# POLYURETHANE / POLY(ETHYL METHACRYLATE) INTERPENETRATING POLYMER NETWORK ORGANOCLAY NANOCOMPOSITES

by

**Boonnak Sukhummek**

A Doctoral thesis submitted in partial fulfillment of

the requirements for the award of

Doctor of Philosophy

of

Loughborough University

**Supervisor : Professor D.J.Hourston**

Institute of Polymer Technology and Material Engineering

# ACKNOWLEDGEMENTS

This research could not have been fulfilled without help of a number of people. First of all, I would like to express my sincere thanks to my supervisor, Professor D.J. Hourston, for his friendship, enthusiasm, invaluable guidance and advice and excellent supervision throughout this project.

I would like to give my thanks to Dr. Mo Song for his useful advice. Special thanks go to Dr. John Bates for his invaluable help in preparing the transmission electron micrographs, and to Dr. David Ross for making the wide angle X-ray diffraction measurements.

I also would like to extend my thanks to Ray Owens, Trevor Atkinson, all technicians and to my fellows in the research group and the Institute without whom this research would not have been so fruitful and enjoyable.

Finally, I deeply appreciate the financial support from the Thai Government for funding all the work in this study.

## ABSTRACT

A number of polyurethane (PU) / poly(ethyl methacrylate) (PEMA) interpenetrating polymer network nanocomposites were investigated with regard to morphology and energy absorbing ability. The nanoclays used were unmodified sodium montmorillonite clay and three different types of organically-modified clays: C15A, C20A and C30B. The nanoclays were incorporated into the IPNs by using an in-situ polymerisation method. The clay dispersions were characterised by wide angle X-ray diffraction (WAXD) and transmission electron microscopy (TEM). The morphologies of the IPNs were determined with dynamic mechanical thermal analysis (DMTA), TEM and modulated-temperature differential scanning calorimetry (M-TDSC), while the mechanical properties were investigated using tensile testing and hardness measurements.

Firstly, the original synthesis procedure and formulation was adjusted by varying the nanoclay C20A content, IPN composition ratio, nanoclay mixing time and PU catalyst, including a study of the PU and PEMA homopolymer composites. All IPN composites showed only partially intercalated nanocomposites as revealed by WAXD and TEM results. 70PU/30PEMA (70:30 composition ratio) IPN nanocomposites exhibited potential as materials for damping applications as it had a broad loss factor $\geq 0.3$ spanning a wide temperature range. Secondly, the synthesis procedure was modified by changing the order of nanoclay mixing with homopolymer components. All IPN composites were based on a composition ratio of 70PU/30PEMA, 5 wt% C20A content, 1.2 wt% of PU catalyst and 30 min mixing time. High intensity ultrasonic waves were also introduced in the nanoclay mixing step for one hour. However, the ultrasonication showed only a marginal change in damping properties. Finally, a number of other nanoclays were incorporated into the 70PU/30PEMA IPN. All IPN composites achieved only a partial intercalation, except for the C30B-filled IPN where no changes were revealed by WAXD. All nanoclays caused a decrease in the glass transition of both homopolymers. IPN nanocomposites tended to reveal a higher extent of phase separation with increased clay content, but only the Na clay-filled IPN still showed a broad loss factor value, even at higher clay content. Improved modulus of elasticity was shown by all nanoclays, with increased clay loading. Whereas a moderate increase in the tensile strength was only shown at 1 wt% clay content.

# TABLE OF CONTENTS

**Page**

## CHAPTER 3 : EXPERIMENTAL

# ABBREVIATIONS

| Abbreviations | Meaning |
|---|---|
| AIBN | Azoisobutyronitrile |
| C15A | Cloisite 15A |
| C20A | Cloisite 20A |
| C30B | Cloisite 30B |
| $CO_2$ | Carbondioxide |
| DMTA | Dynamic mechanical thermal analysis |
| DSC | Differential scanning calorimetry |
| DVB | Divinyl benzene |
| EMA | Ethyl methacrylate |
| EPDM | Ethylene-propylene-diene rubber |
| IPN | Interpenetrating polymer network |
| IR | Infra-red spectroscopy |
| LA | Area under linear loss modulus-temperature curve |
| MMT | Montmorillonite |
| M-TDSC | Modulated-temperature differential scanning calorimetry |
| NMR | Nuclear magnetic resonance spectroscopy |
| OMMT | Montmorillonite |
| $OsO_4$ | Osmium tetroxide |
| PAni | Polyaniline |
| PCL | Poly(ε-caprolactone) |
| PDMS | Poly(dimethyl siloxane) |
| PEA | Poly(ethyl acrylate) |
| PEMA | Poly(ethyl methacrylate) |
| PEO | Poly(ethylene oxide) |
| PET | Polyethylene terephthalate |
| PI | Polyimide |
| PMA | Poly(methyl acrylate) |
| PMMA | Poly(methyl methacrylate) |
| PP | Polypropylene |

| | |
|---|---|
| PPG | Poly(oxypropylene) glycol |
| PS | Polystyrene |
| PTMEG | Poly(tetramethylene ether) glycol |
| PU | Polyurethane |
| RIM | Reaction injection molding |
| $RuO_4$ | Ruthenium tetroxide |
| SAN | Small angle neutron scattering |
| SAX | Small angle X-ray diffraction |
| SBR | Styrene-butadiene rubber |
| SBS | (Styrene-butadiene-styrene) block copolymer |
| SEBS | Styrene-ethylene/butylene-styrene block copolymer |
| SEM | Scanning electron microscopy |
| SIN | Simultaneous interpenetrating network |
| SnOct | Stannous octoate |
| Tan $\delta$ | Damping factor |
| TEGDM | Tetraethylene glycol dimethacrylate |
| TEM | Transmission electron microscopy |
| Tg | Glass transition temperature |
| THAM | Tris(hydroxy methyl) aminomethane |
| TMP | Trimethylol propane |
| TMXDI | 1,1′, 3, 3′-Tetramethylxylene diisocyanate |
| WAXD | Wide angle X-ray diffraction |

# CHAPTER 1

# INTRODUCTION AND OBJECTIVES

# CHAPTER 1
# INTRODUCTION AND OBJECTIVES

## 1.1 Introduction.

Polymers are ubiquitous in daily life. Major industries depend on them. Neither the food packaging industry nor the modern electronics industry could exist without polymers. Polymers are also used in building/construction, household goods, toys, appliances, transportation, furniture and agriculture. Their rapid growth was due to easy processing, inexpensive raw materials, and a wide range of useful and often essential properties. In spite of this, the development of other novel polymers is needed and is now of great interest to scientists.

In the era of the 1960s, multi-component polymer materials were recognised[1]. Polymer blends, grafts, and blocks, of existing polymers, and/or combining them with suitable fillers provided further options for investigation and application. Another type of polymer blend is the interpenetrating polymer network (IPN). It is defined as a combination of two polymer networks, at least one of which is synthesised and/or crossslinked independently in the immediate presence of the other[1,2]. Many IPNs exhibit better mechanical properties than their individual networks due to a synergistic effect induced by forced compatibility of the components. Because of their mechanical properties being changed over a wide range by changing the ratio of components and conditions used in their preparation, IPNs are of great interest in commercial materials for automotive parts, tough plastics, ion-exchange resins, outdoor weathering, controlled drug delivery agents, artificial teeth and sound and damping components[2].

Amongst these applications, IPNs are now an important class of materials for damping purposes[1,2]. Sound and vibration damping are very important in the world today. IPNs are known to introduce forced polymeric interactions between immiscible polymers, which are then able to present high connectivity between the phases, allowing the formation of fine, controllable and stable dispersed phases. IPN synthesis and compositions can be designed in such a way that interaction forces and volume of interface between phases are maximised in order to achieve the highest damping.

Many studies have examined the damping behaviour of IPNs and it has been shown to be dependent on intensity of specific interaction[3-5], crosslink density[3,6-12], phase domain size or morphology [3-6,11,12] and combinations of these[4,6]. Specific interactions amongst immiscible, dissimilar components tend to increase damping ability as they contribute to an increase in the cohesiveness and the connectivity between phase-separated components, whilst the intramolecular crosslink density increases the cohesiveness of each phase and its influence on damping ability depends on the morphology of the resultant system. Therefore, the presence of crosslink bonds can limit the chain segmental motion and fine dispersed domain phases can be set by its actuation.

The phenomenon of phase separation in IPNs is governed by the kinetics of the formation process and polymer component interactions[3-13]. It is well known that a simultaneous interpenetrating network (SIN) formation offers the best inter-segmental contact for a given composition by reaching simultaneously the gel point of the two independent polymerisation reactions, resulting in an interlocked polymeric system[2]. The broadening and/or shift of individual thermal transitions can be used as indicative of the degree of dispersity and/or miscibility of the phases[2].

During the past decade, much attention has been paid to polymer nanocomposites based on organophilic layered silicates[14,15]. Because of the nanometric dispersion of the silicate layers, this new family of materials shows properties that are completely different from those of composites in which the inorganic component is dispersed at the micrometre level[14-17]. Unexpected properties, such as a large increase in mechanical strength[18-23], thermal stability[24-26], and an increase in flame retardency[27,28] and permeability to gases, such as oxygen and moisture[29-31], have been noticed.

Depending on the polymer, different methods have been reported for nanocomposite preparation. The most important ones are in-situ polymerisation and melt intercalation. In the first method, the organoclay has to be swollen in monomer[14]. The key is to control the polymerisation occurring between the layers whereas clay is mixed with the melted preformed polymer in the second method[14]. There are two extreme structures

for nanocomposites, i.e. intercalated nanocomposites in which polymer chains are intercalated between the silicate layers with formation of well-ordered multi-layers with a repetitive thickness of a few nanometres and delaminated, or exfoliated, nanocomposites in which the individual silicate sheets are fully dispersed in the polymer matrix. Moreover, intermediate structures in which silicates are partially intercalated/partially exfoliated can also be obtained[14,32-34].

Many investigations[35-40] proposed that the combination of a glassy polymer and a rubbery polymer at room temperature produce IPNs possessing a broad transition temperature and properties which also depend on the composition ratio and which component forms the continuous matrix. In the present study, the simultaneous polymerisation technique was used for the preparation of IPNs, consisting of an elastomeric (polyurethane) component and a glassy (poly(ethyl methacrylate)) component. Polyurethane polymers provide a good span for the spectrum of properties, including very good elasticity, excellent abrasion resistance and damping properties, high impact strength, and elongation which have been widely used in many applications[41]. Nevertheless, polyurethanes can not be utilised in some applications because of their low modulus[42]. Whilst poly(ethyl methacrylate) possesses a high modulus and very good hardness, it is too brittle to be utilised in many instances. Therefore, a blending technique is applied utilising IPNs of the two polymer components that can amend the deficiencies of each individual polymer. Since the composition ratio is one of the significant factors controlling the miscibility of IPNs, so a ratio of 70/30 polyurethane/poly(ethyl methacrylate) IPN composition (by weight) was first investigated. This composition ratio revealed a broad loss factor, tan $\delta$, of $\geq$ 0.3 spanning a temperature range of 132°C[43,44].

Until now, there has been no work reported regarding the synthesis and characterisation of organoclay IPN nanocomposites. Therefore, in the early stage of this study, the organoclay, Cloisite 20A, was incorporated into the IPNs by using an in-situ polymerisation method, in order to obtain the polyurethane/poly(ethyl methacrylate) IPN organoclay nanocomposites and to investigate the effect of concentration of organoclay on the mechanical and dynamic mechanical behaviours of the IPN. The influences of organoclay, Cloisite 20A, on the polyurethane and

poly(ethyl methacrylate) homopolymers were conducted as well. Consequently, the variation of mixing time, amount of polyurethane catalyst and the composition ratio of polyurethane/poly(ethyl methacrylate) were also examined. In addition, because of its crucial influence in determining the morphology of simultaneous IPNs, the method and order of synthesis were varied, including the use of ultrasonication. Studies[45-47] have reported that the introduction of high intensity ultrasound in a mixing process has led to exfoliated nanocomposites and the clay aggregates in the ultrasonically processed nanocomposites were also more finely dispersed than in the simple mixing methods. Furthermore, a number of other nanoclays were incorporated into the IPNs in order to investigate the effect of types and concentration of nanoclays on the IPN properties, which, hopefully, would be improved especially in damping behaviour.

## 1.2 Objectives of the study.

The purposes of this study were to prepare and characterise novel high damping IPN organoclay nanocomposites based on polyurethane/poly(ethyl methacrylate) with a high energy absorbing ability spanning a broad temperature range.

The objectives of the present study were the following.

1. To synthesise polyurethane/poly(ethyl methacrylate) IPN organoclay nanocomposites.
2. To examine the effect of organoclays on the damping properties, morphology and mechanical properties of these IPN nanocomposites by appropriate characterisation techniques.
3. To investigate the effect of synthesis variables, including mixing time, the amount of PU catalyst and the composition ratio of polyurethane/poly(ethyl methacrylate) on IPN nanocomposite properties.
4. To elucidate the relationship between the morphology of IPN organoclay nanocomposites and their dynamic mechanical and general mechanical properties.
5. To develop high damping IPN organoclay nanocomposites by selection of a suitable method of synthesis, and to characterise their damping characteristics and mechanical properties.

# CHAPTER 2

# BACKGROUND AND LITERATURE REVIEW

# CHAPTER 2

# BACKGROUND AND LITERATURE REVIEW

## 2.1 Interpenetrating polymer networks.

### 2.1.1 An introduction to interpenetrating polymer networks.

**Definition.**

Polymer blends and composites have received increased attention because of the continuous need for engineering polymers with improved properties. Interpenetrating polymer networks (IPN) are an important class of material with broad interest from both the fundamental and industrial points of view. By definition, an IPN is an intimate combination of two or more cross-linked polymers, at least one of which has been synthesised and/or cross-linked in the immediate presence of the other[1,2]. IPNs are related most closely to block copolymers and polymer blends. An IPN can be distinguished from the multi-phase polymers for two reasons. The first reason is an IPN swells in the presence of solvent, but it does not dissolve. The second reason is creep and flow, are suppressed. It is also widely accepted that most IPNs are phase separated. The phenomenon of phase separation in IPNs is governed by polymer component interactions and the kinetics of the formation process[1].

**Types of IPN.**

From the synthesis point of view, IPNs can be made in many different ways as follows[1,2].

- ***Sequential IPNs.*** Polymer network I is polymerised first. Monomer, crosslinker and activator of the second polymer are then swollen into network I and polymerised in situ[1,2]. See Figure 2.1 (a).

- ***Simultaneous interpenetrating networks (SINs).*** Both monomers, plus their crosslinkers and activators, are mixed and synthesised simultaneously by non-interfering reactions. This is often accomplished by polymerising one network by a step reaction polymerisation, while the other network is formed by a chain polymerisation [2]. See Figure 2.1 (b).

(a) Sequential Interpenetrating Polymer Network.

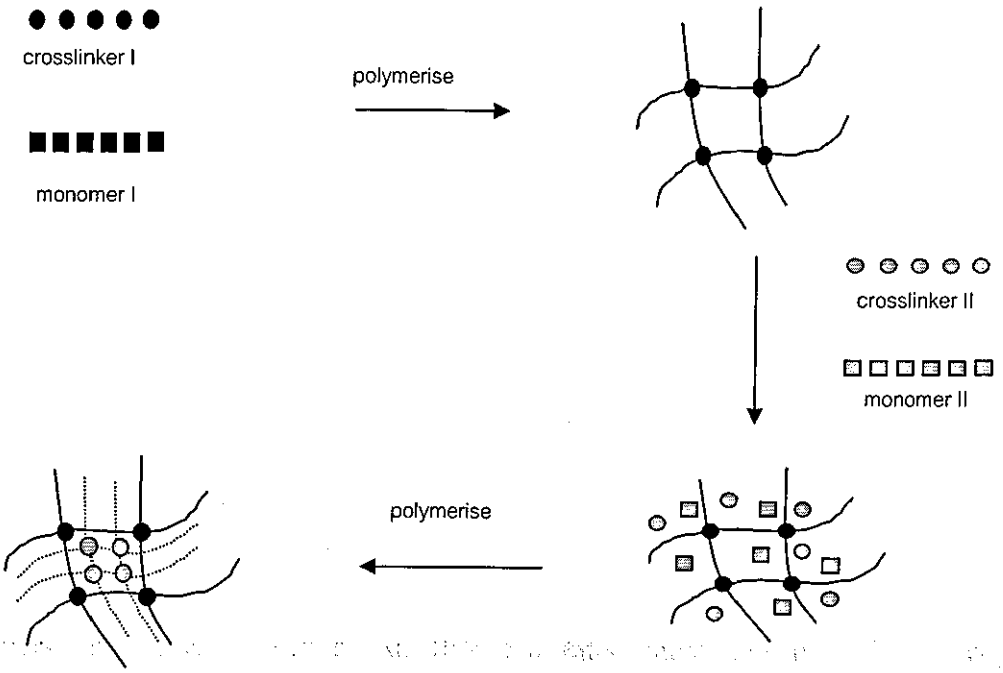


(b) Simultaneous Interpenetrating Polymer Network.

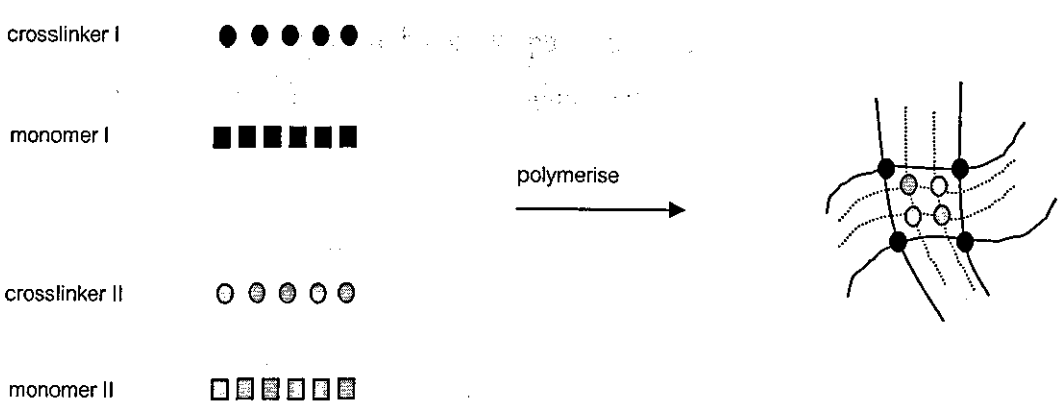


***Figure 2.1*** A schematic diagram of the two basic polymerisation methods to form IPNs: (a) a sequential IPN; (b) a simultaneous interpenetrating polymer network (SIN)[2].

- ***Latex IPNs.*** A latex IPN is synthesised by a sequential emulsion polymerisation method. The morphology of the IPN depends on how the IPN components are polymerised. In case monomer I is first polymerised to form a latex and monomer II then added, the morphology depends on how fast monomer II diffuses into the

first latex. It can have either a homogeneous morphology or a core-shell morphology in which most of monomer II reacts near the surface of the latex particle[1,2].

- ***Gradient IPNs.*** In this system, the overall composition of the material varies systematically from location to location on the macroscopic level. For instance, network I could be predominantly on one surface of a film, network II is prevalently on the other surface, and the interior composition gradually varies from one surface to the other[2].

- ***Thermoplastic IPNs.*** Thermoplastic IPNs are hybrid polymer blends formed using physical crosslinks rather than chemical crosslinks. Thus, they are mouldable and they behave like thermosets and IPNs at the used temperature[2].

- ***Homo IPNs.*** Homo IPNS are IPNs in which both polymers used in the networks are the same[2].

- ***Semi or Pseudo-IPNs.*** Semi- or pseudo-IPNs are materials in which one of the components has a linear or branched structure instead of a network structure[2].

**IPN Applications.**

Most IPNs are combinations of elastomers and plastics. So they exhibit both tough plastic and reinforced elastomer properties, depending on which phase predominates. IPNs have a wide range of applications. A partial list of the commercial materials is shown in Table 2.1[2].

Homo-IPNs based on styrene provide excellent ion-exchange materials for applications such as water-purification[48]. The Rohm and Haas company is well established in this product applications area. IPNs can be designed as mechanical energy absorbing materials if one component is a rubbery material, low Tg, and the other is a rigid, glassy material, high Tg[2,40,41,48]. One example of a sound damping material are the full-IPNs composed of rubbery vinyl polymers and phenolic compounds developed by Hitachi Chemical[48].

*Table 2.1* Commercial IPN materials[2].

| Composition | Application | Trade Name | Manufacturer |
|---|---|---|---|
| SEBS-polyester | Automotive parts | Kraton IPN | Shell Chemical Company |
| Silicone rubber-PU | Gears or medical | Rimplast | Petrach Systems Inc. |
| PU-polyester-styrene | Sheet molding compounds | ITP | ICI Americas Inc. |
| rubber-PE | Tough plastic | - | Shell Research B.V. |
| Anionic-cationic | Ion exchange resins | - | Rhom & Haas |
| EPDM-PP | Tyres, hoses, belts, gaskets | Santoprene | Monsanto |
| EPDM-PP | Outdoor weathering | Somel | Du Pont |
| EPDM-PP | Paintable automotive parts | Vistalon | Exxon |
| Acrylic-urethane-PS | Sheeting molding compounds | Acpol | Freeman Chemical |
| Acrylic-based | Artificial teeth | Trybyte | Dentspy International |
| Vinyl-phenolics | Damping compounds | - | Hitachi Chemical |

Glassy-glassy IPNs have also found good applications. For example, homo-IPNs made of poly(methyl methacrylate) by Dentsply International are used as artificial teeth[49]. Artificial teeth can be made of porcelain or polymers, but polymers are much more tough and resist chipping. According to the Dentsply patent, IPNs exhibit advantages. One is the reduction of swelling by solvents. Another one is it can be ground as a fine powder.

Reaction of functionlised silicones in a thermoplastic melt, such as Nylon-6, 6, can form a thermoset material that interpenetrates the thermoplastic, known as Rimplast thermoplastic IPNs[48] The IPNs based on the silicone and thermoplastic can be prepared by reaction injection moulding (RIM) process, which both constituents are injection moulded and reacts to form the IPNs in the mould. Petrach Systems Inc. uses this process to increase tensile, flexural strength and creep resistance of the IPNs[48].

Impact modifiers in thermoset resins, especially, those based on styrene and unsaturated polyesters can be provided by rubber-based IPN latexes[48,50,51] with surface functionality because they have a core-shell morphology. One of the specific

materials are crosslinked butyl acrylate acting as the rubbery core and methyl methacrylate and glycidyl methacrylate acting as the shell material.

A microporous semi-IPN based on tetrafluoroethylene and silicone[48,52] is used as a wound dressing material. It is sold under the trade name Silon-IPN from Bio Med Sciences. The tetrafluoropolymer component contributes physical strength and the silicone component contributes elasticity and transparency. The combination of these two biocompatible materials provides a film that has a soft and compliant character. This thin film allows oxygen and moisture to diffuse through the material. Therefore, this material is "breathable", which is vital in wound care applications.

One of the interesting applications for gradient IPNs is delivery of medication. In this system, the first network is formed into suspension - sized particles. The extra amount of the drug to be delivered and one of the components of a condensation polymer[53] are dissolved into the network. After rolling in the particles, the second component of the condensation polymer swells into the suspension particles. During its diffusion, the second component meets and reacts with the first component to form a network.

Other applications include flexible, solid electrolytes[54], adhesive bonding of denture teeth[55], latex printing ink compositions[56], latex binders for non-woven products[57], and high temperature polymers as semi-IPNs[58].

### 2.1.2 Morphology of IPNs.

The outstanding behaviour of most IPNs and other multi-component polymer systems is usually derived from the phase separated nature of these materials. The phases vary in amount, domain size and shape, sharpness of their interfaces, and degree of continuity. The morphological detail strongly influences the physical and mechanical properties of the materials. Two major mechanisms of phase separation are proposed in multi-component polymer systems: nucleation and growth, and spinodal decomposition[2]. IPNs can undergo both mechanisms.

**Nucleation and Growth.**

Nucleation and growth mechanism[2,59] generates initial fragments of a new and more stable phase within a metastable phase. Firstly, nucleation forms an unstable intermediate embryo, the so-called a nucleus. After these nuclei are formed, the system decomposes with a decrease in free energy, and the nuclei grow. This mechanism is the growth process, resulting in a two-phase system with dispersed droplets or domains. Figure 2.2 shows the nucleation and growth kinetic mechanism of a multi-component solution of composition $C_o$ which has a tie-line $C_a$-Ca′. If a nucleus of composition Ca′ is formed, the individual molecules within the concentration Co will diffuse downhill into the lower concentration Ca. During the growth process, the concentration within the nuclei remains constant at Ca and Ca′, but the interfaces between two phases vary with time. The final droplet sizes and the distances between them depend on time and rate of diffusion. Later, the droplets become larger by coalescence, coarsening until the phase separation appears.

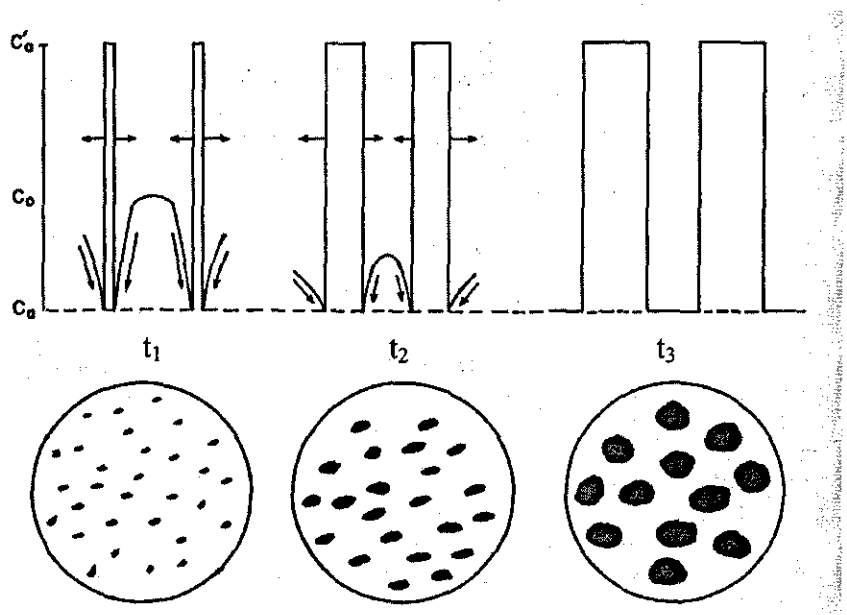


*Figure 2.2* A schematic concentration profile of the nucleation and growth mechanism with the corresponding phase structure[59].

**Spinodal Decomposition.**

The spinodal decomposition mechanism[2,59] generates a spontaneous and continuous growth of new phase within an unstable phase. The growth originates from small amplitude composition fluctuations of the sinusoidal composition modulation with a certain maximum wavelength. Spinodal decomposition tends to form interconnected

cylinders of the second phase. These cylinders grow by increasing their wave amplitude. Figure 2.3 shows the spinodal decomposition mechanism of a multi-component system of composition Co.

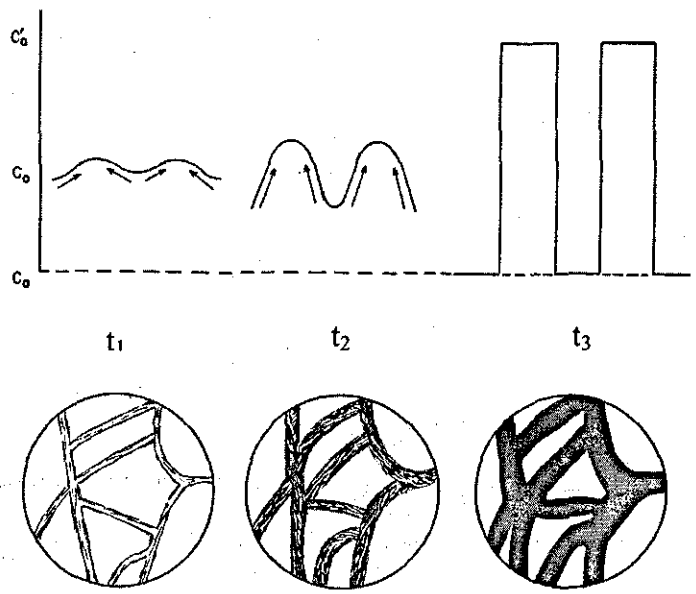


***Figure 2.3*** Schematic concentration profile of the spinodal decomposition mechanism with the corresponding phase structure[59].

If the individual molecules of the new phase component continually diffuse uphill from the low concentration region into a cylinder domain, the system will spontaneously and continuously decompose into two phases of composition $C_a$ and $C_a'$. The domain shape and size may be changed in the coarsening and coalescence as shown in Figure 2.4. However, phase separation might be restricted by crosslinking which keep the domains small.

It is believed that IPNs undergo both nucleation and growth and spinodal decomposition mechanism[2]. The morphology development during IPN polymerisations may be outlined in four distinct stages[2]. Firstly, monomer II may be dissolved in polymer or network I, obtaining an optically clear mixture. Then it suddenly clouds up in the polymerisation stage 2, which means phase separation occurs by the nucleation and growth mechanism to control the spheres of the new phase. Further proceeding to stage 3, interconnected cylinders are created and increase in number during the latter stages of polymerisation, indicating the spinodal

decomposition mechanism. Finally, the resulting morphology may become less distinct because of the high viscosity of the system, leading to a reduction of diffusion towards the equilibrium state. The model[2] of the progress of morphology development is shown in Figure 2.5.

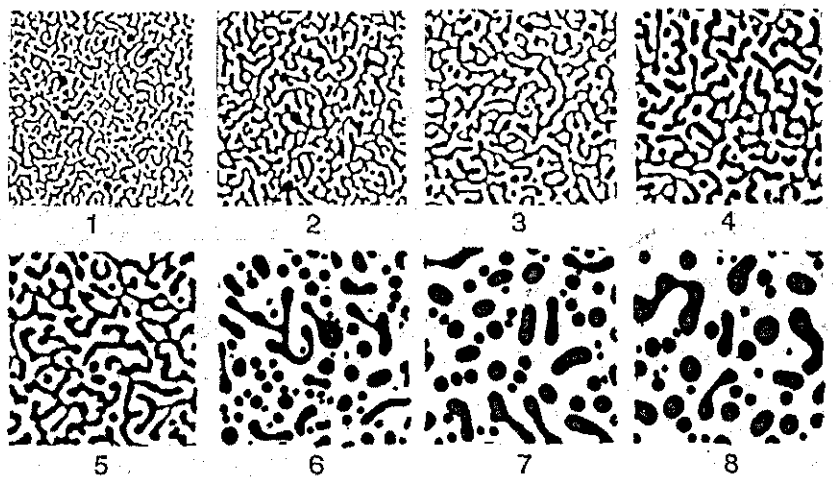


*Figure 2.4* Coarsening and coalescence in the final stage of spinodal phase separation[60].

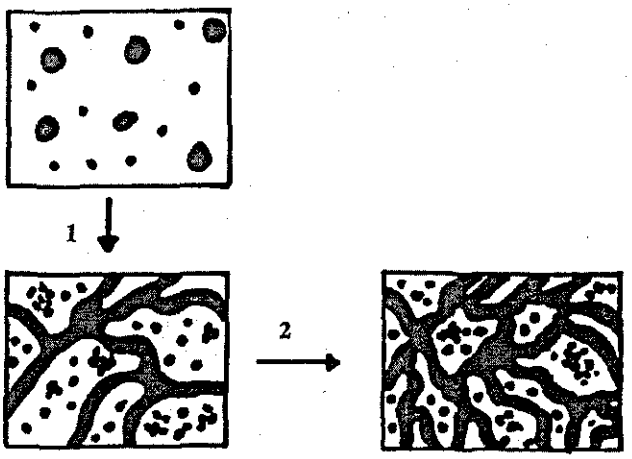


*Figure 2.5* A model of the progress of morphology development[2].

### 2.1.3 Factors influencing IPN morphology.

The prominent behaviour of an IPN is the dual morphology[2], defined as the continuity of both phase I and phase II domains throughout the macroscopic sample, which strongly influences the physical and the mechanical properties of the material. The important factors that control the morphology include: chemical compatibility of the polymers; crosslink densities of the networks; polymerisation method and conditions,

and the IPN composition ratio[1]. These factors may be inter-related or varied independently.

**Chemical compatibility.**

The miscibility of polymer materials indicates the ability of two or more polymer substances to mix together at the molecular level without objectionable separation. Many multi-component polymer systems show a large degree of phase separation and two distinct glass transitions. Thus, the compatibility, or homogeneity, of a multi-component polymer can be defined in relative terms of the dimensions of the separated phases.

Kaplan[61] has treated compatibility as a relative term and defined it by a compatibility number, $N_c$.

$$N_C = \frac{Experimental\ probe\ size}{Size\ of\ phase\ domains} \quad (2.1)$$

The experimental probe size can be provided as the scale of resolution of an instrumental technique. The domain size is the average dimensions of the dispersed phase in the polymer blend. Figure 2.6 represents a two-phase system which illustrates the definition of compatible, incompatible and semi-compatible systems. When $N_c$ approaches zero, two distinct transitions corresponding to each component are observed. This is because the dimensions of each existing phase are much greater than the probe size of the instrument. A change in peak heights could be found if volume fraction of the component change, but not shifts along the temperature axis.

When $N_c$ approaches $\infty$, the compatible case, the phase dimension is much smaller than the probe size. Thus, the instrument is unable to detect small compositional fluctuations. Then a single Tg, which is an average of the contributions of each component, is detected. Therefore, in a two-phase system a single or double transition detected by an instrument would give an indication of the dimensions of the phases present in the system. Many techniques can be used to characterise IPN morphology such as differential scanning calorimetry (DSC)[62-69], dynamic mechanical thermal analysis (DMTA)[62,65,66,69], microscopy[62-65,66,68], x-ray techniques[65-67,70] and light

scattering techniques[69]. The approximate useful range of each technique is shown in Figure 2.7.

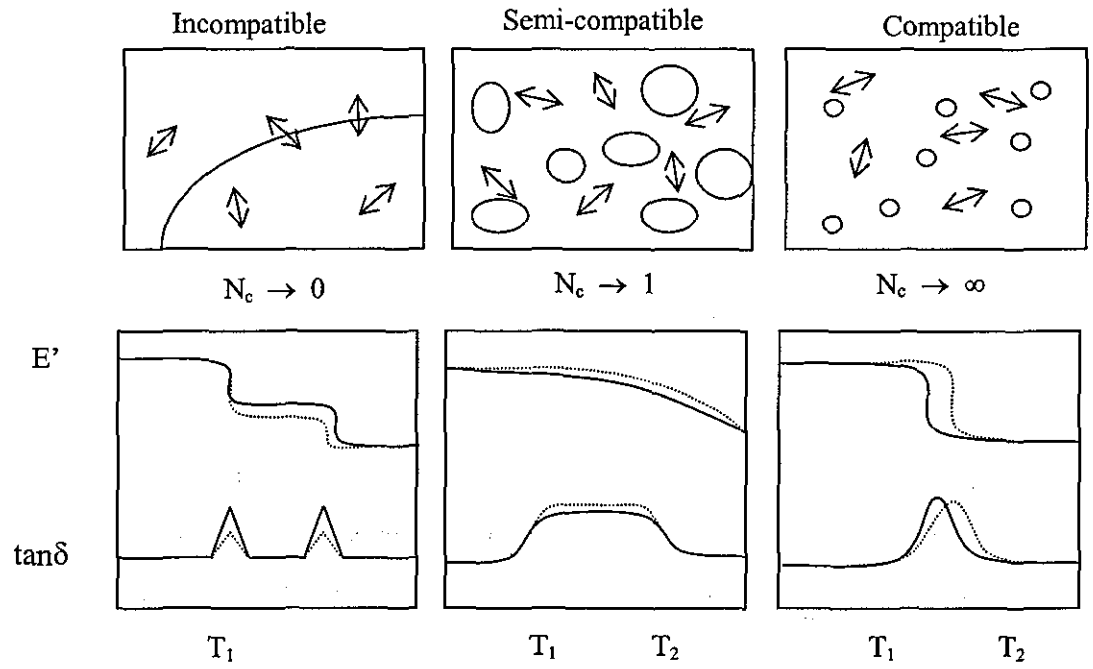


***Figure 2.6*** Schematic diagram of electron micrographs of two phase systems. Arrows represent the probe size[61].

From the thermodynamic point of view[1], the compatibility of multi-component polymers can be explained by the Gibbs free energy of mixing, $\Delta G_m$, which is expressed as follows.

$$\Delta G_m = \Delta H_m - T\Delta S_m \qquad (2.2)$$

where $\Delta H_m$ and $\Delta S_m$ are the enthalpy and entropy of mixing, respectively, and T the absolute temperature in K. The spontaneous mixing process occurs only when $\Delta G$ is negative. Equation (2.2) can be written more precisely in terms of molecular chain structure and interactions as shown by equation (2.3).

$$\Delta G_m = V(\delta_1 - \delta_2)^2 v_1 v_2 + RT(n_1 \ln v_1 + n_2 \ln v_2) \qquad (2.3)$$

where V is the molar volume of the mixture, $\delta_1$ and $\delta_2$ are the solubility parameters of the two components, $n_1$ and $n_2$ are the number of moles of the two polymers, and $v_1$ and $v_2$ are their volume fractions. The first term implies the heat of mixing, and the second term infers the entropy of mixing. Generally, the entropy of mixing is positive because of the entropic term increasing with temperature. In contrast with small

molecules, the entropic changes on mixing of long chain molecules are very low. Thus, the enthalpy of mixing becomes the decisive factor.

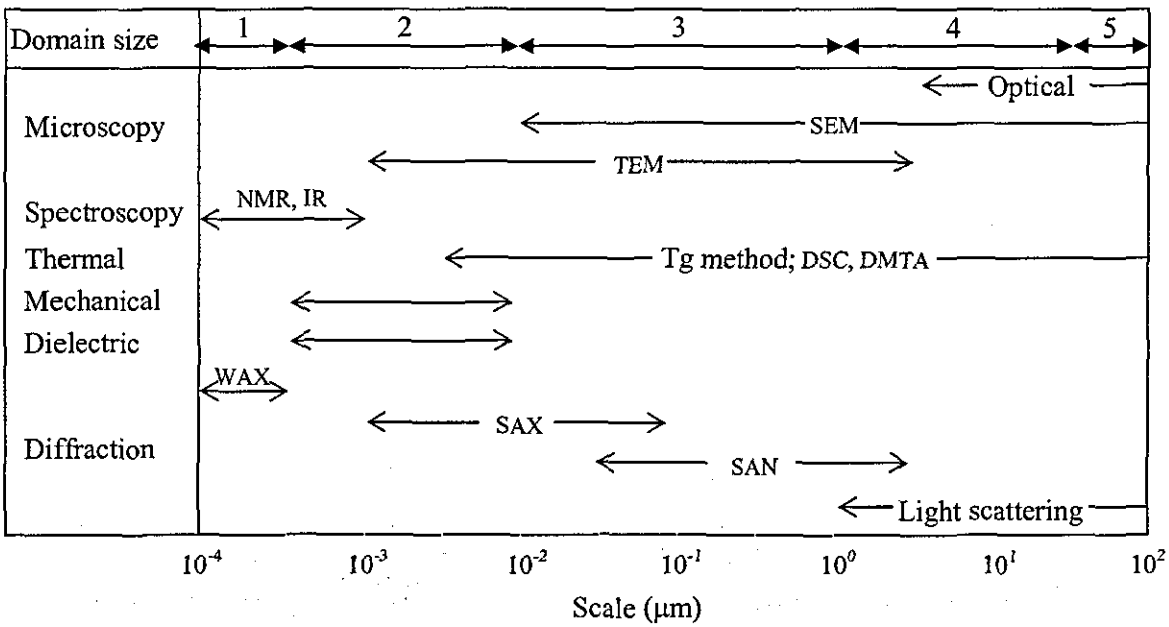


***Figure 2.7*** Approximate ranges of experimental techniques to study blend morphology of: 1) interatomic; 2) molecular, spherulites; 3) filler aggregates, compatibilised blends; 4) reinforcements, non-compatible blends; 5) voids[60].

The enthalpy term is governed by the solubility parameters as shown in equation (2.3). Thus, the compatibility of two polymers can be expected if their solubility parameters are nearly the same, which results in a small $\Delta H_m$ term.

Thus, phase separation occurs when the Gibbs free energy of mixing changes sign, from negative to positive during molecular weight increase in the polymerisation process. However, permanent entanglements in IPNs tend to confine chain mobility, and, consequently, they prevent phase separation from taking place completely. So, two kinetic terms are used to control the phase separation: the rate of network formation and the rate of phase separation. Roughly speaking, if phase separation occurs before gelation, the phases will be relatively large, but normally reduced compared to those occurring in normal blends because of the presence of crosslinks[71]. On the other hand, if gelation happens before phase separation, crosslinking will impede the amount of phase separation and domains might be very small, depending on the crosslink densities of both polymer networks[71].

**Crosslink density.**

It is believed that the crosslink density is an important factor influencing the network morphology[72]. Since, in the presence of crosslinking, the tightened networks, especially the first network, restrict the size of the phase domains, and thus increase the compatibility.

Donatelli et al.[73] proposed that an increased crosslink density in polymer network I decreased the domain size of polymer II in styrene-butadiene rubber/polystyrene (SBR/PS) IPNs, as shown in Figure 2.8. However, variation of crosslink density in the second network, PS, had little effect on the IPN morphology, indicating that the first network was the major control of morphology[73].

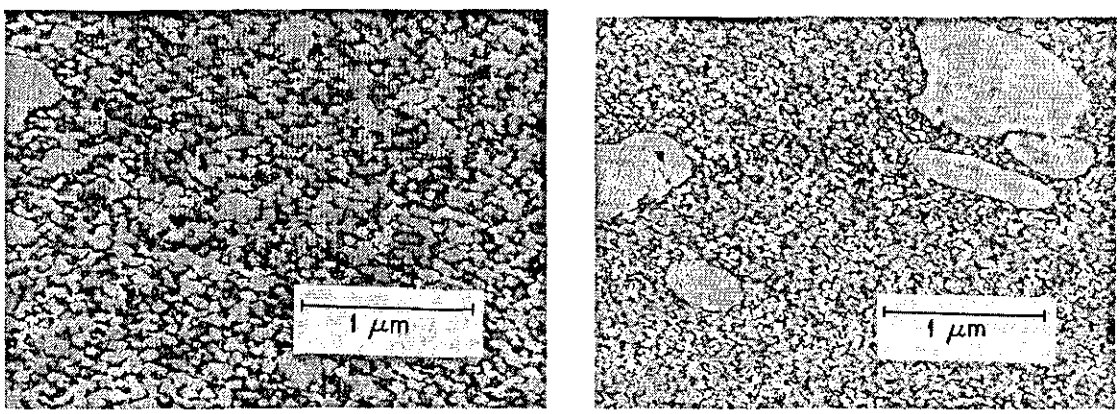


(a) (b)

***Figure 2.8*** Electron micrographs of 20/80 SBR/PS IPNs. The rubber is crosslinked with (a) 0.1%, (b) 0.2% dicumyl peroxide[73].

Hourston et al.[74-76] studied the relationship between crosslink density, morphology and mechanical properties in polyurethane/poly(methyl acrylate) (PU/PMA) sequential IPNs. From electron micrographs, the PU component was presented as a continuous phase, and, as the divinyl benzene (DVB) content increased, the PMA domain size was marginally reduced, suggesting that the PMA component became more continuous[76]. They also found that a semi-2 IPN, in this case a linear PU synthesised in MA which was then itself polymerised and crosslinked, showed a dramatic shift of the loss factor peak of the PU-rich phase towards higher temperature as the crosslinking agent content increased. This indicated an increasing degree of mixing[75]. Similar tends were

obtained from the dynamic storage modulus, showing both transitions were broad, again indicative of an increasing degree of mixing with increasing crosslinking agent. Their former study on semi-1 IPN, showed clearly that increasing the crosslink density in the first formed network produced more effects than when increasing the crosslink density in the second network. Nevertheless, the loss factor values decreased with increased levels of crosslinker, which meant the material tended to be more stiff and brittle.

In contrast, some studies exhibited phase separation as the crosslink level was raised. Felisberti et al.[77] studied the morphology of the poly(vinyl methyl ether)-cross-polystyrene semi-IPNs. Homogeneous, single-phase networks were obtained at low levels of crosslinking (1 and 2 mol% of crosslinker). Phase separation occurred as the amount of crosslinker was increased.

Studying a deuterated polystyrene/poly(vinyl methyl ether) IPN by using SANS, Bauer et al.[78,79] also found phase separation even at low levels of crosslinking agent, indicating the large effect crosslinking had on thermodynamics and compatibility.

**Polymerisation method and condition.**

In sequential IPNs, the network formed first tends to be continuous, having the greater degree of continuity[1]. Even though the order of polymerisation is reversed in sequence, the new morphology is again controlled principally by the first network[80]. Dual phase continuity tends to occur at the mid-range and high concentration of polymer II. Because of its synthesis procedure, the maximum incorporation of monomer II depends upon the equilibrium swelling of polymer I. For simultaneous IPNs, sometimes called the one-shot technique, with both networks forming at the same time, but not necessarily at the same rate[1], this allows for a wide range of compositions to be produced where any composition of monomers can be combined, but the morphologies are more complicated. Simultaneous IPNs tend to show less dual phase continuity than sequential IPNs.

Huelck et al.[80] examined poly(ethyl acrylate) - poly(styrene-co-methyl methacrylate) IPNs by inverting the order of preparation. Electron micrographs showed that the

network synthesised first controlled the morphology of the IPNs, comprising the more continuous phase. A similar finding was made by Donatelli et al.[81] on styrene-butadiene (SBR) copolymer - polystyrene IPNs.

Many comparisons between the IPN morphology prepared by the sequential and the simultaneous techniques have been made. Fox et al.[82] studied the influence of sequential and simultaneous PU/poly-(n-butyl acrylate-co-n-butyl methacrylate) IPNs on the morphology. From dynamic mechanical results, they showed that the simultaneous IPNs exhibited the lower and broader loss factor peaks indicating greater phase separation, or crosslinking, than the corresponding sequential IPNs.

In contrast, Akay et al.[39] compared simultaneous and sequential PU/PMMA IPNs by using scanning electron microscopy. The appearance of the PMMA fracture surfaces in simultaneous IPNs was uniform, implying an intimacy of mixing between the component polymers. In sequential IPNs, however, the non-uniformity of interpenetration could be seen from the respective fracture micrographs, where PMMA aggregates were clearly visible in all the IPN compositions. Also, the simultaneous systems indicated much higher elongations to failure and greater tensile strengths than the sequential ones.

It was also believed that the synthesis conditions have a major effect on morphology and properties of IPNs. PU/PMA IPNs of a fixed composition (50/50 weight ratio) were studied for the effect of synthesis temperatures by Hourston et al.[83] Dynamic mechanical results showed that, with decreasing synthesis temperature, the PMA loss factor transition shifted to lower temperatures and merged with the PU transition, which also shifted to higher temperatures. The merging of the peaks at lower synthesis temperature indicated improved mixing. As a consequence, also greater values for the half-peak width of loss factor peaks were found at the lower temperature, indicating greater phase separation.

On the contrary, there was no significant effect of synthesis temperatures on the physical properties of the IPNs. This was probably a consequence of thermal damage to the PU network, rather than to any phase separation.

**IPN composition ratio.**

Literature[35-37] shows that the relative amounts of the two phases present after polymerisation strongly relate to the IPN composition and polymerisation method. The combination of a glassy polymer with an elastomeric one can produce IPNs possessing a wide range of properties depending on which component forms the continuous matrix. Therefore, IPNs may exhibit the properties from reinforced elastomers through to rubber reinforced high impact plastics.

Kim et al.[84,85] investigated PU/PMMA IPNs with varied composition ratios. Electron micrographs showed finer phase domains than PU/PS IPNs[86], indicating higher compatibility in PU/PMMA IPNs. They also found that phase inversion occurred between the 15/85 and 85/15 composition ratio. The continuous morphology happened only when either PU or PMMA content exceeded 85 wt%. This morphology occurred probably because the relative rates of the two polymerisations were about the same, so the network formed first generally tended to be the more continuous phase. Thus, the concentration here seemed to be a significant factor of the continuity.

Akay et al.[38] investigated the influence of composition ratio on the morphology of PU/PMMA sequential IPNs. The dynamic mechanical behaviours showed that at the extreme IPN compositions, i.e. PU/PMMA ratio of 80/20 and 20/80, single relatively sharp loss factor peaks were obtained and at the intermediate IPN compositions broad loss factor peaks were obtained. This was corroborated by the results of the various mechanical properties. The elastic modulus, ultimate tensile strength and hardness increased, but impact strength decreased with increasing PMMA content.

Schäfer[44] studied simultaneous PU/PEMA IPNs and PU/PS IPNs. He found that no gross phase separation was observed for all PU/PEMA IPN compositions, whereas the PU/PS IPNs showed the phase domains of spherical shape, indicating better component mixing in PU/PEMA IPNs. Both IPNs changed their morphology considerably with composition ratio, especially the PU/PEMA IPNs. He also found that phase inversion occurred between the 30:70 and 20:80 PU/PS IPN compositions.

### 2.1.4 Physical behaviour of IPNs.

The general properties of IPNs depend on three main factors[87]: the properties of the component polymers; the phase morphology and the interactions between the phases. As with other two-component materials, some properties of IPNs are approximately simple averages of the properties of the component polymers.

**Density.**

The density behaviour of IPNs has been debated. Millar[88] found increased densities in PS/PS sequential IPNs. He suggested that some of the "holes" in the comparatively loosely packed amorphous PS structure were filled by self-entanglement of the forming network. However, Klempner et al.[89] results agreed with those of Shibayana and Suzuki[90], who found practically no difference in density between IPNs and the constituent networks in a similar system of PS/PS sequential IPNs. Frisch et al.[91,92] also found no difference in density in PU/polyacrylate latex IPNs.

Kim[84] found the density-composition curve showed significantly increased density in PU/PS IPNs, while there was a slight increase in PU/PMMA IPNs. This seemed to contradict the morphological and glass transition behaviours of the two IPN systems, where the degree of mixing in PU/PMMA IPNs was shown to be higher than that of PU/PS IPNs from the observed dispersed phase domain size and the shift in glass transition, Tg.

**Clarity.**

Clarity, or optical transparency, is one of the practical indications of compatibility[1] of two component materials. Because of the different refractive indices of phase domains, they scatter light which results in a hazy, translucent, or milk-white appearance[1].

This property depends on the amount of light scattered by the material, which is proportional to the square of the difference of the refractive index of the two components and to the sixth power of the radius of the dispersed phase, assuming very small particles[93]. Therefore, optical transparency depends on the type of phase separation and domain size. If the refractive indices of the two polymers match, the

mixtures should be clear, otherwise the result may be a hazy, or milk-white, appearance. Suppression of phase separation is required for high clarity[94-96].

Lipko et al.[97] synthesised a fluorocarbon elastomer/acrylic semi-II IPN system. They showed the grafting effect of high energy β or γ irradiation versus UV irradiation. The former two suppress domain formation through grafting, resulting in a clearer appearance than the latter. The UV-irradiated samples always exhibited significant haze levels. They also proposed that a critical concentration level of acrylic was 3%. Above that level, the material became hazy, indicating the phase separation. In conclusion, high clarity can be maintained if phase separation is suppressed, phase domains are made smaller, and/or the composition within the phase is made more alike[98,99].

**Glass transition behaviour.**

The most commonly used method for establishing compatibility in multi-component systems, or partial mixing, is through determination of the glass transition[58]. A miscible polymer blend exhibits a single glass transition between the Tg's of the components with the sharpness of the transition similar to that of the components. With cases of limited compatibility, such as polymer blends, in general, and IPNs in particular, two separate transitions between those of the constituents occur, depicting a component 1-rich phase and a component 2-rich phase. Shifts and broadening of the transitions indicate the extent of molecular mixing[100].

Huelck et al.[80] evaluated the loss and storage moduli of poly(ethyl acrylate)/polystyrene (PEA/PS) and PEA/PMMA IPNs. Because of increased attractive forces, PEA/PMMA became more compatible, showing one broad glass transition, indicating an extensive overlap of the two primary transitions. On the other hand, PEA/PS IPNs exhibited two separate glass transitions and loss peaks, as shown in Figure 2.9. No IPN has been found that behaves in a manner similar to the equivalent random copolymer, that is, one sharp glass transition[87]. The effect of composition on the modulus of an incompatible polymer pair, cis-polybutadiene/polystyrene (PB/PS), was examined by Curtius et al[101]. Two distinct transitions were observed for all IPN compositions. The peak shifts were minimal as

illustrated in Figure 2.10 (a). The morphology of these IPNs exhibited a relatively sharp phase domain separation.

For the composition ratio comparison of semi-compatible IPNs, Huelck et al.[80] studied the modulus behaviour of PEA/PMMA IPNs. They found only one broad transition for all IPN compositions, as shown in Figure 2.10 (b). More probably the combined transitions of all possible compositions could contribute independent transitions[100].

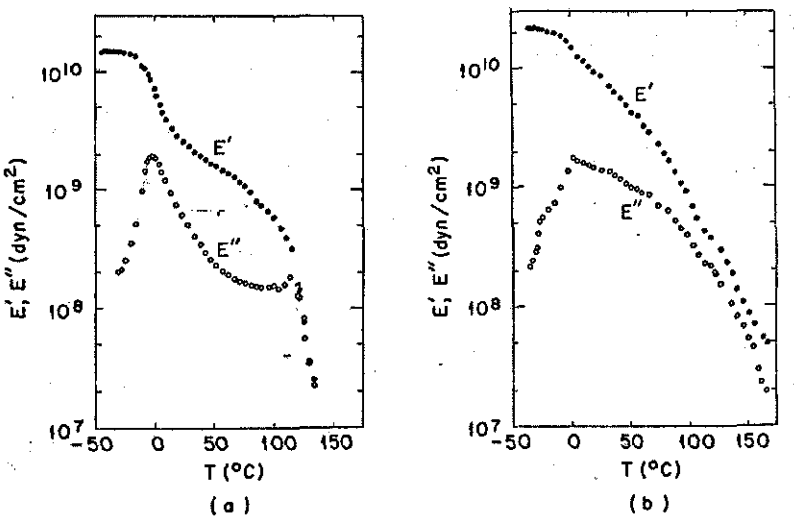


***Figure 2.9*** Storage (E') and loss (E") moduli : (a) 48.8/51.2 PEA/PS; (b) 47.1/52.9 PEA/PMMA IPNs. Both at 110 Hz [80].

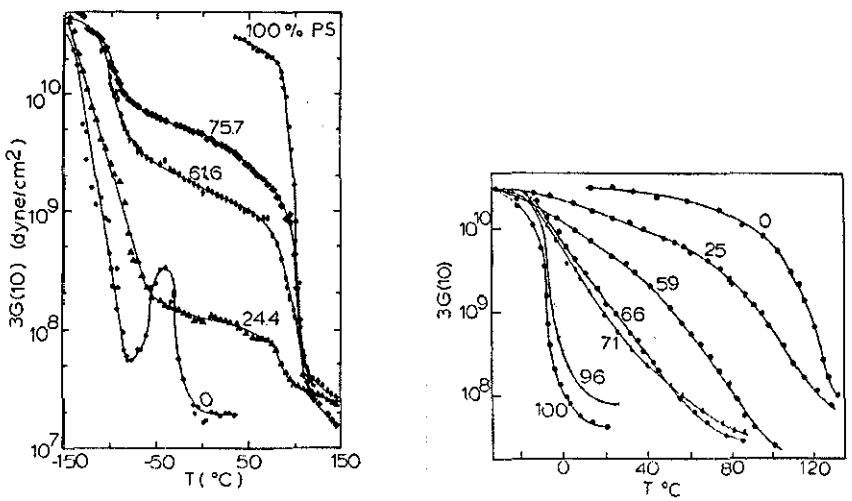


(a) (b)

***Figure 2.10*** Modulus-temperature behaviour of (a) incompatible cis-PB/PS IPNs[101] and (b) compatible PEA/PMMA IPNs[81].

## 2.2 Dynamic mechanical behaviour and damping with IPNs.

Damping behaviour of materials is of practical importance as the degree of damping affects the behaviour under vibratory loading. In particular, higher damping results in lower stresses under forced vibration near resonance, and also in more rapid decay of free vibrations. Damping behaviour may, thus, affect the choice of materials in vibration-sensitive applications. Damping behaviour is characterised in dynamic mechanical terms.

### 2.2.1 Dynamic mechanical properties of polymers.

Polymers commonly exhibit a combination of liquid (viscous) and solid (elastic) behaviours under deformation. They are called viscoelastic materials. Generally, viscoelasticity refers to both the time and temperature dependence of mechanical behaviour[102].

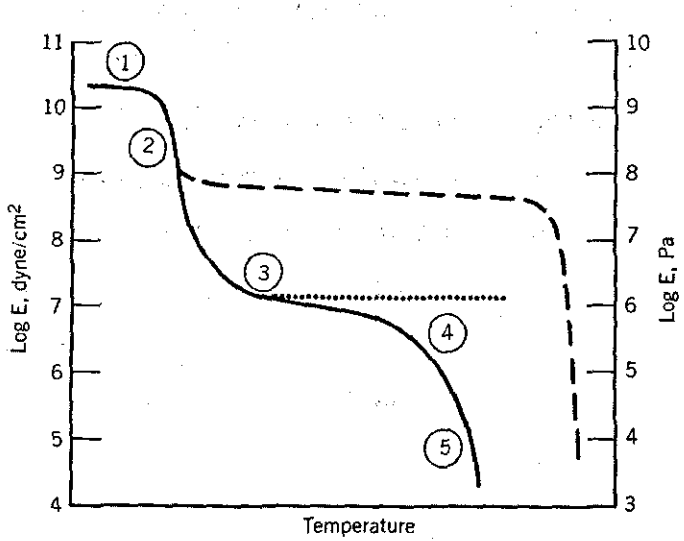


***Figure 2.11*** Five regions of viscoelastic behaviour for a linear, amorphous polymer. Also illustrated are effects of crystallinity (dashed line) and cross-linking (dotted line)[102].

As shown in Figure 2.11, viscoelasticity can be sub-classified into five types[102]. In region I, the glassy state, the polymer is glassy and frequently brittle, where chain segmental motion is quite restricted and involves mainly only bond bending and bond angle deformations[103]. Region II is the glass transition state. The behaviour of polymers in this state is best described as leathery. The glass transition temperature,

Tg, is often taken at maximum rate of turndown of modulus or at a discontinuity of the thermal expansion coefficient. From the qualitative point of view, the glass transition region can be interpreted as the onset of long-range, coordinated molecular motions, where some 10-50 chain atoms attain sufficient thermal energy to move in a coordinated manner. With increasing temperature, polymers change from the glass transition state to the rubbery plateau, state III, where polymers exhibit long-range rubber elasticity, meaning the elastomer can be stretched, and snap back to substantially its original length on being released, This stage is involved with both side-chain and main chain rotations. Region IV, the rubbery state, where local segmental mobility occurs, but total chain flow is restricted by a physical and/or chemical network matrix structure. Finally, the liquid flow region where irreversible bulk deformation and slippage of chains pass one another occurs.

The ability of polymers to damp vibrations and absorb sound is a function of their viscoelastic nature, especially their glass transition behaviour, which can be characterised in dynamic mechanical terms. When a viscoelastic polymeric material undergoes repeated small-amplitude strains in a cyclic manner, a portion of the energy is stored elastically and is represented as the storage modulus, E′. Another portion of energy is dissipated in the form of heat and is represented as the loss modulus, E″. Figure 2.12 illustrates a viscoelastic ball during dropping onto a perfectly elastic floor, indicating the simple definition of E′ and E″.

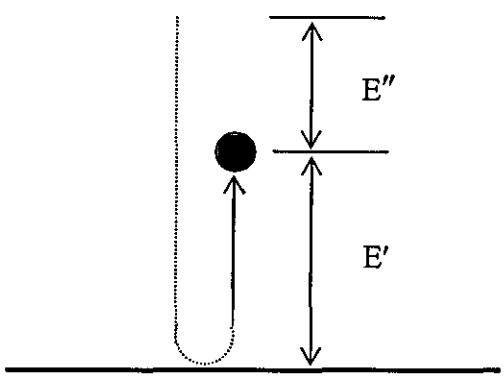


***Figure 2.12*** Simplified definition of E′ and E″ [102].

Dynamic mechanical analysis yields both the elastic modulus of a material and its mechanical damping, or energy dissipation, characteristics, which can be determined

as a function of frequency, time, and temperature. For linear viscoelastic behaviour, when a sinusoidal stress is applied to a specimen, a strain will be produced with the same frequency as, but out of phase with, the stress[104]. This can be represented schematically in Figure 2.13.

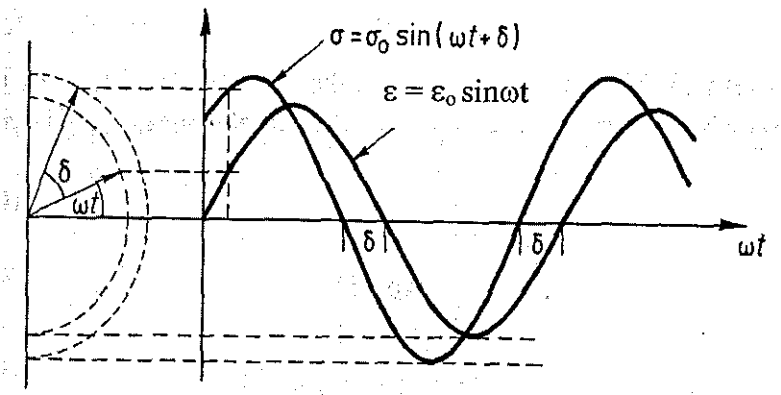


***Figure 2.13*** Vector diagram representation of an alternating stress leading an alternating strain by a phase angle, δ[105].

Thus, the stress, σ, and strain, ε, at any time, t, can be written as the following equations.

$$\sigma(t) = \sigma_0 \sin(\omega t + \delta) \quad (2.4)$$

$$\varepsilon(t) = \varepsilon_0 \sin(\omega t) \quad (2.5)$$

where ω is the angular frequency and δ the phase lag as shown in Figure 2.13.

Using trigonometry, equation (2.4) can be rewritten as equation (2.6).

$$\sigma(t) = \sigma_0 \sin\omega t \cos\delta + \sigma_0 \cos\omega t \sin\delta \quad (2.6)$$

$$\sigma(t) = (\sigma_0 \cos\delta) \sin\omega t + (\sigma_0 \sin\delta) \cos\omega t \quad (2.7)$$

This equation can be separated into the in-phase and out-of-phase stress with the strain as in the equations below.

$$\sigma' = \sigma_0 \cos\delta \quad (2.8)$$

$$\sigma'' = \sigma_0 \sin\delta \quad (2.9)$$

So, the vector sum of these two components gives the overall or the complex stress on the sample.

$$\sigma(t) = \sigma' \sin\omega t + \sigma'' \cos\omega t \quad (2.10)$$

$$\sigma^* = \sigma' + i\sigma'' \quad (2.11)$$

where $i = \sqrt{-1}$. $\sigma^*$ is the complex stress.

From the familiar relation, $e^{i\theta} = \cos\theta + i\sin\theta$, the stress and strain can alternatively be written as:

$$\varepsilon^* = \varepsilon_0 e^{i\omega t} \quad (2.12)$$

$$\sigma^* = \sigma_0 e^{i(\omega t + \delta)} \quad (2.13)$$

The stress-strain relationship defines the dynamic complex modulus as follows.

$$E^* = \frac{\sigma^*}{\varepsilon^*} \quad (2.14)$$

Substitute by equations (2.12) and (2.13)

$$E^* = \frac{\sigma_0 e^{i(\omega t + \delta)}}{\varepsilon_0 e^{i\omega t}} = \frac{\sigma_0 e^{i\delta}}{\varepsilon_0} \quad (2.15)$$

$$E^* = \frac{\sigma_0}{\varepsilon_0}(\cos\delta + i\sin\delta) \quad (2.16)$$

Then $$E^* = E' + iE'' \quad (2.17)$$

and $$E' = \left(\frac{\sigma_0}{\varepsilon_0}\right)\cos\delta \quad (2.18)$$

$$E'' = \left(\frac{\sigma_0}{\varepsilon_0}\right)\sin\delta \quad (2.19)$$

where E′ is the real part in-phase with the strain called the storage modulus, and E″ is the loss modulus defined as the ratio of the component 90° out-of-phase with the strain[103]. See figure 2.14.

For a viscoelastic polymer, E′ characterises the amount of the stored energy, while E″ exhibits the amount of energy dissipated by the material.
Another equation in wide use is

$$\tan\delta = \frac{E''}{E'} \quad (2.20)$$

where tan δ is called the loss tangent, indicating the ratio of the energy stored to the energy lost per cycle.

The maximum peak in E″ and tan δ are sometimes used as the definitions of Tg. The dynamic mechanical behaviour of an ideal polymer is shown in Figure 2.15.

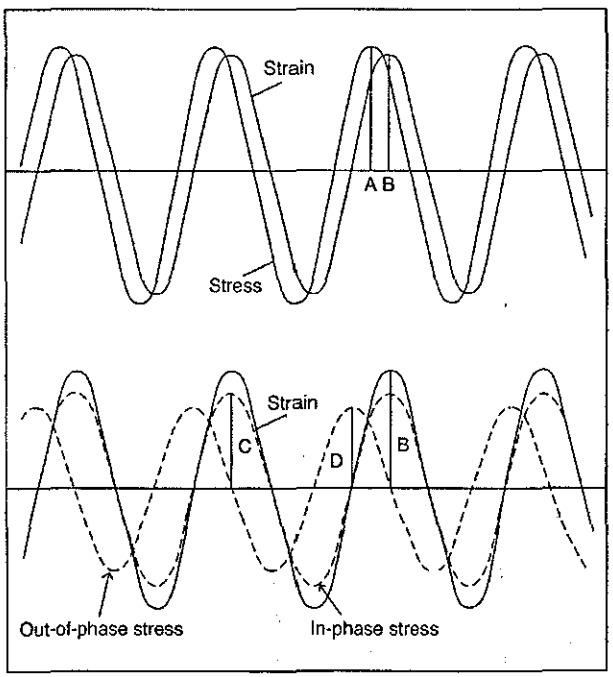


***Figure 2.14*** Sinusoidally varying stress and strain in a dynamic mechanical experiment[106].

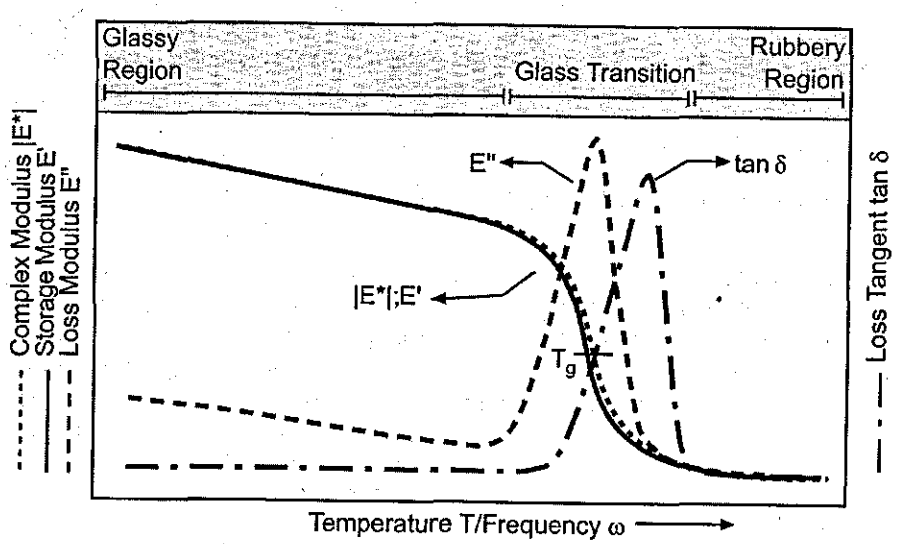


***Figure 2.15*** Dynamic mechanical analysis in oscillatory mode of an amorphous thermoplastic as a function of the temperature[107].

### 2.2.2 Damping with polymers and IPNs.

Many different efforts have been made in recent years to broaden the useful temperature range of damping. Effective ways to broaden, or shift, the Tg range include the use of plasticisers and fillers, blending, grafting, copolymerisation, or the formation of IPNs.

Simple homopolymers and copolymers are common types of damping material used. Their efficient damping is limited to a narrow temperature range of approximately 20-30°C, centered about the glass transition of the polymer involved[108]. Incompatible polymer blends and grafts show two damping ranges with low damping in between. Semi-compatible polymer blends and grafts with high extent of component mixing, but incomplete, lead to a broad temperature use range. IPNs are one way of attaining the required intimate mixing. Ideally, interpenetration occurs only through physical crosslinks. This is catenane-type structures[41], and mixing is on a molecular scale as long as no covalent bonds exist between the different polymers. In this case, a single phase material results when dynamic mechanical measurements are used. However, these materials possess some level of phase separation, if mixing is incomplete, such as when crosslinking occurs after phase separation, then two phases result. However, micro-heterogeneous morphologies can occur and result in broad glass transition regions with respect to temperature and frequency. The advantages that IPNs present over other transition broadening techniques include more control over the resulting morphology, longer phase stability, and broader glass transition regions, leading to the desired high damping property.

The use of IPNs as energy damping materials was first reported by Huelck et al[80]. Latex IPNs based on poly(ethyl acrylate) and poly(methyl methacrylate) were observed to exhibit high tanδ values that stayed high over a broad temperature range of 100°C. Because the polymer components were isomers, it was reasoned that the heat of mixing would be near zero and, therefore, the IPN must lie near the phase boundary; that is the IPNs exhibited a micro-heterogeneous morphology.

Chang et al.[109] assumed that the area under the linear loss modulus-temperature curve, LA, was a function of the glassy modulus, rubbery modulus, average activation

energy of glass transition and the glass transition temperature. LA was controlled by the structure of the polymers. They used this concept to develop a relationship between the extent of damping and the contribution from each molecular structure of the homopolymers, statistical copolymers, and IPNs based on acrylic, vinyl, and styrenic monomers.

Foster and Sperling[110] found a good damping material in a series of acrylic/methacrylic sequential IPNs. 75/25 full PnBA/PnBMA IPN exhibited tanδ values between 0.4-0.5 over nearly a 100°C temperature range, whilst PnBMA/PnBA semi-2 IPNs showed tanδ of 0.4-0.85 over 100°C.

Hourston and McCluskey[111] characterised poly(vinyl isobutylether)/PMMA sequential IPNs which exhibited tanδ over 0.4 from 10 to 60°C. It had also been observed[75,76,112] in various studies of PU/PMMA IPNs that broad loss tangent transitions exhibiting good damping behaviour occured.

### 2.2.3 Extensional and constrained layer damping.

Sound attenuation can occur by four mechanisms[113]: 1) scattering by a inhomogeneity; 2) mode conversion at boundaries; 3) redirection; and 4) intrinsic absorption by conversion to heat with viscoelastic materials. When a viscoelastic polymer is coated on a vibrating substrate, segmental chain motions create internal friction. Subsequently, heat buildup within the polymer occurred because of absorption of the vibrating waves. Common damping configurations consist of two types: extensional and constrained damping[108]. A single viscoelastic layer on a vibrating substrate is called extensional damping in which energy dissipation evolves primarily from the flexural and extensional motions of the damping layer. The composite loss factor of the extensional system is given by equation (2.21).

$$(\tan\delta)_{composite} = k\,(E_2/E_1)\,(h_2/h_1)^2 \tan\delta_2 \qquad (2.21)$$

where E and h represent the Young's modulus and thickness, respectively. Subscript 1 and 2 represent the substrate and viscoelastic layer, respectively, and k is a constant.

A further important configuration in damping is attained by covering the damping layer with a stiff constraining layer. When the substrate material vibrates, the

constraining layer will, in general, respond with vibrations that are out-of-phase with the substrate. The resulting shearing action on the intermediate damping layer causes enhanced degradation of the mechanical energy to heat. The shear action in combination with flexure and extension greatly increases the amount of energy dissipated per cycle over the extensional configuration. The composite loss factor of the constrained layer system is given by equation (2.22).

$$(\tan \delta)_{composite} = k\,(E_3/E_2)\,(h_3/h_1)^2 \tan \delta_2 \qquad (2.22)$$

where subscripts 1, 2, and 3 represent to the substrate, viscoelastic layer, and constraining layer, respectively. Thus, damping depends upon the material loss factor, the material modulus, the substrate modulus, and the constraining layer modulus.

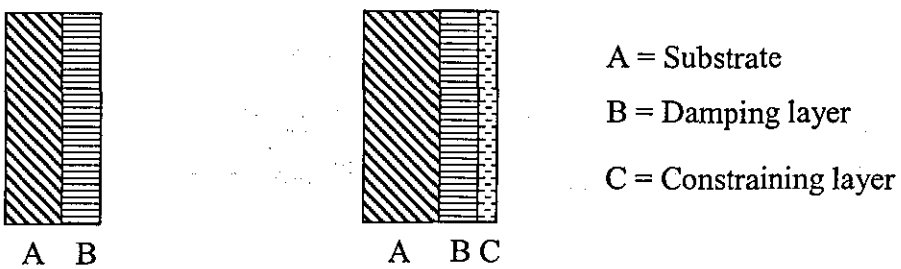


***Figure 2.16*** Two mechanisms of the use of polymers in damping[114].

**2.3 Nanocomposites.**

Polymers are filled with particles in order to get superior properties, such as stiffness and toughness, barrier properties, fire retardance and ignition resistance or cost reduction. Nanocomposites are a new class of composites. They are particle-filled polymers, where at least one dimension of the dispersed particles is in the nanometre, $10^{-9}$ m, range. Amongst all the potential nanocomposite precursors, those based on clays and layered silicates have been most widely studied, probably because the starting clay materials are easily available and their intercalation chemistry has been studied for a long time[115,116]. Because of the nanometre size particles obtained by dispersion, these nanocomposites can show markedly improved mechanical, thermal, optical, physical, and chemical properties when compared with the pure polymer or conventional (microscale) composites as firstly published by a group of researchers from Toyota[117] for nylon-clay nanocomposites. They showed dramatic improvements in mechanical properties, barrier properties and heat distortion temperature. These improvements were obtained at very low contents of the layer silicate, ca. 4 wt%.

### 2.3.1 Structure of layered silicates.

The term "layered silicates" refers to natural clays, but also to synthesised layered silicates. Both natural clays and synthetic layered silicates have been successfully used in the polymer nanocomposite synthesis.

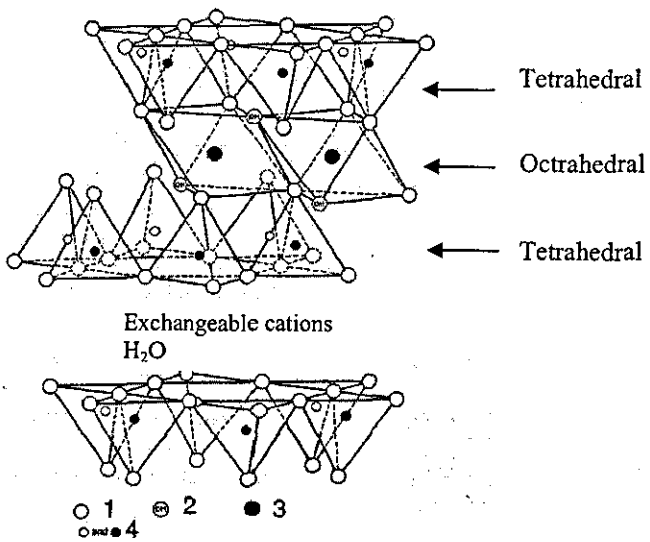


***Figure 2.17*** Structure of 2:1 phyllosilicates. (1) oxygen, (2) hydroxyl, (3) aluminium/magnesium, (4) silicon[119].

Montmorillonite, a natural clay from the smectite family is nowadays the most widely used nanofiller clay because it has a suitable layer charge density. The layered silicates usually used in nanocomposites are based on the structural family known as the 2:1 phyllosilicates[118]. See in Figure 2.17. Their crystal lattice consists of two fused silica tetrahedral sheets, sandwiching an edge-shared octahedral sheet of either alumina or magnesia. The layer thickness is around 1 nm and the lateral dimensions of these layers may vary from 30 nm to several microns, depending on the particular silicate. These layers form stacks with regular van der Waals forces in between them called the interlayer or the gallery. Isomorphic substitutions within the layers, for example, $Al^{3+}$ replaced by $Mg^{2+}$ or by $Fe^{2+}$ in the tetrahedral lattice and $Mg^{2+}$ replaced by $Li^{+}$ in the octahedral lattice cause an excess of negative charges that are counter-balanced by alkali or alkaline earth cations situated in the interlayers. Because of the high hydrophilicity of the clay, water molecules are usually also present between the layers. To make clay more compatible with organic polymers, the hydrated cations of the interlayer can be exchanged with cationic surfactants such as alkylammonium or

alkylphosphonium (onium ions). It usually results in a larger interlayer spacing. The amount of negative surface charge is known as the cation exchange capacity (CEC)[14]. It is measured in milliequivalents per gram (meq/g), or more regularly, per 100 gram (meq/100g). The CEC of montmorillonite can be varied from 80 to 150 meq/100g. The charge of the layer is not locally constant as it varies from layer to layer. So, it must be considered as an average value over the whole crystal.

The cation exchange process[120] of a linear alkylammonium ion is illustrated in Figure 2.18. Because of the negative charge originating in the silicate layer, the cationic head group of alkylammonium molecule preferentially resides at the layer surface and the organic tail leads away from the surface. Depending on the cation exchange capacity of the layered silicate and the chain length of the organic tail, the alkylammonium ions adopt different structures between the silicate layers, forming mono or bilayers or, mono or bimolecular tilted "paraffinic" arrangements as shown in Figure 2.19.

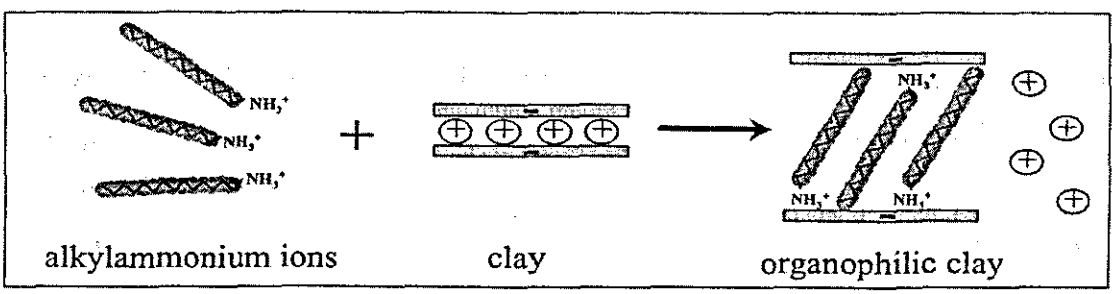


***Figure 2.18*** The cation-exchange process between alkylammonium ions and cations initially intercalated between the clay layers[120].

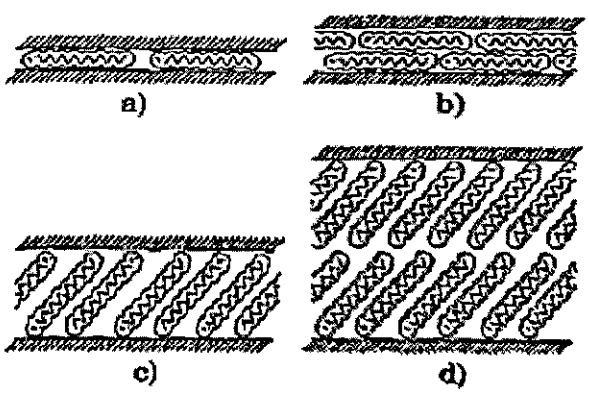


***Figure 2.19*** Alkyl chain aggregation in layered silicates: a) lateral monolayers; b) lateral bialyer; c) paraffin-type monolayer and d) paraffin-type bilayer[121].

### 2.3.2 Structure of nanocomposites.

Polymer-clay composites can be categorised into "conventional composites" and "nanocomposites"[118]. In a conventional composite, the polymer is unable to intercalate between the silicate layers and a phase separated composite is obtained, where clay acts mainly as a filling agent. Two types of nanocomposite can be found. Intercalated nanocomposites are formed when a single or a few extended polymer chains are intercalated between the silicate layers with fixed interlayer spacings. Exfoliated nanocomposites are formed when the silicate layers are completely and uniformly dispersed in a continuous polymer matrix. The latter structure shows greater phase homogeneity because each nanolayer contributes fully to interfacial interactions with the matrix. This is the reason why the exfoliated clay leads to the most dramatic changes in mechanical and physical properties.

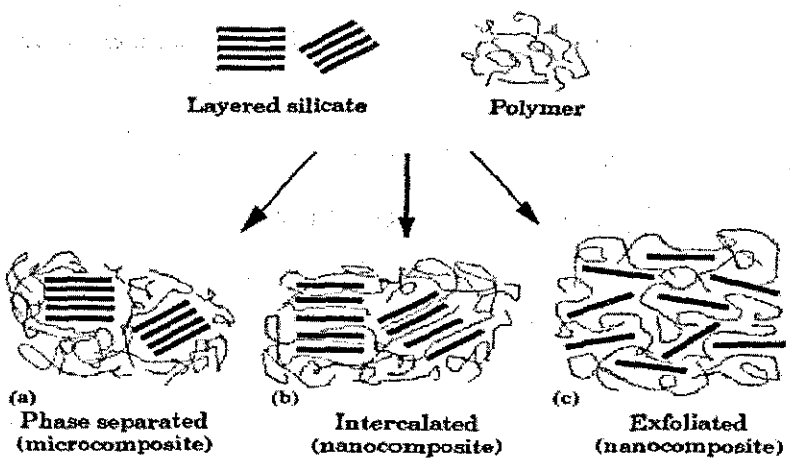


***Figure 2.20*** Schematic of the different structures of composite arising from the interaction of layered silicates and polymers: a) conventional; b) intercalated nanocomposite; c) exfoliated nanocomposite[14].

Two main techniques are used to characterise the structure of polymer-clay nanocomposites. The most straight forward is X-ray diffraction (XRD) because it is used to identify the interlayer spacing between the clay galleries. The intercalation of the polymer chains usually increases the interlayer spacing when compared with the spacing of the organoclay used, causing a shift of the diffraction peak towards lower angle values as shown in Figure 2.21. The angle and interlayer spacing values are related through Bragg's law.

$$n\lambda = 2d\sin\theta \qquad (2.23)$$

where n refers to the degree of the diffraction, λ corresponds to the wave length of the X-ray radiation used, d the spacing between the galleries, and θ the incident angle.

For exfoliated nanocomposites[14], all of the X-ray diffraction patterns are characterised by the absence of the diffraction peaks because there are too large interlayer spacings or the layers are no longer organised in stacks. XRD only gives the distance between the clay layers, thus revealing the relationship of the clay layers to themselves, not of the clay layers to the polymer. XRD does not reveal how well dispersed the clay is throughout the polymer. To complete the XRD results, transmission electron microscopy (TEM) can be used. It is a powerful technique to characterise the nanocomposite morphology. At low magnification, TEM will reveal how well dispersed the clay is throughout the polymer matrix, and it can also show the degree of intercalation and exfoliation which has occurred. Therefore, this technique is widely used to define the overall structure.

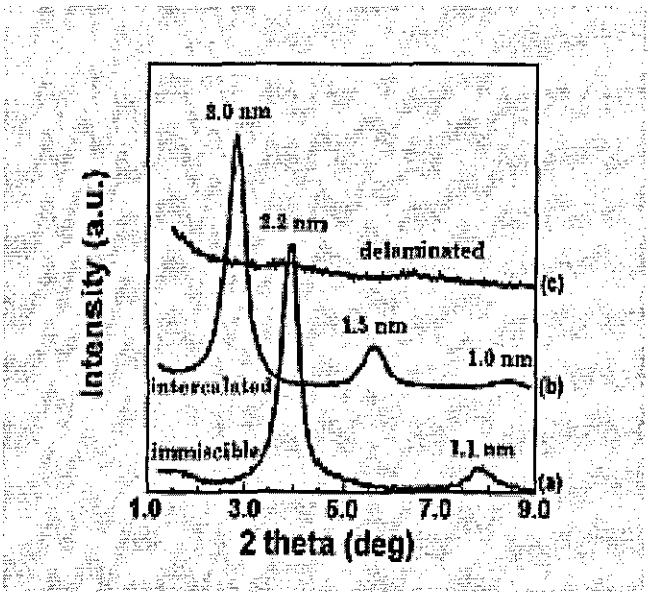


***Figure 2.21*** XRD patterns of: a) phase separated microcomposite; b) intercalated nanocomposite; c) exfoliated nanocomposite[118].

### 2.3.3 Nanocomposite preparation.

Depending on the polymer, three different methods[122] have been widely considered to prepare polymer-layered silicate nanocomposites.

**In-situ intercalative polymerisation.**

In-situ polymerisation was the first process used to prepared polymer-clay nanocomposites based on polyamide-6[117]. Firstly, the organoclay has to be swollen in the monomer and the curing agent is added and then polymerisation occurs between the silicate layers. How well swollen is the organoclay depends on the polarity of the monomer molecules, the surface energy of the organoclay, and the swelling temperature. For thermosets, the curing agent is added to initiate the polymerisation. A curing agent or an elevated temperature can initiate the polymerisation for thermoplastic [31].

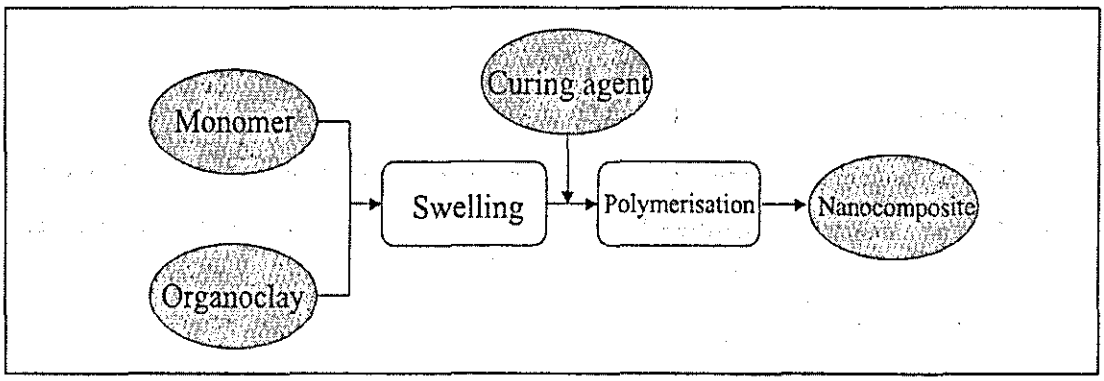


**Figure 2.22** Flow chart representing the two steps of the "in-situ polymerisation" approach[123].

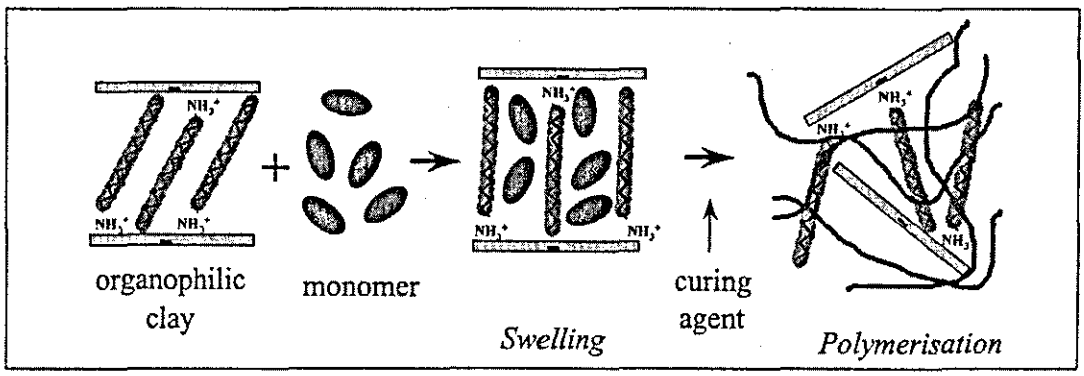


***Figure 2.23*** The in-situ polymerisation showing polar monomer molecules diffusing between the layers. The alkylammonium ions adopt a perpendicular orientation in order to optimise solvation interactions with the monomer[123].

The driving force of the in-situ polymerisation method is associated with the polarity of the monomer molecules. It is believed that during the swelling phase, the high

surface energy of the clay reacts to polar monomer molecules so that they diffuse between the clay layers as shown in Figure 2.23. The diffusion process stops, when an equilibrium is reached, and the clay is swollen in the monomer to a certain extent corresponding to a perpendicular orientation of the alkylammonium ions[124]. The polymerisation is initiated when the monomer starts to react with the curing agent added. Consequently, the overall polarity is lower and displaces the thermodynamic equilibrium. So, more polar molecules can diffuse between the clay layers. Eventually, the delaminated nanocomposite can occur by this mechanism.

**Melt intercalation.**

Vaia et al.[17] were the first group reporting the melt intercalation process. It consists of blending an organoclay with a thermoplastic in the molten state in order to optimise the polymer-clay interactions. Figure 2.24. The mixture is then annealed at a temperature above the glass transition temperature of the polymer, consequently, a nanocomposite forms. During getting intercalated between the clay layers, the polymer chains loose some of their conformational entropy. In this technique, no solvent is required as shown in Figure 2.25. The driving force for this mechanism associates with the enthalpic contribution of the polymer/organoclay interactions during the blending and annealing steps. Because of its great potential for application in industry, especially for production by extrusion processing, this process has become increasingly popular.

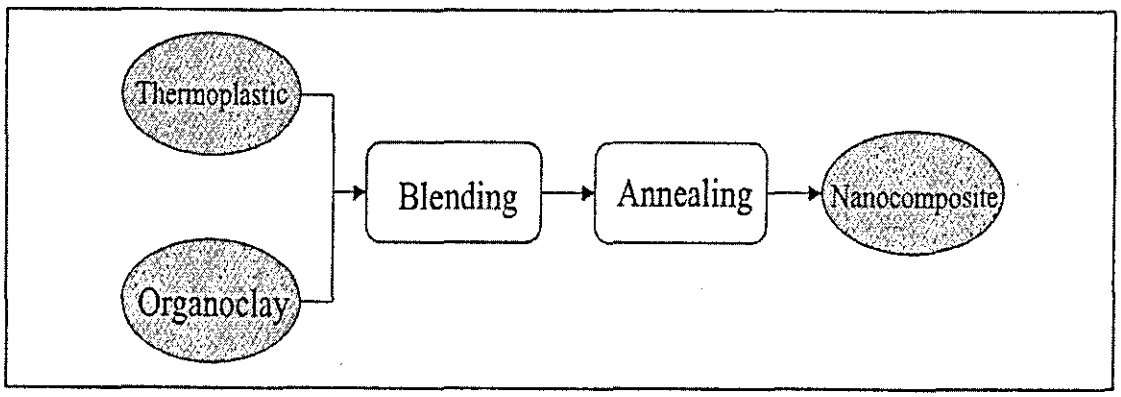


***Figure 2.24*** Flow chart representing the difference steps of the melt intercalation process[123].

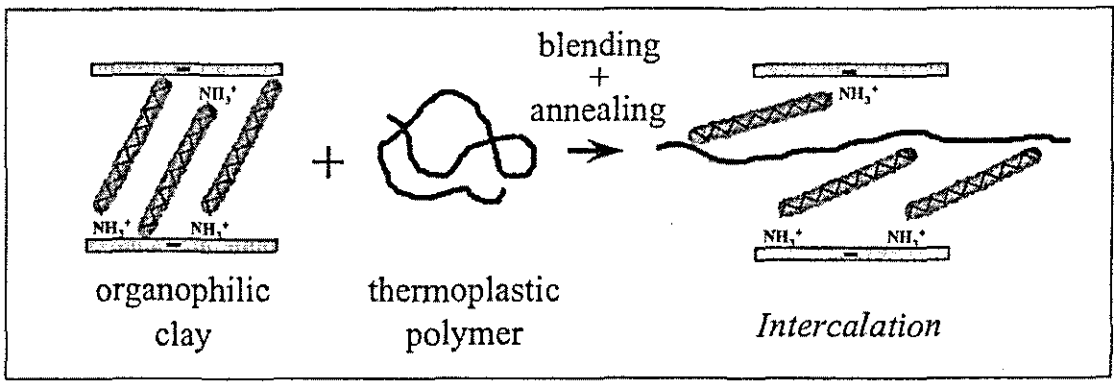


***Figure 2.25*** The melt intercalation process showing the polymer chains losing conformational entropy as they get intercalated between the clay layers[123].

**Solution polymerisation.**

Firstly, the organoclay is swollen in an organic polar solvent. Then the solvated polymer is added into the solution and intercalates between the clay layers. The solvent evaporation, normally under vacuum, is the last step. Finally, the solvent was removed by evaporation under vacuum, subsequently, the intercalated nanocomposite results. The entropy gained by the desorption of solvent molecules allows polymer chains to diffuse between the clay layers, which compensates for the decrease in conformational entropy of the intercalated polymer chains[125]. Hence, a relatively large number of desorbed solvent molecules from the clay accommodate the incoming polymer chains. The major advantage of this method is that it offers the possibilities to synthesise intercalated nanocomposites for polymers with low, or even no, polarity. Because of using large quantities of solvent, however, this process is difficult to apply in industry.

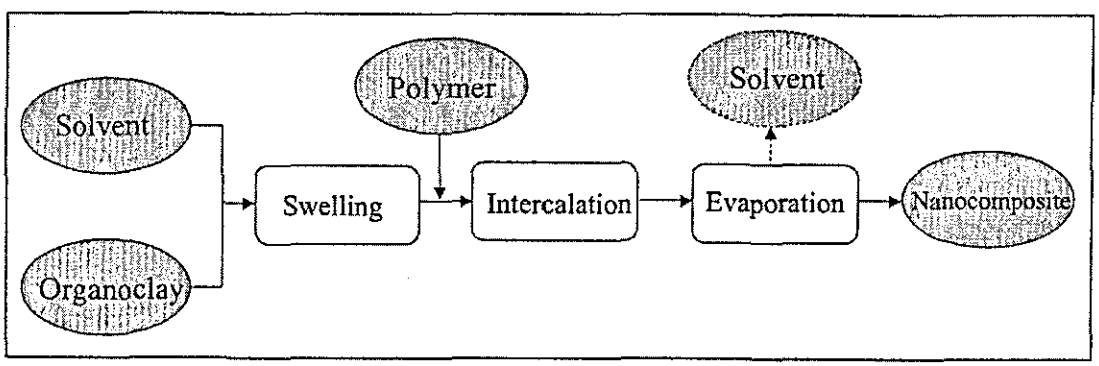


***Figure2.26*** Flow chart representing the different steps of the solution process[123].

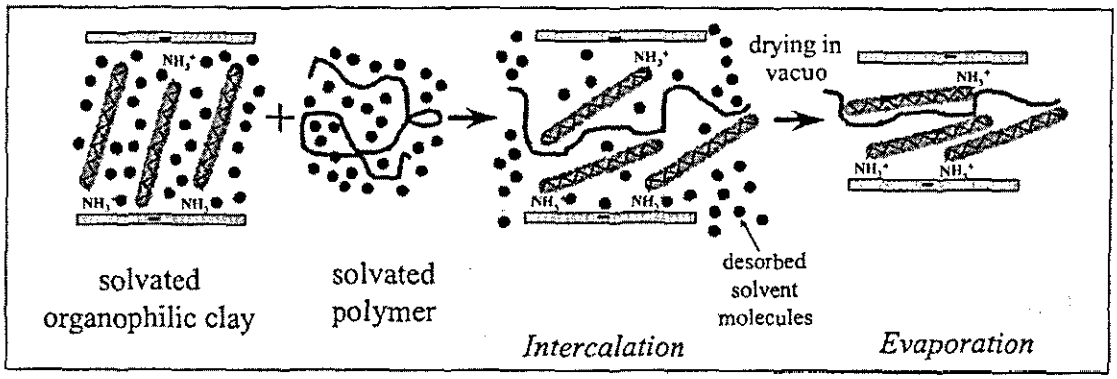


***Figure 2.27*** The intercalation of the polymer by the solution process. The black dots represent the solvent molecules[123].

### 2.3.4 Properties.

The layered silicate nanocomposite structure has provided dramatic improvement in not only the mechanical properties of the polymer, but also some of its other physical properties. The most characteristic changes are brought by the delaminated nanocomposite structure in which layer silicate nanofillers are fully dispersed.

**Mechanical properties.**

The tremendous improvements in tensile strength and tensile modulus provided by the exfoliated nanocomposite structure in polyamide-6-clay hybrids were first reported by the Toyota researchers[117]. The drastic increase in Young's modulus by 90% was obtained with the addition of only 4 wt% of filler. They proposed that the ability of dispersed silicate layers to increase the Young's modulus was related to the average length of the silicate layers. Moreover, the difference in the extent of exfoliation strongly influences the measured modulus values. Similar explanations have also been reported for polypropylene nanocomposites[126] obtained by melt interaction. A large increase in the tensile modulus for an exfoliated structure was also observed for the thermoset matrix[20,21] of the various amine-cured epoxy-based nanocomposites filled with 2 wt% montmorillonite previously modified by alkylammonium cations of different length[21]. Meanwhile the montmorillonite modified with butylammonium ions only gave an intercalated structure with a low tensile modulus. The other three nanocomposites with alkyl chains of 8, 12, and 16 carbons were characterised by exfoliated structures, and, consecutively, give much higher modulus values.

Contrary to the above results, where simply intercalated structures (without any exfoliation) are concerned, such as for PMMA[18] or PS[127] based nanocomposites obtained by emulsion polymerisation in the presence of water-swollen Na-montmorillonite, the increase in Young's modulus is relatively weak. This attests to the inefficiency of intercalated structures to improve the stiffness of nanocomposites. However, Zilg et al.[22] have commented on the rather low stiffness improvements in the case of anhydride-cured epoxy-based nanocomposites. The improvement resided in the formation of supramolecular assemblies obtained by the presence of dispersed anisotropic laminated nanoparticles. They also discussed the stiffening effect when the montmorillonite was modified by a functionalised organic cation (carboxylic acid or hydroxyl groups) that could interact with the matrix during curing.

For thermoplastic-based nanocomposites, the stress at break could vary strongly depending on the nature of the interactions between the matrix and the filler. Filled polymers such as nylon-6-based exfoliated nanocomposites prepared by different methods[19,128], or PMMA-based intercalated nanocomposites[18], exhibited an increase in the stress at break that was normally explained by the presence of polar (PMMA) and ionic interactions (nylon-6 grafted onto the layers) between the polymer matrix and silicate layers. For polypropylene-based nanocomposites[127], no or only very slight tensile stress enhancement was measured. One of the reasons was the lack of interfacial adhesion between a non-polar PP and polar layered silicates. For epoxy resin-based nanocomposites, the stress at break depended upon their glass transition temperature, located above or below room temperature. In high Tg epoxy thermosets[21,22], neither intercalated nor exfoliated nanocomposites lead to an enhancement of the tensile stress at break. Rather they made the materials more brittle. In contrast, nanocomposites based on both epoxy[20,129] and polyurethane[130] elastomeric matrices showed a substantial increase in tensile stress a break upon addition of a small amount of nanofillers.

The elongation at break was reduced for thermoplastic-based nanocomposites such as intercalated PMMA[18] and PS[127] or intercalated-exfoliated PP. On the other hand, in elastomeric epoxy[129] or polyol polyurethane matrices[130] a loss in ultimate elongation did not occur. Moreover, the addition of a nanosilicate into the matrices tended to

increase the elongation at break. The enhancement in elasticity can be attributed, in part, to the plasticising effect of the gallery oniums and to their contribution to the formation of dangling chains, but also probably to conformational effects at the polymer-clay interface.

For an intercalated PS nanocomposite[127], no significant difference in the storage modulus could be seen in the investigated temperature range, indicating that intercalated nanocomposites did not strongly influence the elastic properties of the matrix. Meanwhile, the shift and broadening of the tanδ peak towards higher temperatures indicated an increase in the glass transition temperature together with some broadening of this transition for this nanocomposite. This behaviour has been attributed to the restricted segmental motions at the organic-inorganic interface. In contrast, intercalation of PS sequences in a symmetric (styrene-butadiene-styrene) block copolymer[131], when this SBS was melt blended with a montmorillonite modified by dimethyl didodecylammonium cation, provided a sizable improvement of the storage modulus at 25°C. At a given temperature, higher storage moduli resulted from the better nanofiller dispersion and the influence of the length of the layered particles as shown in case of an exfoliated mica-based polyimide nanocomposite[132]. The storage modulus markedly improved, especially above Tg, such as a well-ordered exfoliated nanocomposite in an epoxy matrix[125] and a nitrile rubber[133]. A possible explanation could be the creation of a three-dimensional network of interconnected long silicate layers, strengthening the material through mechanical percolation.

**Thermal stability and flame retardant properties.**

The first study of thermal stability improvement was provided by the case of PMMA intercalated within montmorillonite by free radical polymerisation[24]. The result showed that a 10 wt% clay intercalated PMMA degraded at a temperature of 40-50°C superior to the degradation of the unfilled PMMA matrix. The author proposed that the enhanced thermal stability of the PMMA-based nanocomposites was not only due to differences in chemical structures, but also to restricted thermal motion of the macromolecules in the silicate interlayers. The improvement of thermal stabilisation of cross-linked poly(dimethyl siloxane)[25], at 10 wt% of exfoliated organomontmorillonite, showed a drastic shift of the weight loss towards higher

temperature, being increased by 60°C at 50% weight loss. It has also been reported that increase in thermal stability has found for intercalated nanocomposites prepared by emulsion polymerisation of methyl methacrylate[18], styrene[132], and epoxy precusors[134] in the presence of water swollen Na-montmorillonite. The decomposition onset temperature increased in every case.

The chemical nature of the studied polymeric material and its degradation mechanism played an important role such as in the case of poly(imide) exfoliated nanocomposites[135]. Their thermal stability was only improved by about 25°C at 50% of weight loss which was much less than the 140°C jump observed in exfoliated poly(dimethyl siloxane) nanocomposites[26].

The flame retardant properties of nanocomposites have been proposed by Gilman[136]. A 63% reduction in the peak heat release rate was observed during combustion of polyamide-6 exfoliated nanocomposite at only 5 wt% of exfoliated montmorillonite. Other nanocomposites have been studied out such as exfoliated nylon-12 (2 wt% organoclay), exfoliated poly(methyl methacrylate-co-dodecylmethacrylate)[137], intercalated PS (3 wt%) or intercalated PP (2 wt%). Each material showed a significant decrease in the peak heat release rate, while the heat of combustion, smoke and the carbon monoxide yields were not increased. The flame retardant effect of nanocomposites mainly arose from the formation of char layers obtained through the collapse of the exfoliated and/or intercalated structures[27]. This multi-layered silicate structure may act as an excellent insulator and mass transport barrier as observed in nylon-6 and thermoset nanocomposites[28]. It slowed down the escape of the volatile decomposition products.

**Gas barrier properties.**

High reduction of gas permeability can be achieved from films prepared from exfoliated nanocomposites. The permeability to carbon dioxide was measured for partially-exfoliated polyimide-based nanocomposites[30]. It was expressed as a function of the length and width of the filler particles as well as their volume fraction within the PI matrix. The decrease in $CO_2$ permeability was due to the large volume fraction of fillers which increases the tortuosity of the gas diffusion path.

The effect on water permeability of both partially and totally exfoliated polyimide-based nanocomposites was reported by Yano et al.[29], using 2 wt% of organoclay with the different layer lengths. It was shown that as the length of the clay platelets increased the relative permeability decreased substantially. This meant that the best gas barrier properties were obtained by fully exfoliated rather long layered silicates. Poly (ε-caprolactone)-exfoliated nanocomposite[31], synthesised by in-situ intercalated polymerisation of the lactone monomer inside 4.8 vol% organo-modified montmorillonite, showed a 80% decrease in water permeability. However, recent investigations[138] showed that the constrain brought by the nanocomposite structure to the mobility of polymer chains situated in the neighbourhood of the silicate layers may be the most important factor.

## 2.4 Polyurethanes.

Polyurethanes have fascinated engineers and scientists by their unique combination of unusual properties and ability to be processed, shaped, and formed by almost all known manufacturing techniques. The original discovery was by Bayer and his co-workers at I.G. Farben Industries, Germany in 1937, at about the same time as the work on isocyanates began in the United States by Carothers of Du Pont[139].

The versatile polyurethanes can yield a wide spectrum of polymeric products including foams (flexible and rigid), elastomers, coating resins, adhesives, sealants, fibres, and films[140]. The largest use is as foams in such industries as automotive, furniture, building construction, recreation, and footwear[41].

### 2.4.1 Polyurethane chemistry.

Polyurethanes contain not only the urethane linkage[139], the basis for a urethane, but also includes other groups as integral units in, or on, the polymer chains, which leads to widely versatile properties.

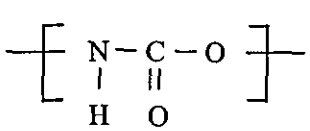

The urethane linkage

Polyurethanes can be formed by a variety of methods, although the most widely used is an addition polymerisation of di- or polyisocyanate and di- or polyol functional hydroxyl compounds, e.g. hydroxyl-terminated polyesters or polyethers[141]. The general structure of a linear polyurethane derived from a dihydroxy compound and a diisocyanate can be represented by the following general formula.

$$\underset{\text{glycol}}{n\,HO-R-OH} \;+\; \underset{\text{diisocyanate}}{n\,O=C=N\text{-}R'\text{-}N=C=O} \;\downarrow$$

$$HO-[R\text{–}OCONH\text{–}R'\text{–}NHOC\text{–}O]_{(n-1)}\text{–}R\text{–}OCONH\text{–}R'\text{–}NCO \qquad (2.24)$$

Polyurethane

Linear products are obtained if the reactants are bifunctional, but higher functionality brings the formation of branched chain or crosslinked materials[139]. The complexity of a polyurethane is formed in a broad variety of variables such as polyol and polyisocyanate, functionality and molecular weight, chain extender used to modify the hard and the soft segment content of the polyurethane, which affect the chemical and physical properties of the final polyurethane.

Polyurethanes are processed by various methods[142] as follows.

- The medium of preparation : solvent-free, in solution, in water.
- The sequence of the addition of the reactions : one-shot process, prepolymer process.
- The type of cure : one-component systems, two-component systems.

Catalysts are frequently added in order to accelerate the polyaddition reaction[142]. In this study, no solvent was used in the preparation process. Therefore, the following description will be restricted to only the solvent-free preparation.

In the solvent-free process, there are two main methods of reaction control: the one-shot process and the prepolymer process.

The one-shot process[142] is carried out by simultaneous mixing together of a polyol, a diisocyanate, a chain extender, a catalyst, and other additives. The reaction is very

exothermic depending on the catalyst applied. The one-shot system is schematically represented in Figure 2.28.

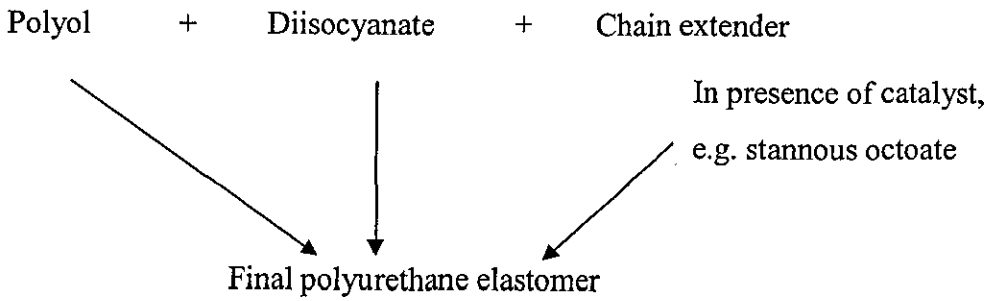


***Figure 2.28*** One-shot process for polyurethane elastomer preparation.

Prepolymer process consists of two separate steps. Initially, the diisocyanate and polyol are reacted together to form an intermediate polymer of molecular weight $15x10^3$-$20x10^3$ called a "prepolymer"[139]. Then, it is converted into the final high molecular weight by further reaction with a diol or diamine chain extender. The prepolymer process is schematically represented in Figure 2.29.

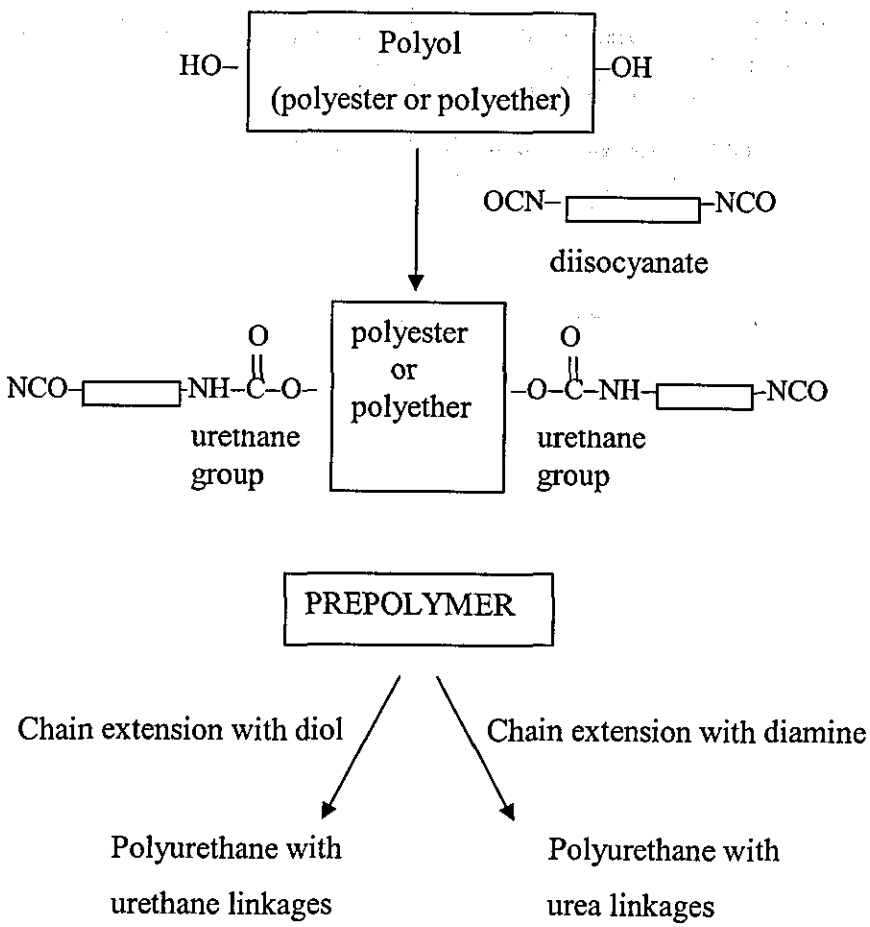


***Figure 2.29*** Prepolymer route for the formation of a polyurethane elastomer.

### 2.4.2 Raw materials.

**Polyol.**

Polyols are considered as hydroxy functional chemicals, or polymers, covering a wide range of molecular weight, hydroxyl functionality, and composition. An average molecular weight of the polyols used in polyurethane manufacture is between 200 to $10x10^3$ depending on the applications[142]. The reactivity, compatibility with the other compounds in the polyurethane formulation, hydroxyl functionality and its distribution, composition of the polymer chain, and the structure of the hydroxyl group are the important characteristics of polyols for polyurethane applications[140]. The polyol properties affect the properties of the resulting polyurethane polymer. The polyols used in polyurethane synthesis have been classified into three classes, namely, polyesters, polyethers, and, polycaprolactones. Their representations of chemical structures are shown below. Polyether polyols share about 90% of the global polyurethane polyol used[140] because of their structural versatility, cost, ease of handling, and product performance.

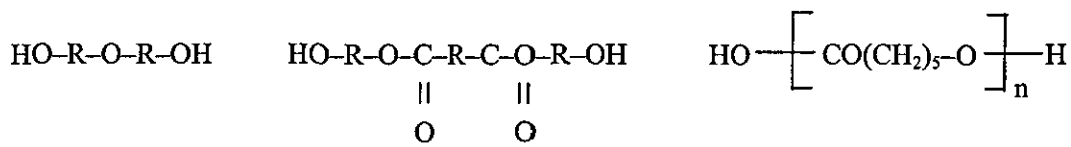


Polyether polyols | Polyester polyols | Polycaprolactone diol

**Isocyanates.**

The isocyanate group, –N=C=O, is very highly reactive, as it has two cumulative double bonds, creating a positive charge on the C-atom. The possible resonances[41] of the isocyanate group are shown as follows.

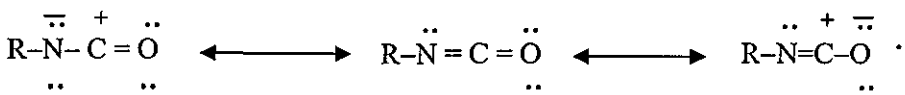


The negative charge can be delocalised into R, if R stands for an aromatic radical. Thus, the isocyanate can react with both electron donor and acceptor groups. Electron donors attack the carbonyl carbon atom, whilst acceptors attack the oxygen or nitrogen atoms, The isocyanate reactions can be classified into the following three main groups:

primary reactions with hydrogen active compounds; secondary reactions with isocyanate adducts, and auto-addition.

- **Primary reactions of isocyanates with active hydrogen compounds.**

The isocyanate can react generally with compounds containing active hydrogen atoms, providing addition to the carbon-nitrogen double bond, i.e. the hydrogen becomes attached to the nitrogen of the isocyanate and the remainder of the active hydrogen compound becomes attached to the carbonyl carbon as follows[139,141].

**With water.**

$$\underset{\text{isocyanate}}{R\text{-}N{=}C{=}O} + H_2O \longrightarrow \underset{\text{carbamic acid (unstable)}}{R\text{-}NH\text{-}CO\text{-}OH} \quad (2.25)$$

$$\underset{\text{carbamic acid (unstable)}}{R\text{-}NH\text{-}CO\text{-}OH} \longrightarrow \underset{\text{amine}}{R\text{-}NH_2} + CO_2 \quad (2.26)$$

The amine then reacts with the isocyanate group.

**With amines.**

$$R\text{-}N{=}C{=}O + R'\text{-}NH_2 \longrightarrow \underset{\text{urea}}{R\text{-}NH\text{-}CO\text{-}NH\text{-}R'} \quad (2.27)$$

**With carboxylic acids.**

$$R\text{-}N{=}C{=}O + R'\text{-}COOH \longrightarrow \underset{\text{amide}}{R\text{-}NH\text{-}CO\text{-}R'} + CO_2 \quad (2.28)$$

Polymer formation can take place if the reagents are di- or poly-functional. These reactions usually occur at different rates, such as the most rapid rate is in the reaction leading to urea formation. However, they can be influenced appreciably and controlled by use of a catalyst. Gaseous carbon dioxide is formed and acts as a blowing agent. It is valuable for forming foamed products, but it causes a problem in bubble-free products[139].

- **Secondary reactions of isocyanates with isocyanate adducts.**

The excess, or unconsumed, isocyanate in the reaction mix can react with the products of the primary reaction, i.e. urethane, urea, and amide, possibly during the initial

polymer formation. The secondary reactions of isocyanate are particularly important in polyurethane chemistry because they introduce chain extension, branching or crosslinking of the polyurethane. The molecular size is increased due to the formation of allophanate, biuret, and acylurea links onto the main chains[139].

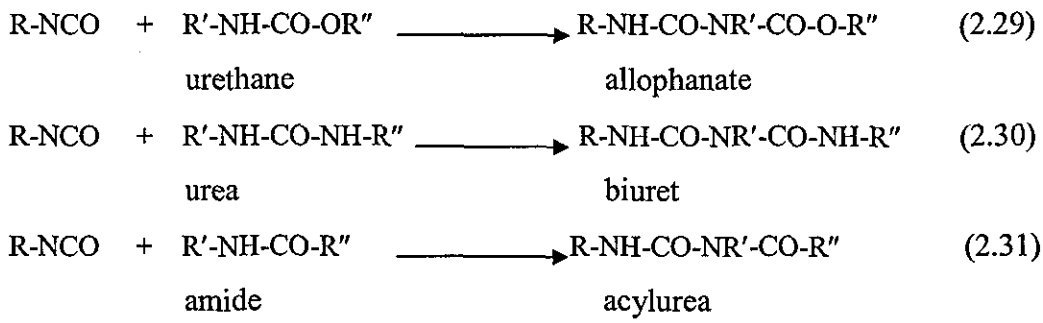


- **Auto-addition of isocyanate.**

There are also reactions of isocyanates with themselves which lead to the formation of polymers and thus have gained technical importance for the formation of polyurethanes. Even the linear polymerisation of monoisocyanates leads to polymeric products[142].

**Dimerisation.**

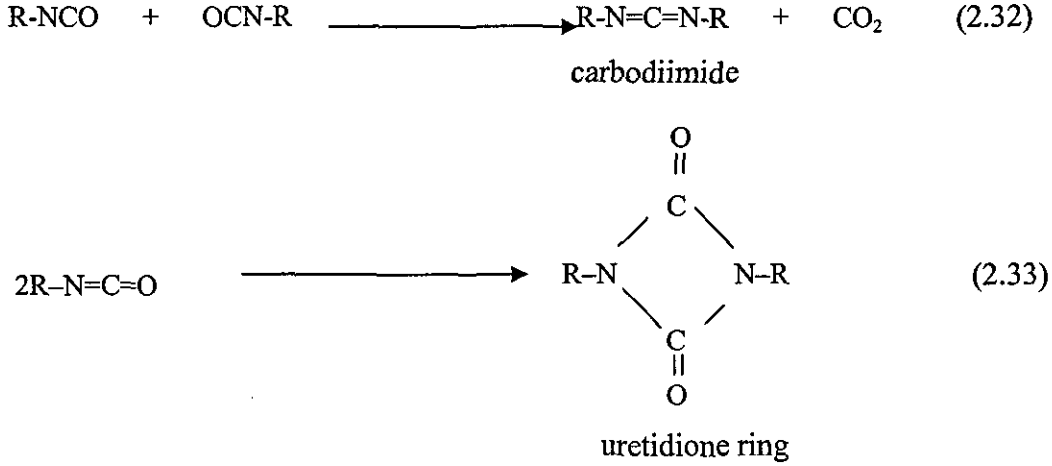


The cabodiimide can occur at room temperature under the presence of a special catalyst. Otherwise, it will occur only at high temperatures. The carbodiimide formation reaction also produces carbon dioxide[142]. The uretidione formation must be run at low temperature because of its thermal instability.

**Trimerisation.**

The reaction is irreversible and occurs in the presence of basic catalysts[41]. However, on vigorous heating, it also can form even in the absence of a catalyst. The isocyanates trimerise to form isocyanurates: a ring structure consisting of alternating nitrogen and carbon atoms, resulting in high stability.

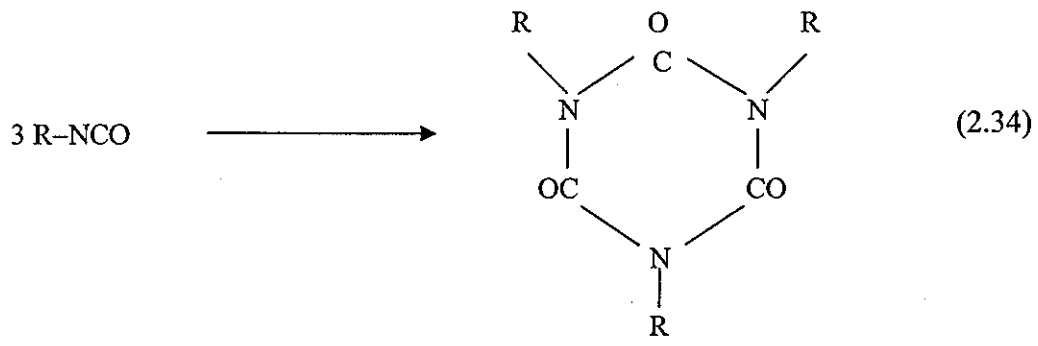


(2.34)

isocyanurate

The degree of crosslinking in polyurethanes depends upon a combination of the extent of polyfunctional monomers present and the amount of biuret, allophanate, and trimerisation reactions[143]. The overall stoichiometry and the specific catalyst present control the latter reactions. The extent of the different reactions also depends upon the temperature used. Significantly high temperatures, higher than 120°C, are avoided because polyurethanes can form various different types of degradation reaction[41,143], such as:

$$\sim R\text{–}NH\text{–}OCO\text{–}CH_2\text{–}CH_2 \sim \longrightarrow \sim R\text{–}NCO + HO\text{–}CH_2\text{-}CH_2 \sim \quad (2.34)$$

$$\sim R\text{–}NH\text{–}OCO\text{–}CH_2\text{–}CH_2 \sim \longrightarrow \sim R\text{–}NH_2 + CH_2{=}CH \sim + CO_2 \quad (2.35)$$

$$\sim R\text{–}NH\text{–}OCO\text{–}CH_2\text{–}CH_2 \sim \longrightarrow \sim R\text{–}NH\text{–}CH_2\text{–}CH_2 \sim + CO_2 \quad (2.36)$$

**Chain extender and crosslinking agent.**

The two terms are often erroneously used as synonyms. Crosslinking agents and chain extenders are both low molecular weight diols or triols or diamines. So, the same chemical can even perform both roles. In other words, the process rather than the specific chemical determines whether a diol is a crosslinking agent or chain extender[144].

Chain extending agents increase the size of the rigid segments as well as the hydrogen bond density and the relative molecular weight of the polyurethane. It shows a remarkable effect on the polyurethane properties, even though it usually constitutes a minor part of the polymer[41].

Crosslinking agents lead to crosslinked final polyurethanes. Large increases in the degree of crosslinking make amorphous polymers more rigid and cause them to have higher softening points and higher modulus, reduced elongation and swelling by solvents, and increased the glass transition temperatures[141]. Some of the significant crosslinking agents/chain extenders are shown below.

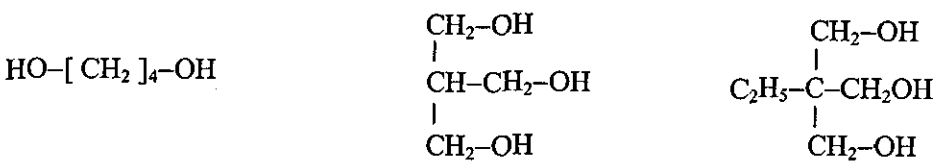

1,4-Butanediol Glycerol Trimethylol propane

### 2.4.3 Basic morphology of polyurethanes.

A polyurethane elastomer can be considered as a linear block copolymer of the type shown in Figure 2.30. Its properties can be varied over a wide range of strength and stiffness by modification of its three basic building blocks: the polyol, the diisocyanate, and the chain extender[139].

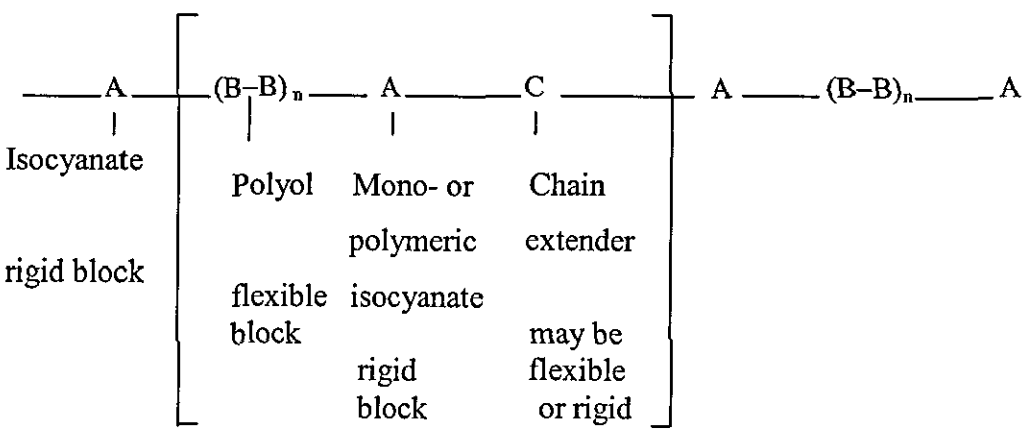


*Figure 2.30* The basic units in a urethane block copolymer.

Polyurethanes can be regarded as segmented polymers built from altering rigid (hard) and flexible (soft) segments, which are chemically and hydrogen bonded together. The hard segments consist of diisocyanate and chain extender, while the soft segments consist of polyester or polyether polyols, as shown in Figure 2.31.

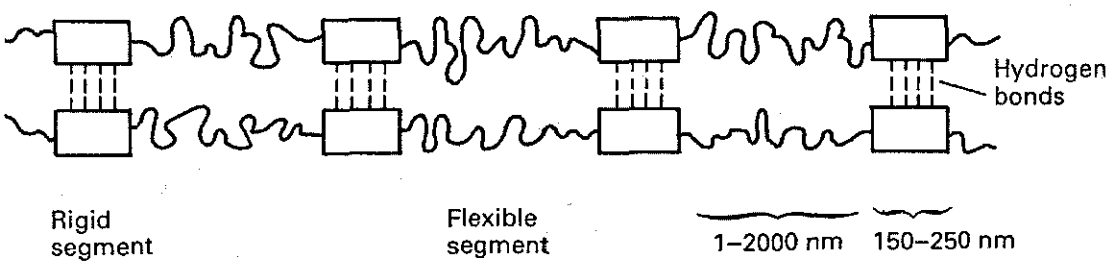


***Figure 2.31*** Flexible and rigid segments in a polyurethane elastomer[41].

If the chain extender is a diamine, a urea linkage is formed, whilst urethane linkages are formed, when the diol is the chain extender[145]. Degree of segregation between hard and soft segments depends on the interaction of hard segments with each other or with the soft segments, respectively. The interactions between the hard segments also depends on the symmetry of the diisocyanate and on the specific chain extender used (diol or diamine)[142].

**2.5 Poly(ethyl methacrylate).**

Poly(ethyl methacrylate), PEMA, is a linear thermoplastic. It has a bulky side group and lack of stereoregularity. Therefore, it is amorphous. PEMA has excellent optical clarity, high mechanical strength and good thermal properties. Ethyl methacrylate monomer has the chemical structure shown below.

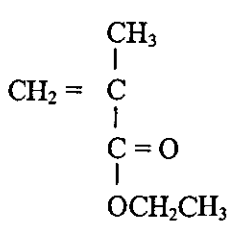

This monomer can be polymerised by a free radical mechanism, a rapid reaction which consists of the characteristic chain-reaction steps, namely, initiation, propagation, and termination[143,146].

**Initiation.**

The initiation step[103,143] involves two reactions. The first is the creation of free radicals. The usual case is the homolytic dissociation of an initiator, I, undergoing thermal or photolytic scission to yield a pair of radicals, R•. The second step is addition of these free radicals to the first monomer molecule to produce the chain initiating species.

$$I \xrightarrow{k_d} 2R\bullet \qquad (2.37)$$

where $k_d$ and $k_i$ are the rate constants for the initiator dissociation and the initiation steps, respectively.

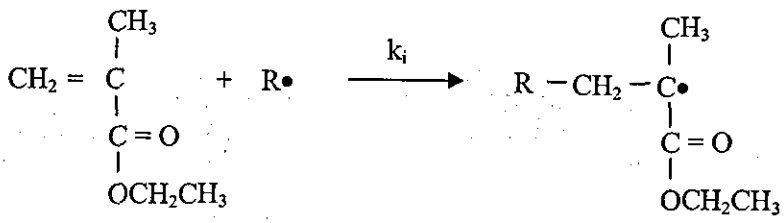

(2.38)

The initiating free-radicals can come from many sources. Thermal decompositions of compounds with azo and peroxy groups are common sources of such radicals. The radicals can also be obtained from redox reactions or through various light-induced decompositions. Initiating radicals can be formed by ionising radiation[147].

Azo compounds contain weak valency bonds in their structure. An elevated temperature causes these bonds to cleave homolytically and to dissociate the compound into free-radicals. For this study, 2, 2′-azo bis-isobutyronitrile (AIBN) was used as the initiator. The final products of its decomposition are two cyanopropyl radicals and a molecule of nitrogen gas. The thermal dissociation of AIBN is illustrated below[103].

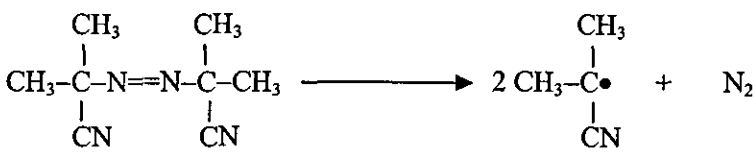

(2.39)

**Propagation.**

The propagation step is a bimolecular reaction, which takes place by the addition of the new free radical to another molecule of monomer usually very rapidly. By many repetitions of this step, the free radical becomes much larger. It is based on an assumption that $k_p$ and $k_i$ are independent of the sizes of the radicals because the radical reactivity is not affected when the chain length exceeds dimer or trimer dimensions [148]. The successive addition may be represented by equation (2.40).

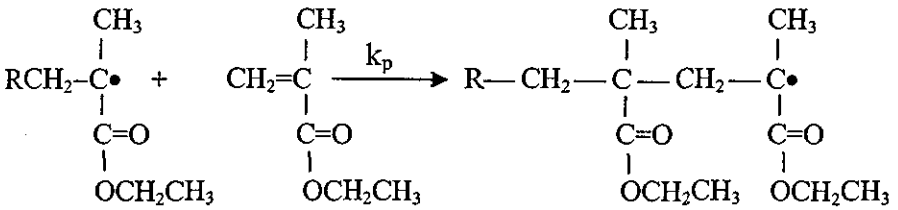

(2.40)

$k_p$ = the rate constant for propagation

**Termination.**

The final steps can take place in three ways[147]: combination; disproportionation; and chain transfer. Two radicals react with each other by combination (coupling). In termination by disproportionation, a hydrogen atom transfers from one chain to another, resulting in the formation of two polymer molecules, one saturated and the other one unsaturated. In chain transfer, a new chain initiates at the expense of the one currently growing.

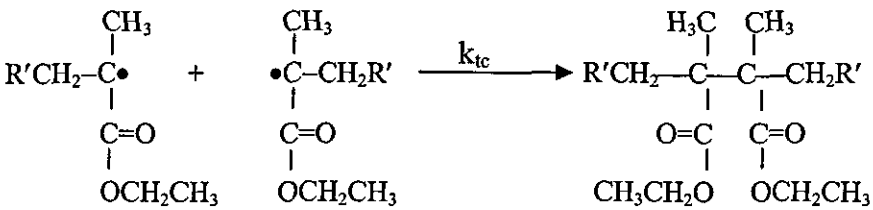

(2.41)

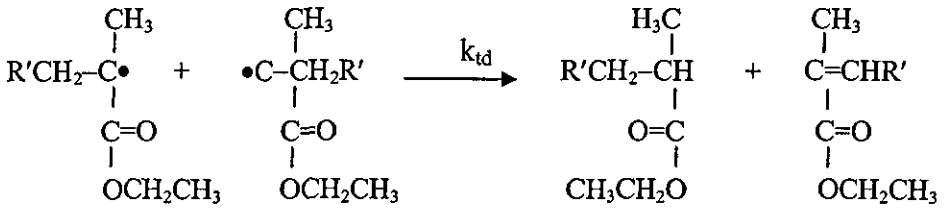

(2.42)

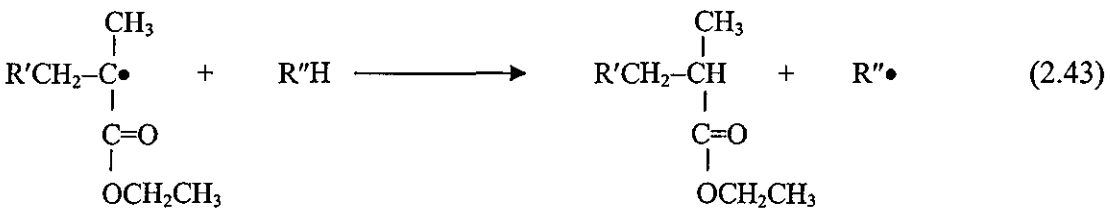


(2.43)

where $k_{tc}$ = the rate constant for termination by combination

$k_{td}$ = the rate constant for termination by disproportionation

# CHAPTER 3

# EXPERIMENTAL

# CHAPTER 3

# EXPERIMENTAL

## 3.1 Materials.

All raw material used in this research were obtained from commercial sources. They are described in Table 3.1. The crosslinked polyurethane (PU) network consisted of alternating soft rubbery segments and glassy hard segments. The hard segments were formed from meta-tetramethylxylene diisocyanate (m-TMXDI) and the crosslinking agent, trimethylol propane (TMP). The soft segment was polypropylene glycol of a molar mass of 1025 (PPG1025). The PU catalyst was stannous octoate.

The glassy polymer network was polymerised from ethyl methacrylate (EMA) using tetraethyleneglycol dimethacrylate (TEGDM) as the crosslinker and azoisobutyronitrile (AIBN) as the initiator.

Nanoclays were incorporated into the IPN formulations to achieve IPN nanocomposites.

## 3.2 Synthesis.

In the present study, all polyurethane/poly(ethyl methacrylate), PU/PEMA, simultaneous IPN nanocomposites were prepared in bulk in various proportions along with different types and amounts of nanoclays according to the IPN formulae in Table 3.2. Variations of mixing time and synthesis procedures were also conducted in these IPN nanocomposite preparations.

### 3.2.1 Purification of chemicals.

Prior to IPN nanocomposite preparations, the hygroscopic PPG1025 had traces of moisture removed at 80°C under vacuum for 2 hours, preventing the formation of $CO_2$ bubbles during polymerisation. After that, it was kept in a desiccator. The EMA monomer and TEGDM crosslinking agent were freed from inhibitor by passing them through neutral aluminum oxide columns (alumina, Brockmann Activity I, Aldrich Chemical Co.) and kept in a refrigerator until used. The nanoclays were dried at 60°C in an open air oven for at least 8 hours before being used. All other chemicals were used as supplied.

***Table 3.1*** Chemicals used in the research.

| Materials | Abbreviation | Function | Supplier |
|---|---|---|---|
| *Polyurethane network* | | | |
| 1,1′, 3, 3′-Tetramethylxylene diisocyanate | TMXDI | Diisocyanate | Aldrich |
| Poly(oxypropylene)glycol (M.W.1025) | PPG1025 | Polyol | BDH |
| Trimethylol propane | TMP | Crosslinker | Aldrich |
| Stannous octoate | SnOct | Catalyst | Sigma |
| *Poly(ethyl methacrylate) network* | | | |
| Ethyl methacrylate | EMA | Monomer | Aldrich |
| Tetraethyleneglycol dimethacrylate | TEGDM | Crosslinker | Fluka |
| Azobisisobutyronitrile | AIBN | Initiator | BDH |
| *Nanoclay* | | | |
| Na clay | Na clay | Nanofiller | Southern Clay |
| Cloisite 15A | C15A | Nanofiller | Products, Inc. |
| Cloisite 20A | C20A | Nanofiller | supplied all |
| Cloisite 30B | C30B | Nanofiller | nanoclays |

***Table 3.2*** IPN nanocomposite formulations.

| Composition | Ratio | Units |
|---|---|---|
| PU /PEMA | 50/50, 70/30, 80/20 | Weight % |
| *PU network* | | |
| Isocyanate / hydroxyl | 1.1 / 1 | mole |
| Diol / triol | 3 / 1 | mole |
| PU catalyst | 1.2, 1.4, 1.5, 1.6, 1.8, 2.0 | PU wt% |
| *PEMA network* | | |
| Monomer | 1 | mole |
| Initiator | 1 | PEMA mole% |
| Crosslinking agent | 5 | PEMA mole% |
| *Nanoclay* | 0, 1, 3, 5, 10, 15 | PU wt% |

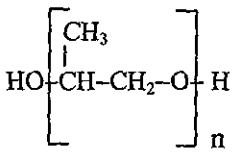

Poly(oxypropylene) glycol (PPG1025)

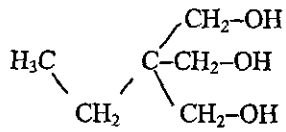

Trimethylol propane (TMP)

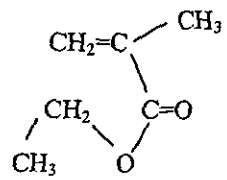

Ethyl methacrylate (EMA)

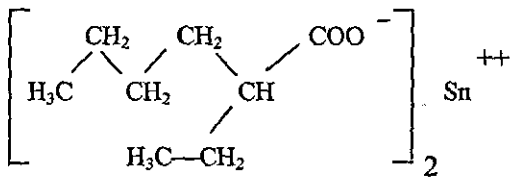

Stannous octoate (SnOct)

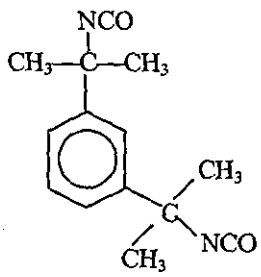

1, 1′, 3, 3′-Tetramethylxylene diisocyanate (TMXDI)

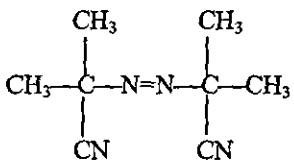

Azobisisobutyronitrile (AIBN)

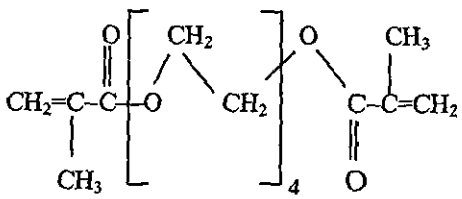

Tetraethyleneglycol dimethacrylate (TEGDM)

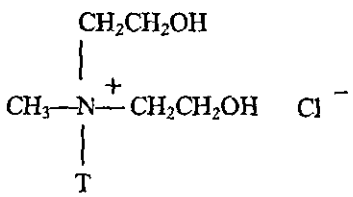

Modifier of Cloisite 30B (C30B)

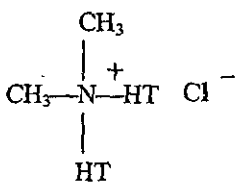

Modifier of Cloisite 15A/20A (C15A/C20A)

T = ~65% $C_{18}H_{35}$, ~30% $C_{16}H_{31}$, ~5% $C_{14}H_{27}$
HT = ~65% $C_{18}H_{37}$, ~30% $C_{16}H_{33}$, ~5% $C_{14}H_{29}$

***Figure 3.1*** Chemical structures of the raw materials.

### 3.2.2 Preparation of IPN nanocomposites by Original Process, P0.

**PU component mixture.**

Nanoclay was weighed and added into the polyol (PPG1025), then homogeneously mixed at room temperature for 30 minutes using a Silverson L2R mixing apparatus at quarter speed. Triol (TMP) was added in the desired mole ratio into the mixture which then was kept at 60°C for 60 mins under vacuum to dissolve completely the solid TMP ($T_m$ = 58°C) in the PPG. After that, the mixture was allowed to cool to room temperature in a desiccator. Finally, the diisocyanate (TMXDI) and catalyst (SnOct), in the desired amounts, were added to the mixture before combining with the PEMA component mixture.

**PEMA component mixture.**

The purified EMA monomer and the crosslinker (TEGDM) were completely mixed with the initiator (AIBN) in the desired proportions by a conventional laboratory stirrer at an angular rotation speed of 200 rpm for 20 mins at room temperature.

**Polymerisation.**

Both of the IPN component mixtures were immediately combined after finishing the preparation of PU and PEMA component mixtures. The homogeneous mixture was prepared at room temperature by vigorous agitation using a conventional laboratory stirrer at an angular rotation speed of 200 rpm for 3 minutes. The final mixture was degassed for 60 seconds in order to remove any air bubbles entrapped during the mixing process. Then the mixture was cast into a steel mould, which had been cleaned and sprayed with silicone mould release agent (Cil Release 1711~Plus, Compounding Ingredients Limited). In between the steel plates, there was a nitrile rubber gasket of diameter 6 mm as shown in Figure 3.3. The steel plates were held together by using spring-loaded screws. Finally, the filled mould was placed in an air oven, preheated to 60°C, for 24 hours in order to prevent the evaporation of volatile monomers and the occurrence of bubbles in the IPN nanocomposite samples. Then, it was heated to 80°C and held for 24 hours and finally this was followed by 24 hours at 90°C.

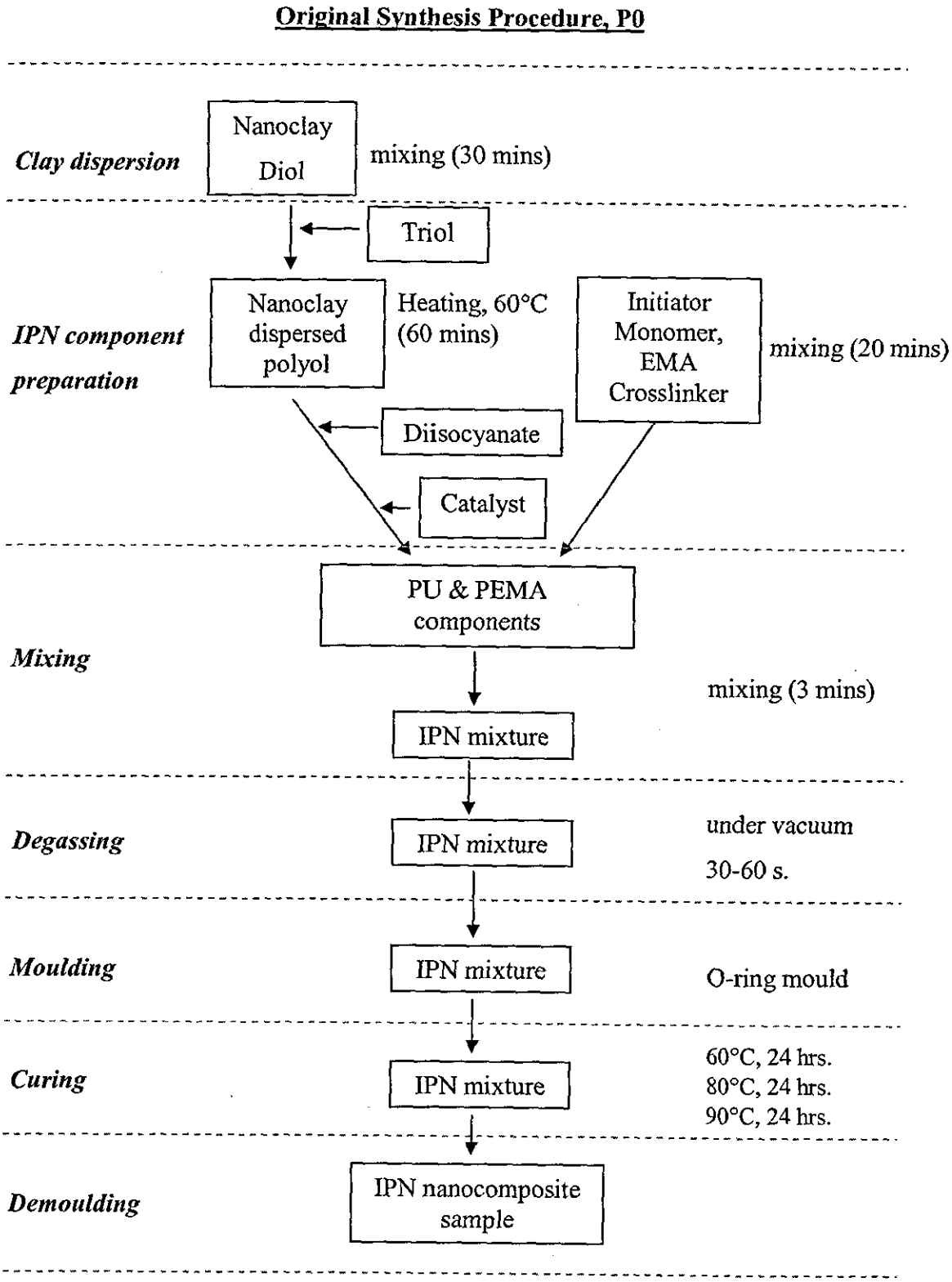


***Figure 3.2*** Diagram of the IPN nanocomposite synthesis by original synthesis procedure, P0.

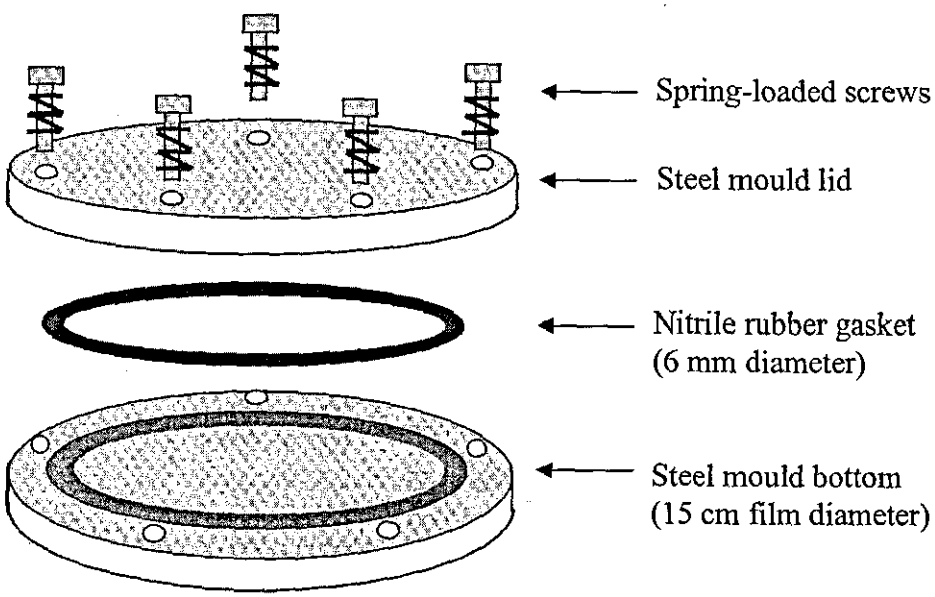


***Figure 3.3*** Schematic representation of the steel mould.

### 3.2.3 Preparation of IPN nanocomposites by Process One, P1.

Synthesis procedure one (P1) allowed both the soft segment polyol and the PU crosslinker, TMP, which had hydroxyl groups in their chemical structures, diffused concurrently into the silicate galleries. Therefore, in this procedure, only the first step of the Original Process was changed. The nanoclay was weighed and added into the mixture of polyol (PPG1025) and Triol (TMP), which the solid TMP was completely dissolved in the PPG under vacuum at 60°C for 60 minutes. Then the nanoclay was homogeneously dispersed in the mixture at room temperature by using a Silverson L2R mixing apparatus at quarter speed. The further procedures were the same as the Original Process as shown in Figure 3.4.

### 3.2.4 Preparation of IPN nanocomposites by Process Two, P2.

Synthesis procedure two (P2) also concentrated on the diffusion of the PU component into the silicate clay layers. In this process, the soft and hard segment included its crossliker were first introduced into the organoclay. Thus, only the PU component mixture preparation was changed in Process Two, compared with the Original Process. Solid triol (TMP) was weighed and added into the polyol (PPG1025) which then was kept at 60°C for 60 minutes under vacuum to dissolve the TMP completely in the PPG.

After the mixture cooled down to room temperature in a desiccator, the nanoclay and the diisocyanate (TMXDI) were added in the desired mole ratio into the mixture, then homogeneously mixed for 30 minutes at room temperature by using a Silverson L2R mixing apparatus at quarter speed. Finally, the catalyst (SnOct) in the desired amount was added into the mixture before mixing with the PEMA component mixture. The PEMA component mixture and the polymerising steps were the same as those in the Original Process as shown in Figure 3.5.

### 3.2.5 Preparation of IPN nanocomposites by Process Three, P3.

Synthesis procedure three (P3) changed the focus point to be the PEMA component. The PEMA constituents were allowed to diffuse into the silicate galleries before combining with the PU component.

**PU component mixture.**

Solid triol (TMP) was weighed and added into the polyol (PPG1025), then the mixture was kept at 60°C for 60 minutes under vacuum to dissolve completely the TMP into the PPG. After that the mixture was allowed to cool to room temperature in a desiccator. Finally, the diisocyanate (TMXDI) and catalyst (SnOct) in the desired amounts were added into the mixture before combining with the PEMA component mixture.

**PEMA component mixture.**

Nanoclay was added in the desired amount into the mixture of the purified EMA monomer and the crosslinker (TEGDM), then homogeneously mixed for 30 minutes at ambient temperature using a Silverson L2R mixing apparatus at quarter speed. Then the initiator (AIBN) in the desired proportion was added into the mixture before combining with the PU component mixture.

Then two homo-component mixtures were combined. A conventional laboratory stirrer was used to mix at room temperature for 3 minutes to obtain a homogeneous mixture. Then the mixture was degassed, poured into the steel mould, cured and demoulded as the rest processes did in the Original Process as shown in Figure 3.6.

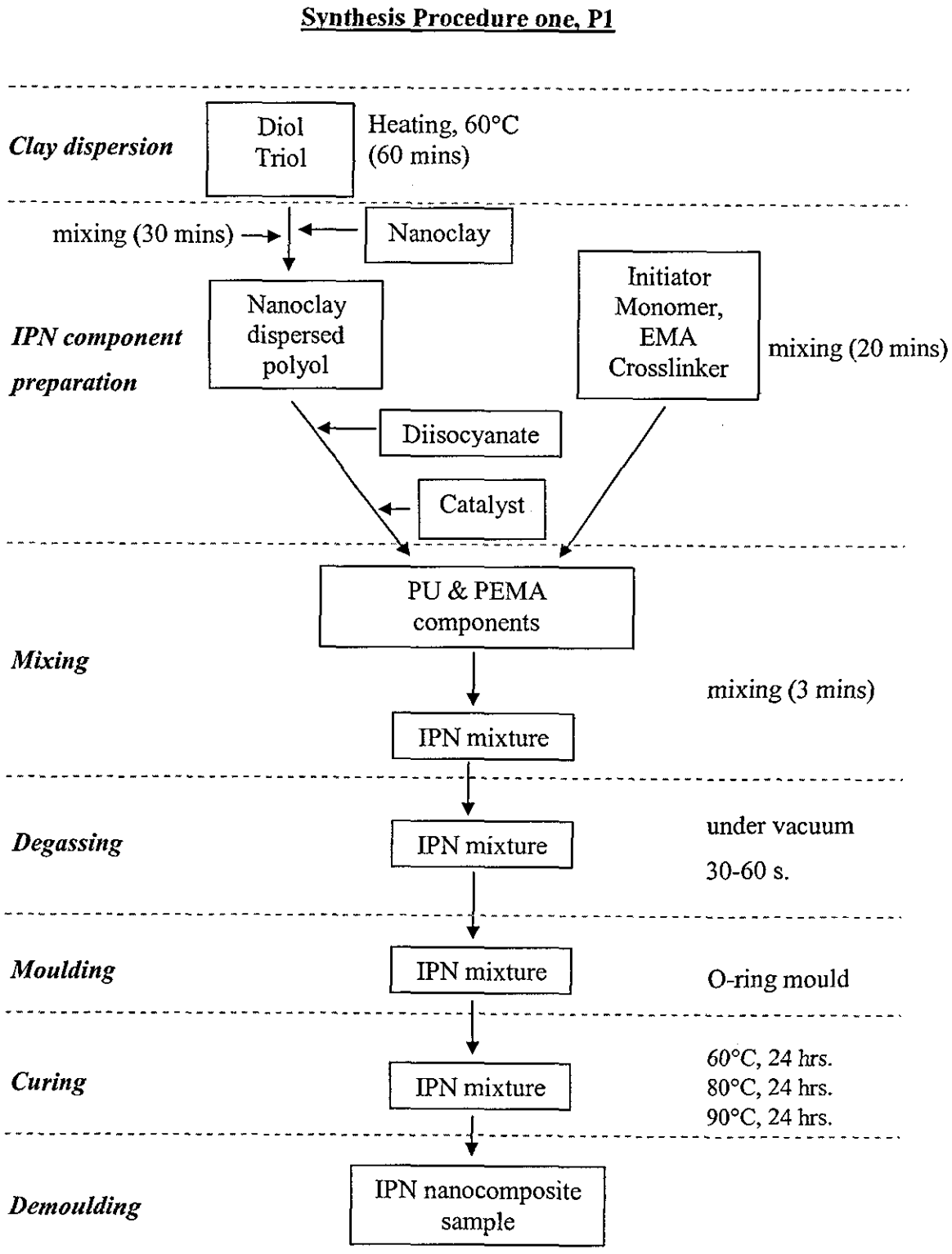


*Figure 3.4* Diagram of the IPN nanocomposite synthesis by synthesis procedure one, P1.

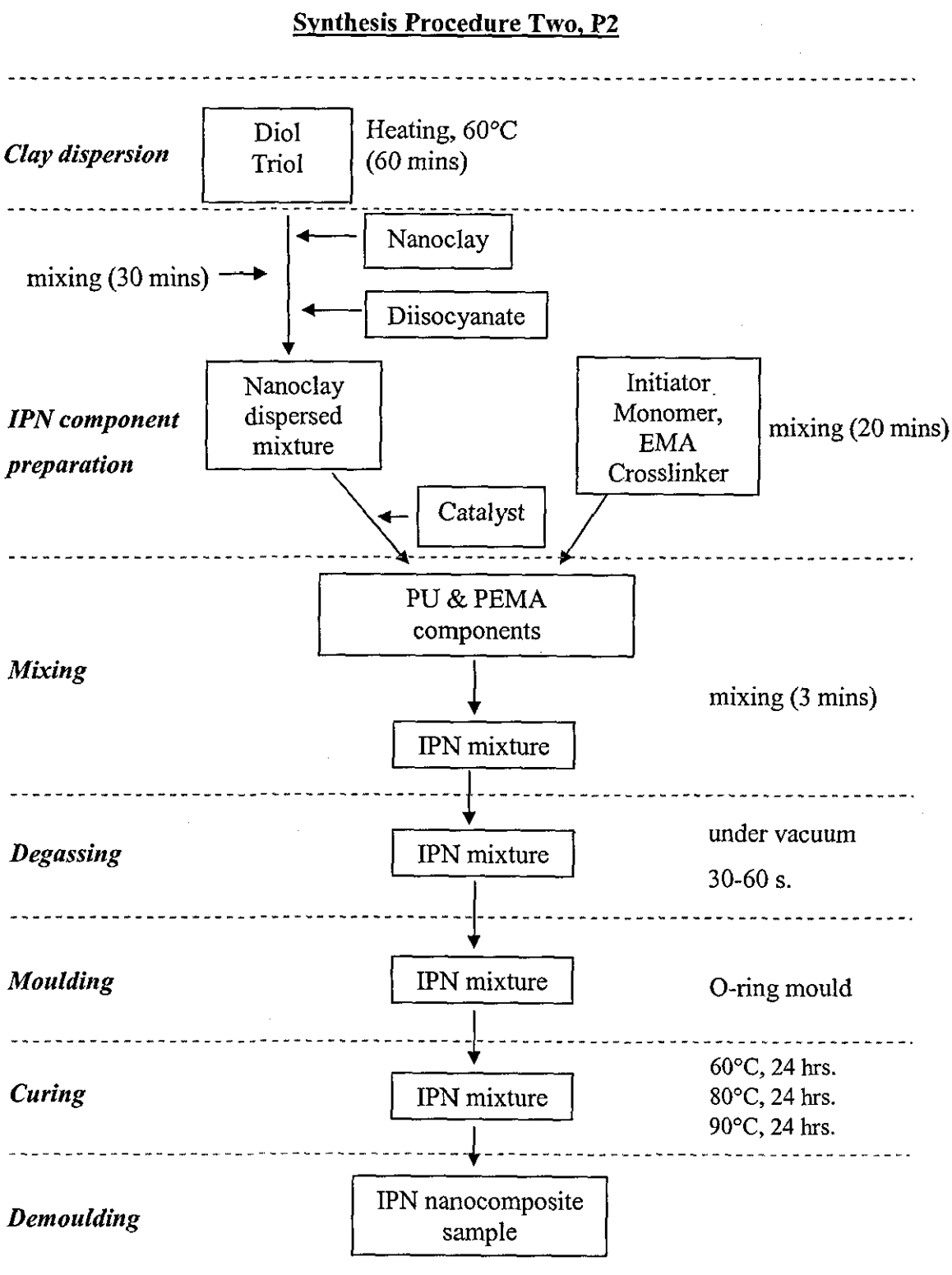


*Figure 3.5* Diagram of the IPN nanocomposite synthesis by synthesis procedure two, P2.

**Synthesis Procedure Three, P3**

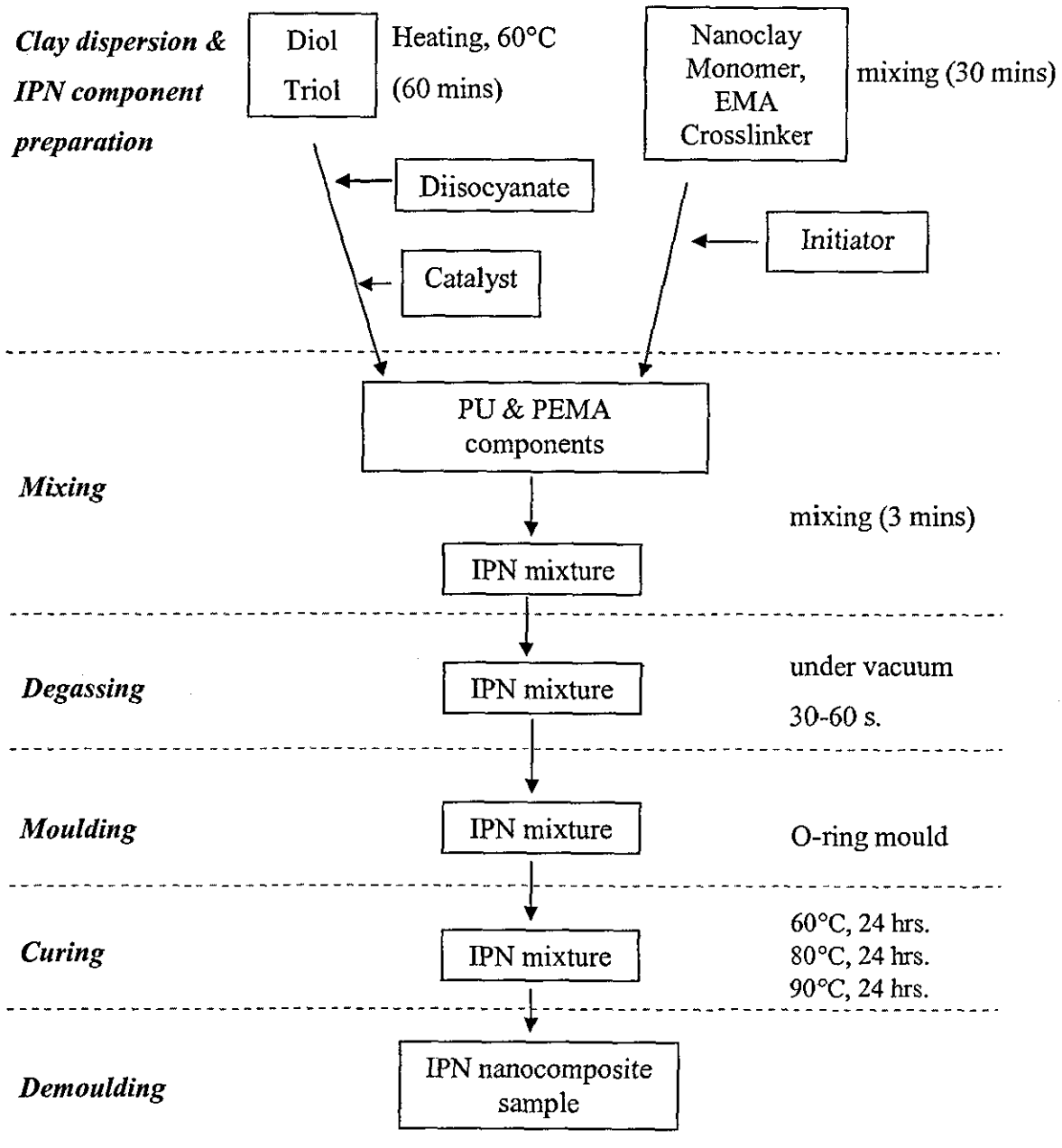


***Figure 3.6*** Diagram of the IPN nanocomposite synthesis by synthesis procedure three, P3.

**Synthesis Procedure Four, P4**

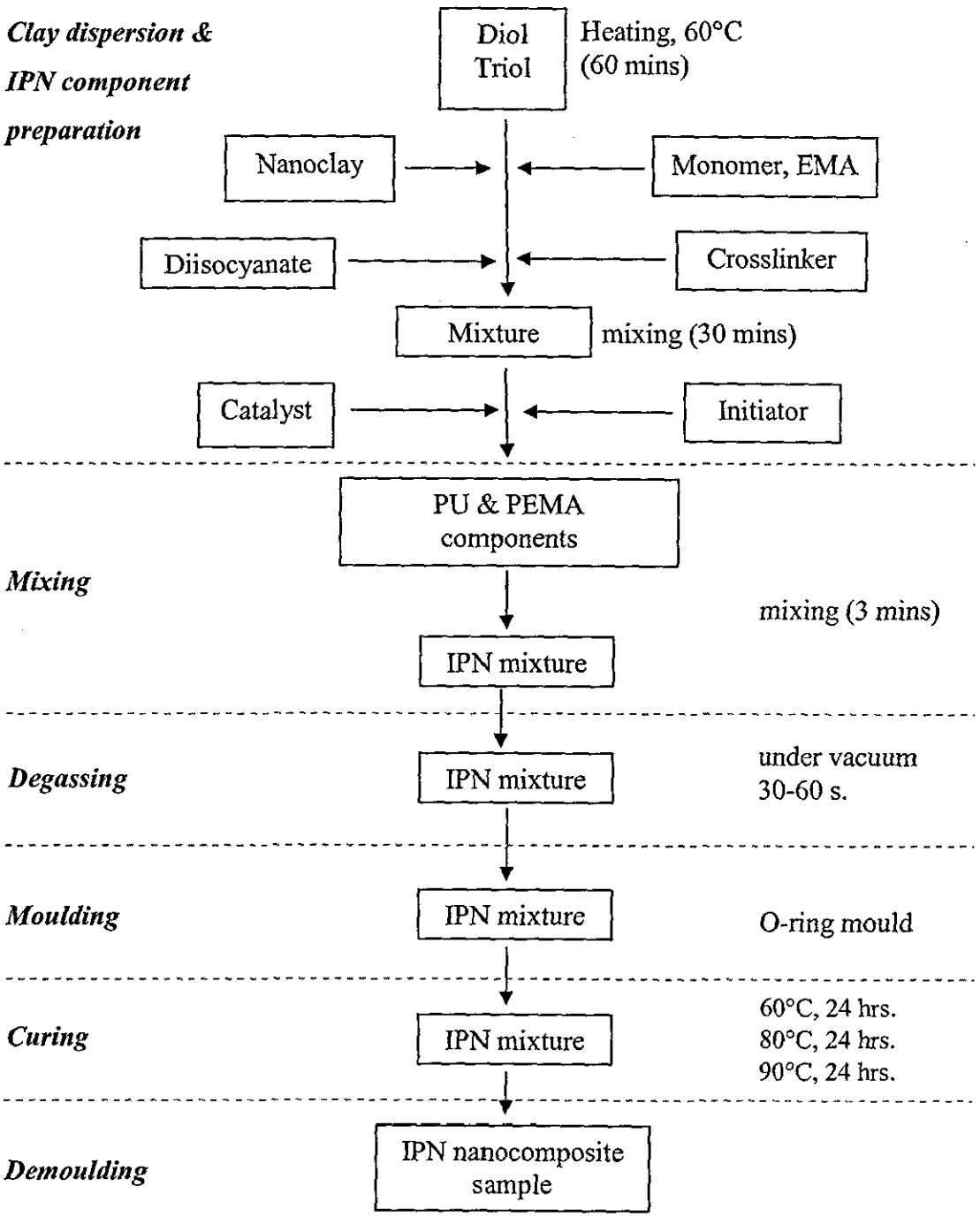


*Figure 3.7* Diagram of the IPN nanocomposite synthesis by synthesis procedure four, P4.

### 3.2.6 Preparation of IPN nanocomposites by Process Four, P4.

Synthesis procedure four (P4) allowed both the PU and the PEMA components to diffuse concurrently into the silicate galleries. Therefore, the PU constituents and the PEMA constituents were mixed in the early stage of the mixing process. Firstly, the triol (TMP) was added in the desired mole ratio into the polyol (PPG1025), then the mixture was kept under vacuum for 60 minutes at 60°C to dissolve completely the solid TMP in the PPG. After that the mixture was left to cool to room temperature in a desiccator. Secondly, the nanoclay, the diisocyanate (TMXDI), the purified EMA monomer and the crosslinker (TEGDM) in the desired amount were added into the mixture, then homogeneously mixed for 30 minutes using a Silverson L2R mixing apparatus. Finally, the catalyst (SnOct) and the PEMA initiator (AIBN) in the desired proportions were added into the mixture and completely mixed for 3 minutes at ambient temperature by using a conventional laboratory stirrer at an angular rotation speed of 200 rpm. The homogeneous mixture was obtained. The degassing, moulding and curing processes were applied as same as in the other procedures. Figure 3.7 represents the P4 synthesis procedure.

In conclusion, the organoclay was first mixed with the PU component in the original synthesis procedure, the synthesis procedure one and two, but in the different stages and various chemicals. Whilst, in the synthesis procedure three, the organoclay was added and mixed with the PEMA component before being combined with the PU component. For the synthesis procedure four, both components were simultaneously combined and mixed with the organoclay. These studies were tried to find a suitable synthesis procedure that provided the IPN organoclay nanocomposite which, hopefully, would reveal enhancement in mechanical behaviour and damping properties.

However, after being demoulded, the samples were left for at least a month at ambient temperature prior to characterisation to complete the curing processes. Besides, the samples were kept at room temperature under vacuum for a week to get rid of the chemical traces remained on the sample sheets before examining their properties in order to yield the good results.

### 3.3 Characterisation techniques.

A number of characterisation techniques were used to investigate the morphology, dynamic mechanical and physical properties. X-ray diffraction and transmission electron microscopy techniques were used to characterise the structure of the polymer-clay nanocomposites. Dynamic mechanical thermal analysis (DMTA), modulated-temperature differential scanning calorimetry (M-TDSC), and transmission electron microscopy (TEM) were the principal techniques used to study the glass transition behaviour and morphology. The other techniques were tensile testing and hardness measurement. The instrumentation and experimental conditions of each technique are briefly stated in the following sections.

#### 3.3.1 Wide angle X-ray diffraction (WAXD).

X-ray diffraction is commonly used in polymer systems to determine the presence of ordered arrangements of atoms and molecules, so called structural parameters. Most polymeric materials are either amorphous, or partially crystalline to varying degrees[149]. Typically, it is used to provide information such as whether the polymer is crytalline or amorphous, oriented or unoriented, and the size of any repeat distance[150]. In addition, structural information such as the unit cell, space group and full structure of a crystalline or semi-crystalline polymer may be determined. For organoclay nanocomposites, it confirms the crystalline structure of the mineral. WAXD measures the average distance between the nanolayers and their relative stacking order. Hence, WAXD provides valuable information about the interlayer spacing of nanoclays. The interlayer distance and stacking order determine the formation and performance of nanocomposites. The principle of X-ray diffraction[151] is shown in Figure 3.8.

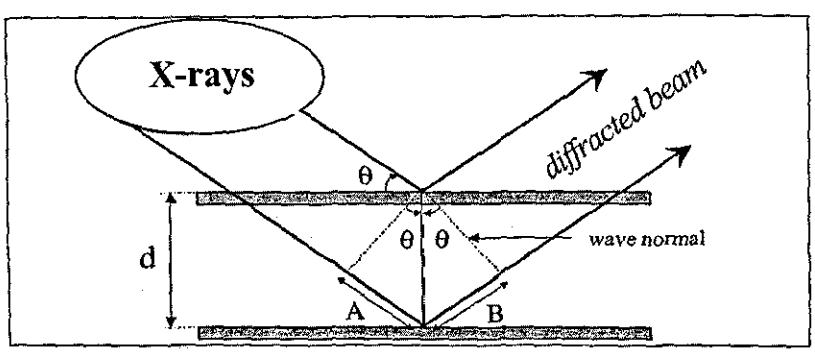


*Figure 3.8* Priciple of X-ray diffraction.

The X-ray of wavelength λ impinges at an angle θ on two adjacent planes separated by an inter-planar distance, d. Diffracted X-rays are shown making the same angle θ with these planes. The wave normals connect points of identical phase for incident and diffracted rays. The difference in path length between the rays diffracted by two adjacent planes is A+B, and must equal a whole number of wavelengths, i.e. nλ, where n is an integer, for total constructive reinforcement to occur between the scattering from these planes. Since the direction of d is normal to the planes, and the wave normal is normal to the wavelets, so the angles opposite A and B are also θ. Thus, from the geometry of the figure, constructive interference occurs when:

$$n\lambda = 2\,d\sin\theta \qquad (3.1)$$

This equation is known as Bragg's law[151]. The case where n = 1 refers to the diffraction of the first order from the given planes.

In the present study, WAXD was used to examine the interlayer spacing of nanoclays dispersed in IPNs. A Bruker model D8 X-ray generator was operated at 40 kilovolts and 40 milliamperes. A graphite monochromator copper $k_\alpha$ radiation (λ = 0.1542 nm) was used throughout. The scan speed was 0.24°/min. and the angle of scan was from 1° to 25°.

### 3.3.2 Transmission electron microscopy (TEM).

Transmission electron microscopy is a powerful technique used to study the morphology at and below the nanometre scale. Therefore, it can be used to confirm results obtained by WAXD about the organisation of the clay layers in the nanocomposite. Furthermore, TEM is widely used to examine the miscibility and phase segregation of IPNs. The information about the extent of molecular mixing, the size and shape of the domains and their distribution can be investigated. TEM can be used only on ultrathin specimens less than 1 μm thick[152]. Thus, the TEM specimen requires special preparation. Figure 3.9 illustrates image formation in a TEM[153].

The electron gun, usually made of a tungsten filament, produces the electrons. These electrons are accelerated by applying a high voltage. The condenser lenses equipped with a diaphragm directs an electron beam onto the specimen with aid of a series of electrostatic and/or electromagnetic lenses. The electrons are scattered passing through

the specimen. Then they are transferred to the objective lens, forming the first image of the specimen. The objective aperture controls the spread of the electron beam and gives contrast to the image. The intermediate lens and projection lens magnify the image and focus it on the viewing screen. The strength of the lenses can be controlled by varying the current through them. In this way, it is possible, easily and rapidly, to change the magnification[153].

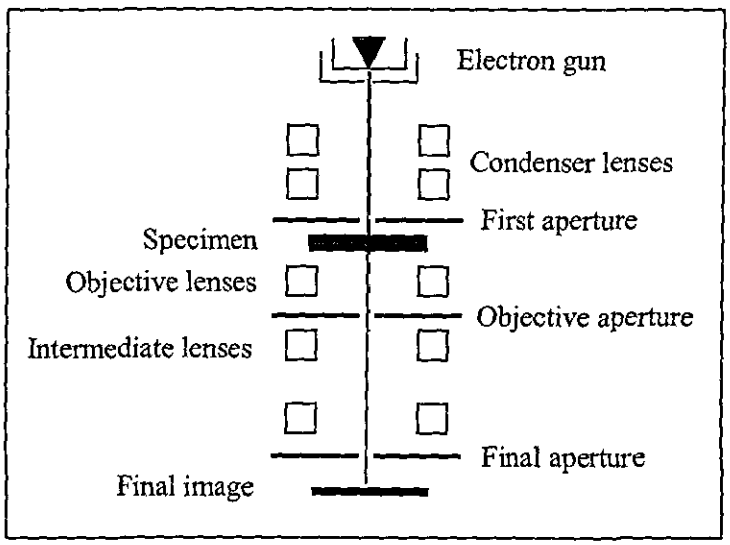


***Figure3.9*** Diagram of image formation in a transmission electron microscope[153].

Because of the soft characteristic behaviour of most IPN nanocomposite sheets at room temperature, prior to sectioning the samples are imbedded in epoxy resin in order to increase the hardness. Ultrathin sections of 100 nm were cut by using a LKA Bromma 8800 Ultratome III ultramicrotome. After that the cut samples are stained with osmium tetroxide, by dipping them into the osmium tetroxide solution for an overnight, or with ruthenium tetroxide vapour for 20 minutes in a closed container. The TEM instruments used in this study were a JEOL JEM 100CX operated at accelerating voltage of 100 kilovolts and a JEOL 2000FX operated at accelerating voltage of 200 kilovolts.

### 3.3.3 Dynamic mechanical thermal analysis (DMTA).

Dynamic mechanical analysis[106,154] is the most common technique to determine degree of phase separation in multi-component systems. A sinusoidal oscillatory stress test is one of the most widely used methods for the experimental measurement of the mechanical behaviour of polymers as a function of temperatures, frequency or time, or

both[106,107]. DMTA can be applied to a wide range of materials using the different sample fixture configurations and deformation modes: bending; shear or tensile.

In this technique,[106,152] a sinusoidal load is applied to the sample and a real, or in-phase, modulus, E′, and an imaginary, or out-of-phase, modulus, E″, are measured. The real and imaginary moduli represent the elastic and viscous behaviours of the sample, respectively. Their ratio, E″/E′, defined as the loss tangent, or damping factor, tan δ, is shown in Figure 3.10.

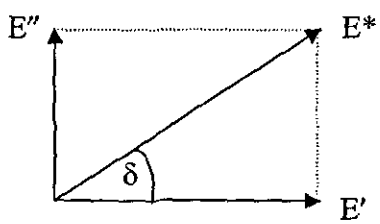


**Figure 3.10** Diagram for complex modulus.

The various degrees of miscibility in multi-component polymer systems can be examined using DMTA results[59]. Figure 3.11 shows generalised relationships for immiscible or heterogeneous, partially miscible, and miscible polymer blends. Two glass transition peaks at the location of their corresponding homopolymers will be observed if the two polymers are immiscible, or mixing is incomplete as when phase separation occurs before crosslinking[59,113]. For partially missible blends, two possibilities are represented. A blend of polymers that exhibit some degree of miscibility will have two transition peaks shifted inwards between those of their two homopolymers[59]. Another possibility is a semi-miscible system. In this system, a broad transition region can be achieved, indicating micro-heterogeneity, in that a large number of phases of differing compositions exist[59,113]. A miscible system will exhibit a single glass transition between the glass transitions of the components with a transition sharpness similar to those of the components[59].

The storage modulus versus temperature profile also can used to identify the degree of miscibility. An immiscible polymer blend exhibits two clearly separated glass

transition peaks, while the miscible polymer blend exhibits only one glass transition. A broad glass transition arises from a micro-heterogeneous structure, or semi-miscible, system.

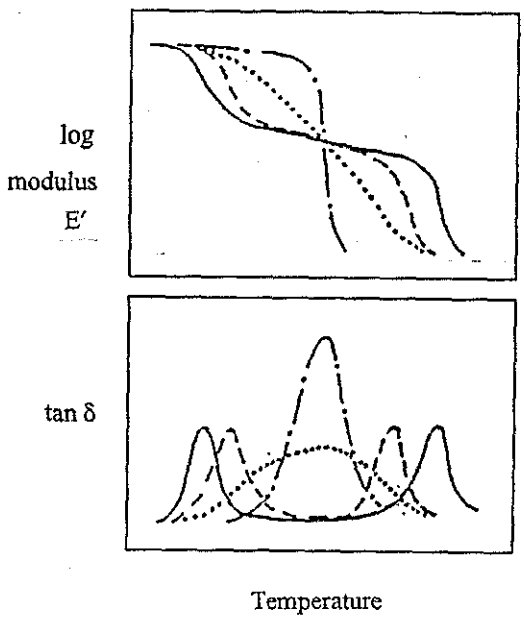


***Figure 3.11*** Generalised mechanical loss and modulus behaviour for different types of polymer blends. a) miscible (dashed-dotted line); b) limited miscibility (dashed line); c) microheterogeneous (dotted line); d) heterogeneous (solid line)[59].

The DMTA instrument used in this study was a Rheometric Scientific dynamic mechanical thermal analyser (Model MK II). It is comprised of five main parts. Namely, i) the mechanical measurement unit, ii) the DMTA analyser, iii) the temperature controller, iv) the control computer, and v) the liquid nitrogen delivery system. A schematic diagram of the measuring head is shown in Figure 3.12.

For the bending mode[149] used in the present study, a sample in the form of a small bar is clamped firmly at both ends and the central point is vibrated by means a ceramic drive shaft. The drive shaft can be driven at frequencies selected from the range 0.01 to 110 Hz. The applied stress is proportional to the A.C. current fed to the drive shaft and the strain is detected using a transducer that measures the displacement of the drive clamp. Temperature can be controlled up to 800°C[106], either isothermally or more normally by ramping up and down at various fixed rates. For sub-ambient operation, a

suitable coolant, recommended is the use of liquid nitrogen, must be passed through the cooling chamber[106].

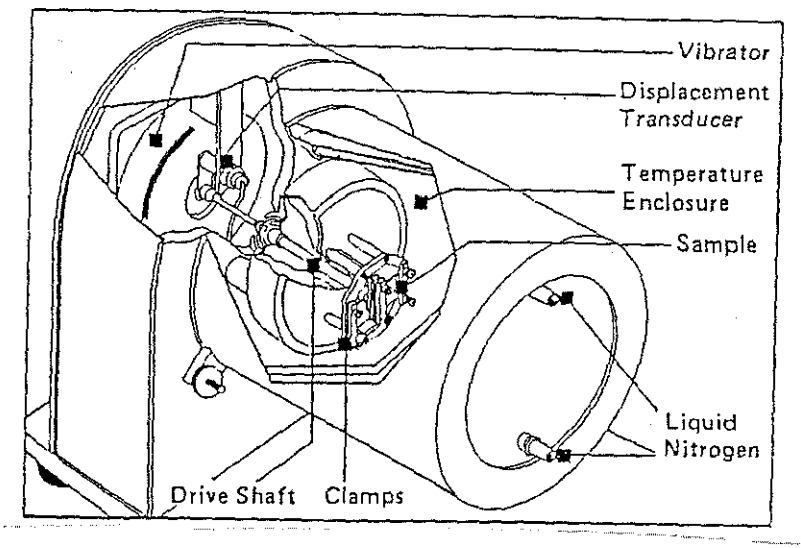


***Figure 3.12*** A schematic diagram of measuring head of a DMTA[149].

The present work used the bending mode in a dual cantilever clamping assembly. Sample specimens in the form of bars with dimensions approximately 25 mm. x 10 mm. x 2 mm. were investigated by varying the temperature from -80°C to 230°C at a heating rate of 3°C/min. The strain amplitude was fixed at a value of x 4, while the frequency was also fixed at 10 Hz.

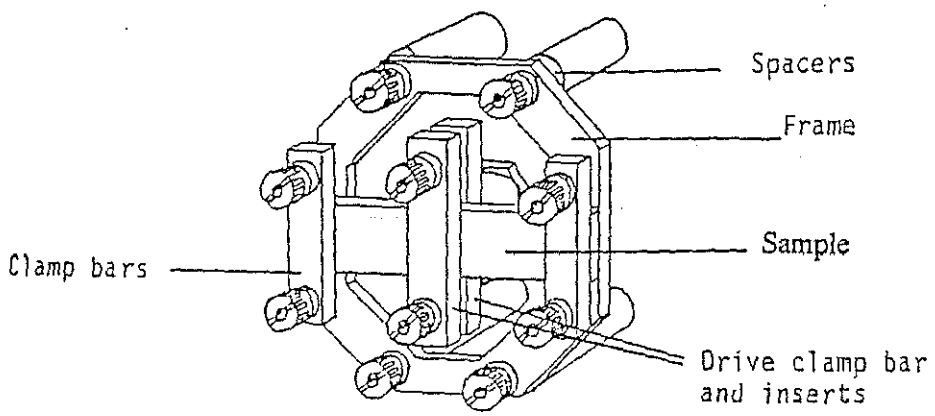


***Figure 3.13*** Clamping arrangement for the dual cantilever bending mode[155].

### 3.3.4 Modulated-temperature differential scanning calorimetry (M-TDSC).

Differential scanning calorimetry (DSC) is a thermal analysis technique used to measure changes in heat flows associated with material transitions. DSC measurements provide both qualitative and quantitative data on endothermic (heat absorbing) and exothermic (heat evolving) processes. DSC instruments can analyse solid and liquid samples by using only a small amount and can vary over a wide temperature range[153]. A sample is placed in an aluminium pan which is sealed using a sample pan crimper. DSC method is schematically presented in Figure 3.14.

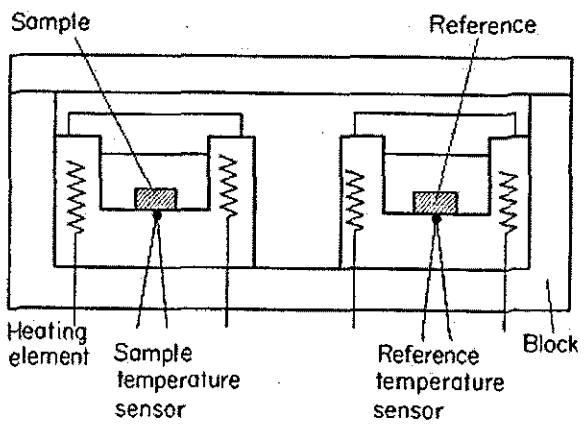


***Figure 3.14*** Essential elements of a DSC cell[153].

The sample and reference are heated separately by individually controlled heater elements. The temperature of the sample holder is kept the same as that of the reference holder by continuous and automatic adjustment of the heater power. The differential power required to achieve this condition is recorded as the ordinate on the recorder, with the programmed temperature of the system as the abscissa[153,156]. A DSC thermogram of an undercooled, potentially semi-crystalline polymer illustrating the measurement principle is shown in Figure 3.15.

At low temperatures, the sample and the reference are at the same temperature. An increase in the heat flow to the sample is required when the glass transition is reached in order to maintain the two at the same temperature. Thus, the change in level of the scanning curve is proportional to $\Delta Cp$. Further heating of this polymer caused crystallisation to occur creating the exothermic peak. The heat flow to the sample in this temperature region should be less than the heat flow to the reference. The integrated difference between the two heat flows, the area under the exothermic peak,

is equal to the crystallisation enthalpy. The melting process, which is an endothermal process, has the heat flow to the sample higher than that to the reference, and the peak points downwards. Thus, the melting enthalpy is proportional to the area under the endothermic peak[156].

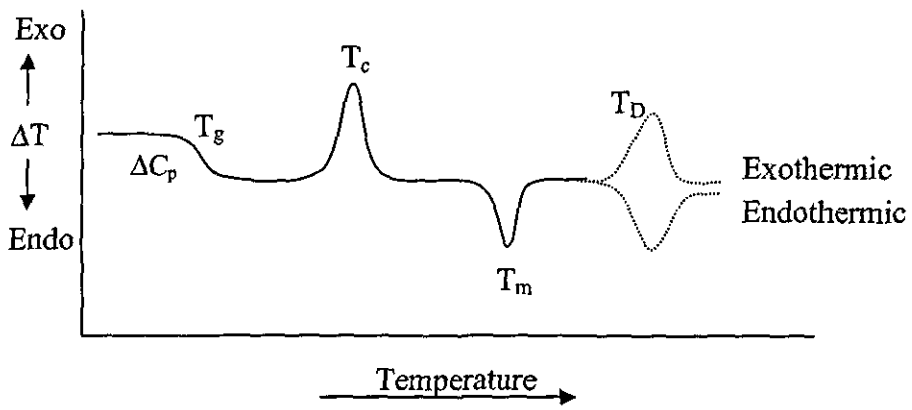


***Figure 3.15*** Schematic DSC traces depicting several transition types[106].

In recent years, a new thermal analysis technique has become available, known as modulated-temperature differential scanning calorimetry (M-TDSC)[157]. It provides the same qualitative and quantitative information about physical and chemical changes as conventional DSC. M-TDSC overcomes certain limitations of conventional DSC. The effects of baseline slope and curvature are reduced, therefore improving the resolution and the sensitivity of the system[158]. M-TDSC uses the same conventional heat flux DSC cell system. Uniquely, it uses a different heating profile, specially a sinusoidal modulation or oscillation which is superimposed on the conventional linear heating rate as shown in Figure 3.16. This modulation in heating rate results in a corresponding modulation in heat flow. This results in three signals, the underlying or average response that is equivalent to a conventional DSC at the same underlying heating rate, the amplitude of the modulation and the phase lag[152]. M-TDSC data analysis separates the total heat flow, or apparent heat capacity, into reversing and non-reversing components[152,158].

This method was first proposed by Reading[159]. The reversing component of the heat flow is obtained from the first harmonic of the heat flow by using a Fourier transform of the data. The non-reversing heat flow is defined as the difference between the

average heat flow and the reversing heat flow. Figure 3.17 shows the M-TDSC data for PET.

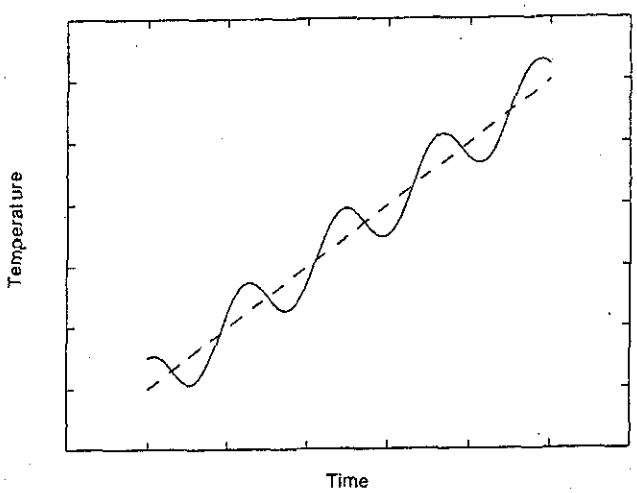


***Figure 3.16*** Typical modulated temperature profile versus time in M-TDSC. The dashed line shows the underlying heating rate[157].

The basic response of an ideal DSC[160] is a combination of a signal that depends on the rate of change of temperature and another one which depends on the value of the temperature. The former depends on the sample heat capacity and the latter on the rate of any kinetically driven process. This can be given by equation (3.2).

$$\frac{dQ}{dt} = Cp\frac{dT}{dt} + f(t,T) \qquad (3.2)$$

where Q is the amount of heat evolved, Cp the thermodynamic heat capacity, T the absolute temperature, t the time, and f(t,T) is some function of time and temperature that governs the kinetic response of any physical or chemical transformation.

The temperature programme is given as a sinusoidal sine wave[158] expressed as follows.

$$T = T_o + bt + B\sin\omega t \qquad (3.3)$$

where $T_o$ is the stating temperature, $\omega/2\pi$ the frequency, b the heating rate, and B the amplitude of the temperature modulation.

So, the derivative with respect to time of the equation (3.3) is

$$\frac{dT}{dt} = b + B\omega\cos\omega t \qquad (3.4)$$

Then, equation (3.2) can be written as

$$\frac{dQ}{dt} = Cp\ [b + B\omega\cos\omega t] + f_1(t,T) + C\sin\omega t \qquad (3.5)$$

where $f_1(t,T)$ is the average underlying kinetic function once the effect of the sine wave modulation has been subtracted, and C is the amplitude of the kinetic response to the sine wave modulation. Therefore, it can be seen that the heat flow signal will contain a cyclic component.

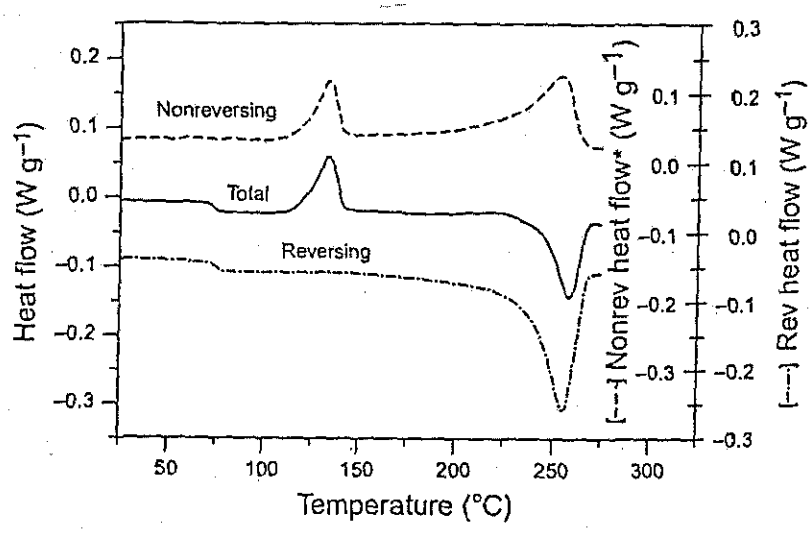


***Figure 3.17*** The M-TDSC results for PET[160].

As is known from the literature[59], information about immiscibility or miscibility in multi-polymer systems can be obtained from Tg studies, because the Tg value is sensitive to many microstructural aspects of the material[157]. Measurement of the Tg transition can be determined easily and accurately from the change in heat capacity of the polymer system by using the M-TDSC technique as shown in Figure 3.18.

The increment of heat capacity over the glass transition can be obtained from equation (3.6).

$$\Delta Cp = \int_{T_i}^{T_f} [dCp(T)/dT]\, dT \qquad (3.6)$$

where $T_i$ and $T_f$ are the initial and final values of the temperature in the glass transition region[158].

For an immiscible polymer blend, the total ΔCp is the linear addition of the ΔCp values of the two constituent polymers[157].

$$\Delta Cp = w_{10}\,\Delta Cp_1 + w_{20}\,\Delta Cp_2 \quad (3.7)$$

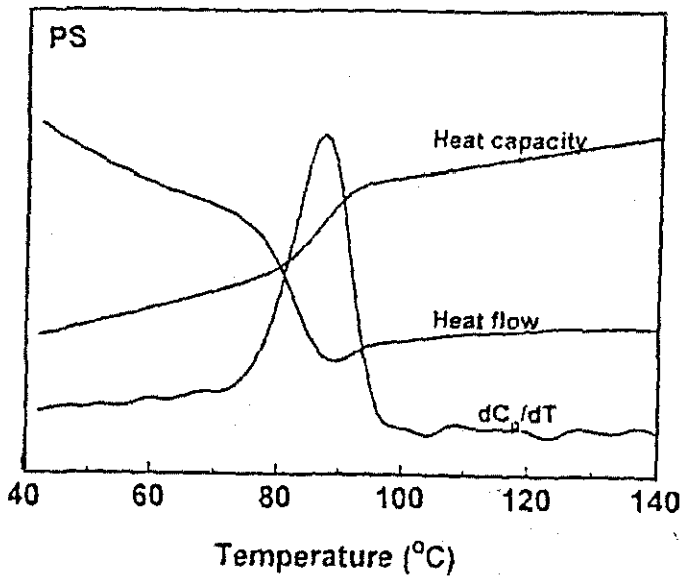


**Figure 3.18** M-TDSC curves show changes in heat flow, heat capacity and dCp/dT with temperature[157].

where $w_{10}$ and $w_{20}$ are the weight fractions of polymer 1 and polymer 2, respectively. $\Delta Cp_1$ and $\Delta Cp_2$ are the values of the increments of heat capacity at the corresponding Tgs.

When the system exhibits an interface, a partially miscible polymer blend, the ΔCp can be obtained by

$$\Delta Cp = \Delta Cp_1 + \Delta Cp_2 + \Delta Cp_i \quad (3.8)$$

$$\Delta Cp = w_1\,\Delta Cp_{10} + w_2\,\Delta Cp_{20} + \Delta Cp_i \quad (3.9)$$

where $w_1$ and $w_2$ are the weight fractions of polymer 1 and polymer 2, respectively, in the mixed phases. $\Delta Cp_i$ is the increment of heat capacity of the interface in its glass transition region. $\Delta Cp_{i0}$ is the increment of heat capacity at the Tgs before mixing. The weight fractions, $\delta_1$ and $\delta_2$ in the polymer1-polymer2 interfacial regions can be obtained as follows[161].

$$\delta_1 = w_{10} - \Delta Cp_1 / \Delta Cp_{10} \quad (3.10)$$

$$\delta_2 = w_{20} - \Delta Cp_2 / \Delta Cp_{20} \quad (3.11)$$

where $w_{i0}$ is the weight fraction of the polymers before mixing.

For a miscible two-polymer blend, Tg depends on the composition ratio. The increment of heat capacity, ΔCp, at Tg, which has been shown to be larger than in an immiscible polymer blend, will vary with the proportion of the two polymers[162].

In this study, a TA Instruments 2920 calorimeter was used. The samples were heated at 3°C/min. with an oscillation amplitude of 0.8°C and oscillation period of 60 s.

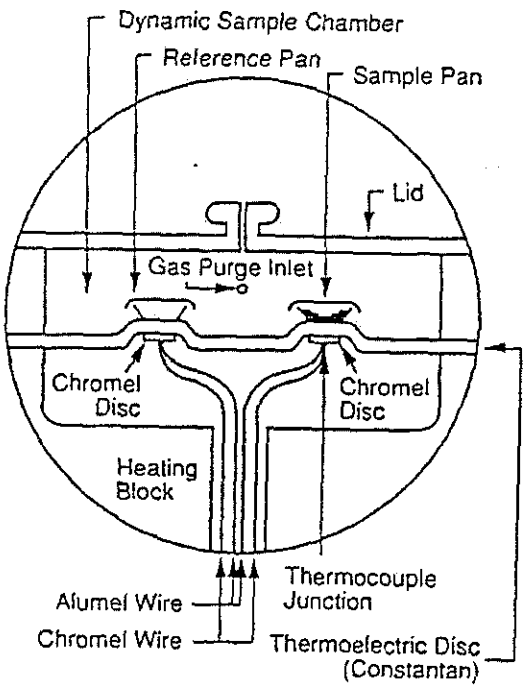


***Figure 3.19*** Schematic diagram of a cross-section of a M-TDSC cell[163].

### 3.3.5 Tensile studies.

Mechanical, or physical, testing of a polymer material is carried out to obtain numerical values of different mechanical properties in order to identify, or classify, materials. A straightforward means of examining the physical properties of polymers is tensile testing or stress-strain experiments[102]. In a stress-strain experiment, a sample is pulled until it breaks. The force applied, or stress, is recorded as a function of strain,

the change in length. The important types of the stress-strain curves are illustrated in Figure 3.20.

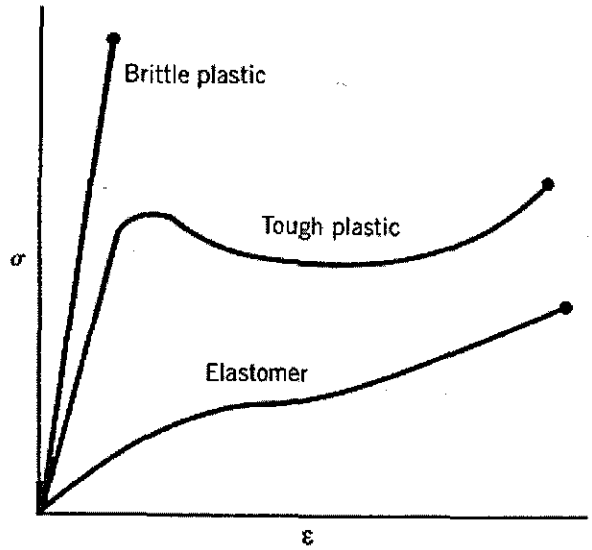


***Figure 3.20*** Stress-strain behaviour of polymeric materials[102].

The tensile parameters are calculated as follows[164].

Tensile strength (σ) defines the maximum tensile stress sustained by a test piece during a tensile test.

$$\sigma\ (\text{MPa}) = \frac{F}{A} \tag{3.12}$$

where F is the force, in N and

A is the cross-section area of the gauge region of test piece, in $mm^2$.

Strain or elongation at break (ε) defines the extent of elongation when the sample breaks.

$$\varepsilon\ (\%) = (\frac{L - L_0}{L}) \text{ x } 100 \tag{3.13}$$

where L = length between gauge marks at break in mm.

$L_0$ = initial gauge length in mm.

Elastic modulus (modulus of elasticity or Young's modulus) defines the ratio of the applied stress to the strain in the linear portion of stress-strain curves.

$$\text{Modulus (MPa)} = \frac{\Delta\sigma}{\Delta\varepsilon} \tag{3.14}$$

where $\Delta\sigma$ = the difference in stress between two points on the straight line

$\Delta\varepsilon$ = the difference in strain between the same two points

In a typical tensile test[164], a sample in the form of a dumb-bell shape, shown in Figure 3.21, is clamped between two sets of grips. One set of grips is fixed and the other is attached to a moving crosshead and load cell arrangement. The thinner portion of the tensile specimen encourages the sample to fail at the centre of the bar and not at the grip sites, where stress concentration may result in premature failure. Crosshead speed depends on the nature of the polymer material. The general purpose is to use a speed that allows all polymers to be tested at the same timescale: fast speeds for extensional materials and slow speeds for rigid materials.

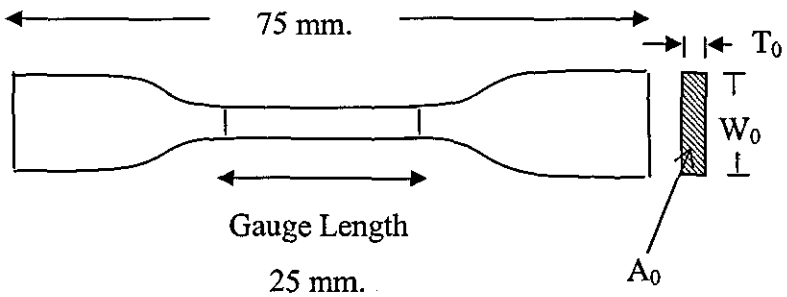


***Figure 3.21*** Typical tensile test piece[164].

Tensometers measure the force necessary to elongate and break the specimen and also usually determine the accompanying elongation, achieved by measurement of the crosshead movement in the case of a straight sample. Force values are converted to stress values, whilst elongation is given as a percentage figure as shown in Figure 3.22. The modulus is usually taken as the initial slope through the zero point. The area under the curve is a measure of the energy required for a failure. In the present study, the tensile tests were carried out by using a Lloyd model 2000 R instrument equipped with a 500 N load cell and a crosshead speed of 50 mm/min. Tests were conducted at room temperature. Three to five specimens were tested to obtain an average value for each sample.

### 3.3.6 Hardness measurement.

Hardness measurement is an easy and rapid measurement. It measures the resistance of materials toward indentation[165]. The indentation hardness of a material is inversely related to the penetration and is dependent on its modulus of elasticity and viscoelastic properties[166]. Generally, an indenter is pressed into the surface of the material to be tested under a specific load for a definite time interval.

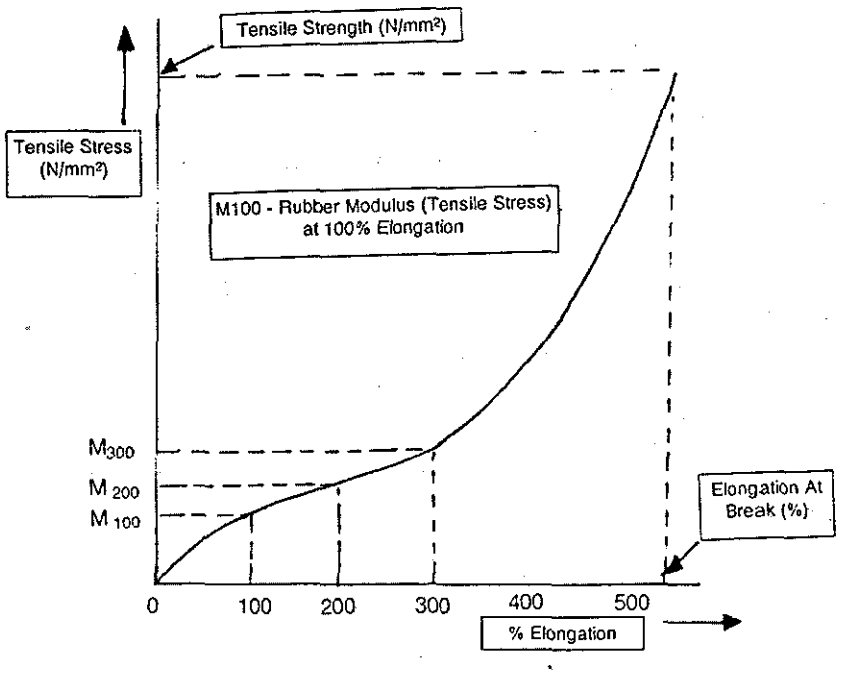


***Figure 3.22*** Typical stress/elongation curve for a rubber compound in tension[164].

The hardness testing of plastics and rubbers/elastomers is most commonly measured by a Shore (Durometer) test, using either the Shore A or Shore D scale. The Shore A scale is used for softer materials, while the Shore D scales is used for harder ones. Figure 3.23 shows shapes of indentors for Shore A and Shore D scales. The scale of a Shore hardness gauge has 100 divisions, ranging from 0 for the full protrusion of 2.5 mm ± 0.04 mm to 100 for nil protrusion obtained by placing the pressure foot and indentor in firm contact with a flat piece of glass[166].

In this present study, Shore A hardness measurements were made using a Durometer (type M) from the Shore Instrument & Mfg. Co., Inc., New York. The testing was conducted at room temperature (22 ± 1° C). A hardness value was read after placing the pressure foot and indentor in firm contact with a sample specimen for 5 seconds. An average of at least 5 readings were taken from the test specimen at random over the entire both top and bottom flat specimen surfaces. Each specimen was composed of three thin layers to obtain the necessary thickness.

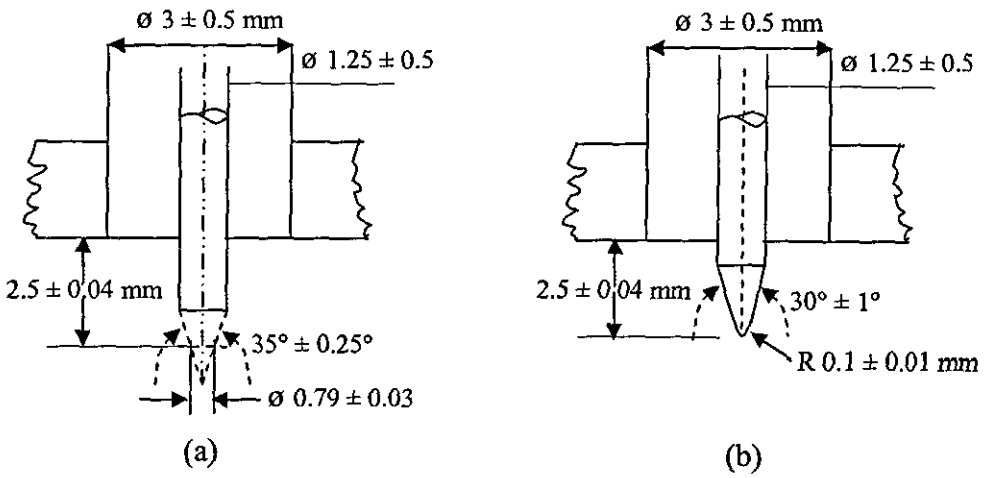


***Figure 3.23*** Indentor geometry for the Shore durometer (a) type A and (b) type D[165].

# CHAPTER 4

# SELECTION OF SUITABLE FORMULATIONS AND CONDITIONS

# CHAPTER 4
# SELECTION OF SUITABLE FORMULATIONS AND CONDITIONS

Most polymer blends, especially IPNs, exhibit phase separation, microheterogeneous morphology, which strongly affects their physical and mechanical properties[102]. There are a number of factors influencing IPN morphology, including the composition of the IPN and the synthesis conditions, as discussed in section 2.1.3. However, the use of filler reinforcement in polymer matrices also improves the stiffness, strength and resistance to temperature and creep of the matrix materials[167]. It has been reported[14-16] that the introduction of organoclays into polymers can result in drastic changes in morphology and mechanical and rheological properties.

In this chapter, there were five sections. The first section is focused on the study of IPN-organoclay nanocomposites based on 70PU/30PEMA IPNs, because of this composition ratio showing a microheterogeneous morphology and great potential for sound and mechanical energy absorption[43,44], by adding various amount of Cloisite 20A, C20A. The influence of the C20A organoclay on the homopolymers, PU and PEMA, is reported in the second section. In the third section, three different composition ratios of PU/PEMA IPNs, in which the component ratio in the PU and PEMA networks were fixed, were investigated in order to get a suitable formulation which broadens and heightens tan δ values and thus, improves the dynamic mechanical properites of the material. Futhermore, the influences of the mixing time and the amount of the PU catalyst, SnOct, on the 70PU/30PEMA IPN properties are reported in the fourth and fifth sections, respectively. However, the original synthesis procedure (see section 3.2.2) was used for all the preparations of the IPN organoclay nanocomposites discussed in this chapter.

## 4.1 Study of PU/PEMA IPN organoclay nanocomposites.

Montmorillonite is the most common type of clay used for polymer nanocomposite formation. Because of its relatively weak forces between the layers, intercalation of

various molecules, even polymers, is possible[168]. However, a number of compatibilising agents are used to improve the polymer dispersion in the clay galleries, by exchanging the hydrated cations in the interlayers with cationic surfactants, such as alkylammonium ions. Organically-modified layered silicates, also known as organoclays, are the most commonly used layered silicates in polymer nanocomposites[118].

Cloisite 20A, C20A, is a natural montmorillonite modified with a quaternary ammonium salt, dimethyl dihydrogenated tallow quaternary ammonium chloride. Its modifier concentration is 95 milliequivalents/100g clay. It is a white powder with a specific gravity of 1.77 g/cm$^3$ and is used as an additive for plastics to improve various plastic physical properties[169].

In this study, C20A at 0%, 1%, 3%, 5%, 10% and 15% by weight of PU were introduced into the 70PU/30PEMA IPN system by using an in-situ polymerisation method, in which the C20A organoclay was first homogeneously mixed with PPG1025 at room temperature for 30 minutes using a Silverson L2R mixing apparatus. The PU network was based on TMXDI, PPG1025, TMP and SnOct, with PPG1025:TMP ratio of 3:1 and SnOct 1.2% by weight of PU, whereas the PEMA network was prepared containing TEGDM at 5 mol% of PEMA and initiated by AIBN at 1 mol% of PEMA (Chapter 3). The simultaneous IPN technique was used to combine intimately the crosslinked elastomeric PU with a high glass transition plastic, PEMA. Polymerisation of the constituent components involves non-interfering steps and radical chain reactions[170]. The PU and PEMA are considered[171] as a semi-miscible polymer pair with solubility parameters, $\delta$, of 20.5 (J/cm$^3$)$^{½}$ and 18.3 (J/cm$^3$)$^{½}$, respectively.

The aim of this work was to synthesis the polyurethane/poly (ethyl methacrylate) IPN organoclay nanocomposites and elucidate the influences of the amount of C20A organoclay on the glass transition behaviour, morphology, damping and mechanical properties of IPN organoclay nanocomposites. The samples were prepared and analysed by several characterisation techniques as outlined below.

### 4.1.1 Wide angle X-ray diffraction (WAXD).

For polymer-clay nanocomposites, the most widely used technique is X-ray diffraction because it is the way to evaluate the spacing between the clay nanolayers and their relative stacking order. The sample preparation is relatively easy and the X-ray analysis can be performed with a few hours. The interlayer distance and stacking order determine the formation and performance of nanocomposites. Hence, WAXD is an effective method used to investigate and confirm that the polymer chain molecules have intercalated into the organoclay layers.

However, dispersion stability of organoclays swollen in the matrix is very important in studying nanocomposites, as poorly dispersed mixtures typically lead to settling of the clay particle during polymerisation. Many studies[34,172,173] showed that the magnitude of property improvement in polymeric systems strongly depended on the state of dispersion of the clay particles in the polymer.

Therefore, X-ray diffraction data were collected from both sides of cast samples to verify a homogenous distribution of the organoclay particles. WAXD patterns for both sides of organoclay C20A-filled 70PU/30PEMA IPNs for 1 and 15 wt% C20A are shown in Figure 4.1. Three diffraction peaks are observed in all the diffraction patterns, which reveal a 2θ angle of 2.25°, ($d_{001}$), corresponding to an interlayer spacing of 4.13 nm and the secondary diffraction, ($d_{002}$), and the third diffraction, ($d_{003}$), at 4.58° and 6.75° respectively. The intensity of the bottom diffraction peaks is higher than that of the top ones for both the studied specimens, indicating that the C20A organoclay particles tend to settle down to the bottom side of the sheets during the polymerisation process. Moreover, the intensity difference between the top and bottom diffraction peaks are systematically decreased with the amount of clay loading. On increasing the amount of organoclay, the overall viscosity of the mixture is increased, consequentially, this restricts the settlement of clay particles during polymerisation. In this case, X-ray diffraction patterns of the bottom sides will be used for further study.

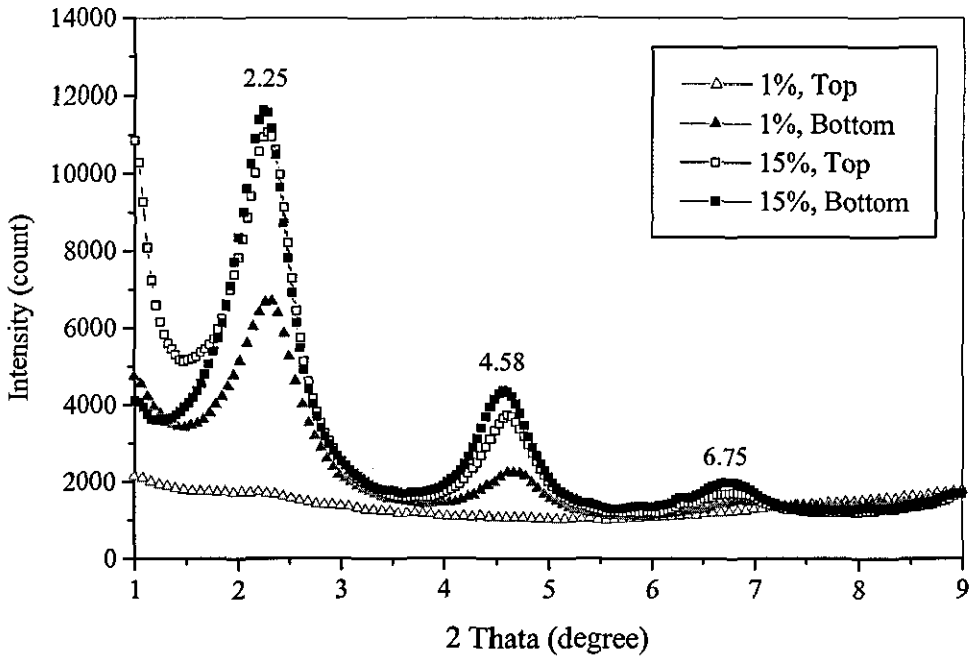


***Figure 4.1*** WAXD patterns for top and bottom sides of C20A organoclay-filled 70PU/30PEMA IPNs containing 1 and 15 wt% of C20A.

The WAXD patterns for C20A organoclay, 70PU/30PEMA IPN, and C20A organoclay-filled 70PU/30PEMA IPNs for 1, 10 and 15 wt% clay are shown in Figure 4.2. No diffraction peak are present in the unfilled 70PU/30PEMA IPNs, because it is an amorphous composites. Two diffraction peaks are observed in the C20A organoclay at 3.85° and 7.42° corresponding to the first and the second diffraction, respectively, of the interlayer spacing of 2.29 nm. After in-situ intercalative polymerisation with 70PU/30PEMA, the diffraction peaks have shifted towards lower angle values of 2.25° and 4.58°, corresponding to the plane (001) and plane (002) respectively, of the interlayer spacing of 3.92 nm, which indicates that the polyether polyol molecules intercalate between the clay nanolayers at all the clay contents. At higher clay content, greater than 10 wt% of C20A, the intensity of the basal diffraction peak does not show any significant increment. This is probably because of agglomeration of organoclay at the higher clay contents. However, it is clear that the variation of amount of C20A has no effect on the intercalation of polyol into the clay galleries.

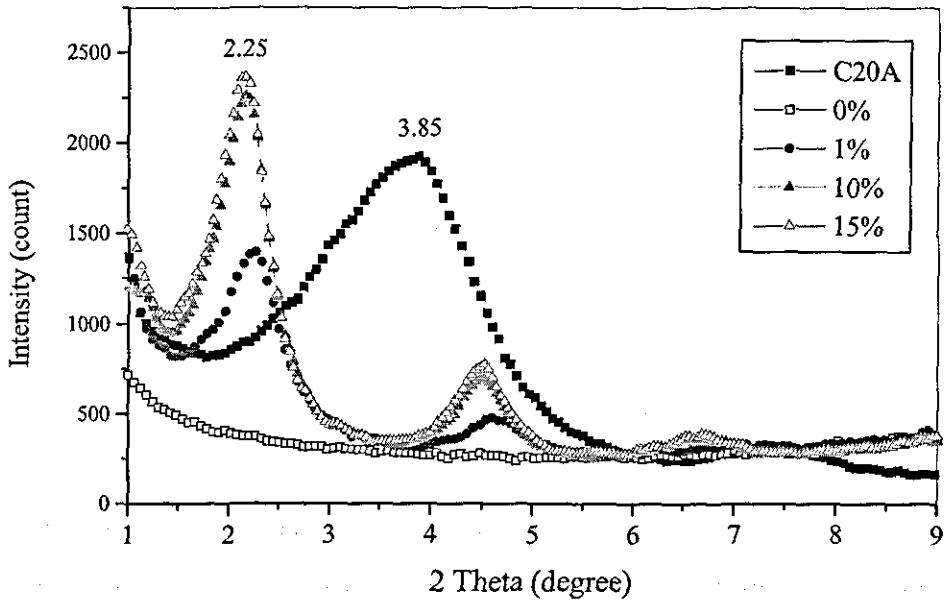


***Figure 4.2*** WAXD patterns for C20A organoclay, the 70PU/30PEMA IPN and the C20A-filled 70PU/30PEMA IPNs containing 1, 10 and 15 wt% C20A.

### 4.1.2 Transmission electron microscopy (TEM).

A TEM investigation was conducted in order to study the morphology of the polymer nanocomposites. The image produced by this technique reveals information about the extent of mixing and the size and shape of domains. It allows a precise observation of the nanostructures. Therefore, this technique is widely used to confirm the results obtained by WAXD about the extent of the filler dispersion in the polymer matrix.

The TEM micrographs showing the morphology of the 70PU/30PEMA IPN and the 70PU/30PEMA IPN organoclay nanocomposites are given in Figures 4.3 to 4.5. For all PU/PEMA IPN composites, no gross phase separation is observed by TEM. They show a fine morphology with light, interconnected PEMA domains in a dark $OsO_4$-strained PU matrix. The phase domains are irregular in shape. The phase boundaries are not clear, indicating that there is high extent of the interconnection in these IPNs. At a high magnification, in addition to a dark PU matrix and light PEMA domains, an interface with different shades of grey is revealed. No further information about the

IPN morphology is provided. However, there is no significant change on the IPN matrix with increasing the organoclay content.

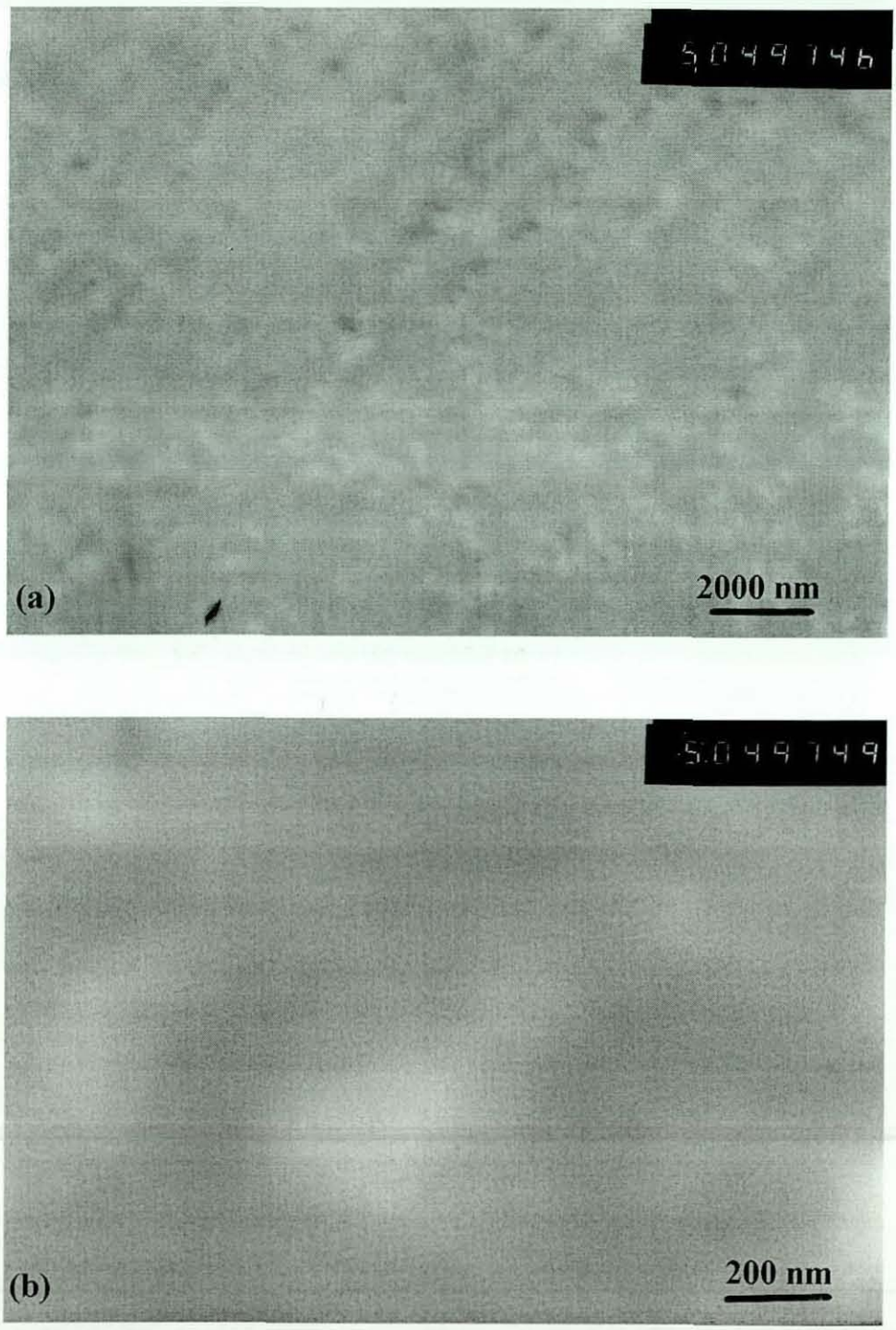


***Figure 4.3*** TEM micrographs for the 70PU/30PEMA IPN.

quantify exfoliation degree ?

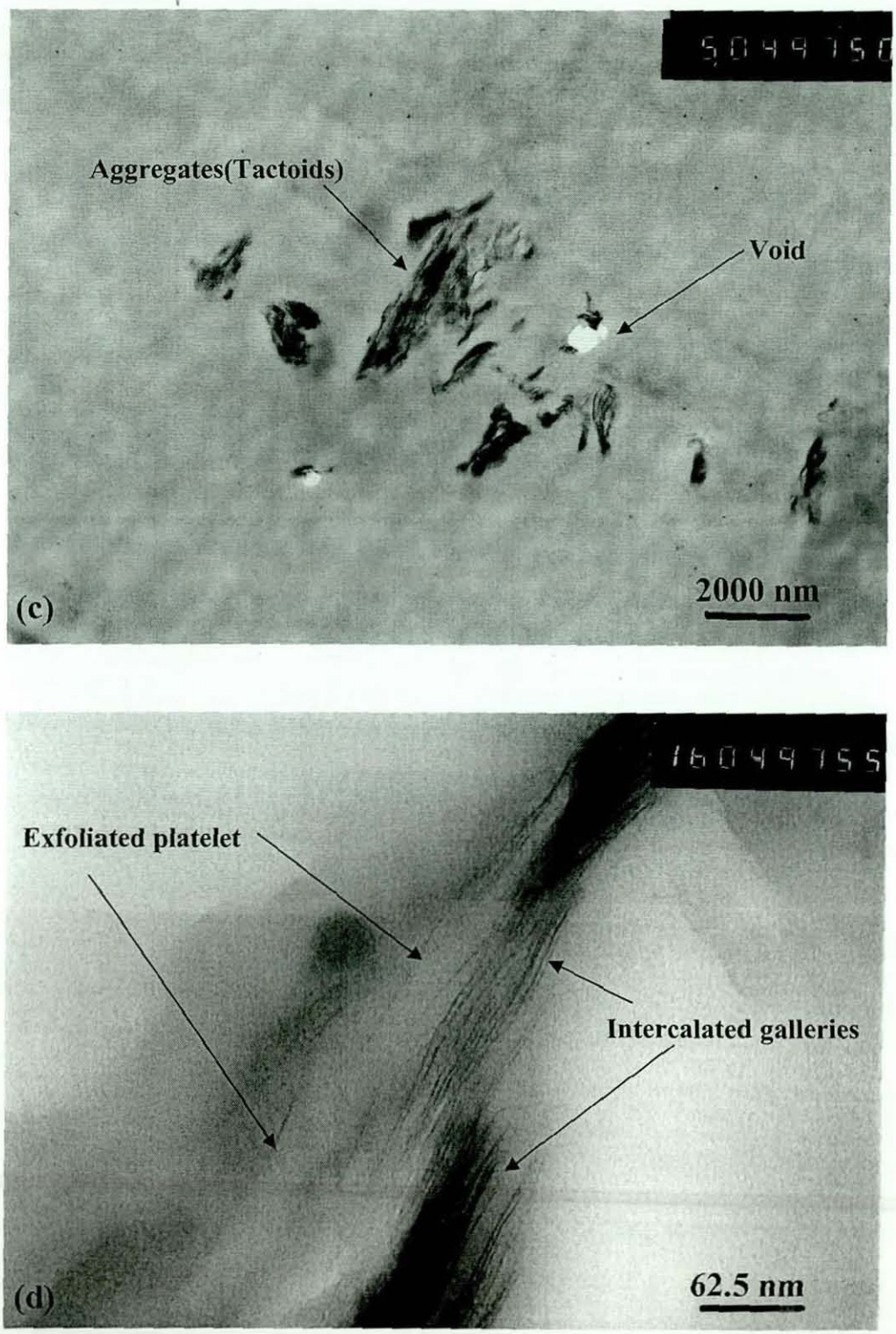


***Figure 4.4*** TEM micrographs for the 70PU/30PEMA organoclay nanocomposite with 5 wt% C20A.

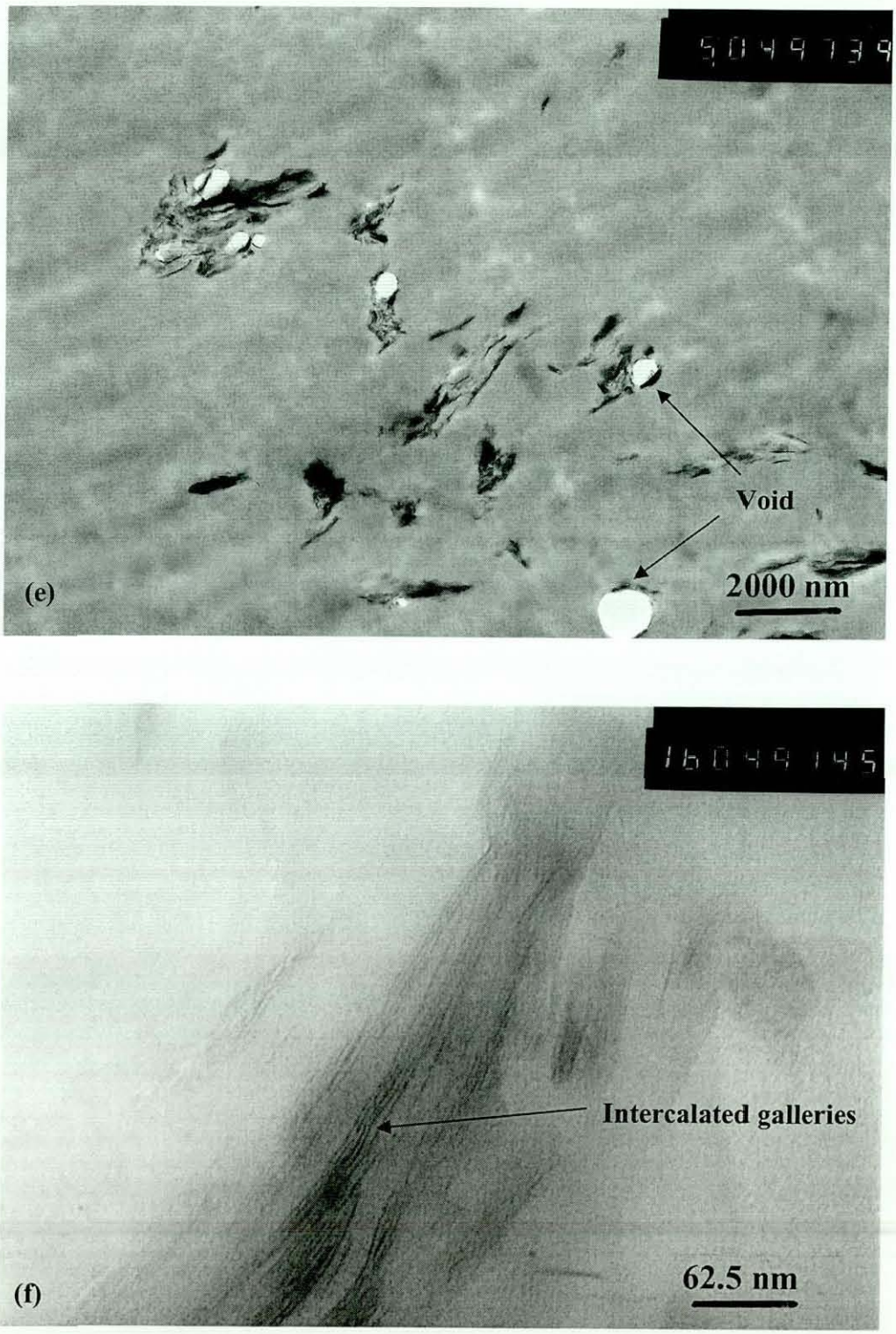


***Figure 4.5*** TEM micrographs for the 70PU/30PEMA organoclay nanocomposite with 15 wt% C20A.

Because organoclays have a much higher electron density than the surrounding polymer matrix, they appear as dark particles in the TEM images. As can be seen from the 70PU/30PEMA IPN organoclay nanocomposites compared with the 70PU/30PEMA IPN, Figures 4.3 to 4.5, the very large and unevenly dispersed organoclay platelets are aggregated in the polymer matrix at low magnification, indicating the relatively poor dispersion of clay particles. High magnification of these materials shows large intercalated tactoids (multi-layer platelets) in which the clay layers are tightly packed together. Only a very little amount of random distribution, exfoliation, is observed. The extensive stacking, with a well defined basal plane spacing consistent with the position of the corresponding first order Bragg peak, is shown in Figures 4.4 (d) and 4.5 (f). Changing the concentration of the organoclay in the polymer matrix does not significantly affect the observed microstructure. However, there are some voids/flaws observed in the IPN organoclay nanocomposites. This evidence supports the WAXD results, showing the significant increase in the interlayer distance. Therefore, the systems presented here do not show complete intercalation.

### 4.1.3 Dynamic mechanical thermal analysis.

Dynamic mechanical thermal analysis (DMTA) was used to complement the morphology studies[80]. While electron micrographs reveal the size, shape and arrangement of the phases, DMTA yields insights about the extent of mixing of the two components, at least semi-quantitatively. The shifting and broadening of transitions are generally[38,61] used as an indicator for the actual occurrence of mixing and interpenetration in IPNs.

The resulting loss factor, storage modulus and loss modulus spectra for the 70PU/30PEMA IPN organoclay nanocomposites with various C20A contents are illustrated in Figures 4.6, 4.8 and 4.10, respectively. Their dynamic mechanical properties are summarised in Table 4.1.

DMTA plots of the PU/PEMA IPNs (Figure 4.6) shows that the two polymers produced a semi-miscible system, where two shoulders corresponding to PU and PEMA-rich regions appeared at 1°C and 90°C, respectively. The feature of the tan δ

curve is that it is broad and almost rectangular in shape with a considerable high damping temperature interval. Glass transition broadening has been reported[174-177] in IPNs prepared from semi-miscible polymers. The reasons for the broadening include micro-heterogeneity of the system with some extent of molecular mixing[38] and a fine dispersion of the component domains[174,177].

***Table 4.1*** Dynamic mechanical properties of 70PU/30PEMA IPN organoclay nanocomposites with various C20A contents.

| C 20A (% wt) | Tg at tan δ max (°C) | | Tan δ max value at Tg | | Peak width tan δ ≥ 0.3 (°C) |
|---|---|---|---|---|---|
| | PU | PEMA | PU | PEMA | |
| unfilled | 1 | 90 | 0.50 | 0.49 | - |
| 3% | -11 | 83 | 0.39 | 0.54 | -21 ↔ 125 (146) |
| 5% | -13 | 82 | 0.36 | 0.58 | -20 ↔ 131 (151) |
| 10% | -14 | 76 | 0.31 | 0.65 | -15 ↔ 125 (140) |
| 15% | -16 | 75 | 0.26 | 0.77 | 0 ↔ 127 (127) |

The PEMA transition reveals at 90°C (tan δ max 0.49) in the absence of the C20A organoclay. Incorporation of C20A organoclay brings down the transition to 75°C (tan δ max 0.77). A gradually increasing damping response at the PEMA Tg is observed for all the studied range.

In addition, there is a downward shift of PU transitions over the composition range of the IPN organoclay nanocomposites in combination with a reduced tan δ max at Tg which strongly contrasts with the finding of the PEMA transition, as shown in Figure 4.6. As the C20A organoclay is added, the PU transitions decrease from 1°C (tan δ max 0.50) shown by the unfilled organoclay to -16°C (tan δ max 0.26) shown by the sample of 15 wt% C20A organoclay. Moreover, the peak width of tan δ ≥ 0.3 seems to be smaller at the higher clay content. A comparison plot of the glass transition and tan delta values is shown in Figure 4.7.

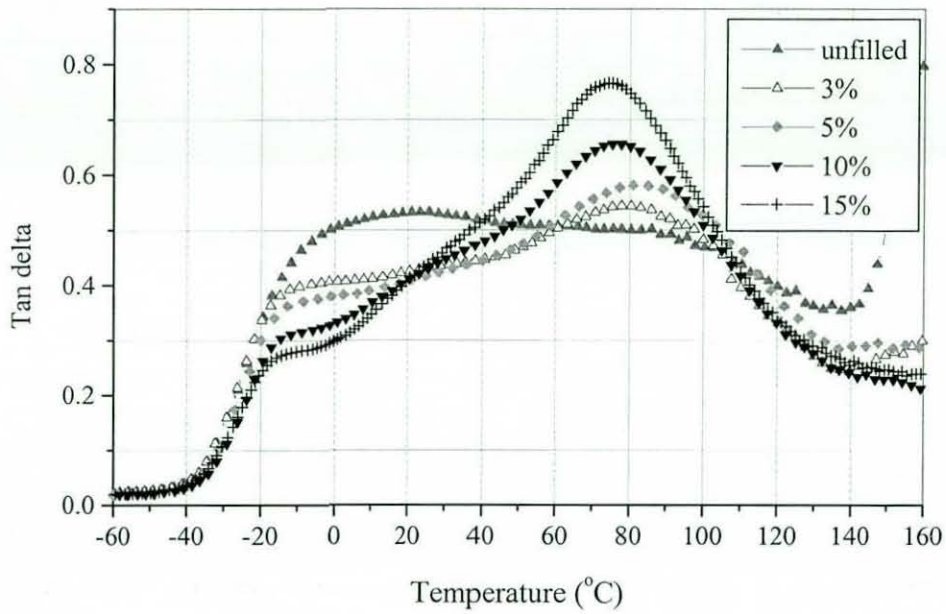


***Figure 4.6*** Loss factor versus temperature plots for the 70PU/30PEMA IPN organoclay nanocomposites: 0, 3, 5, 10 and 15 wt% C20A.

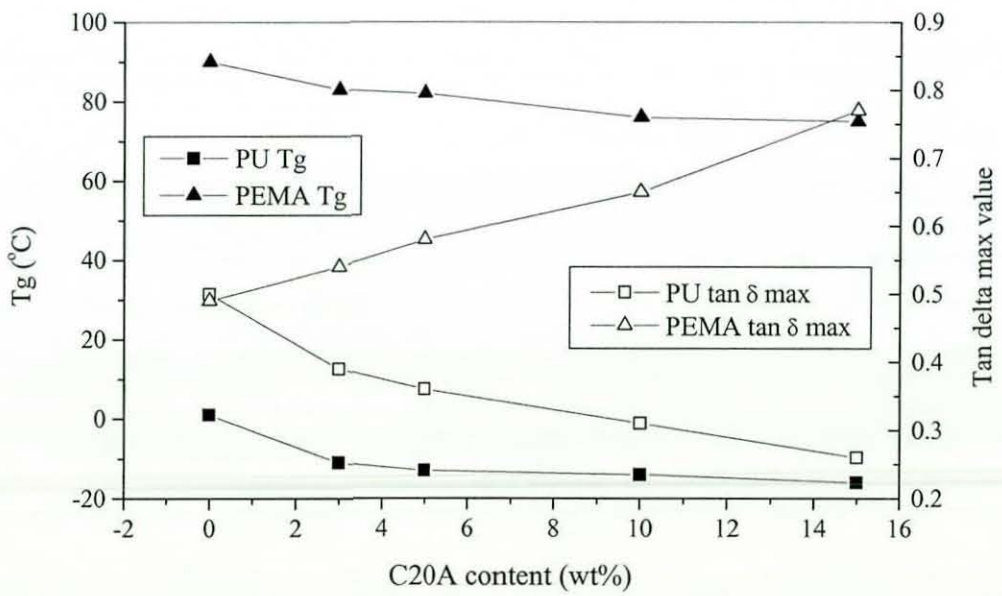


***Figure 4.7*** Glass transitions and tan delta max values corresponding to PU and PEMA-rich phases with various clay contents.

Here, it is necessary to explain why the PU Tg goes down as does its tan δ max and why the PEMA Tg goes down as its tan δ max goes up. It is believed that the polyol, PPG, molecules can intercalate the galleries of the C20A clay as was shown in experiments where the C20A clay was treated with PPG only. Here, the d-spacing changed from 2.29 nm to 3.76 nm. It was found also that the diisocynate, TMXDI, also intercalated (d-spacing changed from 2.29 nm to 3.84 nm). Consequently, it is believed that during the PU network polymerisation there was an imbalance in the hydroxyl : isocyanate ratio resulting in an incomplete network yielding, perhaps, rather branched molecular species rather than a complete network. This would explain both the reduction in glass transition (a more flexible species) and the drop in tan δ max as fewer PPG species were involved. In the case of the PEMA network, it may also be that the degree crosslinking is reduced because of intercalated and non-reacted monomer/crosslinker, yielding a more flexible (lower Tg and higher tan δ max) molecular structure.

Another possible reason of the reduction in the tan δ max at the PU Tg might be due to a restricted mobility of the chain segments in the PU network, where the clay was blended in before mixing. As a consequence, there was a reduced amount of the chain segments in the PU network to interpenetrate with the PEMA network. Therefore, the latter polymer predominated and exhibited the increased tan δ max, compared with that in the IPN themselves.

Lipatov et al.[178] also reported a similar trend in the study of reinforcing silica-filled sequential PU/PS IPNs. They found that the loss factor value at the PU transition decreased with increasing amount of silica. They proposed that when the filler was blended in before curing, the mobility of the chains in PU network was restricted.

Li et al.[179] also studied the influence of filler on the damping properties. They proposed two possible factors in the damping ability for filled polymer systems. One is a decrease in free volume, which limits the mobility of molecular chains so that the damping value decreases. Another is about internal friction between the fillers and

polymer chains, and between the filler particles themselves over the transition range. When the movement of molecular chains becomes more substantial, the transition range will increase so the damping ability increases.

Figure 4.8 shows the storage modulus of IPN organoclay nanocomposites as a function of temperature. As demonstrated in this figure, there is no sign of gross phase separation, which would be noticed as sharp drops at the Tgs of both homopolymers[10].

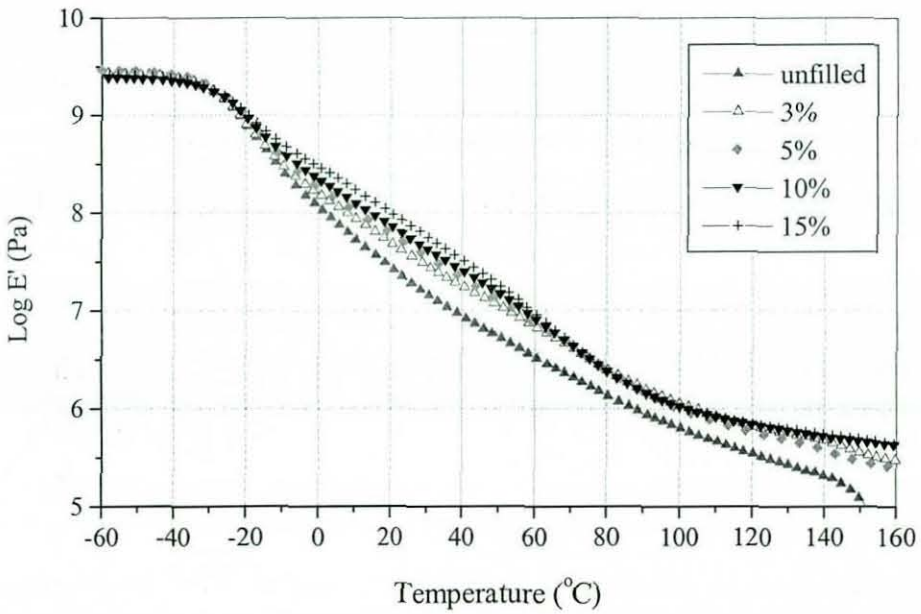


***Figure 4.8*** *Storage modulus versus temperature plots for the 70PU/30PEMA IPN organoclay nanocomposites: 0, 3, 5, 10 and 15 wt% C20A.*

Each IPN organoclay nanocomposite produces a broad transition interval. However, the storage moduli in the glassy state exhibit no significant differences, while in the rubbery state, they reveal a great change, as compared to the unfilled IPN. This could be attributed to the larger modulus ratio between the polymer and the silicate clay particles of the composites when they are in the rubbery state compared to the rigid glassy state. Besides, at the temperature range between the homopolymers, the storage modulus increases with increasing organoclay content. With increasing organoclay

content, the higher storage modulus reflects a gradual change in viscoelastic properties from elastic-like to a more glassy material.

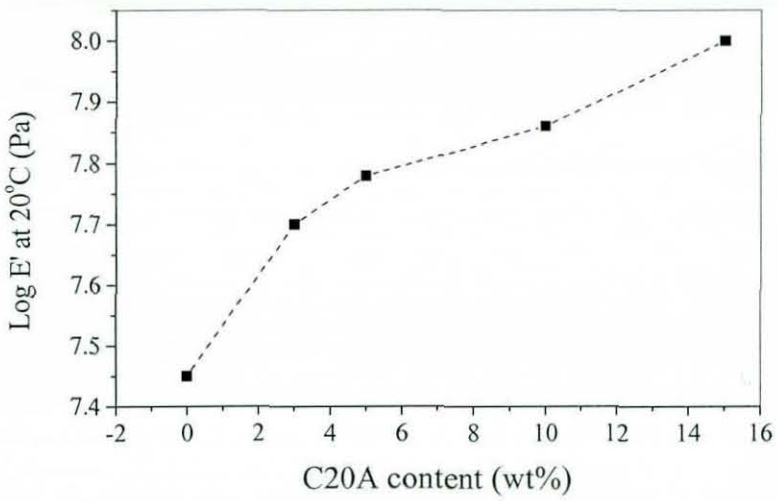


***Figure 4.9*** Storage modulus at 20°C for the 70PU/30PEMA IPN organoclay nanocomposites with various clay contents.

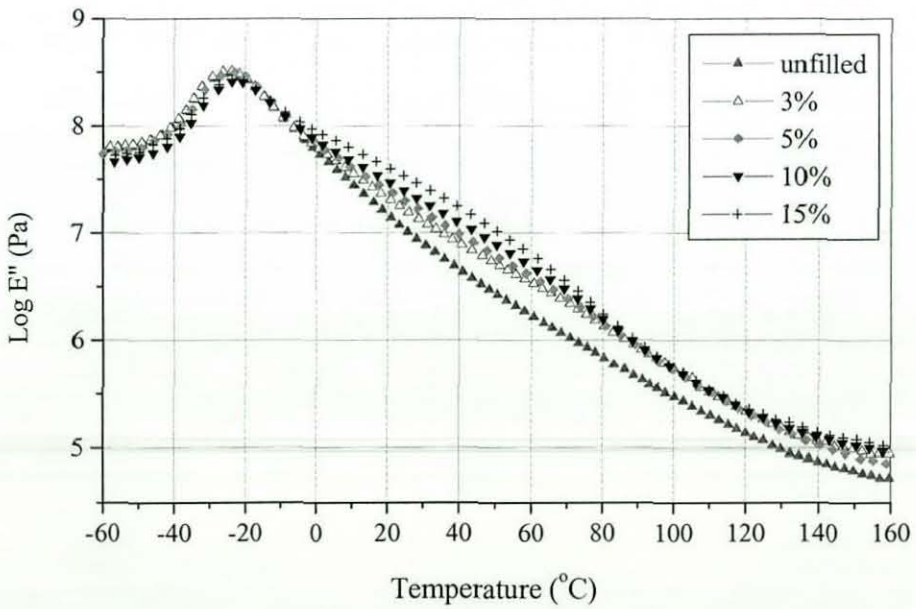


***Figure 4.10*** Loss modulus versus temperature plots for the 70PU/30PEMA IPN organoclay nanocomposites: 0, 3, 5, 10 and 15 wt% C 20A.

Figure 4.10 shows the bending loss modulus of IPN organoclay nanocomposites as a function of temperature. Again, it can be seen that the addition of clay results in an increase in loss modulus at rubbery plateau, although the gradient of the curve does not increase with increasing the clay content. Typical increase in modulus for filled systems has been reported earlier[180].

Corresponding with the data obtained from the storage modulus and the loss modulus, evidence of some degree of phase separation indicated by a two-step broad modulus with slight changes of slope is found from the 15 wt% organoclay content. However, it should be noted that the location of Tgs are difficult to detect accurately, especially, for the PU transition, where a very broad change over a range in loss factor profile was observed for all IPN organoclay nanocomposites.

Many studies[124,126,131] have investigated the influence of organoclay content on dynamic mechanical properties of polymers. They found a similar trend in that the storage modulus appeared to be substantially enhanced at temperatures above Tg for exfoliated nanocomposites with layered silicates of high aspect ratio.

A possible explanation for such an improvement could be the creation of a three-dimensional network of interconnected silicate layers, strengthening the material through mechanical percolation.

However, Noh et al.[127] found no significant difference in the storage modulus could be seen over the investigated temperature range for an intercalated PS nanocomposites, indicating that intercalated nanocomposites did not strongly influence the elastic properties of the matrix. A shift and broadening of the tan δ peak towards higher temperature occured, indicating an increase in the glass transition temperature. They ascribed this to the restriction of segmental motions at the organic-inorganic interface region of these intercalated composites.

### 4.1.4 Modulated-temperature differential scanning calorimetry (M-TDSC).

More detailed information about the morphology of PU/PEMA IPN organoclay nanocomposites was obtained from differential heat capacity, dCp/dT, versus temperature data by M-TDSC. The signals provide useful information because they are sensitive to glass transition temperature, miscibility and degree of molecular mixing of a polymer blend[159].

M-TDSC curves for the 70PU/30PEMA IPN organoclay nanocomposites are shown in Figure 4.11. The M-TDSC data are also listed in Table 4.2. Differential heat capacity signal, dCp/dT, for PU and PEMA homopolymers, show single peaks with dCp/dT values of 0.029 and 0.012 $Jg^{-1}°C^{-2}$, where the transition temperatures are centered at -37°C and 81°C, respectively. Also, the dCp/dT signal for a PU(70%) + PEMA(30%) physical blend shows two single peaks at the locations of the respective homopolymers.

***Table 4.2*** M-TDSC data for the 70PU/30PEMA IPN organoclay nanocomposites with varying C20A clay contents.

| C20A %wt | Tg, °C | | dCp/dT value, $J/g^{-1}°C^{-2}$ | |
|---|---|---|---|---|
| | PU | PEMA | PU | PEMA |
| Pure PU | -37 | - | 0.029 | - |
| Pure PEMA | - | 81 | - | 0.012 |
| Physical blend | -37 | 81 | 0.021 | 0.004 |
| unfilled | -37 | 62 | 0.018 | 0.001 |
| 1% | -37 | 62 | 0.017 | 0.002 |
| 3% | -36 | 62 | 0.016 | 0.001 |
| 5% | -37 | 60 | 0.015 | 0.001 |
| 10% | -37 | 59 | 0.015 | 0.001 |
| 15% | -38 | 58 | 0.014 | 0.002 |

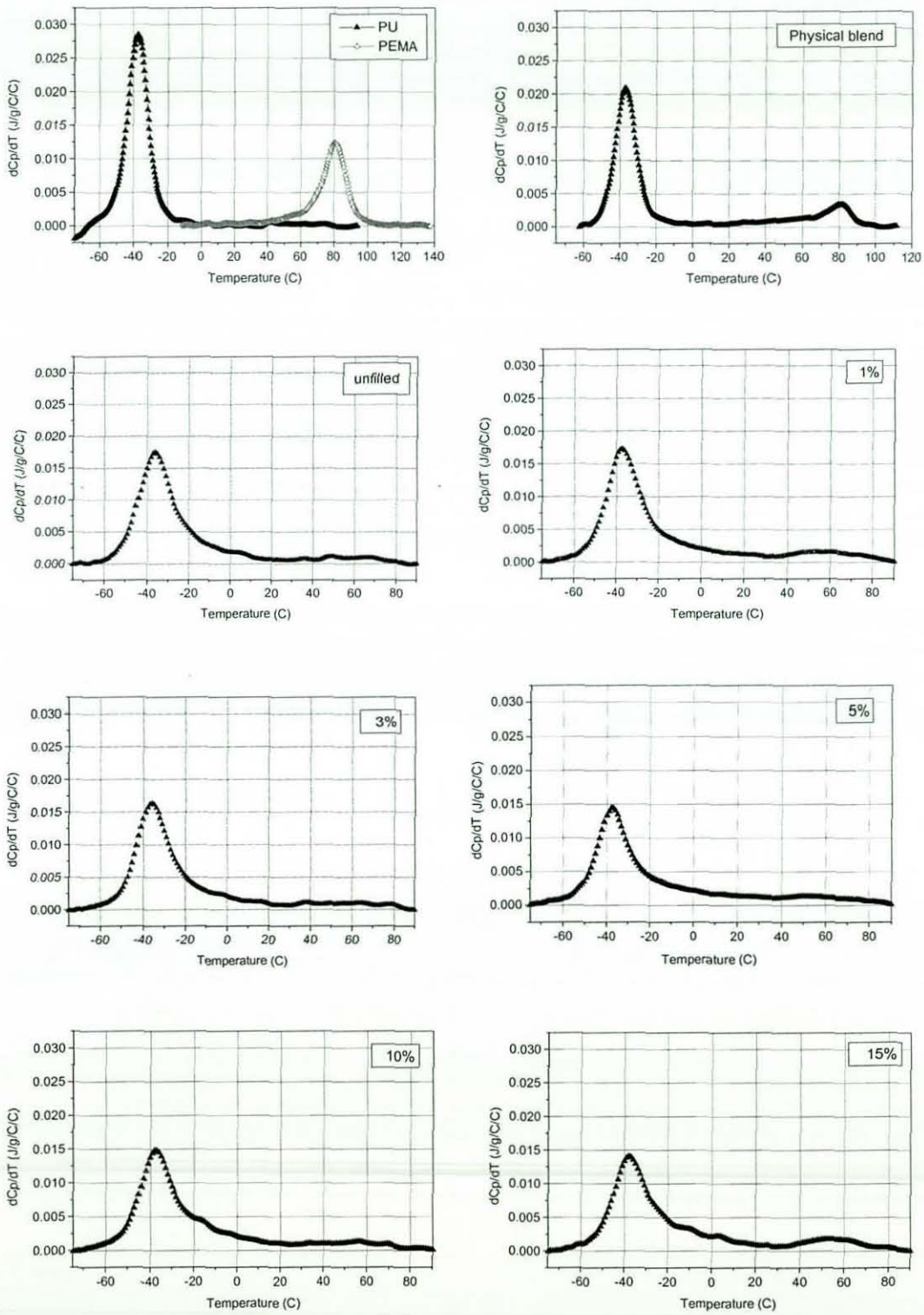


***Figure 4.11*** Differential heat capacity versus temperature plots showing the effect of organoclay content for the 70PU/30PEMA IPN organoclay nanocomposites.

Besides, the PU and PEMA homopolymers, the PU(70%)/PEMA(30%) physical blend, the other IPN organoclay nanocomposites reveal some degree of phase separation and exhibit a broad shoulder at the second transition. However, the spanning of transition spectra over wide temperature ranges between the transitions of pure PU and PEMA implies that gross phase separation did not take place. Hence, this multi-phase behaviour over the whole range of clay contents in these 70PU/30PEMA IPN organoclay nanocomposites is confirmed by the M-TDSC measurements.

It also can be seen that the Tg value of PU network in the IPNs is equal to that of the pure PU network. However, the Tg values of PEMA network exists as a weak, very broad transition and it is difficult to identify the location of Tg. It is lower by at least 19°C than that (81°C) of the pure PEMA network. The presence of organoclay results in similar spectra where a sharp peak appears at the PU transition and a very broad shoulder is revealed at the PEMA transition over the entire clay content range.

Glass transitions of the non-clay containing IPNs are detected at -37°C and 62°C. With an addition of organoclay, the Tg values of PU network are similar to that of the pure PU network. However, the PEMA transitions shift slightly downwards from the PEMA Tg of IPNs, but this is not significant.

Increased clay loading reduced the volume fraction of polymer in the composites, resulting in a slight reduction of heat capacity values at the PU Tgs. However, for PEMA transition, no significant changes are observed. It was noted that the Tg values obtained from M-TDSC technique were typically lower than those obtained from DMTA method, mainly due to lower frequency of M-TDSC as compared to that of DMTA equipment. DMTA also provides a more sensitive measure of this transition as shown in section 4.1.3.

Hence, the presence of organoclays did not cause any significant change in the positions of the glass transition temperatures and shapes of M-TDSC spectra when they are compared to the IPN spectrum.

Many studies examined the influence of organoclay on the thermal properties of the polymer nanocomposites. Lu et al.[181] found that the increasing C30B montmorillonite content on epoxy resin matrix resulted in a shift of Tg to higher temperatures, and the Tg regions became broader relative to the pure epoxy. They stated that the increment of the Tg was attributed to chemical bonding in the interphase between the silicate and epoxy matrix, which retarded the mobility of the epoxy network segments near the solid surface.

Song et al.[182] investigated polyurethane/$Na^+$-montmorillonite nanocomposites. By increasing the weight fraction of layered clay, the peak area of the differential of heat capacity signal, dCp/dT, versus temperature decreased, indicating that the value of $\Delta Cp$ decreased. They ascribed this to the fact that some modified polyether polyol segments were intercalated between the layers in the clay. Therefore, the glass transition of that part which was confined strongly between the silicate layers did not occur.

Gelfer et al.[183] evaluated the effects of C6A organoclays on PS/PMMA blends. The presence of organoclays greatly affected Tg in these PS/PMMA blends, while there was no significant shift on the Tgs of PS and PMMA homopolymers. They found two distinctive peaks at 78°C and 115°C after adding C6A clay, instead of only one peak at about 105°C. The reduction in Tg value was related to the region near the PS/PMMA interface, which was plasticised by the free surfactant from the organoclay. The higher Tg value probably corresponded to small PMMA domains confined by the PS phase.

### 4.1.5 Tensile behaviour.

Fillers can modify the properties of polymer systems in many ways. Some mechanical properties are influenced by the interacting effects between the polymer and the filler and also the reinforcing characteristics of the filler used[184]. Furthermore, layered silicate nanofillers have shown that the intercalated and/or delaminated nanocomposites can show tremendous property improvements[14].

The mechanical properties of the IPN organoclay nanocomposites were also investigated by tensile testing. The results are listed in Table 4.3. Figure 4.12 illustrates the tensile properties: modulus of elasticity; tensile strength and elongation at break versus the organoclay content.

***Table 4.3*** Measured values of maximum tensile strength, extension at break, and modulus of elasticity for the IPN organoclay nanocomposites.

| Clay content (wt%) | Tensile strength (MPa) | Extension at break (%) | Modulus of elasticity (MPa) |
|---|---|---|---|
| unfilled | 4.58 ± 0.24 | 736 ± 37 | 4.52 ± 0.72 |
| 1% | 4.58 ± 0.44 | 652 ± 36 | 6.34 ± 0.99 |
| 3% | 4.06 ± 0.55 | 606 ± 42 | 5.71 ± 1.37 |
| 5% | 3.89 ± 0.34 | 587 ± 41 | 5.67 ± 0.58 |
| 10% | 3.29 ± 0.12 | 505 ± 14 | 7.90 ± 0.48 |
| 15% | 1.62 ± 0.60 | 272 ± 49 | 9.04 ± 1.34 |

As seen from Figure 4.12, at 1 wt% clay loading, the maximum tensile strength at break shows the same value as the unfilled IPNs. Adding more clay, results in a gradual reduction of tensile strength. A drastic decrease is found when the clay loading is more than 10 wt%.

The same behaviour is exhibited by the percentage extension to failure at ambient temperature. The incorporation of C20A organoclay gradually reduces the elongation, whilst adding more than 10 wt% causes a rapid reduction.

These observations could be attributed to the way in which the matrix was restricted in its ability to stretch between the clay galleries and possibly reduced interfacial bonding between the polymer matrix and the organoclay particles.

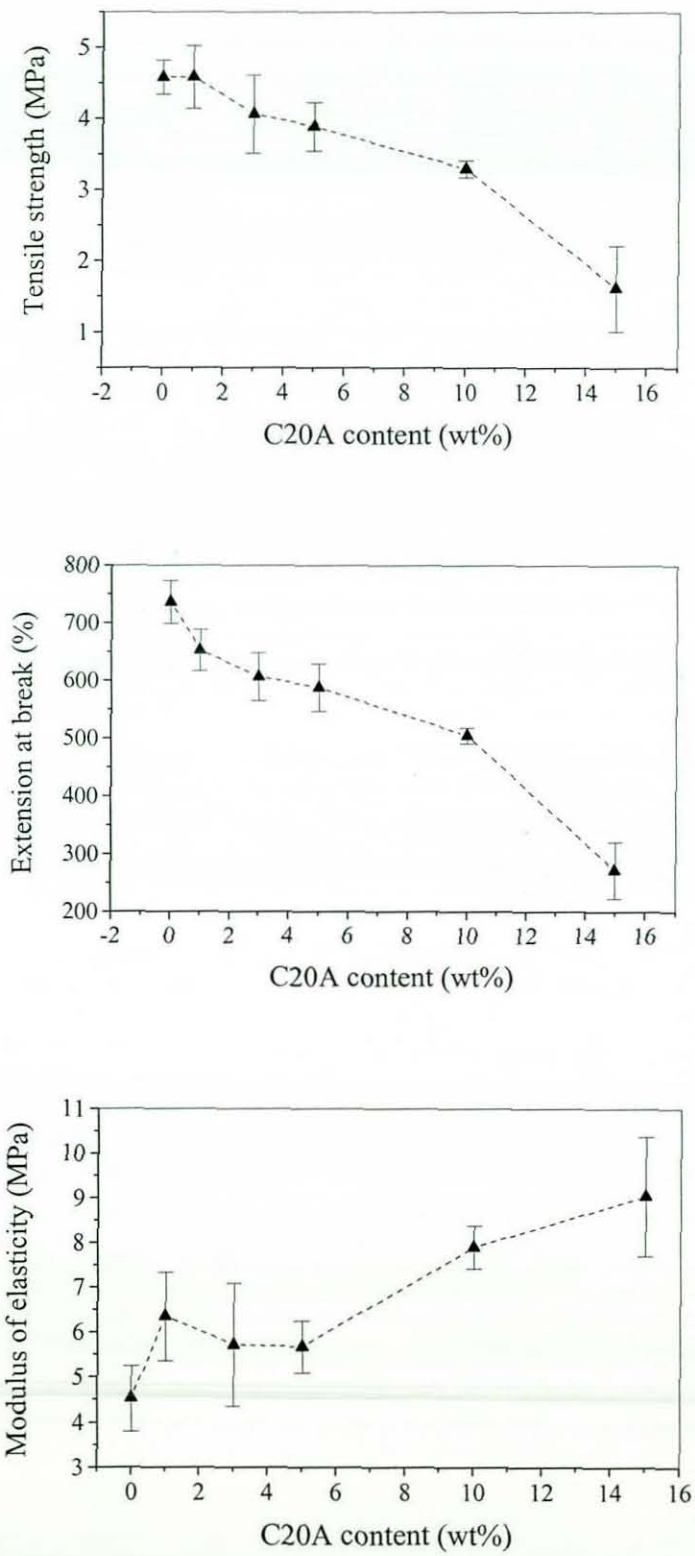


***Figure 4.12*** Tensile properties of the IPN organoclay nanocomposites as a function of clay loading.

By contrast, the modulus of elasticity exhibits an increase with increasing clay content. At 1% clay content, the modulus shows a drastic increase from 4.51 MPa, observed for the unfilled IPN, to a value of 6.34 MPa. 3% and 5% exhibit a similar increase to around 5.7 MPa. Further addition of clay content results in an increase in the elastic modulus as seen in Figure 4.12. This is because the silicate layers are, compared to most polymers, much stiffer and are essentially inextensible materials. Incorporation of filler into a polymer usually provides a composite material of an increased stiffness and reduced strain to failure relative to the unfilled sample, i.e. the composite will be less ductile or less elastomeric. The extent of this change depends not only on the amount of filler, but also on the nature of the polymer[184]. Besides, higher modulus or stiffening effects can be provided by the aggregates, or flocculated particles, because the portion of the matrix that is isolated in the aggregates is less free to react to stress than the continuous phase under the measured conditions[180].

Regarding the TEM results, the overall pictures show that the clay layers are not occupying the full volume and large regions of the polymer matrix are visible. At this scale, considerable inhomogeneity is apparent. The presence of multiplets is observed, indicating all layers are not separated individually upon polymerisation. Only some silicate layers are intercalated. This might be the reason why the mechanical properties have not shown a strong improvement.

Siddaramaiah et al.[185] synthesised and characterised polyaniline-filled PU/PMMA interpenetrating polymer networks. They found that the addition of 2.5% polyaniline (PAni) to PU/PMMA IPN did not affect its original tensile strength. With further addition of PAni, the tensile properties increased with increase in PAni content. This was due to the reinforcing effect of PAni and the formation of hydrogen bonding between –NH– of PAni with –NHCOO– of PU/PMMA polymer network. Consequently, PAni-filled IPN showed better surface hardness values, while it was worse in percent elongation at break than the IPN as PAni content increased.

Many studies[186-188] have found that the properties of nanocomposites were strongly related to their microstructure. They also showed that the reinforcing effects

demonstrated by storage modulus, thermal stability, etc., were directly related to the dispersability of the clay particles in the polymer matrix. The dispersion of sodium montmorillonite in natural and epoxidised rubber was examined by Mark and co-workers[187]. They showed that the dispersion of silicate clay was an important role in its reinforcing effect in the rubber. Zhang et al.[188] also reported similar behaviour for clay-polypropylene nanocomposites.

With clay-polyurethane nanocomposites, Tortora et al.[189] found the exfoliation occurred at low montmorillonite content. As the clay content increased, more intercalated nanocomposites was obtained, associated with higher stress and lower strain at break.

Recently, a theoretical study[190] showed that when the structure changed from an intercalated to an exfoliated structure the morphology of the nanocomposites also changed, accompanied by a moderate change in modulus rather than an abrupt change. There also was a general agreement in the literature that the exfoliated systems had better mechanical properties than those of the intercalated systems, especially in the modulus of elasticity of the polymer matrix[173].

In this research, the decrease in the tensile strength at break should be because of the silicate agglomerates and the reduced extent of the dispersion ability of the individual layered silicates into the IPN matrix. The latter is also a key factor of an improvement in the modulus of elasticity, discussed in the above paragraph. The TEM micrographs showed that the intercalated silicate layers spread out with only a rare amount of delaminated silicate layers. Therefore, a great improvement in the storage modulus was not achieved in the IPN systems studied here.

### 4.1.6 Hardness measurements.

Hardness was determined to complete the studies of mechanical properties. Generally, the hardness of a material relates significantly to its modulus of elasticity and viscoelastic properties[166]. The hardness of the 70PU/30PEMA IPN was also affected by the presence of the C20A organoclay as shown in figure 4.13.

Shore A hardness values exhibit a non-linear curve shape. As expected, by adding the C20A organoclay, the hardness of 70PU/30PEMA IPN significantly increases from Shore A 60, observed for the IPN, to Shore A 70 at 15 wt% clay content, indicating that the IPN nanocomposites are more stiff than the unfilled IPN. Thus, this behaviour is similar to the modulus of elasticity, since, in general, the hardness is directly related to the modulus of elasticity[165].

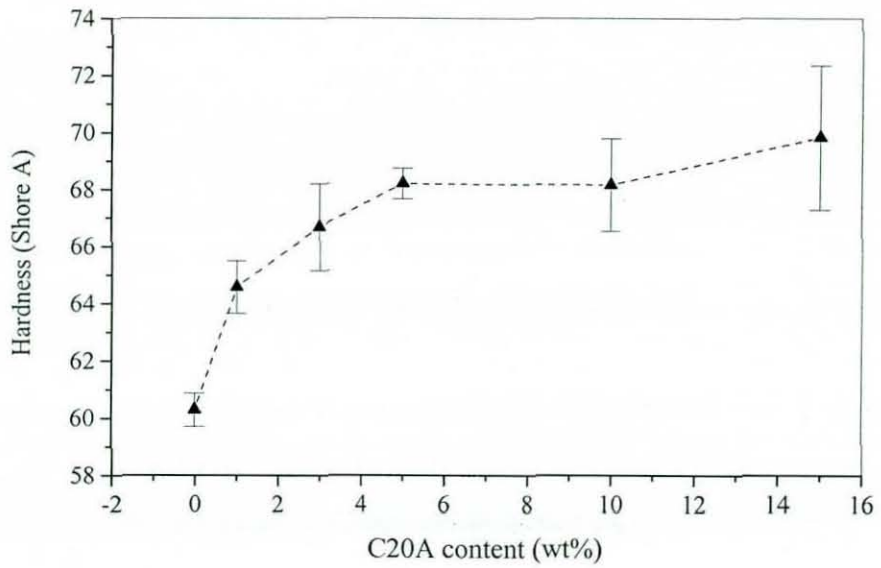


***Figure 4.13*** Shore A hardness values of the IPN organoclay nanocomposites as a function of C20A clay loading.

**4.2 Study of homopolymer PU and PEMA organoclay nanocomposites.**

After having examined the influences of C20A organoclay on the damping properties, morphology, thermal and mechanical properties of the 70PU/30PEMA IPN organoclay nanocomposites, showing the variation of C20A has significantly influenced its damping properties, especially, it was worth to determine the effect of C20A organoclay on the PU and PEMA homopolymers. Thus, the C20A organoclay was incorporated into each of the homopolymers by using an in-situ polymerisation method with the various amount of C20A, i.e. 1%, 3%, 5%, 10% and 15% by weight.

### 4.2.1 PU nanocomposites.

PU-organoclay nanocomposites were prepared by the following general procedure. The C20A organoclay was added and homogenously mixed with PPG 1025 in the desired proportions with a Silverson L2R mixer, at room temperature. The crosslinker, TMP, was added into the mixture and then the mixture was kept under vacuum at 60°C for 60 minutes to completely dissolve the solid TMP. After that the mixture was allowed to cool down to room temperature in a desiccator. Then, the diisocyanate, TMXDI, in the desired amount and the catalyst, SnOct, 0.2 wt%, were added and mixed together by a conventional laboratory stirrer at room temperature for 3 minutes. After being degassed for 60 seconds under vacuum, in order to remove any air bubbles entrapped during the mixing process, the mixture was introduced into a tin mould, which had been sprayed with silicone mould release agent. Then, the filled mould was left in an air oven for 24 hours at 60°C, 24 hours at 80°C, and finally 24 hours at 90°C in order to complete the reaction.

The morphology of the PU-organoclay nanocomposite specimens were investigated by dynamic mechanical and physical properties, with a number of characterisation techniques, i.e., dynamic mechanical thermal analysis, modulated-temperature differential scanning calorimetry, and hardness measurements. As shown and discussed in the section 4.1, the WAXD results showed that the polyol molecules intercalated into the silicate galleries showing an increased interlayer distance of the silicate layers from 2.29 to 3.92 nm. The TEM results also revealed partial intercalation and only a small amount of exfoliation. Non-uniform dispersion of the silicate layers was observed in the 70PU/30PEMA IPN organoclay nanocomposites. Therefore, it can be concluded that intercalated PU-organoclay nanocomposites had been synthesised. The other characterisation techniques are shown and discussed further in the following sections.

**Dynamic mechanical thermal analysis.**

DMTA was used to examine the influences of organoclay on the dynamic mechanical properties of the PU-organoclay nanocomposites. The resulting loss factor, storage

modulus and loss modulus spectra of PU-organoclay nanocomposites are illustrated in Figures 4.14 to 4.16. The dynamic mechanical properties are summarised in Table 4.4.

The glass transitions obtained from the maximum values of tan delta peaks versus the organoclay content plots for PU-organoclay nanocomposites show only a single peak for all specimens. The pure PU shows a very strong and narrow transition at -15°C. Incorporation of 1 wt% organoclay, the transition reveals no change. Further increase in the C20A content brings the transition to higher temperature of -14°C and remains at -14°C, even after increasing the C20A up to 10 wt%. However, the tan δ max value at Tg gradually decreased as the clay content increased. At 10 wt%, the tan delta max value is reduced from 1.21 for the pure PU to 0.96. Nevertheless, the small change of only one degree temperature certainly is within the experiment error range. Thus, the influence of the organoclay, C20A, on the PU transition is quite insignificant, while it significantly affects the tan delta max value at the PU Tg. Moreover, temperature range at which the peak width of tan $\delta \geq 0.3$ is evidently broader at the higher clay content. The lower loss factor peaks could be due to the restricted mobility of chain segments as the clay content increased.

***Table 4.4*** Dynamic mechanical properties of the PU-organoclay nanocomposites.

| C 20A (% wt) | Tg at tan δ max (°C) | Tan δ max value at Tg | Peak width tan $\delta \geq 0.3$ (°C) |
|---|---|---|---|
| unfilled | -15 | 1.21 | -28 ↔ 18 (46) |
| 1% | -15 | 1.12 | -30 ↔ 31 (61) |
| 3% | -14 | 1.05 | -28 ↔ 39 (67) |
| 5% | -14 | 1.04 | -30 ↔ 42 (72) |
| 10% | -14 | 0.96 | -30 ↔ 62 (92) |

Wang and Pinnavaia[130] synthesised intercalated nanocomposites based on elastomeric polyurethanes by using an organo-montmorillonite modified with protonated

dodecylamine or octadecylamine. They found that the tan δ peak was broadened as the nanoparticle content increased, which resulted from the changed motion of polymers at the clay-polymer matrix interface. A similar result was obtained by Yao et al.[182], who studied polyurethane/$Na^+$- montmorillonite nanocomposites.

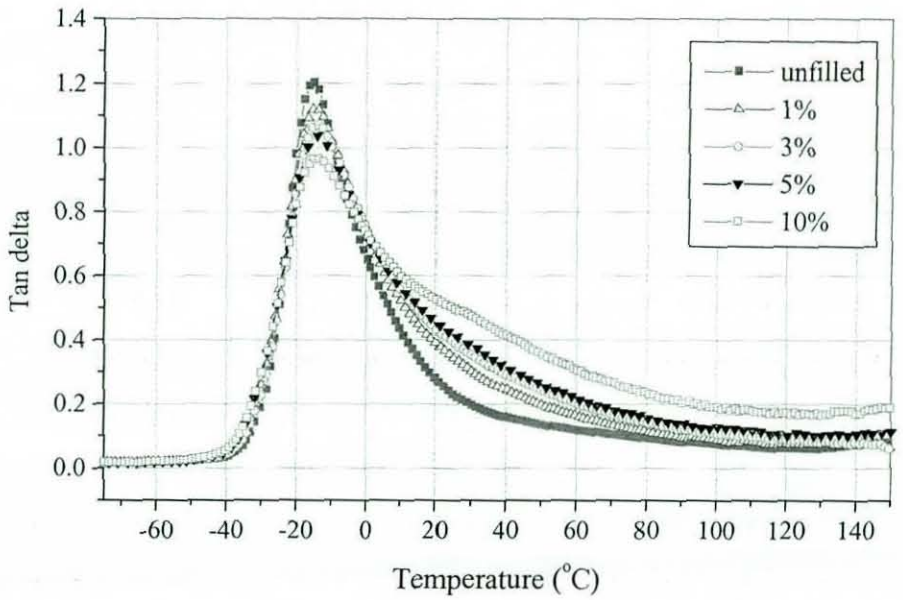


***Figure 4.14*** Loss factor versus temperature plots for the PU-organoclay nanocomposites: 0, 1, 3, 5 and 10 wt% C 20A.

As shown in Figure 4.15, the storage modulus of the PU polymer slightly increases in the glassy state, whilst a significant decrease of the storage modulus is revealed in the rubbery state, as increasing the organoclay content. It also shows that the slope of the storage modulus values versus temperature gradually reduces with an increase in the loading of layered organoclay, indicating compatibility mixing of PU and organoclay particles. The increase of the storage modulus at the glassy state is the typical nature for the filled polymer systems[191,192]. A probable explanation for the reduction of the storage modulus at the rubbery plateau is a reduced amount of diisocyanate in the matrix since some of it may be intercalated in the clay layers, resulting in a lower hard segment content in the PU matrix, and consequently, a lesser degree of cross-linking between the diisocyanate units in the hard segments, which normally play an important role of physical cross-links and acts as a high modulus filler[139,142,193].

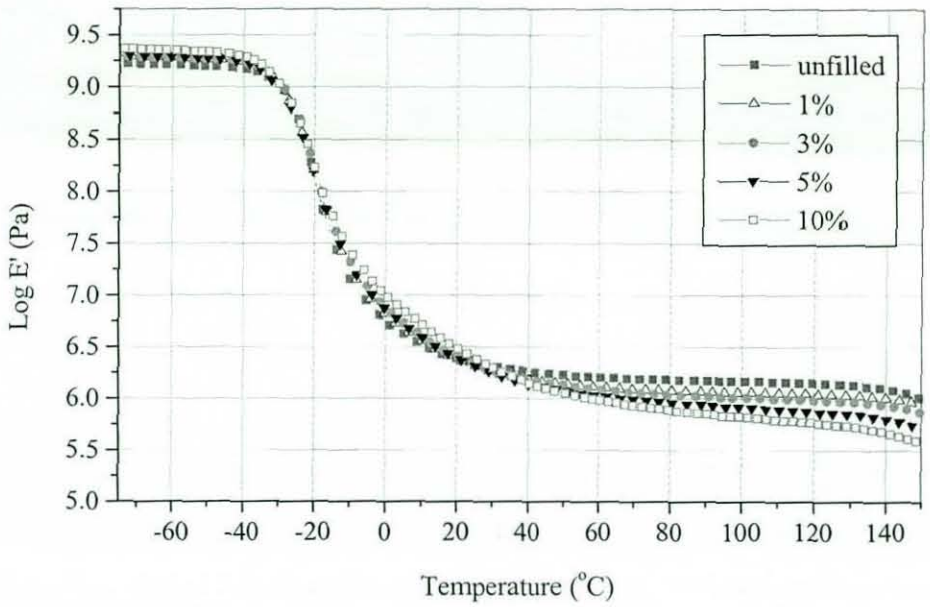


***Figure 4.15*** Storage modulus versus temperature plots for the PU-organoclay nanocomposites: 0, 1, 3, 5 and 10 wt% C 20A.

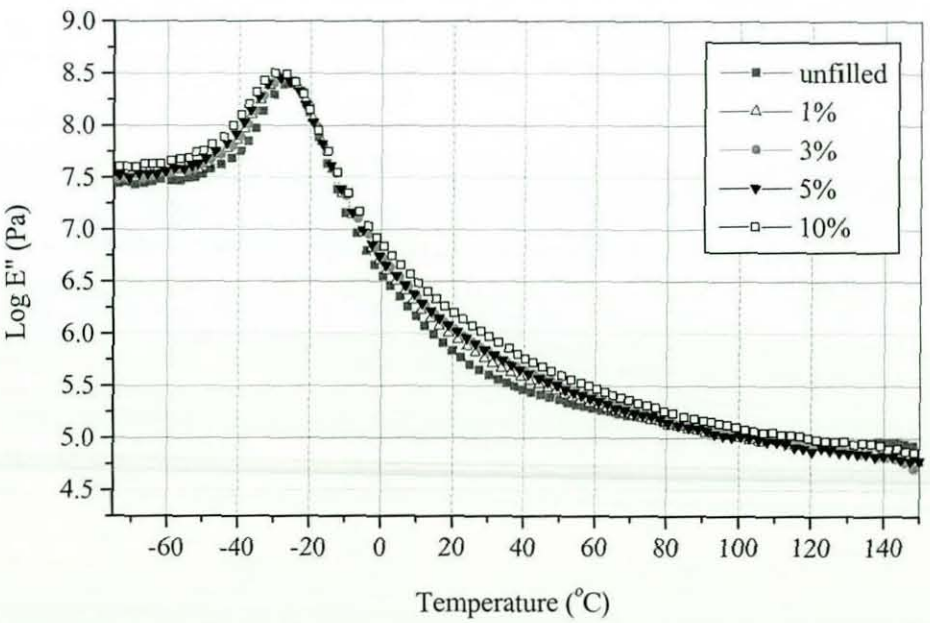


***Figure 4.16*** Loss modulus versus temperature plots for the PU-organoclay nanocomposites: 0, 1, 3, 5 and 10 wt% C 20A.

As can be seen in Figure 4.16, the introduction of organoclay into a PU matrix, firstly, does not effect the glass transition of PU and the loss modulus value at the PU Tg. Secondly, in the glassy stage and also around room temperature, the loss modulus of PU nanocomposites increases considerably in comparison with that of the pristine PU, indicating the effect of the stiffer silicate particles.

Tien et al.[194] studied the effect of nano-sized silicate layers on the glass transition, dynamic mechanical behaviour and thermal degradation of a segmented polyurethane. They found that there was no change in the soft-segment Tg, compared with that of the pure PU, as the amount of swelling agent (organic cation molecules used to replace the metal cations in the intergallery of the silicates), modified by trihydroxyl groups, increased. While, the hard-segment Tg, increased with the amount of swelling agent. They proposed that the hydroxyl groups of the swelling agent reacted with the isocyanate groups of the prepolymer during the synthesis, resulting in a tethering of the silicates onto the PU molecules. Moreover, the urethane bonds in the hard segments could form hydrogen bonding with the dangling hydroxyl groups on the surface of the silicates. Consequently, the dramatic improvement in the storage modulus exhibited at 3 wt% of swelling agent. With further addition of the swelling agent, the storage modulus decreased because of the poorer dispersion of montmorillonite in these PU nanocomposites[195].

**Modulated-temperature differential scanning calorimetry.**

M-TDSC was performed to study the effect of C20A organoclay on the thermal behaviour of the PU. Figure 4.17 shows the differential of heat capacity, dCp/dT, of the PU versus temperature at increasing silicate loading. It can be seen that the presence of organoclays is quite insignificant to the glass transition temperature in any of nanocomposites, showing it almost to be independent of the addition of C20A. This may be because M-TDSC can not detect the glass transition temperature of the polymer chains which are located near the silicates. Therefore, the measured glass transition temperatures are those belonging to the soft-segments which are far away from the silicates and they are the same as that of the bulk polyurethane[196]. On the other hand, the dCp/dT value gradually reduces with increasing C20A. This behaviour

might be attributed to the lesser amount of polyol to participate during the glass transition, because some polyol chains are intercalated and were confined strongly between the silicate layers. Thus, the value of ΔCp decreased because of the incorporation of the organoclay. An estimated weight fraction, ω, of the polyether polyol chains intercalated in the layered silicates can be calculated by a simple equation[197] shown below.

$$\omega = 1 - \Delta C_p(\text{polyol in nanocomposites}) / \Delta C_p(\text{polyol in PU}) \quad (4.1)$$

The values of $\Delta C_p$ for the pure PU and the PU-organoclay nanocomposites with clay content of 1, 5 and 10 wt% are found to be 0.56, 0.53, 0.50 and 0.44 $Jg^{-1}{}^{o}C^{-1}$, respectively. According to the equation (4.1), the ω values are 5, 11 and 21%. Therefore, the polyether polyol molecules have intercalated between the silicate layers into a systematic extent with increasing the organoclay content.

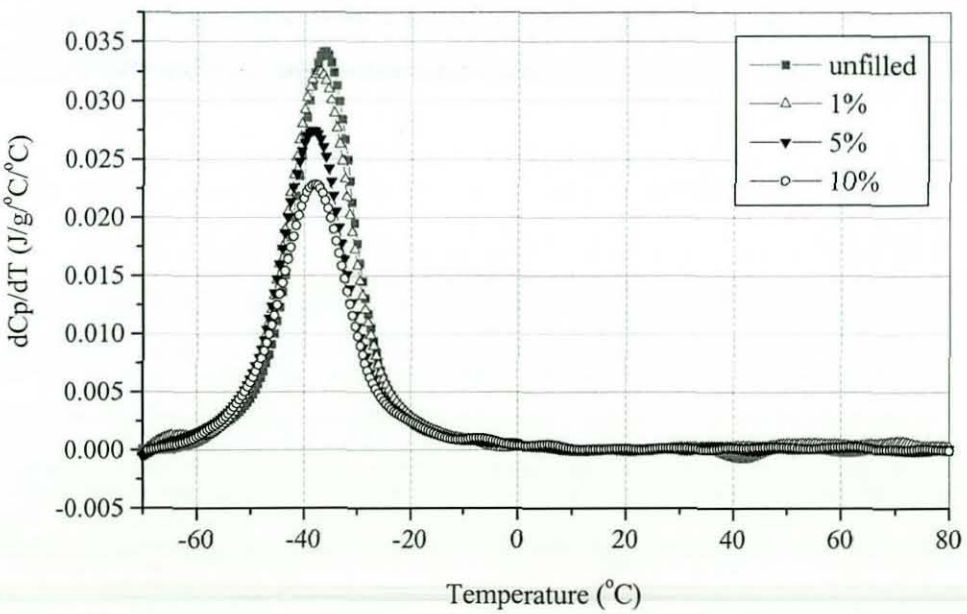


***Figure 4.17*** Differential heat capacity versus temperature plots showing the effect of organoclay content on the PU-organoclay nanocomposites.

Moon et al.[198] reported that there was no significant changes in the glass transition and melting temperatures of the polyurethane and polyurethane/montmorillonite nanocomposites, prepared via in-situ polymerisation from highly crystalline poly(butylene succinate)/poly(ethylene glycol) polyols and 4, 4′-dicyclohexylmethane diisocyanate. The same result was found by Tien and Wei[196], who studied PU/MMT nanocomposites from poly(tetramethylene ether) glycol, PTMEG, polyol and 4, 4′-diphenylmethane diisocyanate.

**Tensile behaviour.**

The influences of C20A organoclay on the tensile phenomena of the PU polymer are listed in Table 4.5. Figure 4.18 illustrates the tensile properties: modulus of elasticity, tensile strength and elongation at break versus the C20A clay content.

***Table 4.5*** Measured values of maximum tensile strength, extension at break, and modulus of elasticity for the PU-organoclay nanocomposites.

| Clay content (wt%) | Tensile strength (MPa) | Extension at break (%) | Modulus of elasticity (MPa) |
|---|---|---|---|
| unfilled | 1.20 ± 0.17 | 586 ± 130 | 0.65 ± 0.03 |
| 1% | 1.00 ± 0.05 | 555 ± 29 | 0.48 ± 0.03 |
| 3% | 1.14 ± 0.12 | 689 ± 69 | 0.48 ± 0.02 |
| 5% | 1.02 ± 0.06 | 1,110 ± 66 | 0.24 ± 0.04 |
| 10% | 1.66 ± 0.43 | 1,390 ± 227 | 0.39 ± 0.03 |

As seen in Figure 4.18, the tensile strength does not show any significant change when C20A clay was added up to 5 wt%. Further increase in the clay content to 10 wt%, the tensile strength significantly increases from a value of 1.20 MPa, observed for the unfilled PU, to a value of 1.66 MPa. The extension at break reveals a similar tendency as the tensile strength. The increase in the elongation at break shows at organoclay contents greater than 3 wt% C20A.

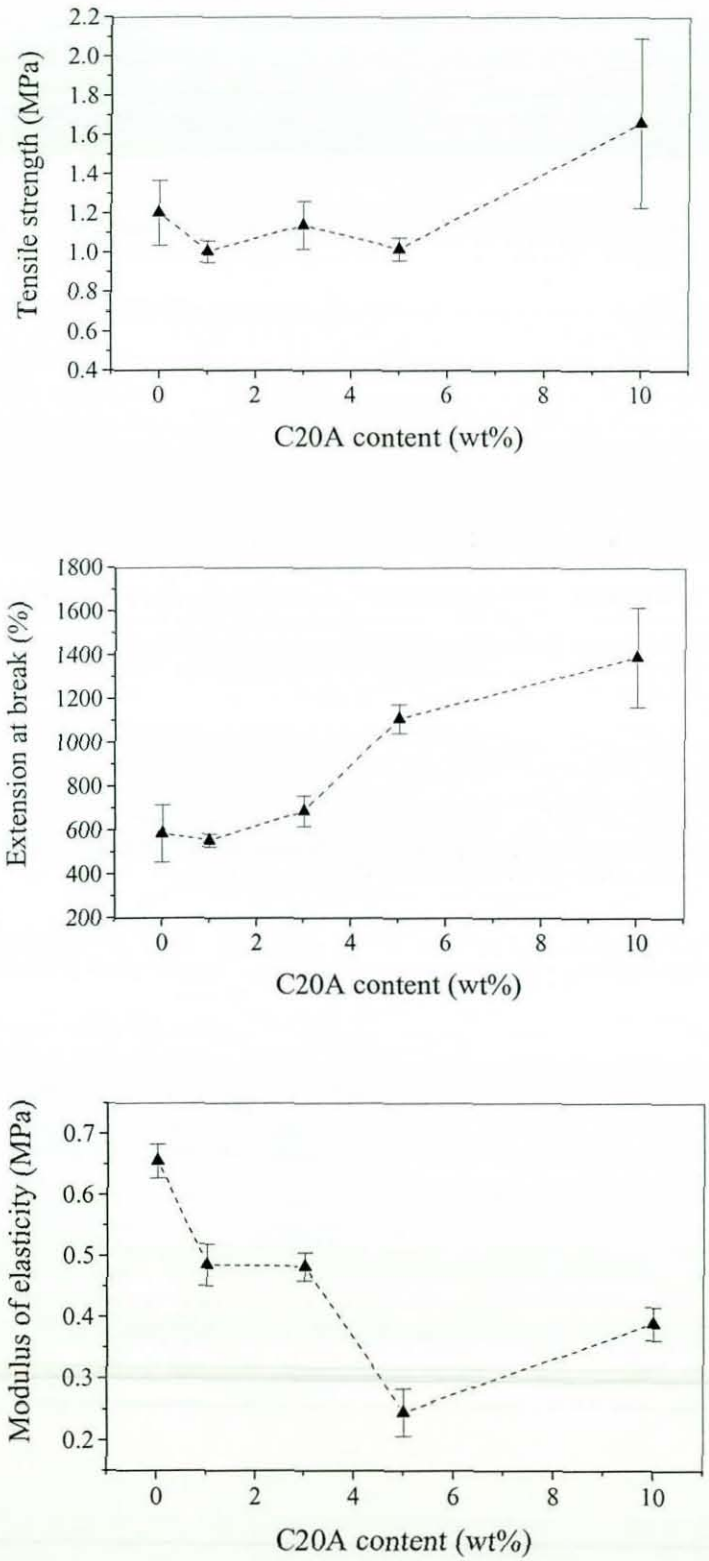


***Figure 4.18*** Tensile properties of the PU-organoclay nanocomposites as a function of C20A clay loading.

Modulus of elasticity, on the other hand, decreases significantly with increased C20A clay content, until it reaches the lowest point at 5 wt% clay. However, 1 and 3 wt% clay have essentially the same modulus values. On further addition of clay, the modulus of elasticity rises again.

The large increase in the elongation at break is probably because of the interfacial interaction between the organic modified silicate surface and the PU matrix, where the modifying ions contributed to the dangling chain formation in the PU matrix and causes a plasticising effect in the polyurethane[195]. Thus, the tensile strength and the elongation at break of PU nanocomposites increases simultaneously. The decreases in the storage moduli, encountered when increasing the content of organophilic layered silicates, may be caused by the reduced amount of diisocyanates and polyols in the matrix since some of them are intercalated in the clay layers, resulting in a lower degree of cross-linking between the diisocyanates themselves in the hard segments. Consequently, a lower storage modulus value results[199]. With further addition of organoclay at more than 5 wt%, the storage modulus increases, acting as a conventional filled system, since the silicate particles are normally many times more rigid than polymers. In addition, an increase in modulus can be obtained by the restricted mobility of polymer chains which were trapped in the aggregates. Subsequently, they are less free to react to stress than those in the continuous phase.

**Hardness measurements.**

The mechanical properties of the PU nanocomposites were also examined by hardness testing. The results are plotted in Figure 4.19.

As can be seen in Figure 4.19, increasing the C20A clay content results in a gradual decrease in hardness from Shore A 20, as measured from the unfilled, to an undetectable value for the 5 wt% clay content. Further increase in the C20A clay content up to 10 wt%, increases Shore A to 3. The hardness relates directly to the modulus of the material. The same behaviour is also shown by the bending storage modulus, E′, results, as shown in Figure 4.15. At the hardness measuring temperature, 22°C±1°C, the hardness values gradually decrease as the C20A clay content increases

to 5 wt%. For 10 wt% content, the hardness value goes up again. The reduction in hardness with clay loading could be attributed to the lesser amount of diisocyanate and polyol reacted in the polymer matrix, since some of them may be intercalated between the clay layers, as mentioned before, resulting in a lower degree of crosslink density. Again, as the loading of clay increases to more than 5 wt%, the polymer composite acts as a conventional polymer composite, showing an increase in the storage modulus and hardness values.

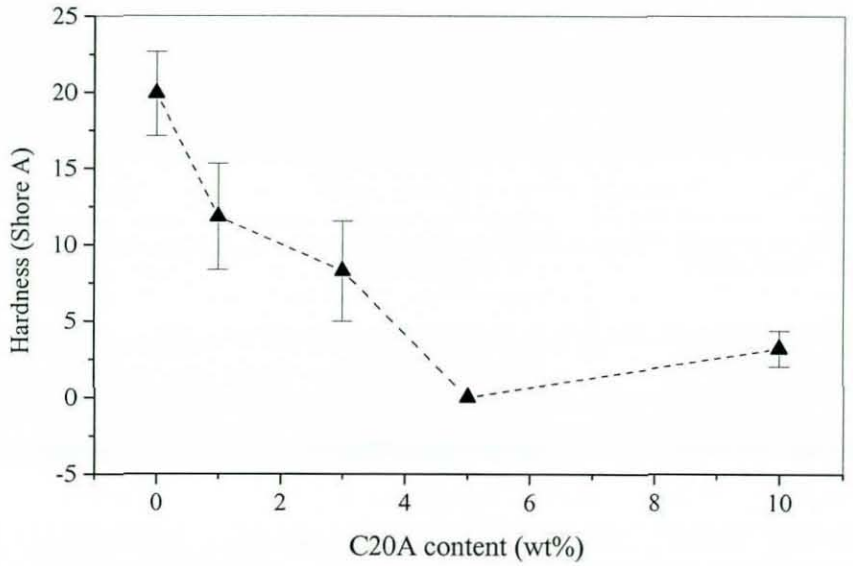


***Figure 4.19*** Shore A hardness values of the PU-organoclay nanocomposites as a function of clay loading.

### 4.2.2 PEMA nanocomposites.

PEMA organoclay nanocomposites were prepared by the following general procedure. The C20A organoclay, in the desired amount, was added into the mixture of EMA monomer, TEGDM crosslinker and AIBN initiatior. Then the mixture was homogenously mixed by a conventional laboratory stirrer at room temperature for 30 minutes. After degassing in a vacuum oven at room temperature for 60 seconds to get rid of any air bubbles entrapped during mixing process, the final mixture was poured into a steel mould which had been sprayed with a silicone release agent and then the filled mould was place into an open air oven for curing at 60°C, 80°C and 90°C for 24

hours per each stage to cure completely. Note that the PEMA nanocomposite samples were very difficult to make in large specimens because the initial viscosity was very low. Consequently, the final mixture poured into the steel mould leaked past the nitrile rubber sealing ring.

The effect of the C20A clay on the PEMA glass transition temperature, damping and mechanical properties were characterised by several techniques as follows.

**Wide angle X-ray diffraction.**

The resulting of WAXD patterns for organoclay based PEMA for 0, 1 and 15 wt% C20A are shown in Figure 4.20.

Again, the X-ray diffraction data were collected from both sides of cast samples to verify homogeneous distribution of the organoclay particles. WAXD patterns for both sides of C20A organoclay-filled PEMA at 1 and 15 wt% C20A clay are shown in Figure 4.20. Three diffraction peaks are observed in the diffraction patterns of 15 wt% C20A clay content, which reveals at 2θ angle of 2.32°, ($d_{001}$), corresponding to an interlayer spacing of 3.81 nm and the secondary diffraction, ($d_{002}$), and the third diffraction, ($d_{003}$), at 4.65° and 6.94° respectively. The intensity of the bottom diffraction peaks is higher than that of the top ones for both the studied specimens, indicating that the organoclay particles tend to settle down to the bottom side during the polymerisation process. Besides, the intensity difference between the top and bottom of the diffraction peaks are systematically decreased with the amount of clay loading. As the same phenomena was shown in the 70PU/30PEMA organoclay IPNs, only the bottom surface of the cast samples will be used for further discussion.

The resulting WAXD patterns for C20A organoclay, pure PEMA, and C20A organoclay-filled PEMA for 1 and 15 wt% C20A are also shown in Figure 4.20. No diffraction peak was present in the pure PEMA, because it is an amorphous composite. Only one diffraction peak is observed in the C20A organoclay at 3.85° corresponding to the first diffraction of the interlayer spacing of 2.29 nm. After in-situ intercalative polymerisation with the pure EMA, the diffraction peak has shifted towards lower

angle value of 2.32° corresponding to the plane (001) of the interlayer spacing of 3.81 nm, which indicates that the PEMA molecules are intercalated between the clay nanolayers. The higher clay content, 15 wt%, reveals the higher intensity of the basal diffraction peak. The polar character of the ethyl methacrylate ester, which contains a –CO–O– functional unit, has not showed any significant change on its intercalation with the modified silicate, C20A clay, as compared with that of the PU polymer. It is clear that the variation of amount of C20A has no effect on the intercalation of PEMA into the clay galleries, indicating that the PEMA molecules do not totally disturb the layer structure of the silicate crystallites.

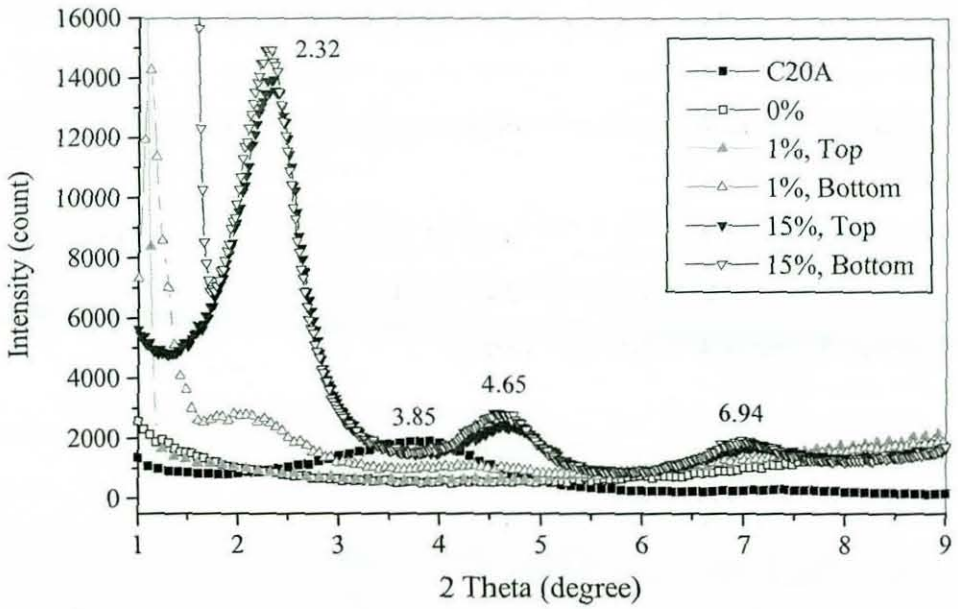


***Figure 4.20*** WAXD patterns for pure C20A clay, pure PEMA and the top and bottom sides of C20A organoclay-filled PEMA containing 1 and 15 wt% C20A.

Fang et al. [200] found a similar result. They synthesised poly(methyl methacrylate)/organophilic montmorillonite, (PMMA)/OMMT, nanocomposites via γ-ray irradiation polymerisation. They found that the nanolayered silicates were orderly dispersed in the matrix at 3 wt% OMMT. When the amount of OMMT increased to 10 wt%, there was no further distinct shift of the X-ray diffraction peak, indicating that

the amount of the OMMT did not affect the distance between the sheets of the PMMA/OMMT. Tabtiang et al.[201] also reported a similar trend for WAXD results.

**Transmission electron microscopy.**

TEM images of the PEMA nanocomposites containing 15 wt% of C20A clay are shown in Figures 4.21 and 4.22.

The TEM analysis tends to support the findings from WAXD, but also shows that the clay is well dispersed at the microscale in this system. At low magnification, the TEM image shows widely dispersed C20A organoclay throughout the PEMA matrix in large and unevenly dispersed primary clay tactoids. While, the highly magnified TEM image shows an intercalated tactoid structure. The clay layers are tightly held together. No sign of single layers is observed. Therefore, the system presented here only shows intercalation.

**Dynamic mechanical thermal analysis.**

DMTA was used to examine the influences of organoclay on the dynamic mechanical properties of the PEMA organoclay nanocomposites. Figures 4.23 to 4.26 show the resulting loss factor, storage modulus and loss modulus spectra of the PEMA organoclay nanocomposites. These dynamic mechanical properties are summarised in Table 4.5.

***Table 4.5*** Dynamic mechanical properties of PEMA organoclay nanocomposites.

| % wt C 20A | Tg at tan δ max (°C) | Tan δ max value at Tg | Peak width tan δ ≥ 0.3 |
|---|---|---|---|
| unfilled | 100 | 1.09 | 67 ↔ 134 (67) |
| 3% | 105 | 0.99 | 75 ↔ 137 (62) |
| 10% | 107 | 0.86 | 77 ↔ 143 (66) |
| 15% | 109 | 0.77 | 82 ↔ 150 (68) |

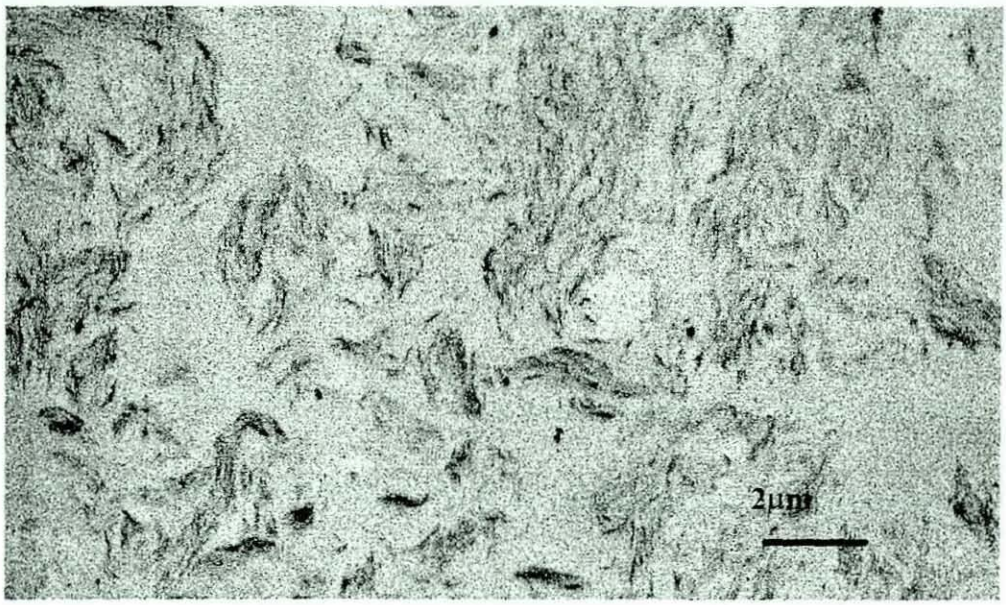


***Figure 4.21*** TEM micrographs for the PEMA organoclay nanocomposites with 15 wt% C20A clay at 3000 magnification.

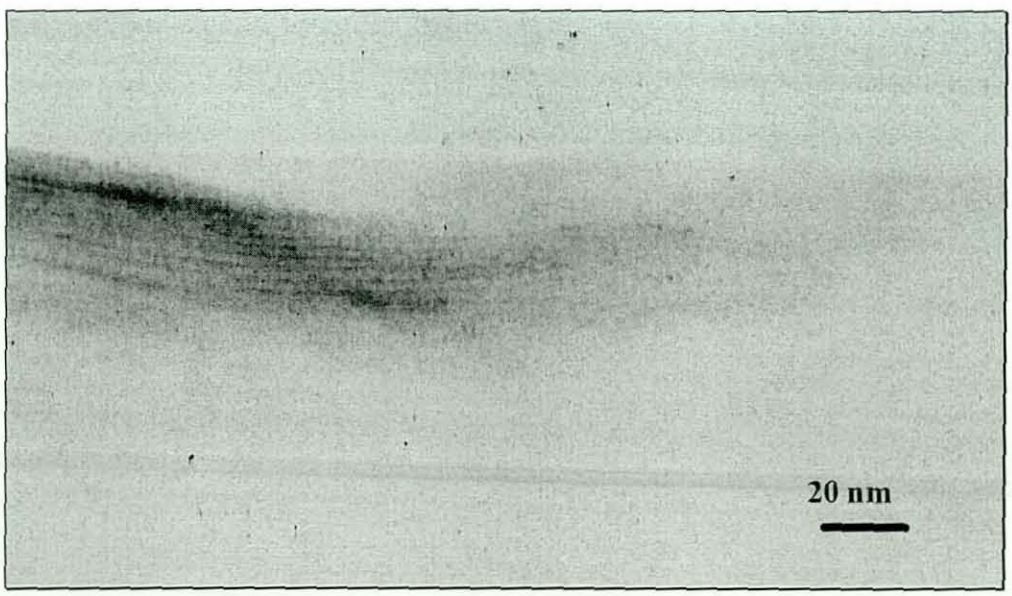


***Figure 4.22*** TEM micrographs for the PEMA organoclay nanocomposites with 15 wt% C20A clay at 200k magnification.

The glass transitions obtained from the maximum values of tan delta peaks versus the organoclay content plots for PEMA organoclay nanocomposite show only a single peak for unfilled and 3 wt%-filled specimens. Adding more C20A clay shows a main peak and a shoulder peak. The pure PEMA shows a very strong transition at 100°C. Incorporation of organoclay gradually shifts the transition up to 109°C at the C20A content of 15 wt%, as shown in Figure 4.23. This is attributed to an increasing number of interactions in the interphase between the silicate and PEMA matrix, as the clay loading increased. However, the tan δ max value at Tg gradually decreased as the clay content increased. At 15 wt%, the tan delta max value is lowered from 1.09 for the pure PEMA to a value of 0.77. Thus, the influence of the C20A organoclay is quite significant on the PEMA transition and the tan delta max value at the PEMA Tg, by decreasing the tan δ max value at the glass transition as the C20A content increased. The shoulder, which appeared when the clay loading was added more than 3 wt%, could be caused by a portion of the PEMA chains which were constrained between the clay galleries. This phenomenon is more obvious at the higher clay contents. Again, the lower loss factor peaks could be due to the limited mobility of chain segments as the clay content increased.

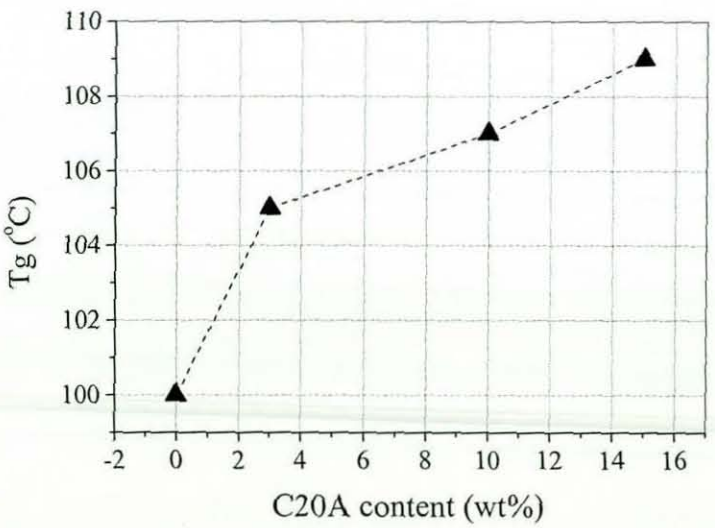


***Figure 4.23*** Glass transitions for the pure PEMA and the PEMA organoclay nanocomposites.

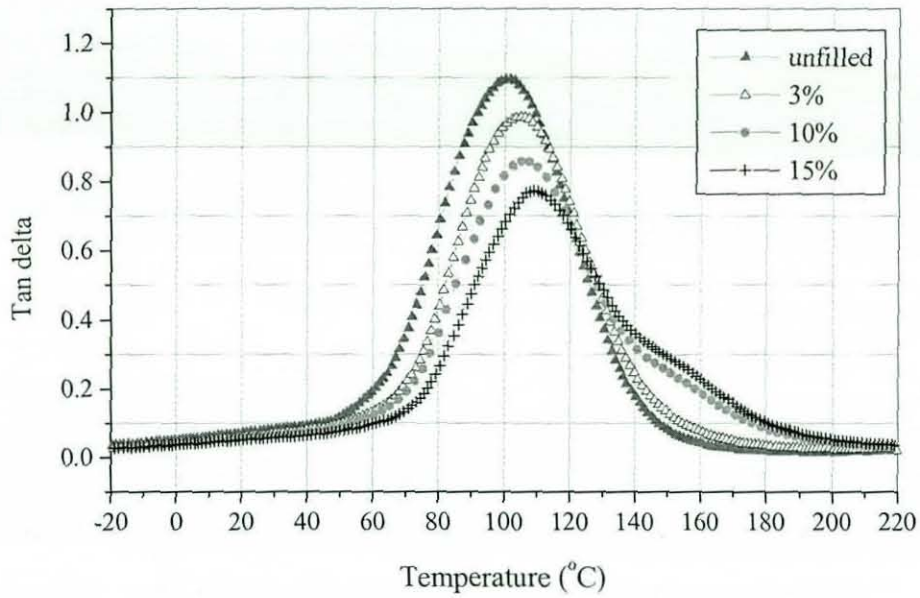


***Figure 4.24*** Loss factor versus temperature plots for the PEMA organoclay nanocomposites: 0, 3, 10 and 15 wt% C 20A.

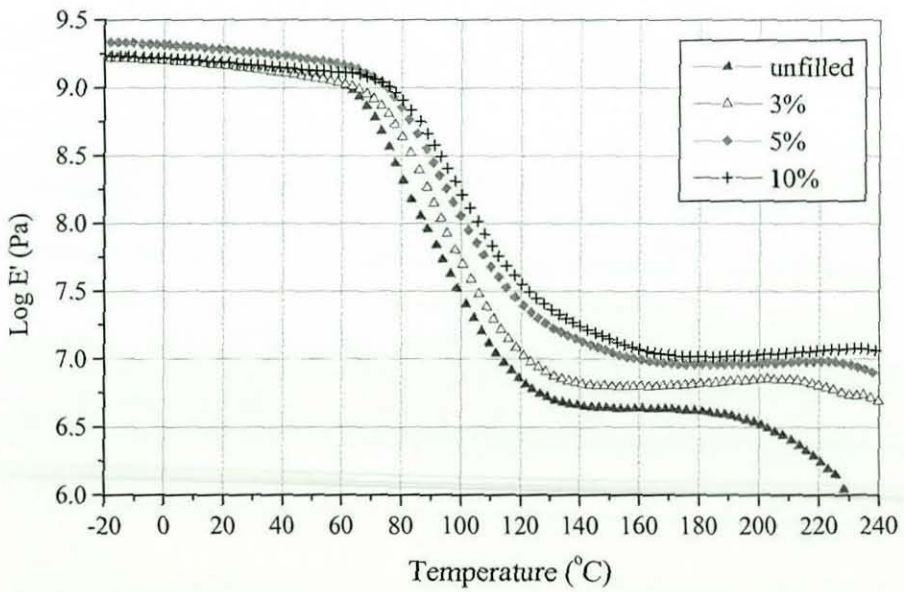


***Figure 4.25*** Storage modulus versus temperature plots for the PEMA organoclay nanocomposites: 0, 3, 10 and 15 wt% C 20A.

The storage and loss moduli gradually increase as clay loading increased above the PEMA transition temperature range in this study. Meanwhile, there is no significant change below the glass transition range. The increment in those moduli is due to the difference in modulus between the polymer matrix and the clay filler. The polymer modulus changes, while that of layered silicates remains rigid throughout the entire temperature range. Moreover, this might partly be because when the content of the silicate layers increased there are plentiful physical crosslinking sites formed, strengthening the interaction between the organoclay and PEMA chains.

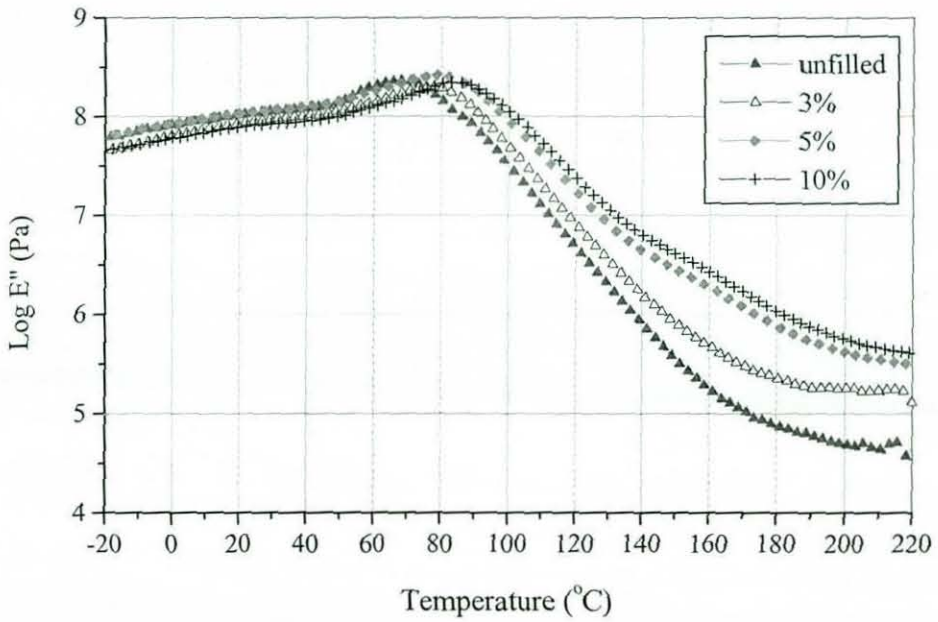


***Figure 4.26*** Loss modulus versus temperature plots for the PEMA organoclay nanocomposites: 0, 3, 10 and 15 wt% C 20A.

Xie et al.[202] studied the influence of a silicone coupling agent on the structure and properties of poly(methyl methacrylate)/montmorillonite, PMMA/MMT, nanocomposites prepared by in-situ bulk polymerisation. They found that the modification of MMT with the silicone coupling agent did not affect the intercalation of the polymer chains, but showed that the dispersion of clay in nanocomposites was more ordered than that in nanocomposites with unmodified organophilic MMT. DSC and TGA analyses showed great improvements in the thermal properties. There was a

6-15°C increase in the Tg and a 100-120°C increase in the thermal decomposition temperature for the nanocomposites as compared to those of the pure PMMA.

### 4.3 Influence of PU/PEMA composition ratio.

The composition ratio is one of the crucial factors that influence the IPNs properties as discussed in section 2.1.3. In this section, three composition ratios of PU/PEMA IPNs, 50PU/50PEMA, 70PU/30PEMA and 80PU/20PEMA, are reported. Similar to the 70PU/30PEMA IPN nanocomposites, the 50PU/50PEMA and 80PU/20PEMA IPNs, were prepared at a PPG1025/TMP ratio of 3:1, by using an NCO:OH ratio of 1.1:1.0 and 1.2 wt% SnOct in the PU component and 5% TEGDM in the PEMA component. 5 wt% of C20A organoclay was used in each preparation via the standard procedure route, in which the C20A clay, in the desired amount, was first mixed with the PPG1025. These materials were investigated via the various characterisation techniques in order to examine the effect of composition ratio on the damping and mechanical properties of these IPN materials. The results were shown and discussed below.

#### 4.3.1 Dynamic mechanical thermal analysis.

DMTA was used to investigate the influence of composition ratio of PU/PEMA on the dynamic mechanical properties of the PU/PEMA IPN organoclay nanocomposites. Figures 4.27 to 4.29 show the resulting bending loss factor, storage modulus and loss modulus spectra of these PU/PEMA IPN organoclay nanocomposites. The dynamic mechanical properties are summarised in Table 4.6.

As can be seen in Figure 4.27, no gross phase separation is observed for all PU/PEMA composition ratios, but the loss factors show phase separation to some extent for all the specimens. At 50PU/50PEMA, the PEMA Tg is clearly revealed, but the PU Tg is appearing as a shoulder. This may partly be explained by a plasticisation effect[203] of the layered silicates, which interact with the polyol and diisocyanate molecules, and, consequently, there may be an incompletely formed PU network[204], containing defects such as loose chain ends. The PU Tg is prominent, whereas the PEMA Tg is ambiguous and very difficult to position at the composition ratio of 80PU/20PEMA.

However, for the 70PU/30PEMA IPN, the difference in the loss factor value at PU and PEMA Tg, is not very high, indicating that it has a high level of an interphase component, which is formed from a micro-heterogeneous structure caused by phase separation. As expected, increasing the PU component ratio, the PU Tg significantly increases, subsequently, the tan delta max value increases. While, the tan delta max value at the PEMA Tg decreased as the PU component increased. The damping of the material, which can be implied by the peak width (tan delta value ≥ 0.3), shows that the 70PU/30PEMA reveals the highest temperature range of 151°C compared with the 50PU/50PEMA and 80PU/20PEMA, which exhibit values of 89° and 115°C, respectively. Thus, 70PU/30PEMA composition ratio could be a useful high damping material in this temperature range.

***Table 4.6*** Dynamic mechanical properties of PU/PEMA IPN organoclay nanocomposites with various composition ratios and 5 wt% C20A clay.

| Composition ratio (% PU/PEMA) | Tg at tan δ max (°C) | | Tan δ max value at Tg | | Peak width tan δ ≥ 0.3 (°C) |
|---|---|---|---|---|---|
| | PU | PEMA | PU | PEMA | |
| 50/50 | -27 | 78 | 0.12 | 0.91 | 29 ↔ 118 (89) |
| 70/30 | -13 | 82 | 0.36 | 0.58 | -20 ↔ 131 (151) |
| 80/20 | -10 | - | 0.52 | - | -24 ↔ 91 (115) |

The storage moduli versus temperature for these PU/PEMA IPN organoclay nanocomposites are shown in Figure 4.28. From these data, it appears that the PU/PEMA IPN organoclay nanocomposites have a semi-miscible morphology because the storage moduli do not show a clear two-step trend, which would be indicative of two-phase polymer blends. For the 70PU/30PEMA IPN, the storage modulus decreases in an almost linear pattern until it reaches the rubbery plateau, indicating a high degree of component mixing in this IPN. The 80PU/20PEMA reveals the lowest storage modulus around their homopolymer Tg range, as compared with the other two composition ratios. Surprisingly, the 70PU/30PEMA exhibits an even lower storage

modulus in the rubbery plateau region than 80PU/20PEMA. This is indicative of a lower apparent crosslink density in this material. This might probably be due to the fact that both networks are continuous, and they retarded the complete formation of the other. However, the 50PU/50PEMA shows the highest storage modulus beyond the PEMA Tg, owning to its higher content of the glassy component. Nevertheless, this material reveals a lower degree of mixing, as is seen in Figure 4.28

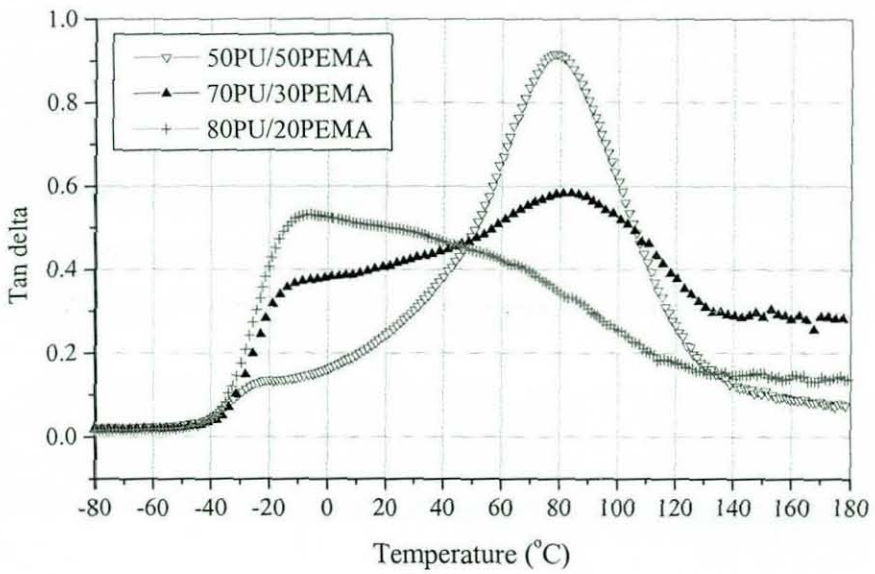


***Figure 4.27*** Loss factor versus temperature plots for the PU/PEMA IPN organoclay nanocomposites with various composition ratios: 50/50, 70/30 and 80/20, and 5 wt% C20A.

The loss moduli versus temperature plots confirmed that no gross phase separation exists as shown in Figure 4.29. Only one clear transition is observed for all IPN composition ratios. However, at 50PU/50PEMA, a broad spectrum with a clear shoulder, indicating some degree of phase separation.

### 4.3.2 Modulated-temperature differential scanning calorimetry.

M-TDSC studies were conducted in order to investigate further IPN miscibility and Tg behaviour of the PU/PEMA organoclay nanocomposites as the composition ratio varied.

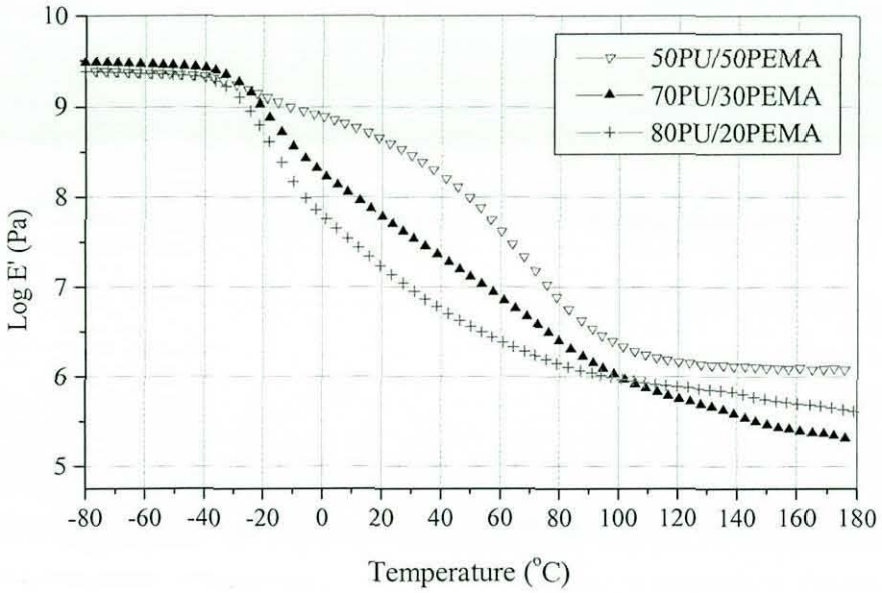


***Figure 4.28*** Storage modulus versus temperature plots for the PU/PEMA IPN organoclay nanocomposites with various composition ratios: 50/50, 70/30 and 80/20, and 5 wt% C20A.

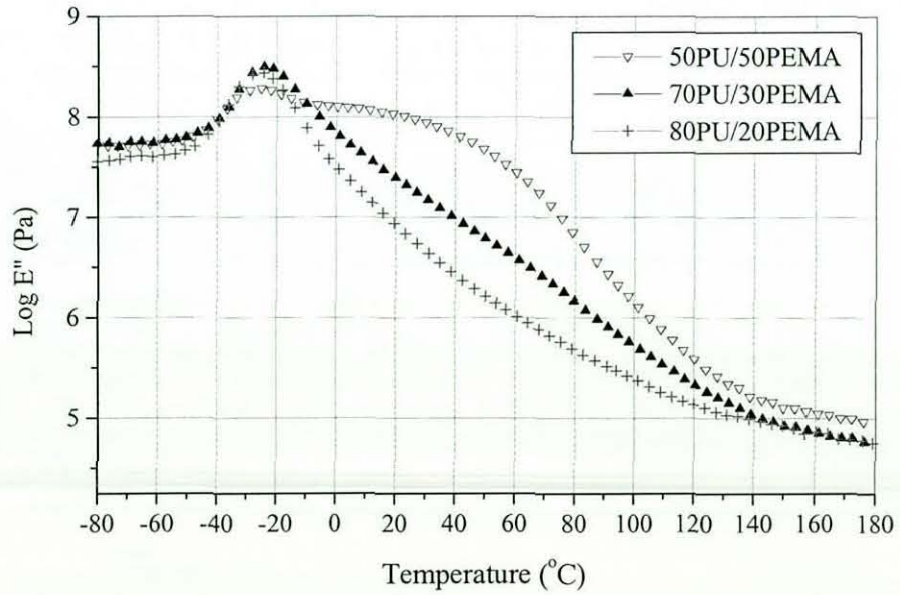


***Figure 4.29*** Loss modulus versus temperature plots for the PU/PEMA IPN organoclay nanocomposites with various composition ratios: 50/50, 70/30 and 80/20, and 5 wt% C20A.

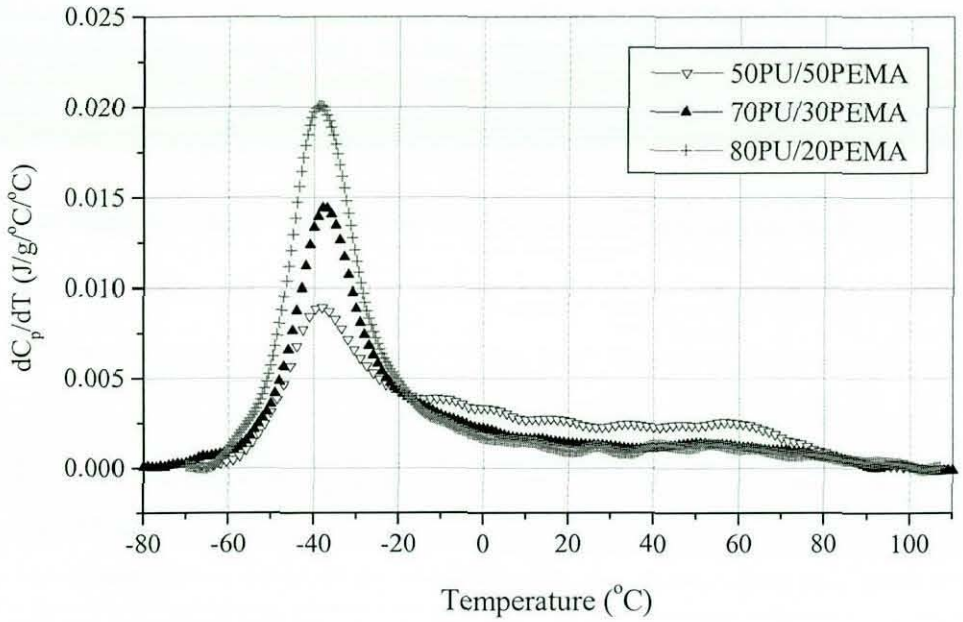


***Figure 4.30*** Differential heat capacity versus temperature plots showing the effect of composition ratio on the PU/PEMA IPN organoclay nanocomposites containing 5 wt% C20A clay.

The influence of the composition ratios on the PU/PEMA IPN organoclay nanocomposites with the addition of 5 wt% C20A is shown in Figure 4.30. As seen in the M-TDSC thermograms, the PU transitions remain at about the same location for all the composition ratios. At the composition ratios of 70PU/30PEMA and 80PU/20PEMA, the transition spectra are very broad and they are very difficult to assign the clear PEMA Tgs. At 50PU/50PEMA, the PU and the PEMA transitions are well defined at -39°C and 60°C, respectively, indicating a two-phase morphology. Also, this composition ratio reveals a high extent of component mixing. Thus, the M-TDSC measurement is one of the most sensitive to the phase separation. Hourston et al.[162] studied the Tg behaviour of PMMA/poly(styrene-co-acrylonitrile) blends. They found that differences in transition temperatures of the constituent polymers as small as 10°C could be readily resolved by using the M-TDSC technique.

### 4.3.3 Tensile behaviour.

The effect of composition ratio on tensile properties was studied. The tensile strength, extension at break, and the modulus of elasticity were calculated from the stress-strain measurements. The results are listed in Table 4.7. Figure 4.31 illustrates the tensile properties: modulus of elasticity, tensile strength and elongation at break versus the composition ratio.

***Table 4.7*** Measured values of maximum tensile strength, extension at break and modulus of elasticity for the PU/PEMA organoclay nanocomposites with variation of composition.

| Composition ratio, wt% PU/PEMA | Tensile strength (MPa) | Extension at break (%) | Modulus of elasticity (MPa) |
|---|---|---|---|
| 50/50 | 8.08 ± 0.51 | 133 ± 8 | 59.59 ± 2.77 |
| 70/30 | 3.89 ± 0.34 | 587 ± 41 | 5.67 ± 0.58 |
| 80/20 | 4.89 ± 0.33 | 982 ± 23 | 2.90 ± 0.14 |

As seen from the Figure 4.31, the tensile strength and modulus of elasticity decreased as the elastomer, PU, component increased. However the 70PU/30PEMA IPN showed a slightly lower value of the tensile strength than that of 80PU/20PEMA. The reverse effect is found for elongation at break.

The tensile strength for 50PU/50PEMA IPN organoclay nanocomposite is 8.1 MPa, which shows the highest value when is compared amongst the three composition ratios. From DMTA data, it was noted that the PEMA constitutes predominantly the matrix. The decrease to 3.9 MPa for the 70PU/30PEMA IPN is around a two-time decrease in the tensile strength. At this composition ratio, the DMTA data had the widest range of the tan delta value, indicating the highest extent of mixing. At 80PU/20PEMA, the tensile strength slightly increases up to 4.9 MPa. However, the increment is not very much, when is compared to that of the 70PU/30PEMA.

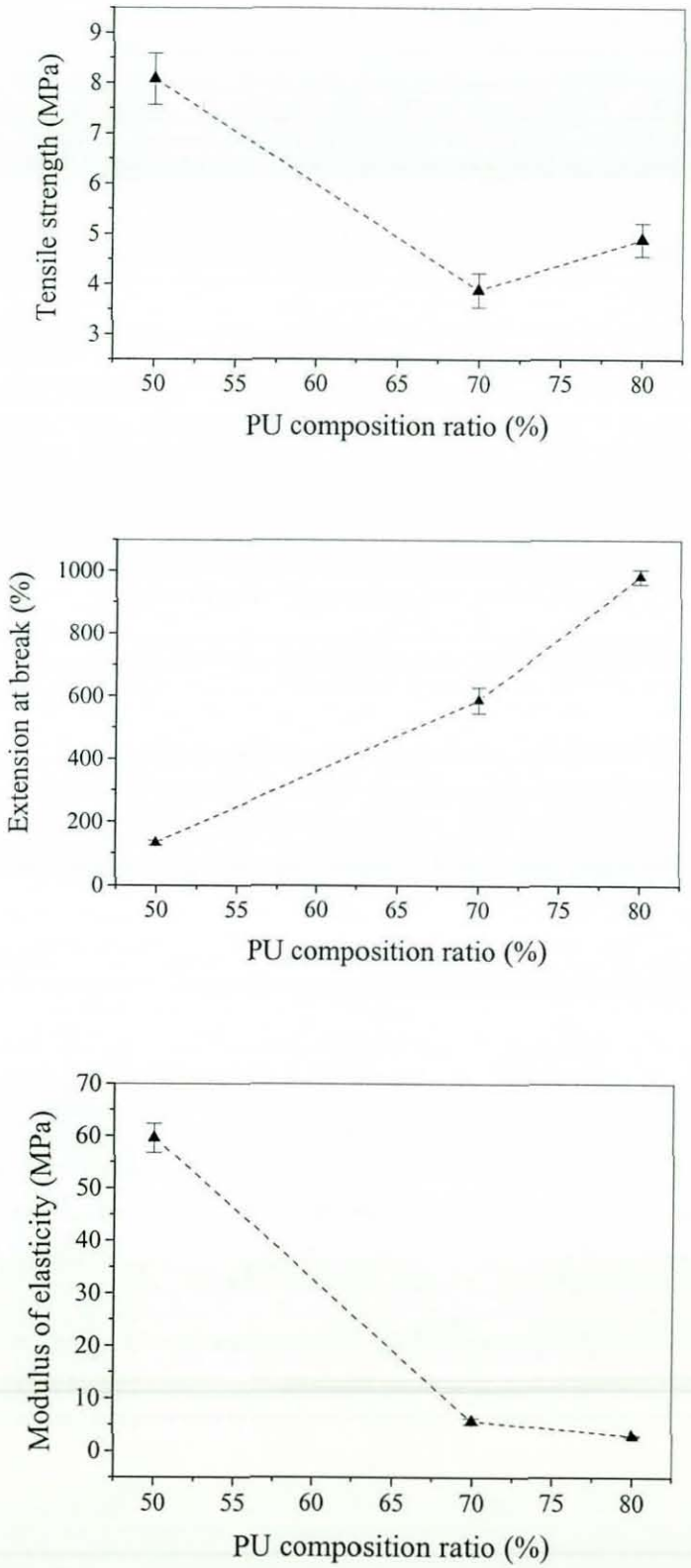


***Figure 4.31*** Tensile properties of the PU/PEMA IPN organoclay nanocomposites as a function of the composition ratio with 5 wt% C20A clay.

Modulus of elasticity shows the same trend as the tensile strength. A large decrease in the modulus of elasticity can be seen from the 50PU/50PEMA (59.6 MPa) to 70PU/30PEMA (5.7 MPa). A slight drop of the modulus was found as the PU constituent increased to 80% (2.9 MPa). On the other hand, data for extension at break shows the opposite trend. Greatly increased elongation at break is shown in the Figure 4.31. The extension at break is very low for the 50PU/50PEMA, at a value of 133%. The values rapidly go up to 587 % and 982% at the composition ratio of 70PU/30PEMA and 80PU/20PEMA, respectively, which are nearly four times and six times greater than that of the 50PU/50PEMA. These findings could be an indication of a change in IPN morphology from the PEMA predominant matrix at 50PU/50PEMA to the PU predominant matrix at the 80PU/20PEMA composition.

### 4.3.4 Hardness measurements.

Shore A hardness values versus IPN composition ratio as percentage of PU component are shown in Figure 4.32.

As was expected, by varying the composition ratio of an elastomer, PU, and the glassy polymer, PEMA, regardless of the fact that they included 5 wt% organoclay C20A, big changes in mechanical properties were observed. A corresponding pattern was revealed from the hardness measurements. As seen in Figure 4.32, a steep decrease in hardness is shown from 50PU/50PEMA towards 70PU/30PEMA composition ratio with values declining from Shore A 90 to 68. Further increase in the PU component shifts the value down to Shore A 50 for 80PU/20PEMA. This evidence supports the results from the DMTA and the tensile measurements, which indicates a change in the morphology of the IPN organoclay nanocomposites as the composition ratio was changed from the predominant glassy PEMA matrix, at the 50PU/50PEMA, to the predominant elastomer PU matrix, at the 80PU/20PEMA composite. Consequently, the properties of the IPN organoclay nanocomposites changed dramatically.

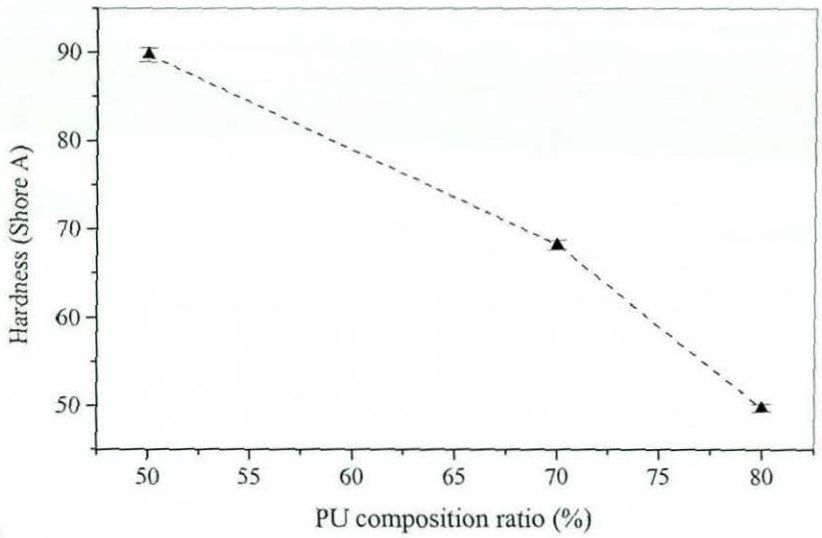


***Figure 4.32*** Shore A hardness values of the PU/PEMA IPN organoclay nanocomposites as a function of composition ratio and 5 wt% C20A clay.

**4.4 Influence of mixing time.**

Many studies[205,206] have found that one of the main issues in preparing good polymer matrix nanocomposite samples is a good dispersion of the nanoparticles in the polymer matrix. The in-situ polymerisation technique, used in this study, is a method in which the nanoparticles are dispersed first in monomer and then the mixture is polymerised. Thus, a mixing time, which allows the nanoparticles to disperse into the monomer, is a first important step in preparing successfully such nanocomposites.

In this section, a further investigation was undertaken on the 70PU/30PEMA IPN organoclay nanocomposite, because, in the previous section, this composition ratio showed a micro-heterogeneous morphology and a great potential for dynamic damping, including other good mechanical properties. The effect of the mixing time on IPN organoclay nanocomposites was examined in an effort to broaden further and heighten the tan delta spectra and, consequently, improve the mechanical properties of the material.

C20A organoclay at 5 % by weight was introduced into the polyol, PPG1025, and then the mixture was stirred by a conventional laboratory stirrer at room temperature to allow the polyol to intercalate into the layered silicate. The mixing time was varied from 30 minutes to 3, 9 and 24 hours. After being mixed, the mixture was then processed further for preparing the 70PU/30PEMA IPN system, which had a PPG:TMP ratio of 3:1, by using an NCO:OH ratio of 1.1:1.0 and SnOct catalyst 1.2 wt% of PU weight in the PU component and at 5 mole% TEGDM crosslinker in the PEMA component. These materials were investigated via the various characterisation techniques in order to examine the effect of the mixing time on the damping and mechanical properties of the IPN materials. The results were shown and discussed as below.

### 4.4.1 Dynamic mechanical thermal analysis.

DMTA was used to examine the influences of mixing time on the dynamic mechanical properties of the 70PU/30PEMA IPN organoclay nanocomposites. Figures 4.33 to 4.35 show the resulting bending loss factor, storage modulus and loss modulus spectra of the 70PU/30PEMA organoclay nanocomposites. The dynamic mechanical properties are summarised in Table 4.8.

***Table 4.8*** Dynamic mechanical properties of the 70PU/30PEMA IPN organoclay nanocomposites with 5 wt% C20A at various mixing times.

| Mixing time (hours) | Tg at tan δ max (°C) | | Tan δ max value at Tg | | Peak width tan δ ≥ 0.3 (°C) |
|---|---|---|---|---|---|
| | PU | PEMA | PU | PEMA | |
| 0.5 | -13 | 82 | 0.36 | 0.58 | -20 ↔ 131 (151) |
| 3.0 | -15 | 76 | 0.34 | 0.64 | -20 ↔ 134 (154) |
| 9.0 | -15 | 80 | 0.31 | 0.67 | – |
| 24.0 | -15 | 73 | 0.31 | 0.71 | -20 ↔ 125 (145) |

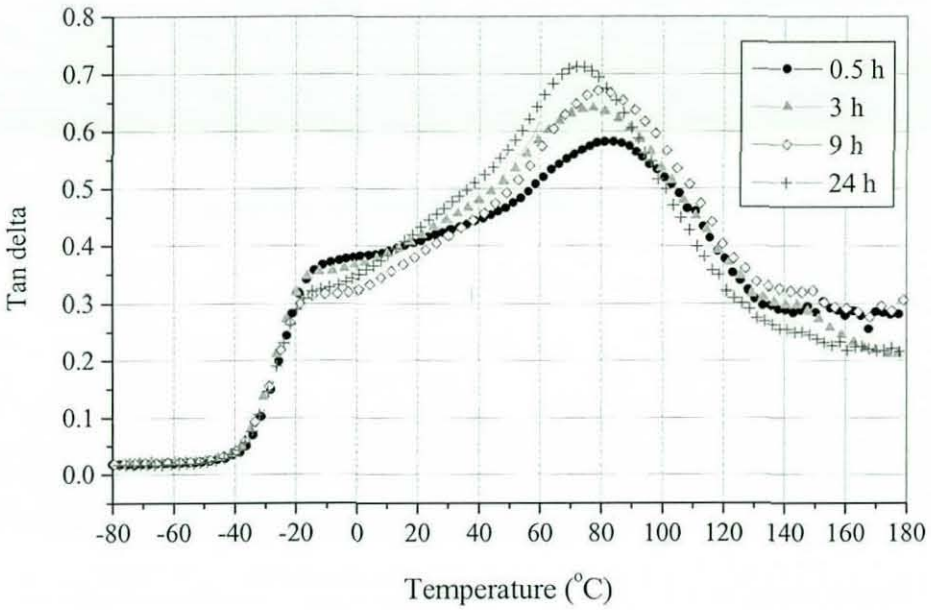


***Figure 4.33*** Loss factor versus temperature plots for the 70PU/30PEMA IPN organoclay nanocomposites with various mixing time: 0.5, 3, 9 and 24 hours and 5 wt% C20A clay.

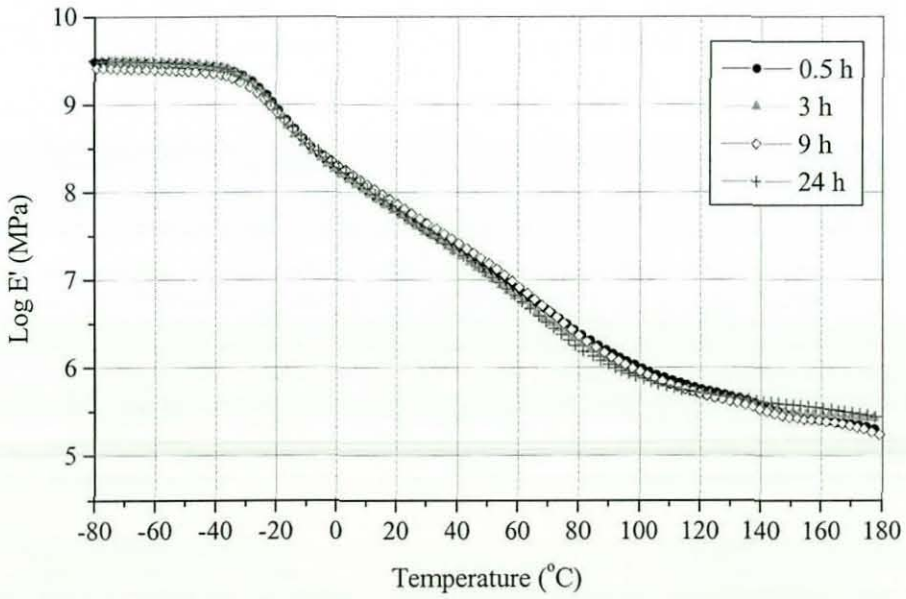


***Figure 4.34*** Storage modulus versus temperature plots for the 70PU/30PEMA IPN organoclay nanocomposites with various mixing time: 0.5, 3, 9 and 24 hours and 5 wt% C20A clay.

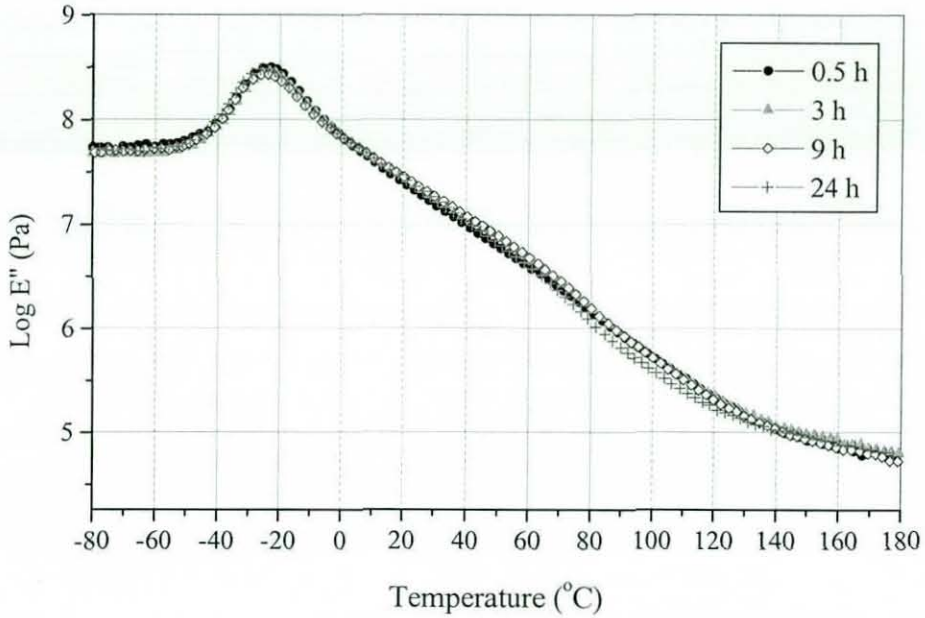


***Figure 4.35*** Loss modulus versus temperature plots for the 70PU/30PEMA IPN organoclay nanocomposites with various mixing time: 0.5, 3, 9 and 24 hours and 5 wt% C20A clay.

As can be seen from the Figure 4.33, the PEMA transition appears at 82°C (tan δ max 0.58) for an original 30 minute mixing time. Further increase in the mixing time brings down the transition to lower temperatures, and gives an enhanced damping response at the PEMA Tg. However, the decrease of the PEMA transition is not an orderly feature, as the mixing time increased. The highest tan delta max value of 0.71 is shown at the 24 hour mixing time. On the other hand, there is a slight decrease in the tan delta max value at the PU transitions with increasing the mixing time. Whilst, the PU transition slightly decrease from -13°C shown by 30 minute mixing time to -15°C for the 3 hour mixing time. Using even more than 3 hour for the mixing process, the PU Tg does not change any further. For 9 and 24 hour mixing times, they exhibit the same tan delta max value of 0.31. Nevertheless, the peak width at tan delta ≥ 0.3 shows no significant regular changes in the range of the mixing time studied.

Again, the reduction in both Tg and tan δ max at PU transition could be because of an incomplete PU network formation and lesser amount of polyol molecules involved in the polymerisation as some of them are intercalated in layered clay. For the PEMA network, some non-reacted monomers/crosslinkers might be trapped in clay galleries. Consequently, a higher molecular weight between crosslinks network (a more flexible network) could be formed, yielding a lower Tg and a higher tan δ max. Besides, the reduction in the PU and PEMA Tgs, can be attributed to a restricted mobility of polymer networks with the presence of clay. However, the morphology seems to show more phase separation as the mixing time increased. This may be due to higher amount of non-reacted constituents of both networks being constrained in the layered clay with increasing mixing time.

There are no obvious changes in shape of the storage and loss moduli, when the mixing time is changed from 30 minutes to 9 hours, as seen in the Figures 4.34 and 4.35. They all show a high extent of the micro-heterogeneous morphology, as shown by a gradual decrease in storage modulus, almost a straight line over the range observed.

### 4.4.2 Modulated-temperature differential scanning calorimetry.

Figure 4.36 shows the effect of the mixing time on the differential of heat capacity of the IPN organoclay nanocomposites at a 5 wt% loading of C20A.

The glass transition of PU was detected at -37°C with the differential heat capacity value of 0.015 J/g/°C/°C for the mixing time of 30 minutes. Further increasing the mixing time, the position of the PU Tg shows no significant change. Moreover, the differential heat capacity still remains the same, showing as the predominant transition because of the higher PU composition. There is a difficulty to identify the PEMA transition, as the mixing time of 30 minutes. Increasing the mixing time, the PEMA transition peaks become more obvious at approximate the same temperature of 56°C. These results indicate that the morphology of the IPN organoclay nanocomposites has changed somewhat from a micro-heterogeneous system to show a slightly greater extent of phase separation, which agrees with the results observed from the DMTA.

Thus, M-TDSC is sensitive to the glass transition temperature, miscibility and molecular mixing of these polymer blends[159].

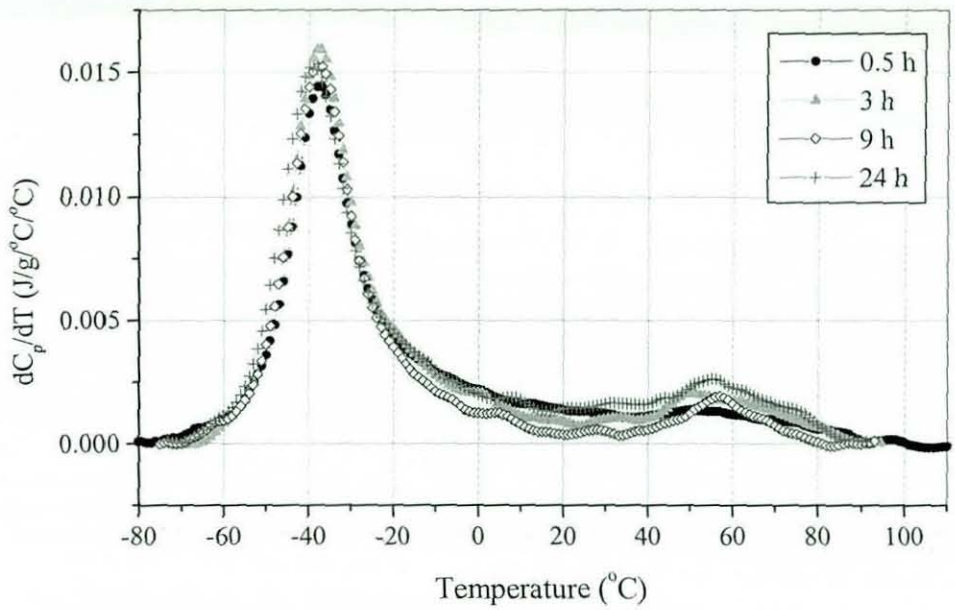


***Figure 4.36*** Differential heat capacity versus temperature plots showing the effect of mixing time on the 70PU/30PEMA IPN organoclay nanocomposites with 5 wt% C20A clay.

### 4.4.3 Tensile behaviour.

Tensile properties of the 70PU/30PEMA IPN organoclay nanocomposites made at various mixing times were investigated. The influences of mixing time on the tensile behaviour of 70PU/30PEMA IPN organoclay nanocomposites are given in Table 4.9. Figure 4.37 illustrates the tensile properties: modulus of elasticity, tensile strength and elongation at break versus the mixing time.

As seen in Figure 4.37, increasing the mixing time to disperse the organoclay, C20A, into polyol, PPG1025, produces the clear trends in mechanical properties. The tensile strength at break shows a slight increase from 3.9 MPa observed for the mixing time of 30 minutes to a value of 4.5 MPa at 9 hours of mixing. Further increase in the mixing time results in a gradual reduction of the tensile strength. At the mixing time of 24 hours, the tensile strength reduces to a value of 2.5 MPa. From these trends it can be

concluded that the use of a long mixing time causes reinforcement up to a certain critical value (at 9 hour mixing time). Further mixing results in a decrease in the tensile strength. This shows that the mixing time is one of the crucial factors in preparing these IPN organoclay nanocomposites. The longer time could create a higher degree of clay dispersion, consequently, an increasing number of interphase interaction between the polymer and the clay particles. At this time it is not clear to us why longer mixing time cause a reduction.

***Table 4.9*** Measured values of maximum tensile strength, extension at break and modulus of elasticity for the 70PU/30PEMA IPNs with 5 wt% C20A organoclay nanocomposites at various mixing times.

| Mixing time (hour) | Tensile strength (MPa) | Extension at break (%) | Modulus of elasticity (MPa) |
|---|---|---|---|
| 0.5 | 3.89 ± 0.34 | 587 ± 41 | 5.67 ± 0.58 |
| 3.0 | 4.00 ± 0.18 | 556 ± 14 | 11.65 ± 0.30 |
| 9.0 | 4.54 ± 0.32 | 591 ± 27 | 12.47 ± 0.80 |
| 24.0 | 2.47 ± 0.15 | 458 ± 24 | 11.02 ± 0.67 |

A similar trend was found in the modulus of elasticity. The modulus of elasticity increases steadily as the mixing time increased. At 3 hours, the modulus of elasticity increases from 5.7 MPa, for 30 minutes of mixing time, to a value of 11.6 MPa. At the mixing time of 9 hours, the modulus of elasticity reaches the highest value of 12.5 MPa. Increasing mixing time further, results in a slight reduction of modulus of elasticity.

The elongation at break shows a marginal change with change of the mixing time from 30 minutes to 9 hours. However, these fluctuations are actually within the uncertainty of the measurement. With further increase in the mixing time, the elongation at break significantly decreases from a value of 591% at 9 hour mixing time to a lower value of 458% for the mixing time of 24 hours. The reduction in the elongation at break can be

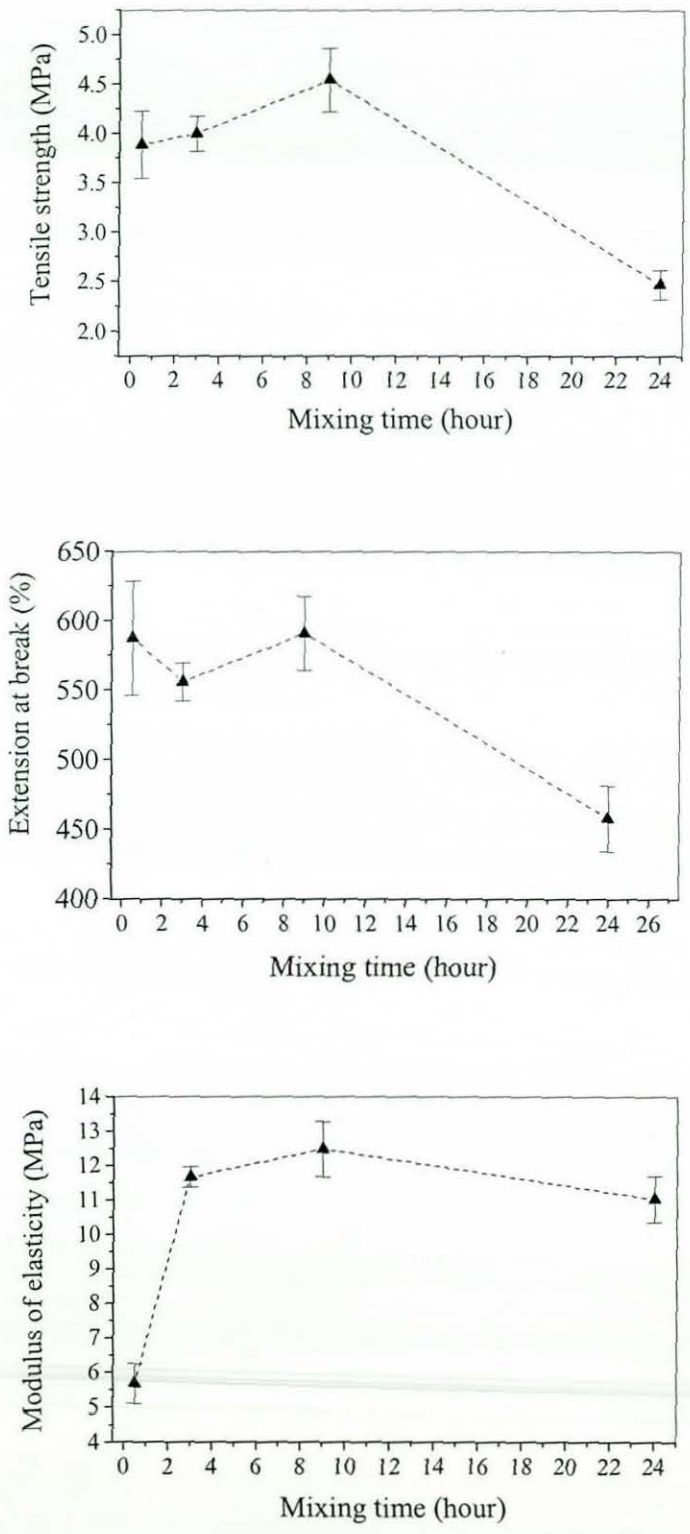


***Figure 4.37*** Tensile properties of the 70PU/30PEMA IPNs with 5 wt% C20A clay as a function of the mixing time.

explained by the high extent of constrained polyol molecules and their limited ability to stretch between the silicate galleries. The restricted mobility of the polymer chains within the clay aggregates is possibly a key factor.

### 4.4.4 Hardness measurements.

Shore A hardness values versus mixing time are shown in Figure 4.38.

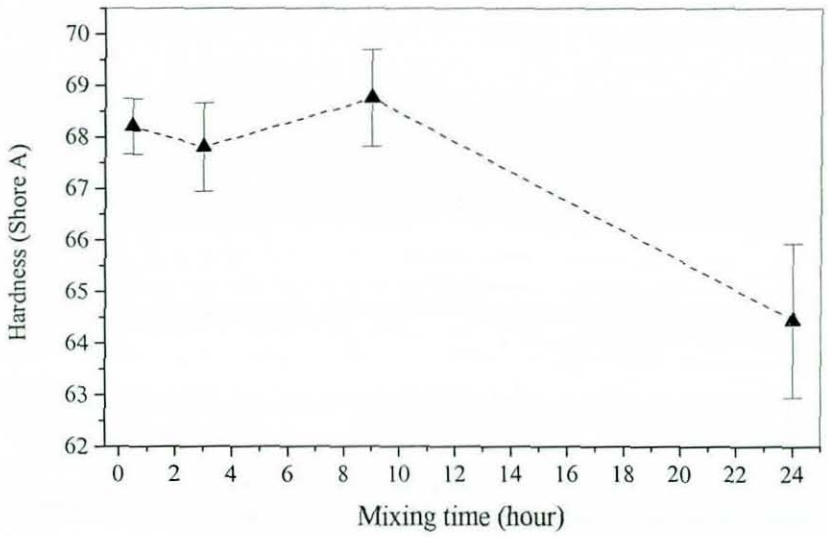


***Figure 4.38*** Shore A hardness values of the 70PU/30PEMA IPNs with 5 wt% C20A organoclay as a function of mixing time.

The hardness values show no significant changes as increase in the mixing time from 30 minutes to 9 hours. With further increase in the mixing time, the hardness gradually decreases to a Shore A value of 64.

## 4.5 Influence of the PU catalyst.

In general, a catalyst is used in PU synthesis to accelerate the reaction rate[207], and also to control the type of reaction favoured. The formation rate of linear polymer increases with catalyst content. In the same manner, the catalyst also has an influence on network formation. Increasing the amount of a catalyst favours the formation of the network, whereas decreasing the amount of the catalyst increased formation of the linear polymer[208]. The result is high tensile strength. Nevertheless, too high a catalyst

content will deteriorate the tensile strength because of a reduction in molecular weight[208].

Commercially, the catalysts most widely used in polyurethane processes are tertiary amines and organotin compounds. The tertiary amines favour the combination reaction of NCO/OH and NCO/$H_2O$. Whereas, the organotin compounds show remarkable activities, promoting reactions of NCO with OH groups, even when used in small trace quantities. Amongst the organotin compounds, tin (II) octoate, SnOct, is widely used, because of its solubility in the reaction mixtures and the advantage of low volatility and little odour[139].

Therefore, in this section various SnOct amounts were added into the 70PU/30PEMA IPN system which included 5 wt% C20A clay. The influence of the concentration of SnOct catalyst on IPN organoclay nanocomposites was then investigated. The 70PU/30PEMA IPN organoclay nanocomposites were prepared by first mixing 5 wt% C20A in the PPG1025, following the original procedure. The IPN system was composed of a PPG1025/TMP ratio of 3:1 and a NCO:OH ratio of 1.1:1.0, in the PU component, and 5% TEGDM in the PEMA component. The catalyst in the desired concentration, was added to the PU components, before being combined with the PEMA components. These materials were investigated via the various characterisation techniques in order to examine the effect of catalyst concentration on the damping and mechanical properties of these IPN materials. The results are shown and discussed below.

### 4.5.1 Dynamic mechanical thermal analysis.

Effects of SnOct catalyst concentrations on the dynamic mechanical properties of the 70PU/30PEMA IPN organoclay nanocomposites were examined. Figures 4.39 to 4.41 show the resulting loss factor, storage modulus and loss modulus spectra of PEMA organoclay nanocomposites. The dynamic mechanical properties of them are summarised in Table 4.10.

***Table 4.10*** Dynamic mechanical properties of 70PU/30PEMA IPN organoclay nanocomposites with various SnOct catalyst concentrations with 5 wt% C20A clay.

| SnOct concentration ( wt% of PU ) | Tg at tan δ max. (°C ) | | Tan δ max value at Tg | | Peak width tan δ ≥ 0.3 (°C ) |
|---|---|---|---|---|---|
| | PU | PEMA | PU | PEMA | |
| 1.2 | -13 | 82 | 0.36 | 0.58 | -20 ↔ 131 (151) |
| 1.6 | -13 | 75 | 0.36 | 0.52 | -20 ↔ 119 (139) |
| 1.8 | -13 | 76 | 0.36 | 0.53 | -20 ↔ 117 (137) |
| 2.0 | -12 | 76 | 0.35 | 0.50 | -17 ↔ 111 (128) |

From Figure 4.39, it can be seen that SnOct catalyst has an effect on the damping ability of the 70PU/30PEMA IPN, especially over the higher temperature range. Adding more catalyst tends to narrow the tan delta peak around the PEMA transition, as well as giving a reduction in the loss factor value over the PEMA-rich phase transition. Moreover, PEMA transition seems to reduce towards lower temperatures, while there was no a significant change in PU transition temperature. Also, the peak width of tan delta value ≥ 0.3 at PEMA glass transition slightly decreases with increasing the catalyst concentration. This can be explained in terms of an increased rate of PU network formation and an increased viscosity of the medium. Therefore, the PEMA could exist as smaller domains in the continuous phase of PU, as the amount of catalyst increased, consequently, there was more extent of micro-heterogeneity, giving the lower tan delta max value and the glass transition of the PEMA. More likely, perhaps, was because of a higher degree of restriction of PEMA segmental mobility, and an incomplete network formation of the PEMA.

As seen in Figure 4.40, the storage moduli show near super-imposition, and decline in an almost linear pattern until they reach the rubbery plateau, indicating a high degree of component mixing in these IPNs. Addition of more catalyst results in an increase of the storage modulus at the rubbery stage. This is probably because of better formed network.

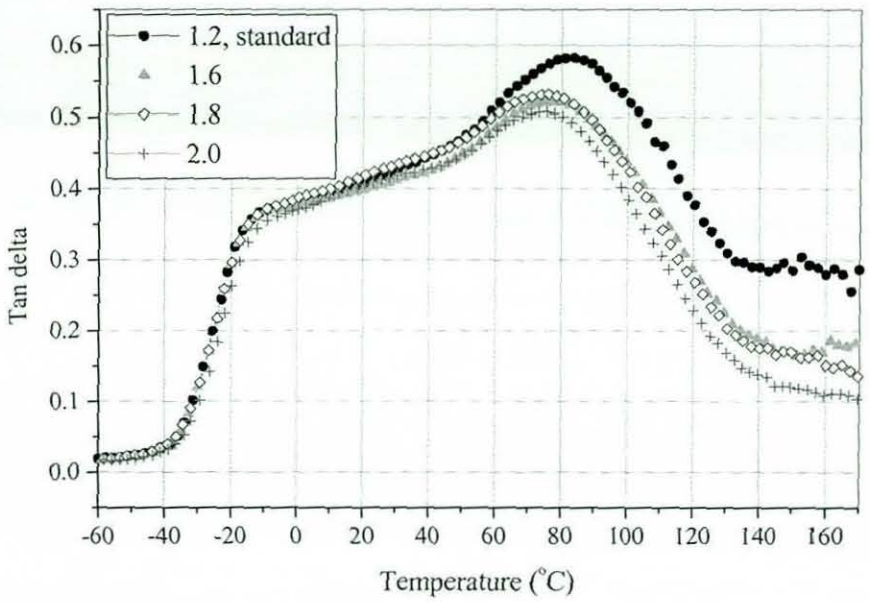


***Figure 4.39*** Loss factor versus temperature plots for the 70PU/30PEMA IPN with 5 wt% C20A organoclay at various SnOct catalyst concentrations.

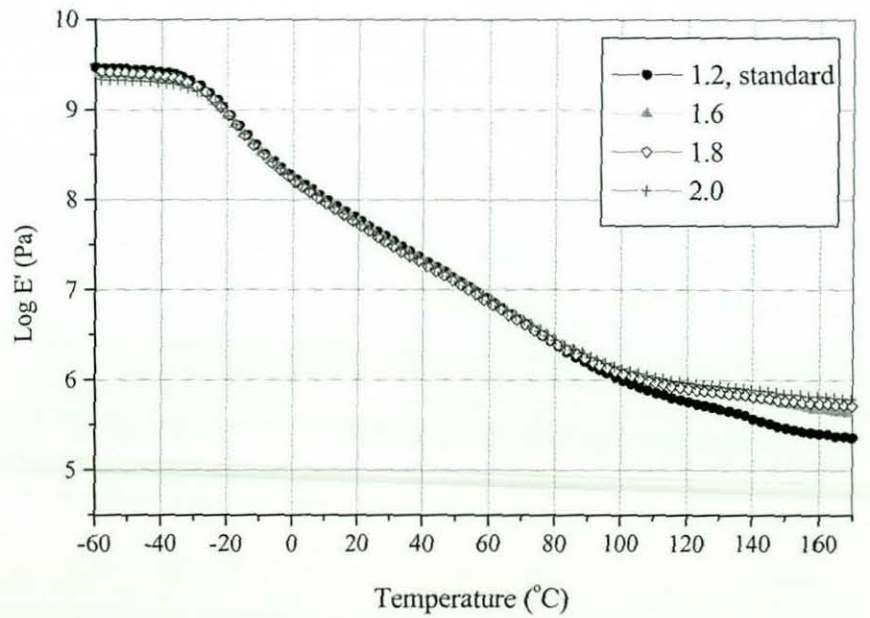


***Figure 4.40*** Storage modulus versus temperature plots for the 70PU/30PEMA IPN with 5 wt% C20A organoclay at various SnOct catalyst concentrations.

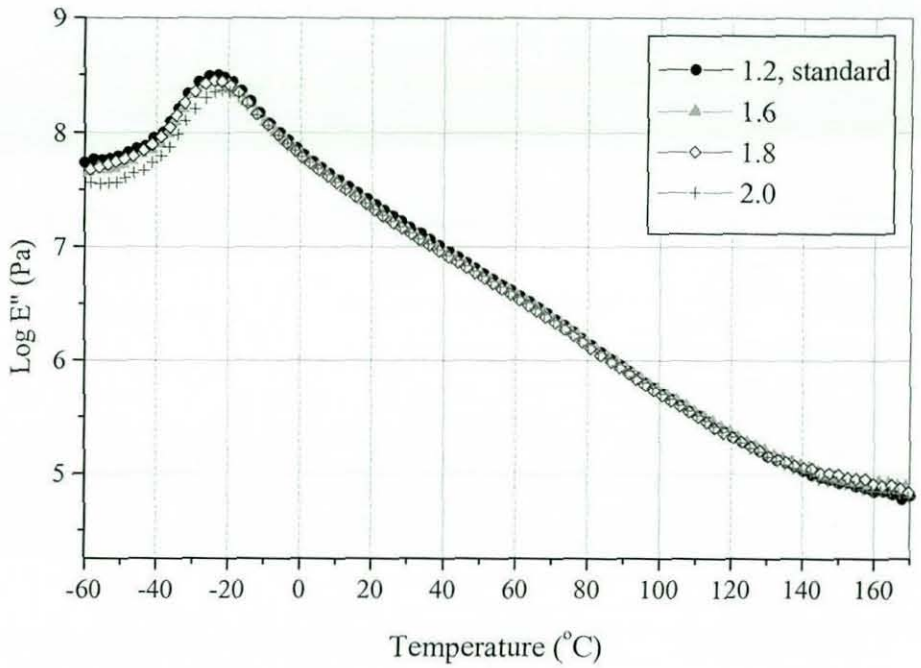


***Figure 4.41*** Loss modulus versus temperature plots for the 70PU/30PEMA IPN with 5 wt% C20A organoclay at various SnOct catalyst concentrations.

Evaluation of the influence of PU catalyst on the loss modulus, Figure 4.41, shows again a near super-imposition of the linear slopes of the loss modulus values, implying a high extent of interphase.

### 4.5.2 Modulated-temperature differential scanning calorimetry.

Figure 4.42 shows the effect of the PU catalyst on the differential of heat capacity of the 70PU/30PEMA IPN organoclay nanocomposites at 5 wt% loading of C20A clay. The PU glass transition temperature and the differential heat capacity measured by M-TDSC are summerised in Table 4.11.

The M-TDSC technique offered corresponding data to those obtained from DMTA in that adding more PU catalyst into 70PU/30PEMA IPN organoclay nanocomposites leads to quite similar thermographs, as seen in Figure 4.42. The PU transition is clear with just a shoulder around the PEMA transition, as is characteristic of this IPN

system. With more SnOct catalyst, no significant change in glass transition is observed for either of the two transitions.

***Table 4.11*** M-TDSC data for the 70PU/30PEMA IPN organoclay nanocomposites with varying SnOct contents.

| SnOct content (wt% of PU) | PU Tg (°C) | dCp/dT value ($J/g^{-1}{}^{o}C^{-2}$) |
|---|---|---|
| 1.2 | -37 | 0.015 |
| 1.4 | -38 | 0.017 |
| 1.5 | -37 | 0.017 |
| 1.6 | -37 | 0.016 |
| 2.0 | -37 | 0.015 |

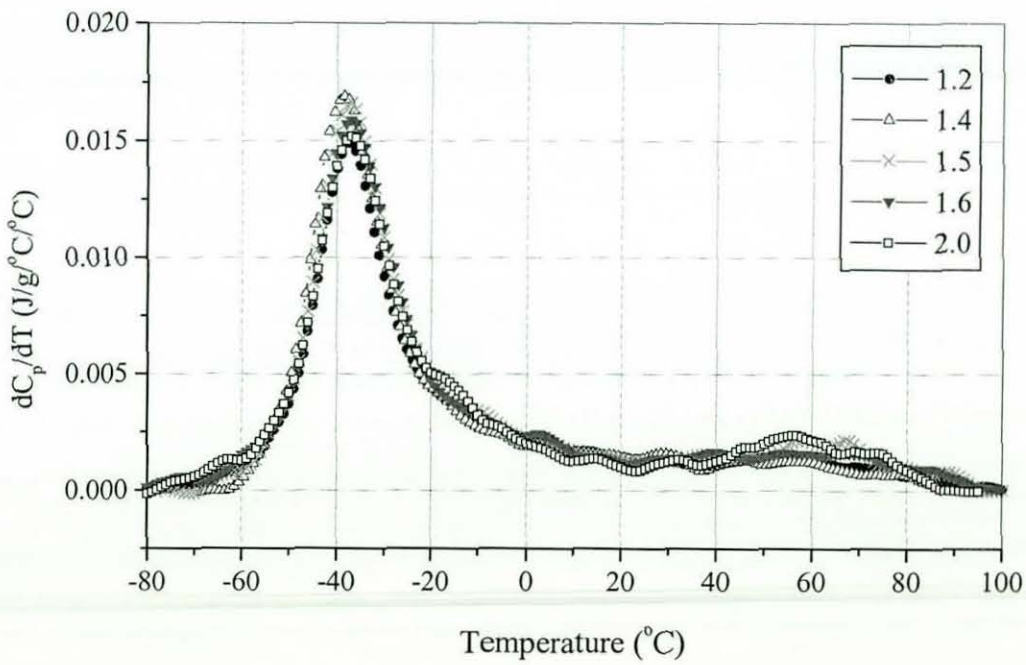


***Figure 4.42*** Differential heat capacity versus temperature plots showing the effect of PU catalyst on the 70PU/30PEMA IPN with 5 wt% C20A organoclay.

### 4.5.3 Tensile behaviour.

In order to investigate the effect of PU catalyst, SnOct, on the mechanical behaviour, tensile properties of the 70PU/30PEMA IPN organoclay nanocomposites with 5 wt% C20A clay were investigated. The influences of SnOct on the tensile properties of 70PU/30PEMA IPN organoclay nanocomposites are given in Table 4.12. Figure 4.43 illustrates the tensile properties: modulus of elasticity, tensile strength and elongation at break versus the PU catalyst content.

***Table 4.12*** Measured values of maximum tensile strength, extension at break and modulus of elasticity for the 70PU/30PEMA IPN organoclay nanocomposites with various SnOct catalyst at 5 wt% C20A clay.

| SnOct content (wt% of PU) | Tensile strength (MPa) | Extension at break (%) | Modulus of elasticity (MPa) |
|---|---|---|---|
| 1.2 | 3.89 ± 0.34 | 587 ± 41 | 5.67 ± 0.58 |
| 1.4 | 4.24 ± 0.32 | 568 ± 34 | 11.27 ± 0.57 |
| 1.5 | 5.08 ± 0.29 | 591 ± 20 | 9.64 ± 0.72 |
| 1.6 | 5.69 ± 0.49 | 639 ± 30 | 10.29 ± 0.26 |
| 1.8 | 4.92 ± 0.32 | 617 ± 40 | 9.54 ± 0.29 |
| 2.0 | 5.30 ± 0.60 | 617 ± 61 | 9.53 ± 0.60 |

As seen in Figure 4.43, increasing catalyst content, the tensile strength shows an increase from 3.89 MPa, observed for a catalyst content of 1.2 wt%, to a value of 5.69 MPa at 1.6 wt% SnOct. Further increase in the catalyst content results in a gradual reduction of the tensile strength. At 2.0 wt% of SnOct, the tensile strength reduced to a value of 5.30 MPa. It can be seen that the presence of the SnOct catalyst causes reinforcement up to a certain critical value. This was a result of an increase in a better formed PU network as increasing the catalyst content. Too high catalyst concentration led to a higher in the PU average molecular weight between crosslinks, consequently the decrease in the tensile strength was observed.

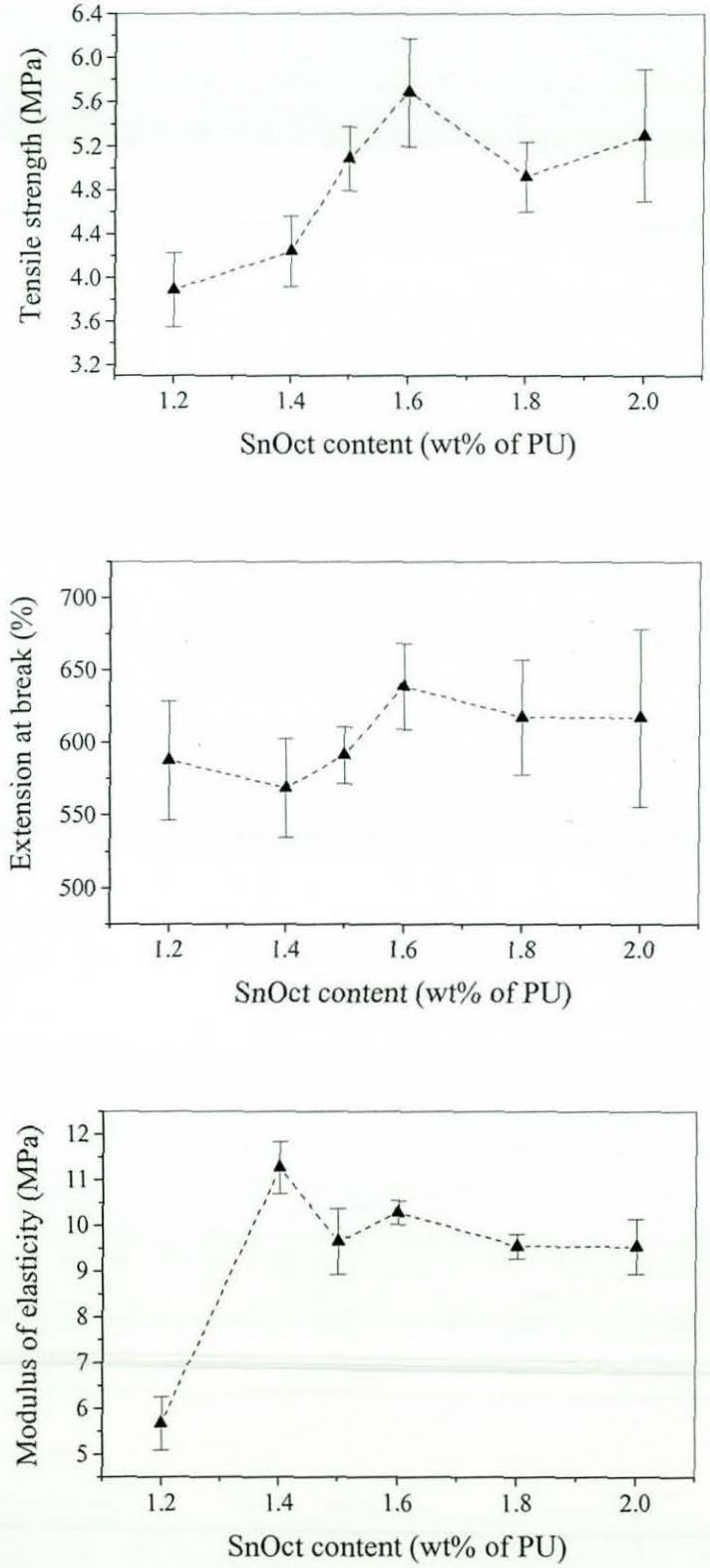


***Figure 4.43*** Tensile properties of the PU/PEMA IPN organoclay nanocomposites as a function of the catalyst content and 5 wt% C20A clay.

The modulus of elasticity reveals a similar trend as found in the tensile strength, even if it shows some scatter. The modulus of elasticity increases steeply from a value of 5.67 MPa at 1.2 wt% to a value of 11.27 MPa at 1.4 wt%. With further catalyst addition to 1.6 wt%, the modulus of elasticity decreases to a value of 9.64 MPa at 1.5 wt% and then, increases towards a value of 10.29 MPa. However, these values fluctuate approximately in an instrument error range. The modulus of elasticity finally drops to a value of 9.53 MPa when the catalyst content is 2.0 wt%.

The extension at break over the whole studied range is within an experiment error. Thus there is no significant trend.

### 4.5.4 Hardness measurements.

The mechanical behaviour was further investigated via Shore A hardness measurements in order to corroborate the findings from the tensile testing.

A plot of Shore A hardness against SnOct catalyst content is shown in Figure 4.44. No significant trend is shown for the hardness measurements for this system.

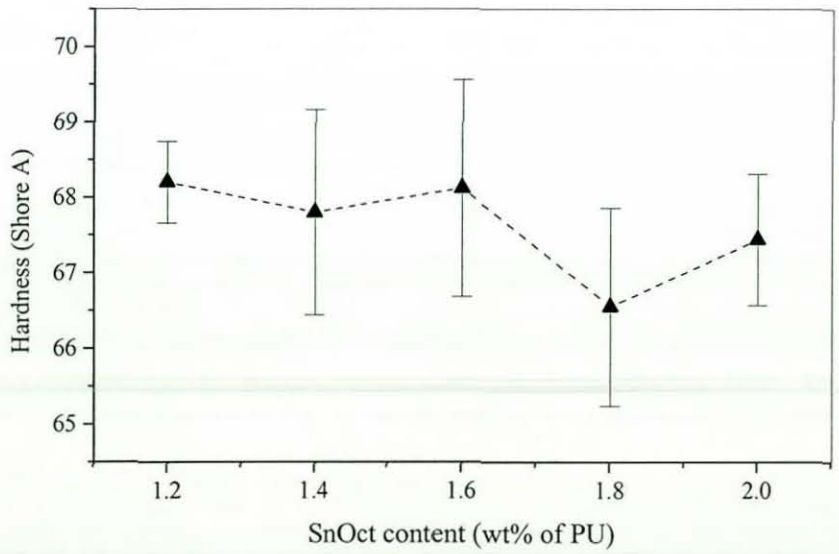


***Figure 4.44*** Shore A hardness values of the 70PU/30PEMA IPN organoclay nanocomposites as a function of SnOct catalyst at 5 wt% C20A clay.

# CHAPTER 5

# OPTIMISATION OF SYNTHESIS PROCEDURES

# CHAPTER 5
# OPTIMISATION OF SYNTHESIS PROCEDURES

Polymer layered silicate nanocomposites have received a considerable amount of attention because they often exhibit improved mechanical, thermal and flammability properties[15,25,129,136,209,210]. Their behaviour is different from conventional composite materials with a microscale structure because of the small size of the structural units and their high aspect ratio[211]. The properties of nanocomposites are greatly influenced by the degree of mixing between the polymer matrix and the nanoparticles[212]. Many methods have been developed to prepare polymer clay nanocomposites such as direct melt blending and in-situ, emulsion or solution polymerisation[46,213]. These methods attempt to prepare true nanocomposites[16] in which the silicate layers are uniformly and individually dispersed in the polymer matrix, creating a three-dimensional network of inter-connected long silicate layers, the so called exfoliated or delaminated nanocomposites. Most research results[20,124,214] showed that the achievement of completely exfoliated clay nanocomposites yielded remarkable isotropic properties, because the high aspect ratio and surface area of the dispersed silicate particles are fully utilised.

Results shown in chapter 4 revealed only partial intercalation with a few exfoliated silicate layers poorly dispersed in all cases. Consequently, limited improvement in damping and mechanical properties resulted. Therefore, synthesis routes had to be designed to achieve complete exfoliation or at least a high extent of exfoliation within fully intercalated systems. This should show a great improvement in IPN properties, especially in damping behaviour.

In this chapter, there were two sections. The first section is focused on the variation of the synthesis procedure by changing the clay dispersion and the IPN component preparation steps, as shown in section 3.2.2. Use of ultrasonic radiation to aid organoclay dispersion is investigated in the second section.

**5.1 Variation of synthesis procedure.**

In this study, the 70PU/30PEMA IPN organoclay nanocomposites, which had a PPG:TMP ratio of 3:1 and 1.2 wt% SnOct in PU component, and 5 mole% TEGDM in PEMA component, were prepared by in-situ polymerisation, using different procedures as explained in section 3.2.2.

In the original synthesis procedure, P0, organoclay was first added and completely mixed with the polyol, PPG1025, after that the mixture was combined with crosslinker, TMP. Then, diisocyanate, TMXDI, and catalyst, SnOct, were added into PU component before being combined with PEMA component. For synthesis procedure one, P1, PPG1025 and TMP was completely mixed first. Then the organoclay was incorporated. After that TMXDI and SnOct were added to the PU component. Finally, the PU and PEMA components were combined together. In synthesis procedure two, P2, the first step was the same as in P1 by mixing PPG1025 with TMP. Then the organoclay and TMXDI were introduced and mixed. After that SnOct was added into the mixture and then the PU component was combined with PEMA components. In synthesis procedure three, P3, organoclay was first added into the PEMA components. The organoclay was mixed with EMA and the crosslinker, TEGDM, and then initiator, AIBN, was finally added into the mixture before the final mixture was combined with the PU component. In synthesis procedure four, P4, organoclay was mixed with both network components, except SnOct and AIBN, which were added into the final mixture before casting.

However, because of the settlement of the organoclay reported during polymerisation in the previous chapter, the filled mould was turned over every 30 minutes for the first four hours of curing. After that it was turned over every one hour for another 3 hours to diminish extent of any clay settlement. The mixing time used to disperse the organoclay into the polymer constituents was 30 minutes in all cases and 5 wt% C20A organoclay was added in all specimens in this study. The influences of the various synthesis procedures on the glass transition behaviour, morphology, damping and mechanical properties of IPN organoclay nanocomposites were examined by several characterisation techniques.

### 5.1.1 Wide angle X-ray diffraction.

In general, the structure of nanocomposites has typically been established using WAXD analysis[15,16,215-217]. By monitoring the position, shape and intensity of the basal diffractions from the distributed silicate layers, the nanocomposite structure can be identified. However, it can only express little about the spatial distribution of the silicate layers or any structural non-homogeneities in nanocomposites. Thus, care must be taken in the interpretation of the nanocomposite structure, i.e. intercalated or exfoliated system, when WAXD data alone are used.

Once again, both sides of the specimens were characterised by WAXD to examine dispersion uniformity of silicate layers in the polymer matrix. WAXD data for both sides of C20A organoclay-filled 70PU/30PEMA IPNs for original procedure, P0, is shown in Figure 5.1 Three diffraction peaks are revealed for both sides of P0 specimen, at the same 2θ angles of 2.30, 4.60 and 6.92, which correspond to a harmonic series of the 001, 002 and 003 planes, respectively. The basal spacing, $d_{001}$, is 3.84 nm, in this case, indicating that polymer chains have intercalated into the layered silicate to some extent, as compared with the interlayer spacing of the C20A organoclay, which has a value of 2.29 nm. However, the intensity of the bottom side is stronger than that of the top side, implying that the C20A organoclay still gradually settled to the bottom side. This might conclude that a turning interval time of 30 minutes was too infrequent to prevent the settlement of clay. Nevertheless, the settlement was retarded to some extent. For all further investigations, only the bottom side of the specimens will be examined.

Figure 5.2 shows a comparison of the diffraction patterns of the original procedure, P0, synthesis procedure one, P1, synthesis procedure two, P2, synthesis procedure three, P3, and synthesis procedure four, P4. All of the specimens prepared by these various synthesis procedures show the same diffraction profiles. They reveal three diffraction peaks of an interlayer spacing, $d_{001}$, of 3.84 nm, increasing from a $d_{001}$ value of 2.29 nm, for the C20A organoclay. This shows a strongly intercalated characteristic. The high intensity peaks imply that polymer molecules do not totally interrupt the layer structure of the silicate crystals. Even though, the organoclay was first mixed with PEMA components before the mixture was then mixed with PU components, or the

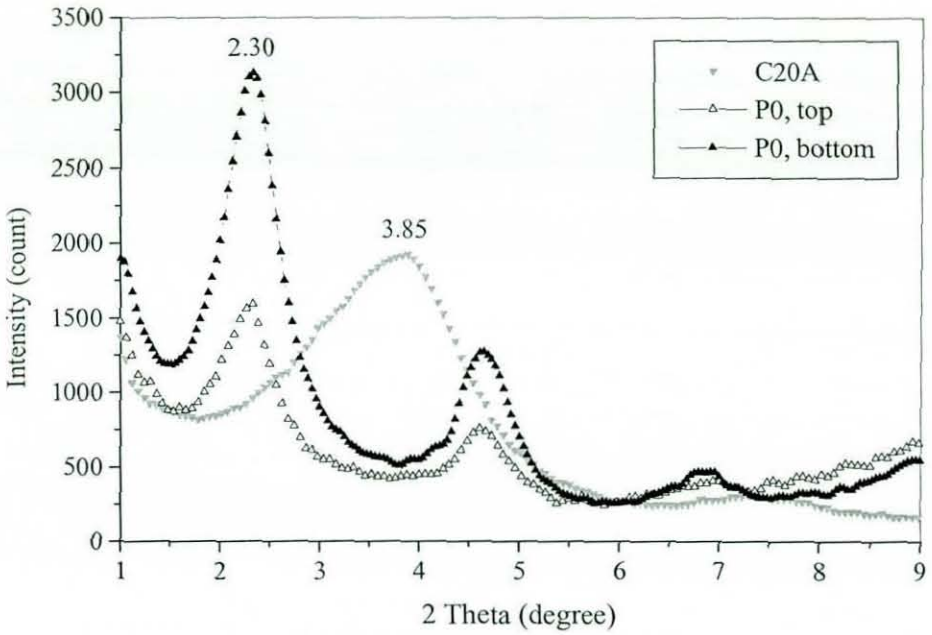


***Figure 5.1*** WAXD patterns from the top and bottom sides of C20A organoclay filled 70PU/30PEMA IPNs prepared by the original synthesis procedure, P0.

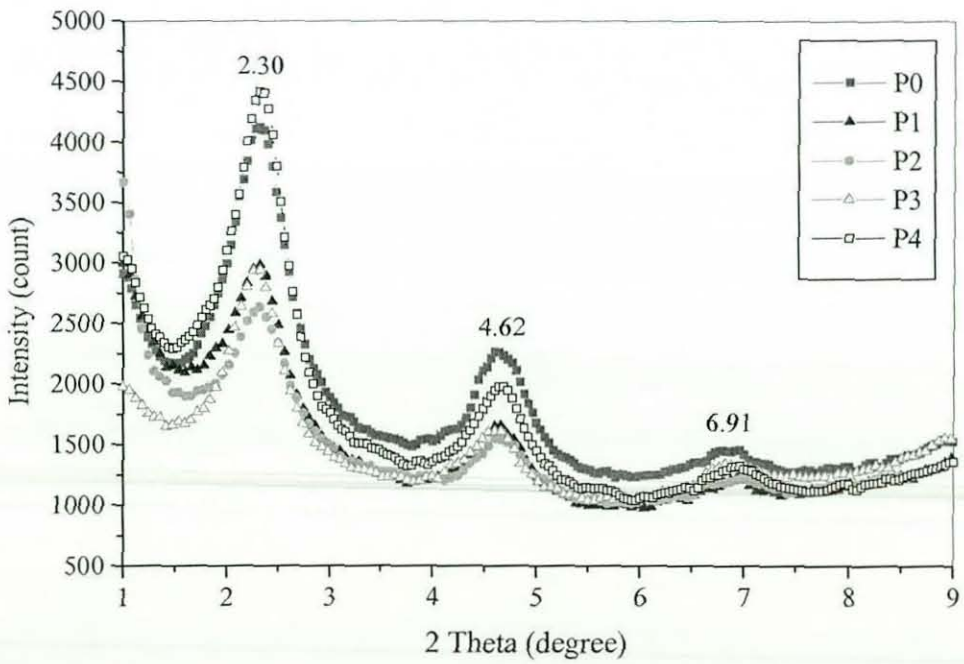


***Figure 5.2*** WAXD patterns of the C20A organoclay filled 70PU/30PEMA IPNs prepared by various synthesis procedures: P0, P1, P2, P3 and P4.

organoclay was mixed with both components, the results do not show any significant change in the position of the diffraction peaks. This may indicate that the swelling ability of the PU and PEMA components into the layered silicates are very similar. These results correspond to the results of the incorporation of the C20A organoclay into homopolymers, PU and PEMA, as investigated in sections 4.2.1 and 4.2.2, where they revealed an approximately equal interlayer spacing for filled-PU and filled-PEMA.

### 5.1.2 Transmission electron microscopy.

WAXD generally describes relationship between clay layers in the polymer matrix, but does not portray the degree of dispersion of the clay to that matrix[218]. TEM allows the degree of dispersal of the clay through direct visualisation[219]. However, TEM is time-consuming, and only gives qualitative information on a very tiny sample of the whole[218]. For a better contrast, the samples were stained with ruthenium tetroxide, $RuO_4$, because it is more reactive than $OsO_4$, which is known[92] to stain the PU preferentially.

TEM images of the unfilled IPN and the filled IPNs prepared by synthesis procedures P0, P1, P2, P3 and P4 are presented in Figures 5.3 to 5.8, respectively.

For the 70PU/30PEMA IPN and all the 70PU/30PEMA IPN organoclay nanocomposites, no gross phase separation was observed by TEM, as can be seen in Figures 5.3 to 5.8. The phase domains are not that well-defined, which indicates some extent of mixing. The unfilled IPN shows fine morphology with light, interconnected domains of PEMA in a dark, dominant PU matrix. At a higher magnification of 30 k, besides, the dark PU matrix and the light, interconnected PEMA domains of 25-300 nm stretching through the PU matrix, the TEM micrograph reveals a high extent of interphase which can be seen by the different shades of grey, indicating that the composition is changing only gradually, whereas in immiscible IPNs[1], clear-cut interfaces were observed. Incorporation of the organoclay, the majority of the layered silicate is not dispersed on an individual level. Agglomerates of the silicate layers, so called tactoids, in the IPN matrix could be seen. The size of these tactoids was in the order of 1-3 μm. Therefore, further studies of the influence of the various synthesis

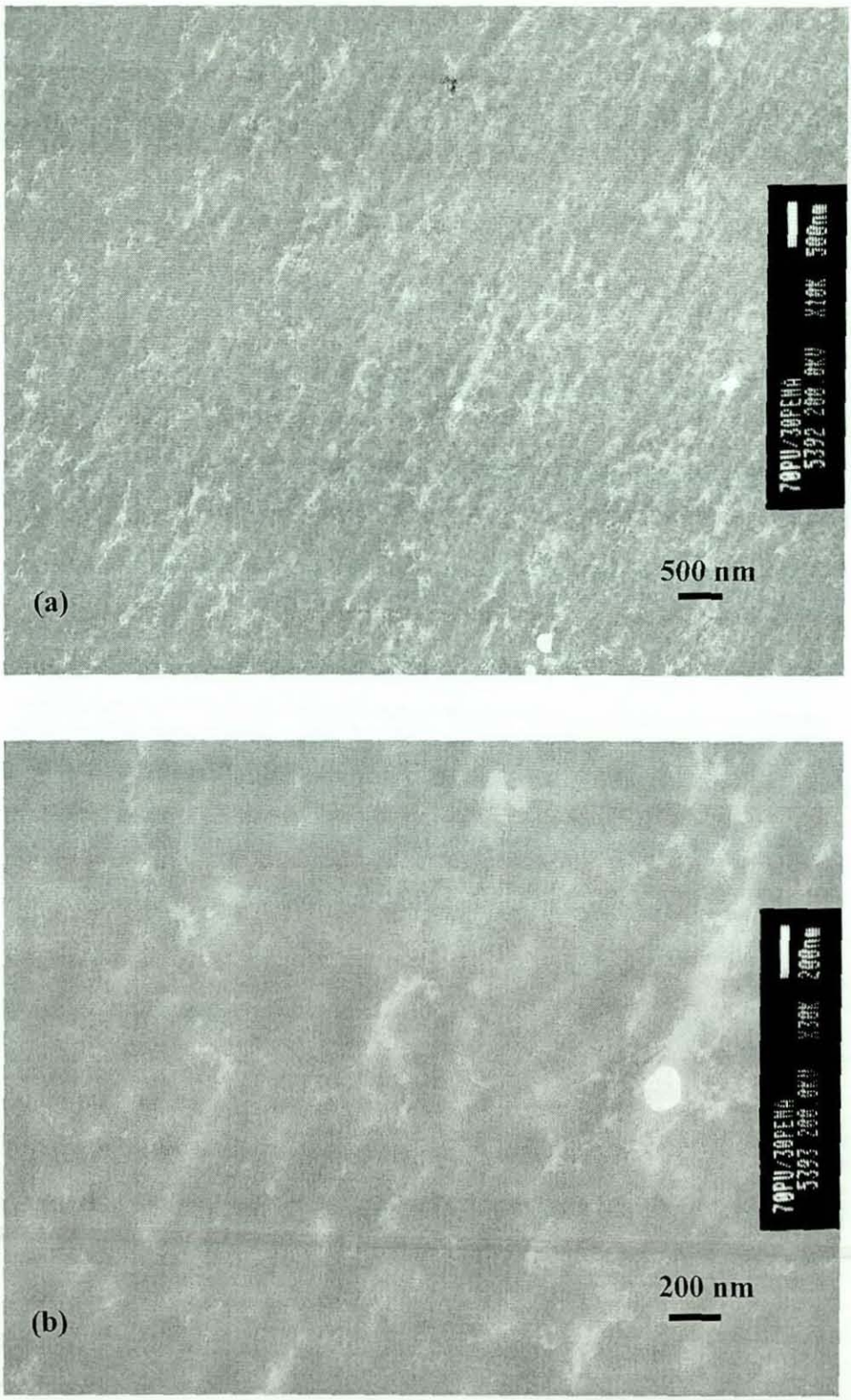


***Figure 5.3*** TEM micrographs of the unfilled 70PU/30PEMA IPN. (a) At 10k magnification. (b) At 30k magnification.

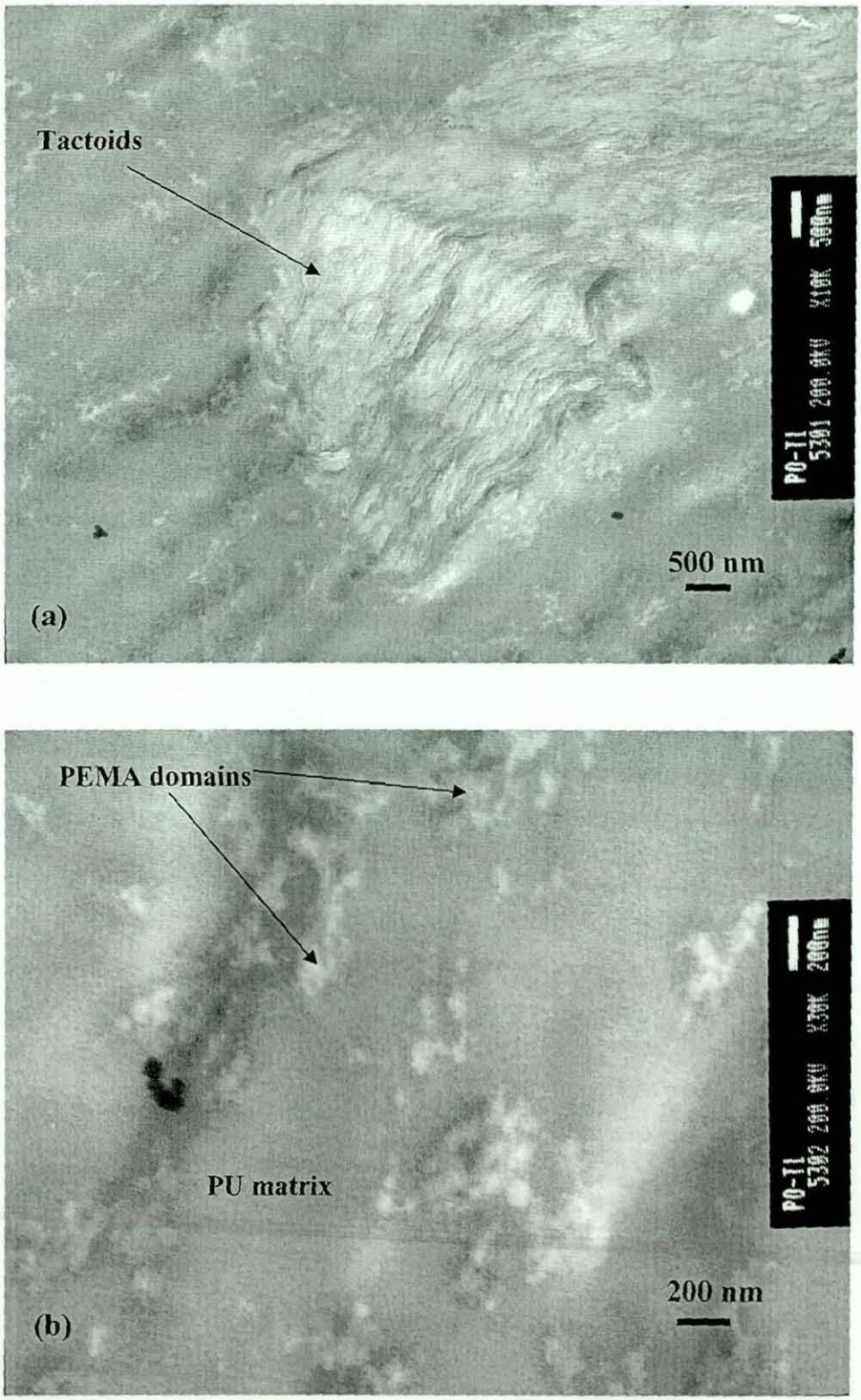


***Figure 5.4*** TEM micrographs of the 70PU/30PEMA IPN with 5 wt% C20A organoclay made by the original synthesis procedure, P0. (a) At 10k magnification. (b) At 30k magnification.

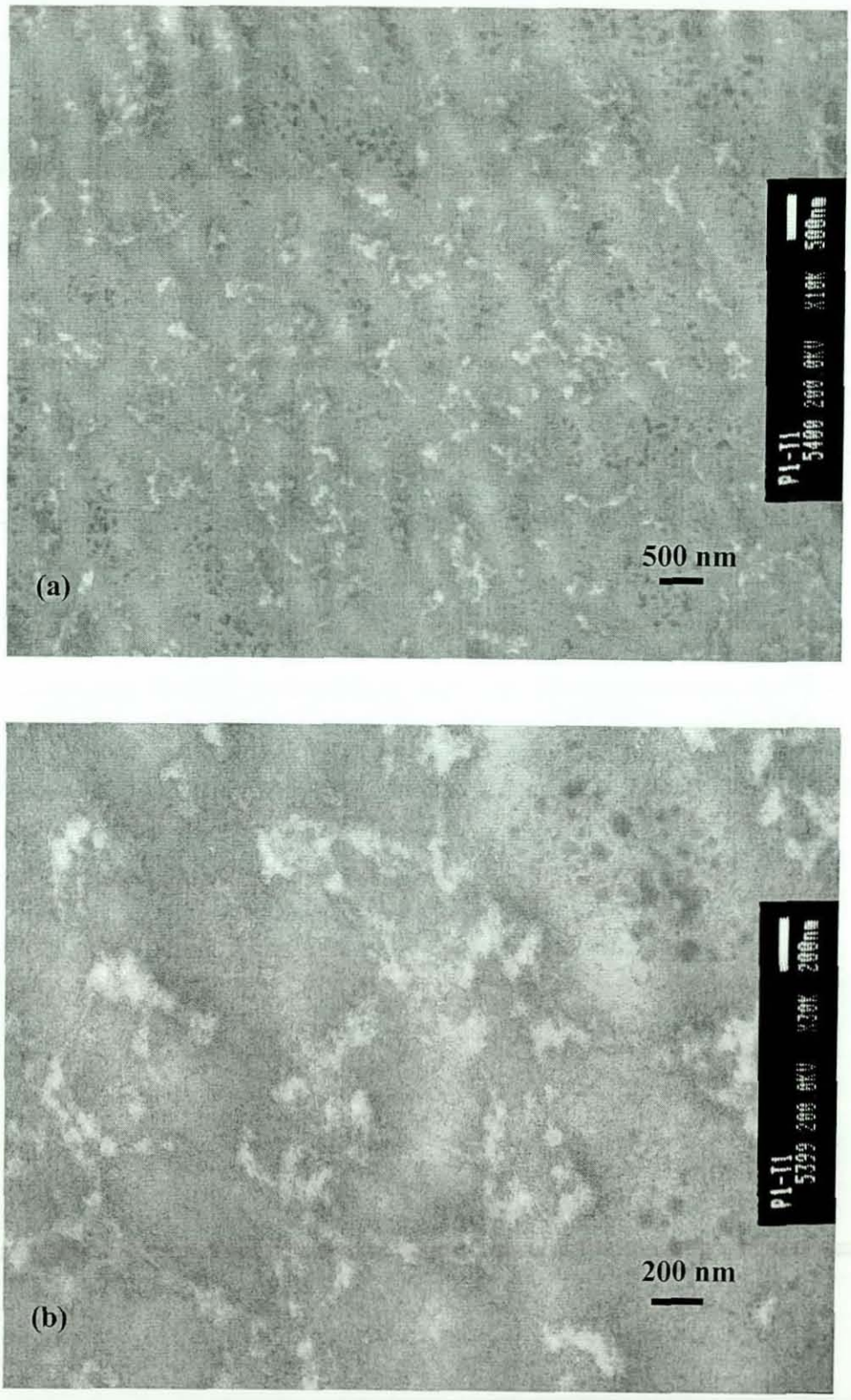


***Figure 5.5*** TEM micrographs of the 70PU/30PEMA IPN with 5 wt% C20A organoclay made by synthesis procedure one, P1. (a) At 10k magnification. (b) At 30k magnification.

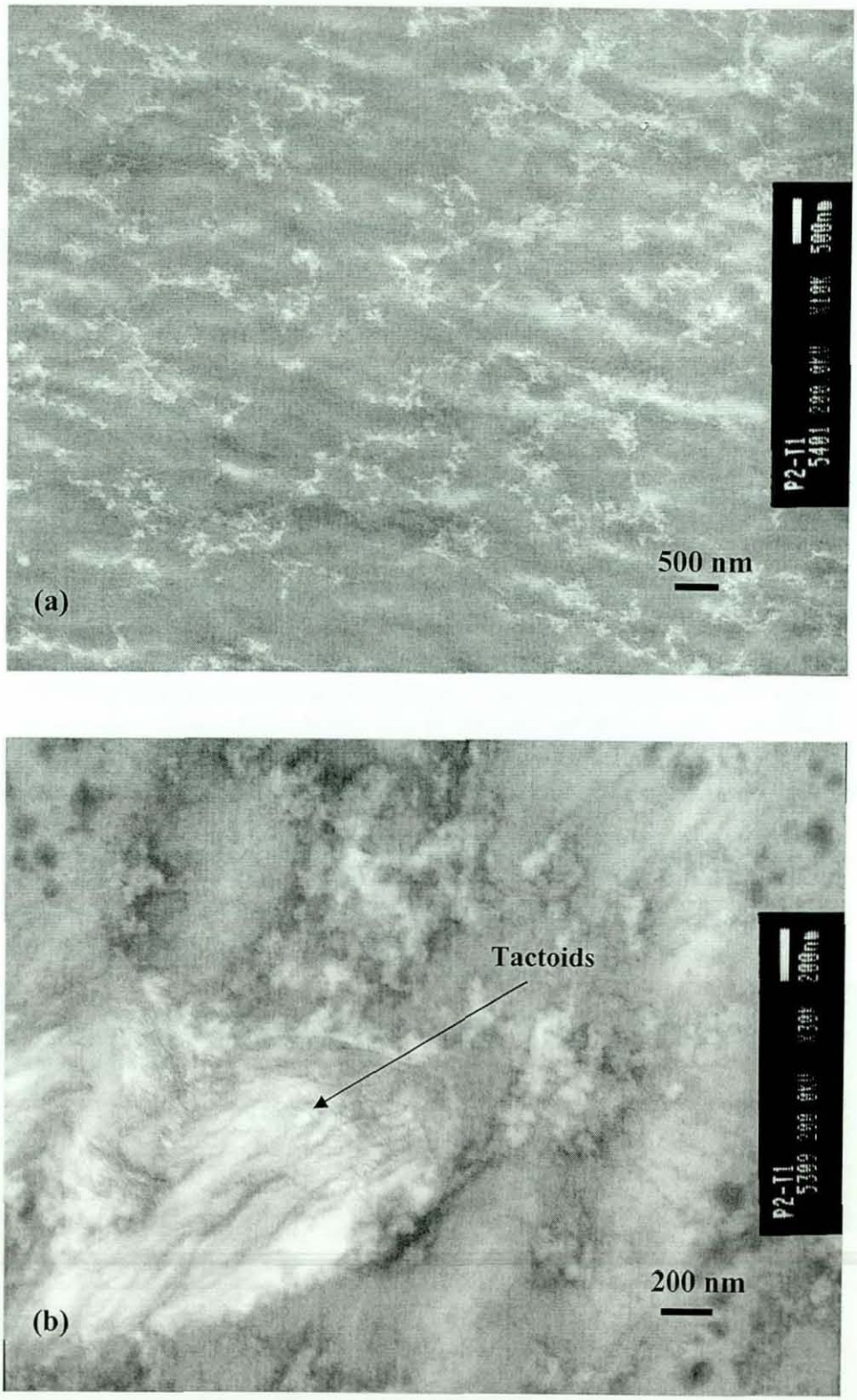


***Figure 5.6*** TEM micrographs of the 70PU/30PEMA IPN with 5 wt% C20A organoclay made by synthesis procedure two, P2. (a) At 10k magnification. (b) At 30k magnification.

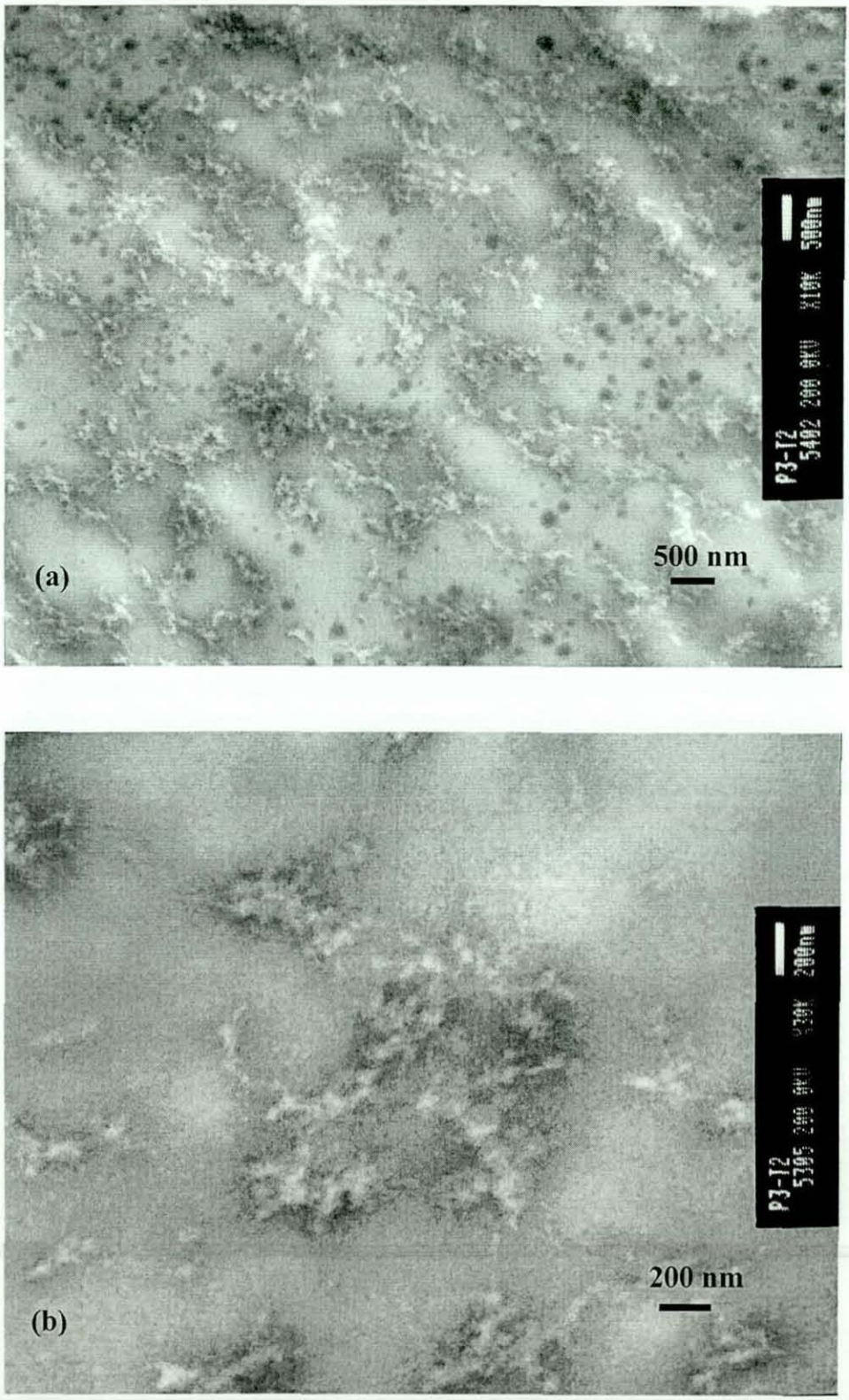


***Figure 5.7*** TEM micrographs of the 70PU/30PEMA IPN with 5 wt% C20A organoclay made by synthesis procedure three, P3. (a) At 10k magnification. (b) At 30k magnification.

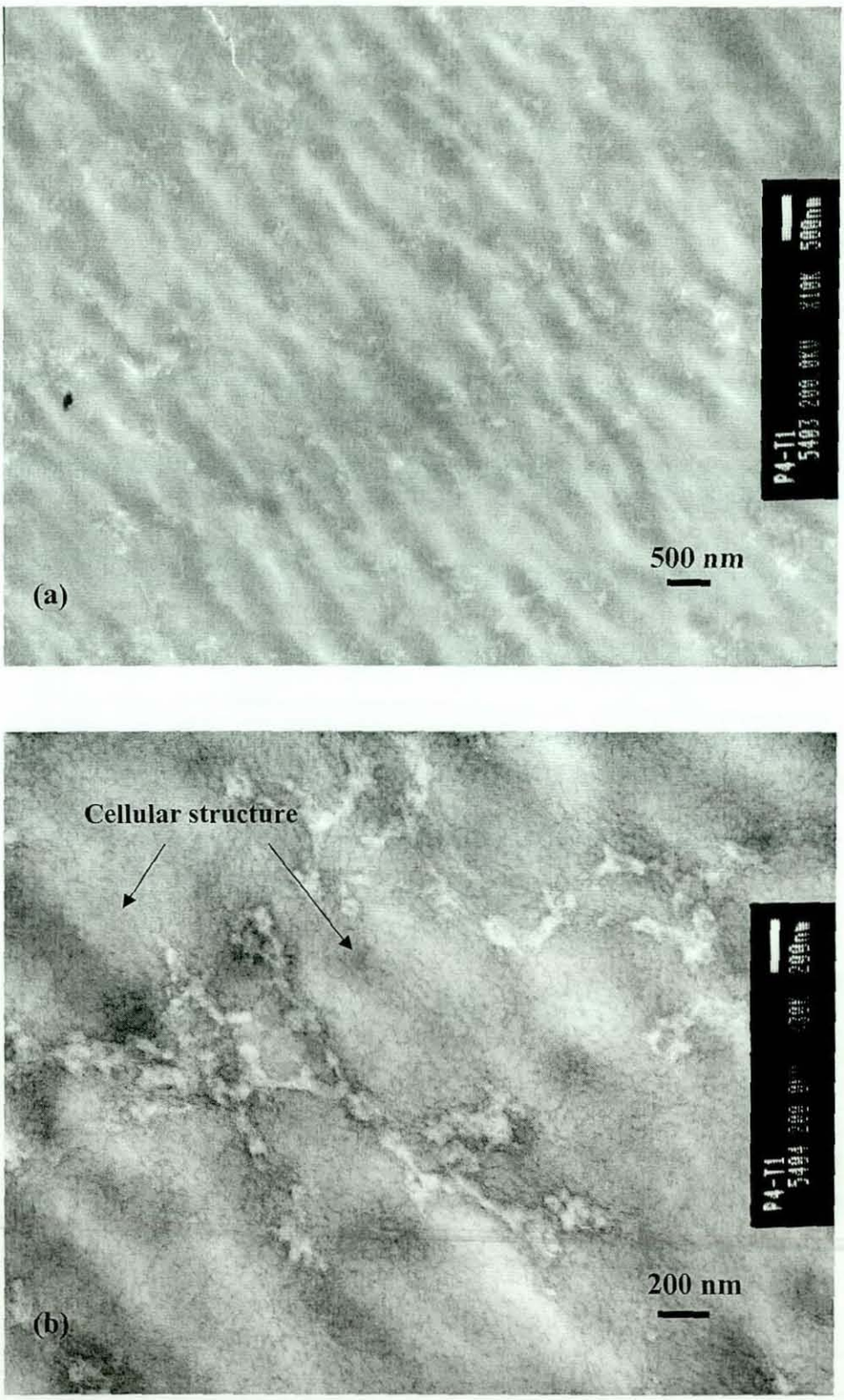


***Figure 5.8*** TEM micrographs of the 70PU/30PEMA IPN with 5 wt% C20A organoclay made by synthesis procedure four, P4. (a) At 10k magnification. (b) At 30k magnification.

procedures on the IPN organoclay nanocomposites will focus only on the morphology changes of the polymer matrix.

Adding the organoclay by the original procedure, P0, the TEM images reveal a significant change in the IPN morphology. The obvious two-phase morphology represented by the light, interconnected PEMA domains is bigger and more distinct in the dark PU matrix. A number of different shades of grey in the continuous PU matrix are present. Since, the phase boundaries are not clear, this material still reveals some extent of molecular mixing.

In synthesis procedure one, P1, the interconnected, light domains of PEMA become bigger and more interconnected as compared to those of the original procedure. Their domains are surrounded by the PU continuous matrix, which forms a cellular structure, showing the light soft segments are surrounded by the dark hard segments. This implies that the PU matrix became more phase segregated. However, many different shades of grey are still revealed. Thus, IPN morphology still exhibits the molecular mixing between the two components.

For the synthesis procedure two, P2, the IPN morphology shows that the interconnected, light PEMA domains become bigger and more interconnected as compared with those of synthesis procedure one. The PEMA domains are surrounded by the cellular PU matrix, which forms a continuous phase, become bigger also. Therefore, the PEMA tends to exhibit a more predominant phase in this IPN.

Incorporation of organoclay by synthesis procedure three, P3, shows a very similar pattern to those of the original synthesis procedure. No cellular structure is revealed. The interconnected, light PEMA domains of 50-200 nm stretch through the PU matrix, which is composed of a number of different shades of grey. Therefore, a high extent of component mixing still exists.

In synthesis procedure four, P4, again, a cellular structure was observed. Thus, the IPN morphology is similar to those of the synthesis procedures one and two. The interconnected, light PEMA domains are 100-300 nm wide in the PU continuous

phase. Nevertheless, it still shows a number of different shades of grey, implying some extent of molecular mixing.

### 5.1.3 Dynamic mechanical thermal analysis.

DMTA can be used to study the morphology and reveal evidence for such miscibility and phase continuity of a polymer blend as has been explained in section 3.3.3. The influence of the various synthesis procedures on these 70PU/30PEMA IPN organoclay nanocomposites are shown in Figures 5.9 to 5.11. The dynamic mechanical properties are also summarised in Table 5.1.

For all synthesis procedures, only a single PEMA transition with a less developed PU transition (shoulder) was observed in these 70PU/30PEMA IPN organoclay nanocomposites as can be seen in Figure 5.9. This implies that they exhibit some degree of phase separation. When the organoclay was mixed first with PPG1025, synthesis procedure P0, a shoulder PU transition appears at -14°C with a tan delta max value of 0.31, whereas an obvious PEMA transition is observed at 75°C with a tan delta max value of 0.64. The PU shoulder occurring in P0 might be due to an incomplete network, as the polyol, PPG1025, molecules have intercalated into the silicate layers. Thus, there are fewer PU constituents in the matrix to interpenetrate with the PEMA component, and, consequently, a predominant PEMA transition can be observed.

***Table 5.1*** Dynamic mechanical properties of the 70PU/30PEMA IPN organoclay nanocomposites made by the various synthesis procedures.

| Synthesis procedure | Tg at tan δ max (°C) | | Tan δ max value at Tg | | Peak width tan δ ≥ 0.3 (°C) |
|---|---|---|---|---|---|
| | PU | PEMA | PU | PEMA | |
| P0 | -14 | 75 | 0.31 | 0.64 | -19 ↔ 119 (138) |
| P1 | -15 | 75 | 0.27 | 0.70 | -3 ↔ 118 (121) |
| P2 | -16 | 71 | 0.30 | 0.74 | -19 ↔ 116 (135) |
| P3 | -14 | 79 | 0.32 | 0.57 | -19 ↔ 119 (138) |
| P4 | -15 | 77 | 0.33 | 0.68 | -19 ↔ 126 (145) |

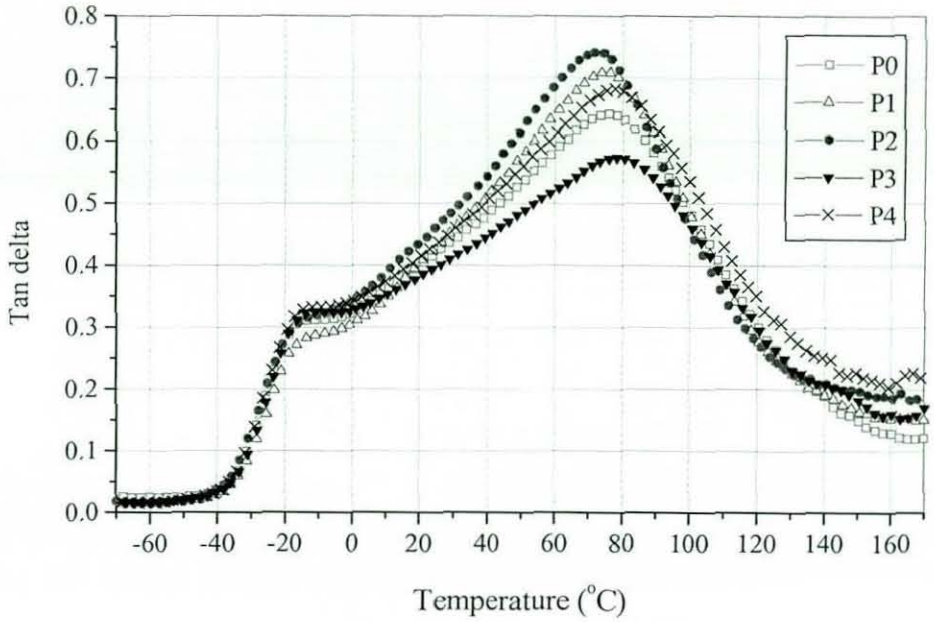


***Figure 5.9*** Loss factor versus temperature plots for the 70PU/30PEMA IPN organoclay nanocomposites made by the various synthesis procedures.

As shown in Table 5.1, when the organoclay was first mixed with a mixture of PPG1025 and TMP, synthesis procedure P1, the PU transition shows roughly at the same location (-15°C) and a significant decrease in tan delta max value from 0.31 to 0.27, as compared to those of P0. While the PEMA Tg occurs at the same temperature, 75°C, but with an increase in tan delta max value from 0.64 to 0.70. This significant reduction of the peak height of the PU transition could be due to more confined PU chains in between the silicate layers, because both polyol, PPG1025, and triol, TMP, could intercalate into the silicate layers at the same time, but might not at the same rate. This leads to a reduced amount of the PU component left to interpenetrate with the PEMA component. Hence, the tan delta profile showed more pronounced phase separation.

The organoclay was first mixed with a mixture of PPG1025, TMP and TMXDI in synthesis procedure two, P2. A shoulder PU transition shows a slight decrease from a value of -14°C to -16°C with the same tan delta max value, while a significant reduction in glass transition from 75°C to 71°C and a significant increase in tan delta max from a value of 0.64 to 0.74 at the PEMA transition are observed, as compared to

those of P0. This IPN seems likely to show the least extent of component mixing. Because TMXDI was also incorporated with the organoclay in concurrence with polyol and triol, so the soft and hard segments can establish within the silicate galleries, even though, they might not be completely formed. Thus, more PU segments may be constrained between the silicate layers. This part may not cooperate in a glass transition within the measured range. Therefore, the lower glass transition was observed. For the PEMA, the reduction in the glass transition and increase in tan δ max could be because the first formed PU network might hinder the PEMA forming. Consequently, a looser PEMA network could be formed. However, the morphology seems most likely to show more phase separation in this synthesis procedure. This may probably be because of the reduced amount of the PU component left to interpenetrate with the PEMA component. Therefore, this IPN showed the predominant PEMA transition.

In synthesis procedure three, P3, the organoclay was first added into a mixture of monomer, EMA, and crosslinker, TEGDM. Its tan delta profile shows evidence of a higher component mixing as compared to that of P0. The tan delta max value at PEMA transition decreases from 0.64, observed for P0, to a value of 0.57, while the glass transition significantly shifted from a value of 75°C, exhibited for P0, to a value of 79°C. On the other hand, no crucial changes are observed at the PU transition. The PU transition with a tan delta max value of 0.32 was at -14°C. This might prove that the PU component could intercalate into the silicate layers faster than the PEMA component. The increase in the PEMA transition could be attributed to a higher interaction at the interface between the silicate and PEMA component, as found before in section 4.2.2. Consequently, a restriction of the mobility of the PEMA network would exist, causing the reduction in the tan delta max value at the PEMA transition. Therefore, this IPN should be composed of smaller phase domains of PU and PEMA, showing more compatibility of component mixture and an increase in the interface component mixing as was found from the TEM micrographs.

In the synthesis procedure four, P4, all the components were mixed first with the organoclay, except the PU catalyst, SnOct, and the initiator, AIBN, of the PEMA component. A PU transition was revealed roughly at the same position (-15°C) and the

same tan delta max value of 0.33, as compared to P0. Whilst, the PEMA transition shows a slight increase from a value of 75°C to a value of 77°C with an increase in the tan delta max value from a value of 0.64 to a value of 0.68. These results can support an explanation that the PU component can intercalate into the layered silicates faster than the PEMA component. Thus, the PU network can establish within and outside the silicate galleries. Consequently, this leads to a decreased amount of the PU component left to interpenetrate with the PEMA component. Also, the PEMA component might be trapped by the first formed PU network resulting in an incomplete network, showing the higher tan delta max value. Therefore, this IPN showed the predominant PEMA transition.

However, these specimens are potentially useful for damping applications since the tan delta values are greater than 0.3 over wide range of temperatures: 138°C, 121°C, 135°C, 138°C and 145°C, for the IPN organoclay nanocomposites via synthesis procedure P0, P1, P2, P3 and P4, respectively.

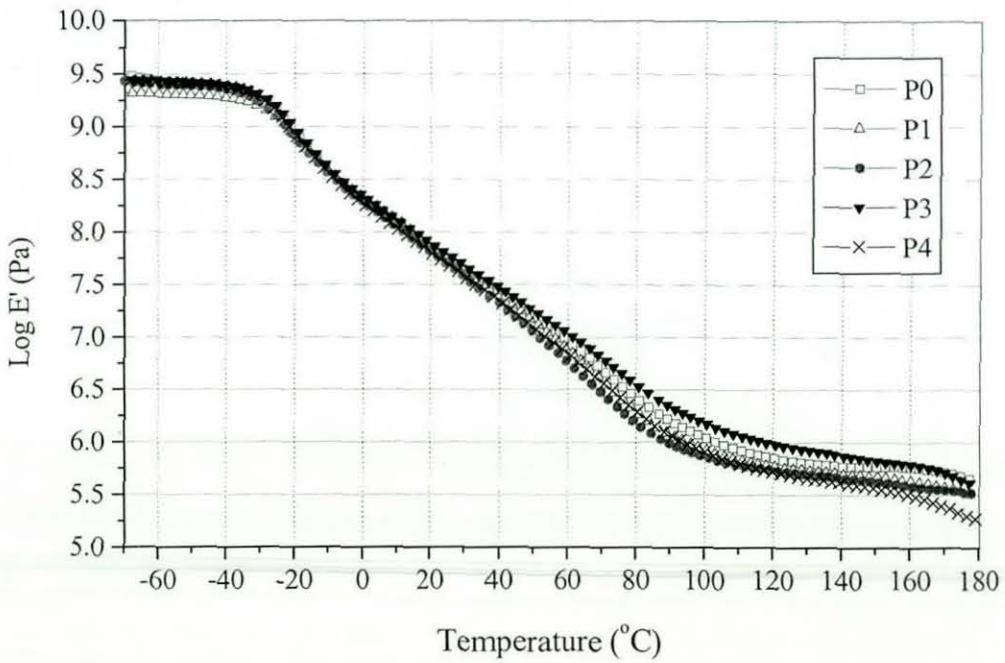


***Figure 5.10*** Storage modulus versus temperature plots for the 70PU/30PEMA IPN organoclay nanocomposites made by the various synthesis procedures.

The storage and loss moduli for all synthesis procedures show a two-step drop through the temperature range studied, as seen in Figures 5.10 and 5.11. This confirms that some extent of phase separation has occurred. The storage moduli in the glassy state do not exhibit much difference with synthesis procedure. While at temperatures beyond room temperature up to the rubbery plateau, the storage modulus of synthesis procedure two, P2, reveals the lowest value and the synthesis procedure three, P3, shows the highest value. These could be explained by using concept of component mixing. From the tan delta profile, P2 showed a higher degree of phase separation than did P3. Therefore, P2 has a reduced phase continuity morphology, and consequently decreases in storage modulus.

The loss moduli versus temperature plots in Figure 5.11 show the same findings as for the tan delta profiles. No significant effect on the PU transition is observed for changing of the synthesis procedure. The loss moduli above room temperature reflect the trends of the storage moduli as shown in Figure 5.10. P2 exhibits the lowest value of the loss modulus, while the highest value is presented by P3.

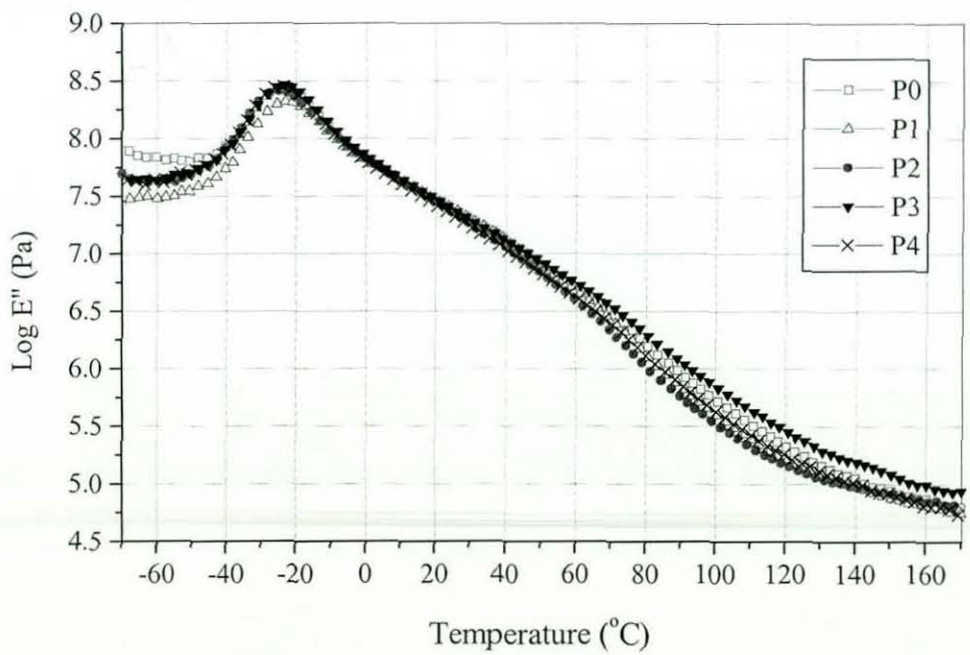


***Figure 5.11*** Loss modulus versus temperature plots for the 70PU/30PEMA IPN organoclay nanocomposites made by the various synthesis procedures.

### 5.1.4 Modulated-temperature differential scanning calorimetry.

The effect of variation of synthesis procedures on the glass transition temperatures of the 70PU/30PEMA IPN organoclay nanocomposites measured by M-TDSC is presented in Figure 5.12.

From the M-TDSC thermograms for all specimens, a prominent dCp/dT peak with a very broad dCp/dT shoulder for the PU and PEMA-rich phase transitions are observed for each specimen, suggesting microphase separation in these systems. However, there exists some extent of molecular mixing as indicated by the fact that the dCp/dT signal is significant over the inter-transition region. Because of the very broad shoulder, it is very hard to assign the Tg of the PEMA-rich phase.

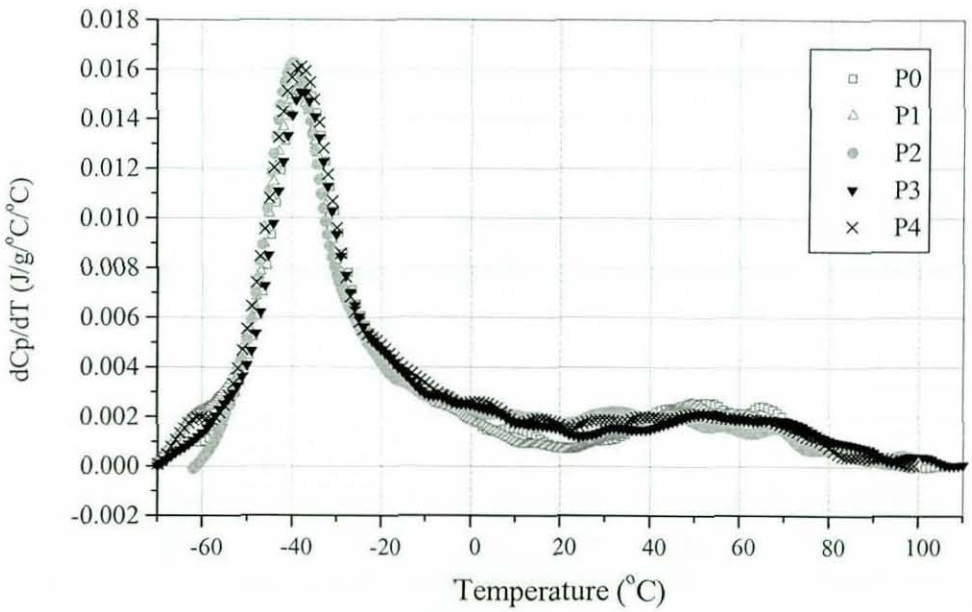


***Figure 5.12*** Differential heat capacity versus temperature plots showing the effect of variation of synthesis procedures on the 70PU/30PEMA IPN organoclay nanocomposites.

As the synthesis procedure was changed, no significant changes are observed in these thermograms. The PU-rich phase transition is at -38°C for the synthesis procedures P0, P1, P3 and P4, but for the synthesis procedure P2, it shows slightly lower at -40°C. The differential heat capacity values show no meaningful difference either at the PU or PEMA-rich phase transitions. The lower PU-rich phase transition in the P2 material

could be caused by incomplete PU network formation which might occur when polyol and isocyanate molecules were constrained between the silicate layers. Consequently, a more flexible PU network could be formed.

### 5.1.5 Tensile behaviour.

In order to study the effect of changing the synthesis procedure, the tensile properties of the 70PU/30PEMA IPN organoclay nanocomposites were evaluated. The tensile strength, extension at break, and the modulus of elasticity were calculated from the stress-strain measurements. The results are listed in Table 5.2. Figure 5.13 illustrates the tensile properties: modulus of elasticity, tensile strength and elongation at break for each synthesis procedure.

***Table 5.2*** Measured values of maximum tensile strength, extension at break and modulus of elasticity for the PU/PEMA organoclay nanocomposites with variation of the synthesis procedure.

| Synthesis procedure | Tensile strength (MPa) | Extension at break (%) | Modulus of elasticity (MPa) |
|---|---|---|---|
| P0 | 4.37 ± 0.45 | 506 ± 61 | 18.88 ± 1.30 |
| P1 | 2.84 ± 0.11 | 392 ± 24 | 17.86 ± 0.94 |
| P2 | 1.96 ± 0.28 | 381 ± 48 | 15.47 ± 1.23 |
| P3 | 5.28 ± 0.31 | 516 ± 27 | 18.35 ± 2.87 |
| P4 | 2.76 ± 0.21 | 471 ± 42 | 10.60 ± 2.08 |

In the original synthesis procedure, P0, where the organoclay was first mixed with PPG1025, the tensile strength, extension at break and the modulus of elasticity have values of 4.37 MPa, 506 %, and 18.88 MPa, respectively. When the order of mixing changed to mix PPG1025 and TMP first, synthesis procedure P1, a drastic reduction in the tensile strength and the extension at break and a slight decrease in the modulus of elasticity are seen. See in Figure 5.13.

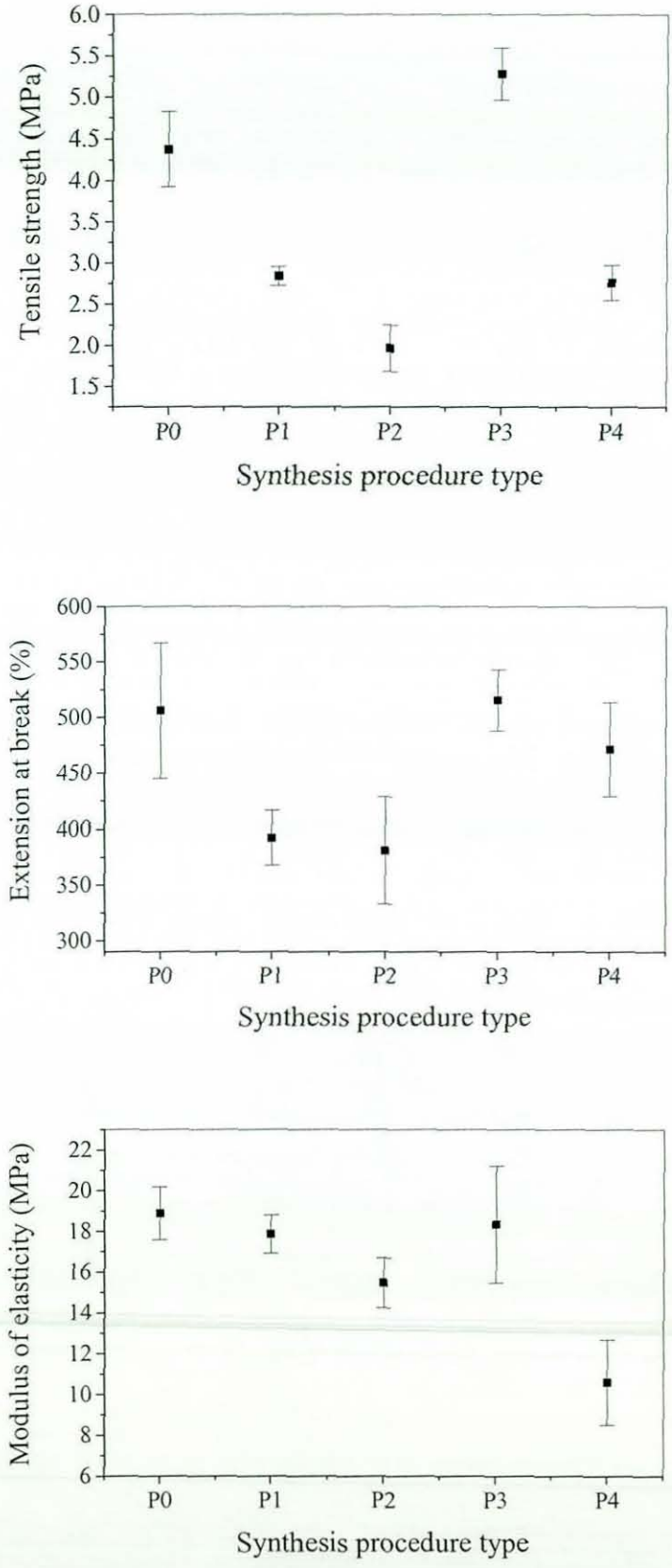


***Figure 5.13*** Tensile properties of the 70PU/30PEMA IPN organoclay nanocomposites (5 wt% C20A) as a function of synthesis procedure.

The tensile strength, the extension at break and the modulus of elasticity for P1 are 2.84 MPa, 392 % and 17.86 MPa, respectively. The reduction in the tensile strength and the elongation at break might be caused by a restricted ability of polymer chains to stretch and possibly a reduced extent of segment mixing between the PU and PEMA networks.

In synthesis procedure P2, all PU constituents were mixed first with the organoclay, except for the SnOct catalyst. The tensile strength and elongation at break severely decrease to the lowest values of 1.96 MPa and 381 %, respectively. Besides, the modulus of elasticity also slightly reduces to a value of 15.47 MPa. These results may be explained by the same reasons as stated above. Consequently, a reduction in the interfacial bonding between the PU and PEMA phases and the layered silicate and the polymer matrix might have occurred.

A slight improvement in the tensile properties, especially the tensile strength and the elongation at break, as compared with the original procedure, was found by the synthesis procedure three, P3. The tensile strength, the elongation at break and the modulus of elasticity have values of 5.28 MPa, 516 % and 18.35 MPa, respectively. The organoclay was first mixed in the PEMA constituents in this procedure, except for the initiator, AIBN. Even when the organoclay was mixed with the EMA and TEGDM, prior to combination with the PU components, the PEMA-rich phase still showed a dominant transition. It might be presumed that the PEMA components could not intercalate as well into the silicate layers as could the PU components. However, both phases seemed to exhibit a degree of continuity as shown in the DMTA results. These findings support the TEM results. This IPN probably presents the finest morphology in the whole series. Therefore, it shows the higher extent of mixing, subsequently, higher interfacial interactions between the polymer matrix itself and the polymer matrix and the silicate layers can be expected. These reasons could explain why the tensile strength increased. However, the modulus of elasticity does not show a significant difference. On the other hand, the slight increase in the extension at break might be due to the PU chains being able to align and the looser network only breaks at higher elongations.

As compared to the original procedure, P0, a great decrease in the tensile strength, the elongation at break and the modulus of elasticity were found for synthesis procedure four, P4. Especially, the modulus of elasticity shows the lowest value amongst the whole series, as can be seen in Figure 5.13. The tensile strength, the elongation at break and the modulus of elasticity are 2.76 MPa, 471 % and 10.60 MPa, respectively. In this procedure, the PU component and the PEMA component were mixed with the organoclay at the same time, except for the PU catalyst, SnOct, and the PEMA initiator, AIBN, which were added into the mixture before moulding. As the polyol, triol and diisocyanate were first mixed together with the organoclay and because of high reactivity of diisocayanate and hydroxyl groups, the PU network was the first polymer formed within and outside the silicate layers. Later on, during the last part of the polymerisation reaction, when the PU constituents were depleted in concentration, some part of the PEMA-rich phase was also constrained in the clay because the EMA monomer also could intercalate into the clay galleries. Therefore, the extent of interpenetration/interlocking of these heterogeneous phases might be reduced. Consequently, a reduction of interfacial reaction became possible. These reasons brought about a reduction in the tensile strength, the extension at break and the modulus of elasticity.

### 5.1.6 Hardness measurements.

Shore A hardness of the materials was evaluated. The indentation hardness, reflecting the resistance to local deformation, is a complex property related to the modulus, strength, elasticity and plasticity[154]. The Shore A hardness of the 70PU/30PEMA IPN organoclay nanocomposites versus synthesis procedure is illustrated in Figure 5.14.

The result presented here can be classified into two groups. The first group consists of P0, P1 and P3, which show approximately the same hardness value at Shore A 69. Another group, P2 and P4, reveals the hardness value around Shore A 63. The possible reason for the lower hardness values for specimens prepared by the P2 and P4 synthesis routes, might be because the diisocyanate was first mixed with the organoclay. Consequently, the degree crosslinking of hard segment in the PU matrix may be reduced, owning to intercalated diisocyanate. Therefore, lower modulus and tensile strength should be occurred to the finishing specimens.

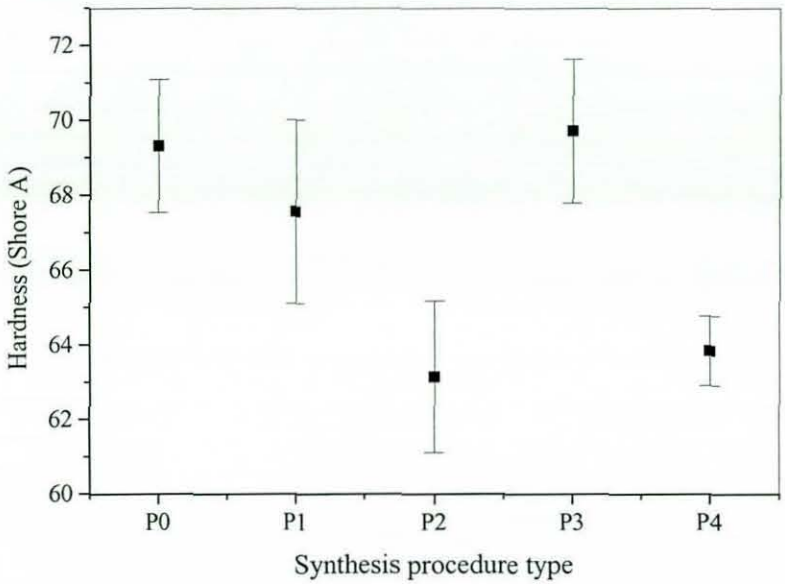


***Figure 5.14*** Shore A hardness values of the 70PU/30PEMA (5 wt% C20A) IPN organoclay nanocomposites as a function of synthesis procedure.

**5.2 Use of ultrasonication.**

Nanocomposites have received considerable attention with the expectation that nanotechnology can lead to lighter and better materials for engineering applications. They achieve their property improvements from interactions at the molecular scale between clay platelets and the polymer matrix. Therefore, exfoliated structures are often preferable. Fabricating nanocomposites where clay platelets are uniformly dispersed within a polymer matrix poses significant synthetic and processing challenges. Of great present interest is the possibility to control the morphology development of IPN organoclay nanocomposites by influencing the processing parameters.

Many researchers[45,220] have used an ultrasonication method for dispersing layered silicate clays into a polymer matrix. They found that composites prepared by ultrasonication showed a better dispersion, and, consequently, better mechanical properties. Thus, in this study, after a step where the organoclay was mixed with the polymer constituents, (for example, the organoclay was mixed with polyol for the P1 synthesis procedure or with polyol and triol for the P2 synthesis procedure etc., see their synthesis flow diagrams in chapter 3), the organoclay mixture was ultrasonicated

at an 8 micron amplitude for 1 hour at room temperature with a 5 minute process alternating with a 2 minute pause. Then, the organoclay mixing was continued following the rest of the steps in each synthesis procedure. Ultrasonic equipment, type KT150 from the Kerry Ultrasonics Ltd., with a power supply of 720 W was used.

It has been reported[45,47,221] that ultrasonic waves may cause a decrease in the molecular weight of a polymer matrix. However, the degradation rate[221] depends upon the molecular weight of the polymer sample, because increased mobility of the polymer molecules favoured harmless energy dissipation, indicating that the influence of the characteristic movements in the ultrasonic wave was relatively weak and the efficiency of degradation was limited in the case of a low viscosity polymer matrix.

Chen et al.[222] studied the decomposition of poly(ethylene glycol), PPG, in nanocomposites. They proposed that PPG with molecular weight 4,000 did not show any sign of the degradation, even after being exposed to some strong treatments, such as high temperatures, high oxygen partial pressures or longer period of times, beyond those used in preparing nanocomposites. However, the degradation of PPG increased with the molecular weight, when the molecular weight was higher than 8000.

The influence of the ultrasonication on the degradation/decomposition of the PPG1025 was also investigated. The results showed no significant change of the average molecular weights of the PPG1025, after being ultrasonicated for 0, 15 and 30 minutes, as seen in Table 5.3. This result agreed with the findings of Chen et al.

***Table 5.3*** Calculated average molecular weights and polydispersities of PPG1025 with variation of the ultrasonication time (expressed as polystyrene equivalents).

| Time (minutes) | $M_w$ | $M_n$ | Polydispersity |
|---|---|---|---|
| 0 | 1910 | 1570 | 1.2 |
| 15 | 1890 | 1580 | 1.2 |
| 30 | 1900 | 1570 | 1.2 |

In the present study, all specimens were ultrasonicated for 1 hour at room temperature. Again, the filled mould was turned over every 30 minutes in the first four hours. After that it was turned over further every one hour for another 3 hours to diminish extent of the clay settlement. The mixing time used to disperse the organoclay into the polymer constituents was 30 minutes and 5 wt% C20A organoclay was used in all the specimens in this study.

The influences of various ultrasonic assisted synthesis procedures on the glass transition behaviour, morphology, damping and mechanical properties of IPN organoclay nanocomposites were examined by several characterisation techniques.

### 5.2.1 Wide angle X-ray diffraction.

Both sides of the specimens were characterised by WAXD to examine dispersion of silicate layers. The WAXD data for both sides of C20A organoclay-filled 70PU/30PEMA IPNs for the ultrasonic assisted procedures: SP0, SP1, SP2, SP3 and SP4, are shown in Figure 5.15. An obvious C20A organoclay diffraction peak occurs at a 2θ angle of 3.85°, which corresponds to a basal spacing, $d_{001}$, of 2.29 nm. Three clear diffraction peaks are detected for both sides of the SP0 specimen, at the same 2θ angles of 2.30, 4.64 and 6.88, which correspond to a harmonic series of the 001, 002 and 003 planes, respectively. A basal spacing, $d_{001}$, is 3.84 nm, in this case, indicating that polymer chains have intercalated into the layered silicates to some extent. However, the intensity of the bottom side is stronger than that of the top side, implying that the C20A organoclay still gradually settled to that side. It can be concluded that the ultrasonic waves have not strongly affected the clay settlement. However, there is weaker diffraction intensity difference between the bottom and the top sides when using ultrasonication.

For a mixture of PPG1025 and TMP first mixed with the C20A organoclay, the ultrasonic assisted synthesis procedure one, SP1, the first diffraction peak shifted towards a lower value of 2.25°, as shown in Figure 5.15 (b), which corresponds to a basal spacing, $d_{001}$, of 3.93 nm, indicating that polymer chains have intercalated between the silicate layers to a higher degree than that of SP0, which extended the layer spacing to a value of 3.84 nm. This could be because both PPG1025 and TMP

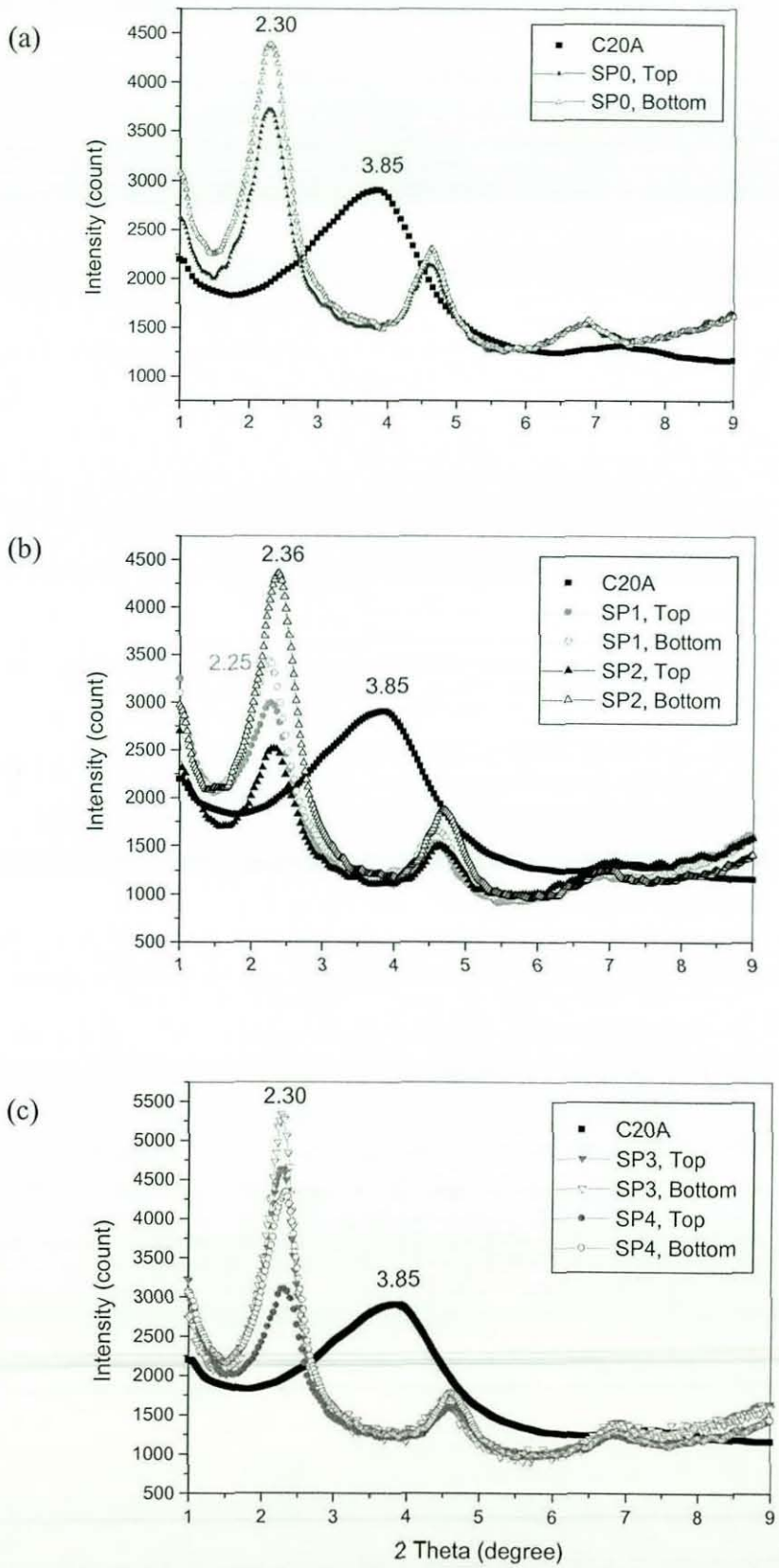


***Figure 5.15*** WAXD patterns for top and bottom sides of C20A organoclay filled 70PU/30PEMA IPNs prepared by the various ultrasonic assisted synthesis procedures.

were intercalated into the clay layers, so stronger repulsion forces of the hydroxyl groups of triol and polyol molecules could exist. Consequently, this caused expansion of the distance between the silicate layers. However, a slight increase in d-spacing only ± 2.3 % is probably within experimental error. Besides, the bottom and the top diffraction results continue to show a difference in peak intensity, indicating the phenomenon of the settlement of clay particles occurred to some extent.

In the ultrasonic assisted synthesis procedure two, SP2, the mixture of diisocyanate, PPG1025 and TMP were first mixed with the organoclay. WAXD results show a shift of the first diffraction peak from a value of 3.85°, observed for the C20A organoclay, to a value of 2.36°, which corresponds to an interspacing distance, $d_{001}$, of 3.74 nm, Figure 5.15 (b), indicating that some polymer chains have intercalated, but to a lesser extent than for SP0, which exhibited $d_{001}$ of 3.84 nm. This may possibly be because the diisocyanate groups reacted with the polyol molecules faster than they intercalated into the clay layers. Therefore, a smaller amount of PU segments occupied the silicate galleries. The intensity difference between the top and the bottom reveals a bigger gap as compared to that of the P0. A possible reason is an increase in overall viscosity of the matrix, as a result of the faster polymerisation of the PU networks, restricted the settlement of clay particles during polymerisation.

As seen in Figure 5.15(c), WAXD results for the ultrasonic assisted synthesis procedure three, SP3, where the organoclay was first mixed with the PEMA components, monomer EMA and crosslinker TEGDM, reveals the first diffraction peak (001) at 2.30°, corresponding to an interlayer spacing of 3.84 nm, which is the same value as the basal spacing obtained for SP0. This indicates that the PEMA can also intercalate into silicate layers to around the same extent as the PU network did. However, the top and the bottom sides still give a difference in the diffraction intensity.

The ultrasonic assisted synthesis procedure four, SP4, where both PU and PEMA components, except the catalyst, SnOct, and the initiator, AIBN, were mixed with the C20A organoclay, shows a shift in the first diffraction peak position from 3.85°, observed for the C20A organoclay, to a value of 2.30°, corresponding to a basal

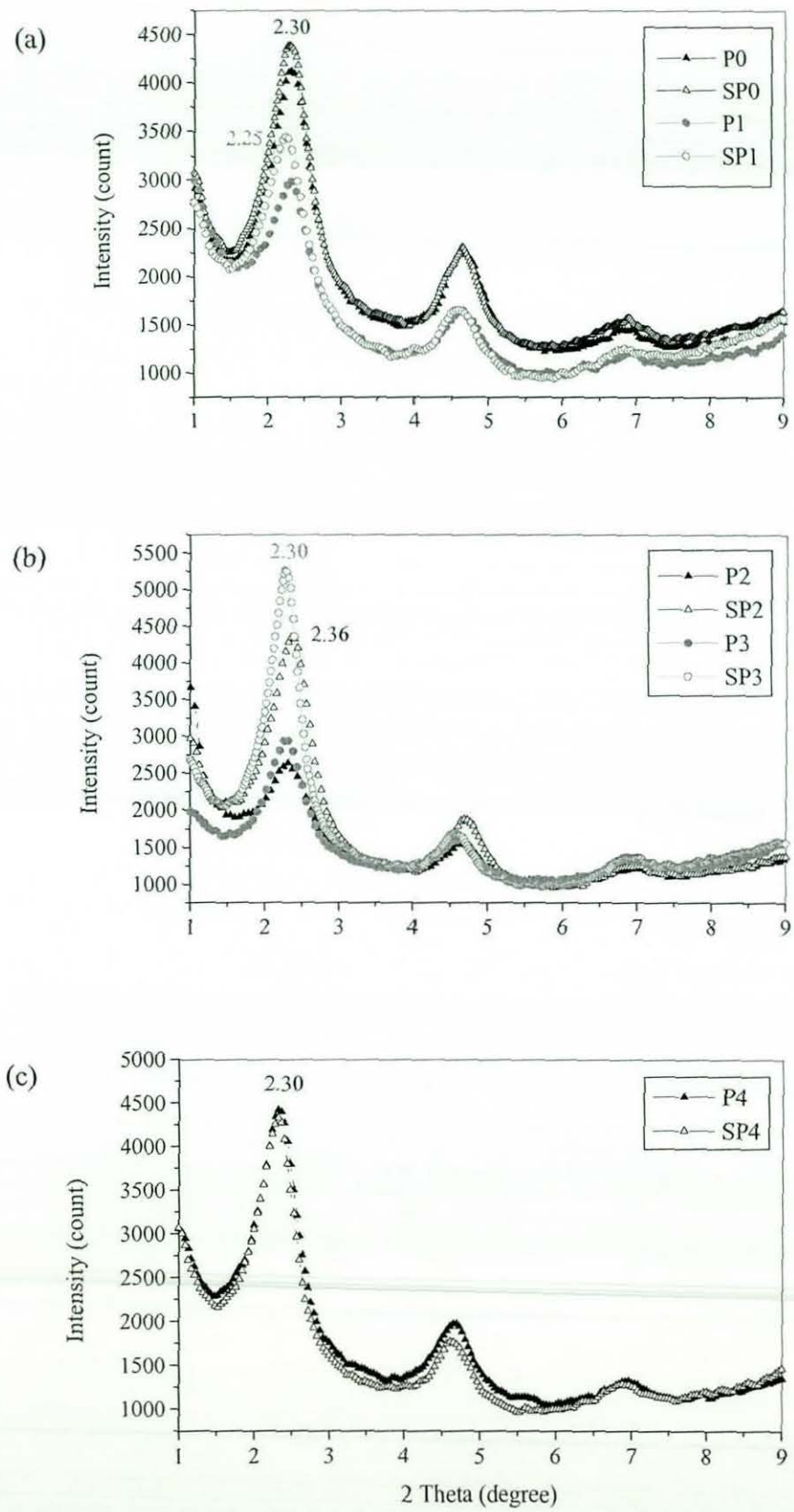


***Figure 5.16*** WAXD patterns of C20A organoclay filled 70PU/30PEMA IPNs prepared by the various synthesis procedures with and without the ultrasonication.

distance of 3.84 nm, which is the same value as that of SP0, shown in Figure 5.15(c). This is not surprising, since both networks could intercalate concurrently into the clay galleries. Their abilities to intercalate into the silicate layers were quite similar, as proven from the results of SP0 and SP3, even though they might not do at the same rate. However, the difference for the top and the bottom sides is quite large. This might be probably be caused by a high overall viscosity, as both networks formed.

Comparison of X-ray diffraction patterns for C20A organoclay filled 70PU/30PEMA IPNs prepared by the various synthesis procedures with and without ultrasonication was also made. After in-situ intercalative polymerisation, WAXD patterns for the specimens prepared with and without the ultrasonication show around the same interlayer spacing for each pair, which were synthesised by P0, P2, P3 and P4. See in Figures 5.2 and 5.15. For P1, the diffraction peak shifted towards a lower value of 2.25° as revealed for SP3, but it showed at a value of 2.30° for P3. However, the fluctuation is within ±2% which is within an experimental error. Therefore, the use of ultrasonic waves has showed that there is no any significant improvement in the dispersion ability of the silicate layers for the C20A organoclay filled 70PU/30PEMA IPN system.

### 5.2.2 Transmission electron microscopy.

TEM and WAXD are complementary characterisation methods[218]. WAXD does not help identify precisely the nanocomposite morphology. TEM, however, can do this.

TEM images of various ultrasonic-assisted synthesis procedures: SP0, SP1, SP2, SP3 and SP4 are presented in Figures 5.17 to 5.21, respectively. As can be seen from Figures 5.17 to 5.21, all IPN nanocomposites show light, interconnected domains of PEMA stretching through the dark PU matrix. The phase domains are not well defined, indicating no gross phase separation occurs. The interphase boundaries between the domains and the matrix are not clear. The high extent of different shades of grey in the PU matrix can be seen, showing some extent of molecular mixing between the two components. Very large and unevenly dispersed primary clay particles, tactoids, are observed in the polymer, strongly suggesting that there is a poor dispersion. The size of these tactoids is in the order of 0.5-3 μm, as seen in Figures 5.17 (a) and 5.21(a).

There is no sign of individual silicate platelets. The systems presented here only show intercalation. Thus, further studies will focus on only the morphology changes in the polymer matrix.

SP0, SP1 and SP4 morphologies reveal a cellular structure with incorporation of light PEMA domains in the PU cellular matrix, the light soft segments surrounded by the dark hard segments. The size of the cellular domains is very fine for SP0, but becomes bigger for SP1 and the biggest cellular domains are found for SP4. However, the different shades of grey areas at the phase boundaries between the PEMA domains and PU matrix can be seen, especially, at the phase boundaries around the PEMA domains, indicating some extent of molecular mixing between the two components. The SP2 and SP3 morphologies show the light PEMA domains stretching through fairly uniform PU matrix of a high amount PEMA as a major part of the matrix, especially, for SP3, can be seen the lighter matrix. These might be explained by variations of the PEMA content dissolved in the predominantly PU matrix. Besides, the darker matrix areas are more frequently observed around the PEMA domains and appeared to be to some extent interconnected. Therefore, the morphology of the whole series reveals some extent of phase separation with the PEMA domains. However, the clear-cut of the two-phase morphology has not been shown.

The morphologies of the C20A organoclay filled 70PU/30PEMA IPNs prepared by the various synthesis procedures, with and without ultrasonication, were also examined. Similar sizes of the light, interconnected PEMA domains in the quite uniform PU matrix were seen in both the P0 and SP0 micrographs. The morphologies of P1 and SP1 also looked very similar to each other. The light PEMA domains became bigger and more interconnected, as compared with those of P0 and SP0, and they stretched through the cellular matrix. Instead of a cellular structure, in P2, but with the same sizes of the PEMA domains spreading in a fairly uniform PU matrix were seen in SP2, suggesting an increase in extent of the component mixing. No cellular structure was observed in both P3 and SP3 morphologies. The interconnected, light PEMA domains of SP3 were slightly bigger and more interconnected than those of P3. Besides, the PEMA acted as a major part of the matrix, which could be seen the lighter matrix also.

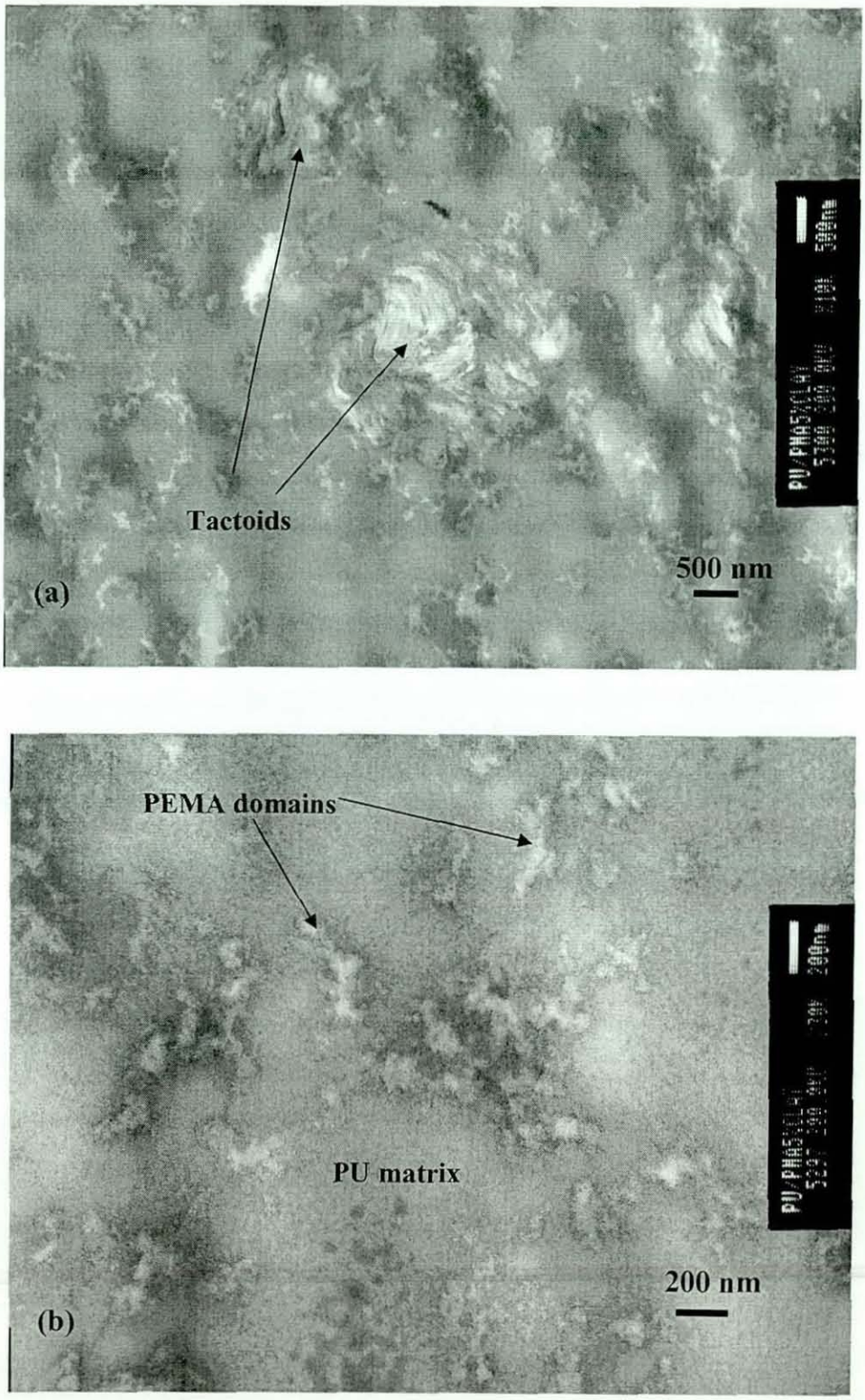


***Figure 5.17*** TEM micrographs for the 70PU/30PEMA (5 wt% C20A) IPN organoclay nanocomposites with ultrasonic assisted original synthesis procedure, SP0. (a) At 10k magnification. (b) At 30k magnification.

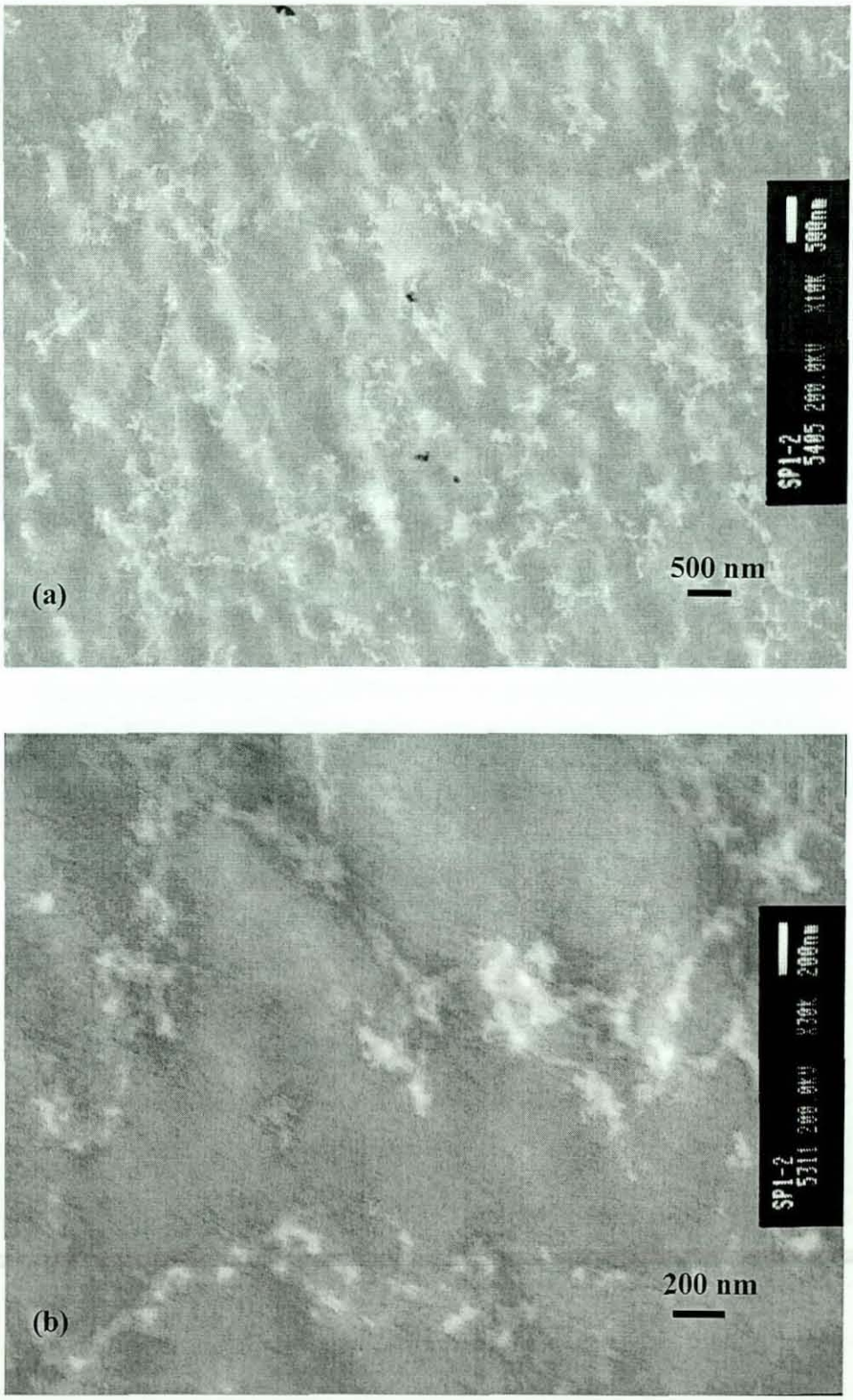


***Figure 5.18*** TEM micrographs for the 70PU/30PEMA (5 wt% C20A) IPN organoclay nanocomposites with ultrasonic assisted synthesis procedure one, SP1. (a) At 10k magnification. (b) At 30k magnification.

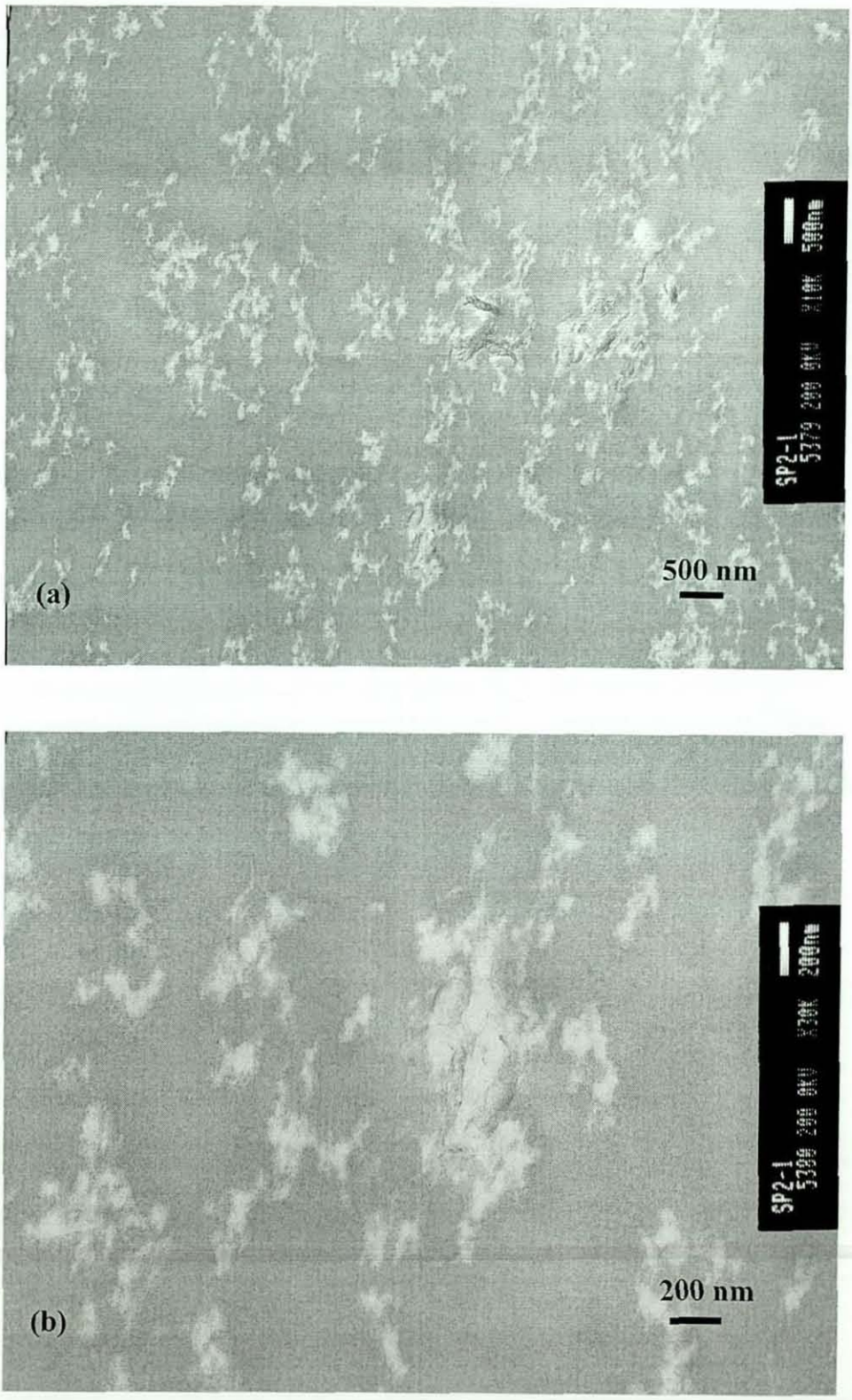


***Figure 5.19*** TEM micrographs for the 70PU/30PEMA (5 wt% C20A) IPN organoclay nanocomposites with ultrasonic assisted synthesis procedure two, SP2. (a) At 10k magnification. (b) At 30k magnification.

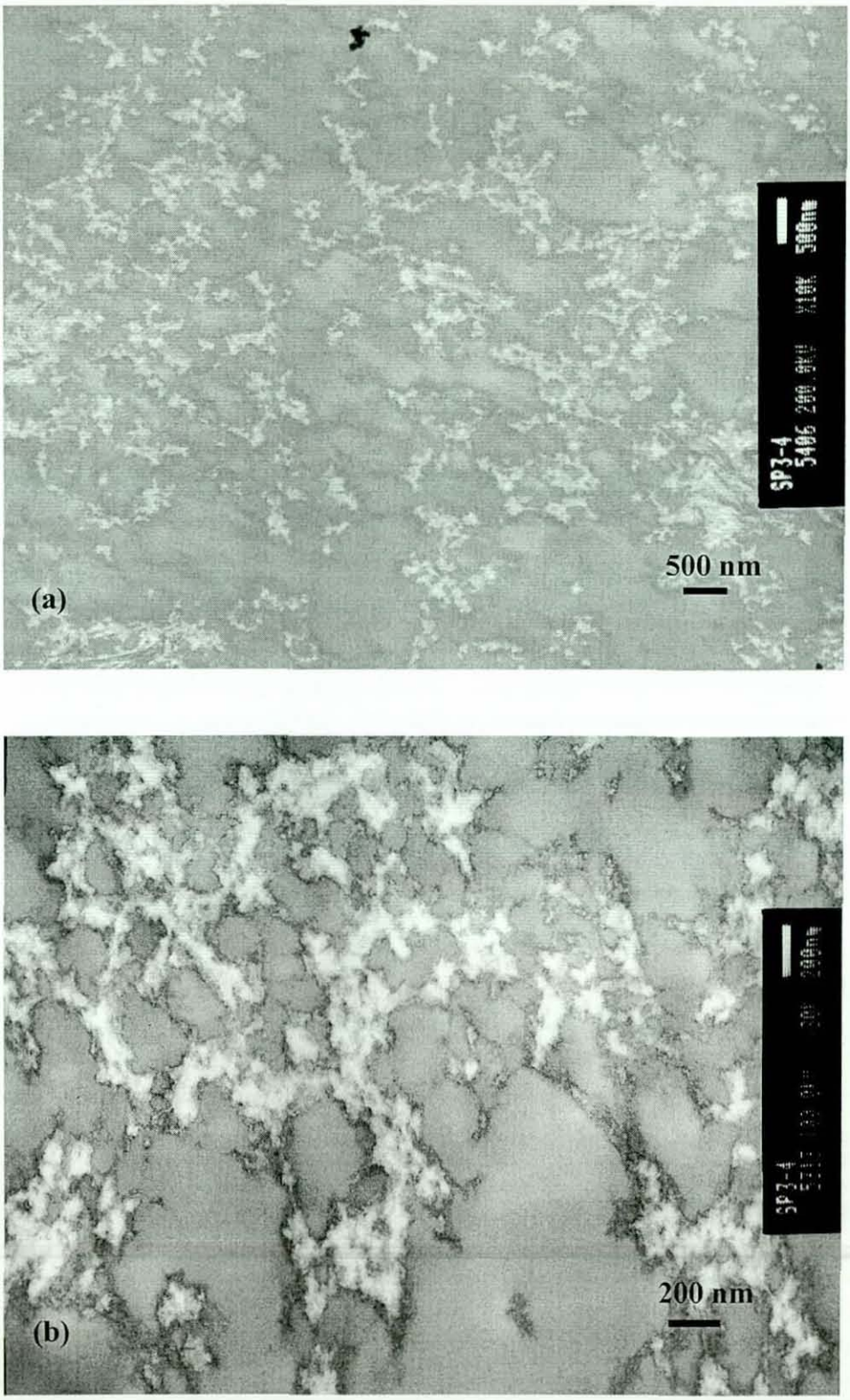


***Figure 5.20*** TEM micrographs for the 70PU/30PEMA (5 wt% C20A) IPN organoclay nanocomposites with ultrasonic assisted synthesis procedure three, SP3. (a) At 10k magnification. (b) At 30k magnification.

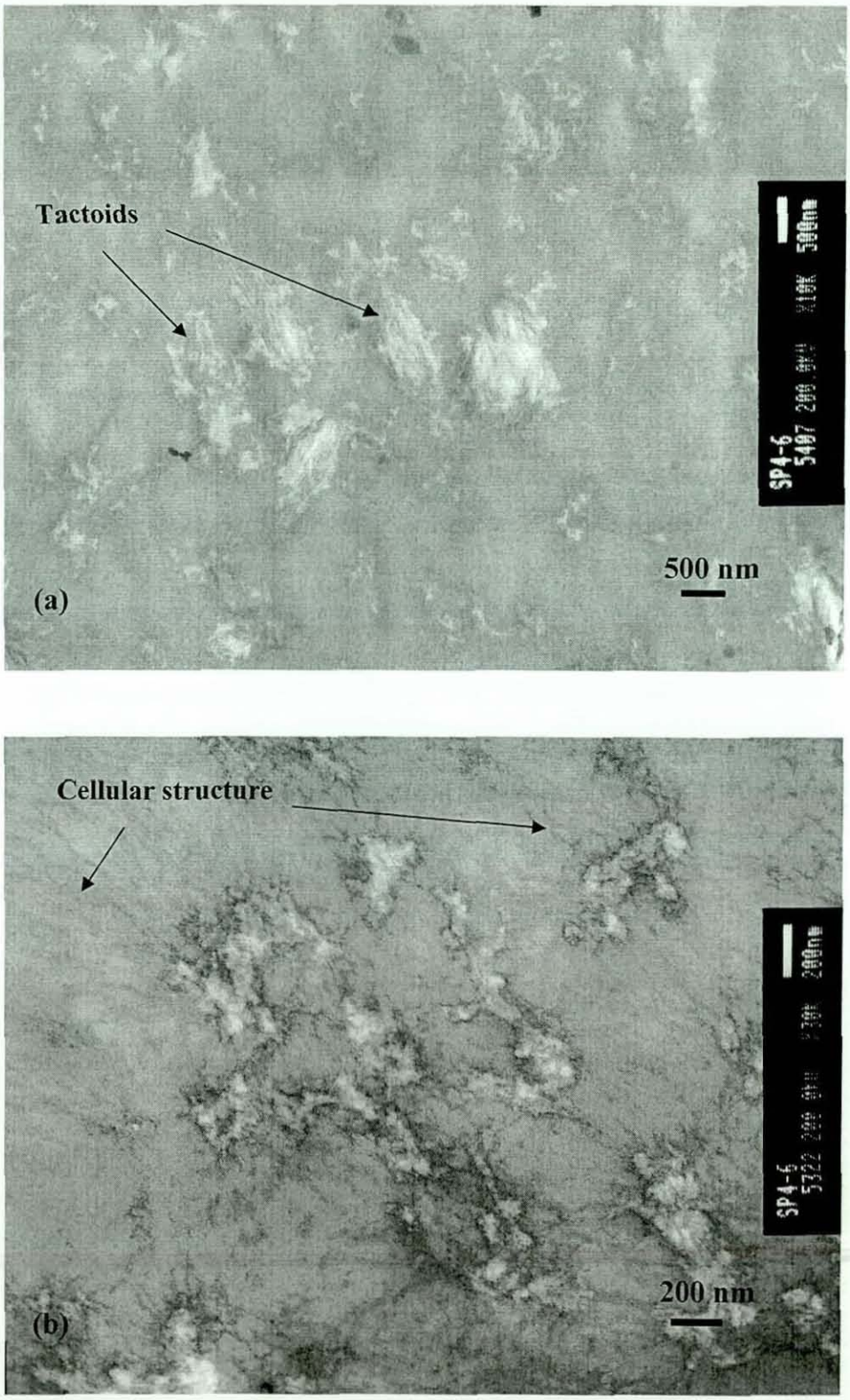


***Figure 5.21*** TEM micrographs for the 70PU/30PEMA (5 wt% C20A) IPN organoclay nanocomposites with ultrasonic assisted synthesis procedure four, SP4. (a) At 10k magnification. (b) At 30k magnification.

There were no obvious distinctive morphology differences between P4 and SP4. Their morphologies showed the light PEMA domains spreading in the cellular PU matrix. However, all specimens showed high extent of molecular mixing, which was revealed by a number of different shades of grey in the PU matrix.

### 5.2.3 Dynamic mechanical thermal analysis.

DMTA was used to examine the influences of ultrasonic-assisted synthesis procedures, coded as SP0, SP1, SP2, SP3 and SP4, on the dynamic mechanical properties of the 70PU/30PEMA IPN organoclay nanocomposites. The resulting bending loss factor, storage modulus and loss modulus spectra of these 70PU/30PEMA IPN organoclay nanocomposites are illustrated in Figures 5.22 to 5.24. The dynamic mechanical properties are summarised in Table 5.4.

***Table 5.4*** Dynamic mechanical properties of the 70PU/30PEMA IPN organoclay nanocomposites with various ultrasonic-assisted synthesis procedures.

| Synthesis procedure | Tg, °C at tan δ max. | | Tan δ max value at Tg | | Peak width, °C tan δ ≥ 0.3 |
|---|---|---|---|---|---|
| | PU | PEMA | PU | PEMA | |
| SP0 | -14 | 80 | 0.30 | 0.59 | -13 ↔ 123 (136) |
| SP1 | -15 | 77 | 0.30 | 0.71 | -17 ↔ 124 (141) |
| SP2 | -16 | 74 | 0.28 | 0.80 | -11 ↔ 117 (128) |
| SP3 | -14 | 75 | 0.29 | 0.64 | -4 ↔ 119 (123) |
| SP4 | -13 | 77 | 0.33 | 0.69 | -20 ↔ 126 (146) |

As observed in Figure 5.22, the dynamic loss factor profiles for all samples, synthesised by the various ultrasonic-assisted procedures were similar in shape and correlative order, compared with those obtained from specimens which were not sonicated, except for the sample prepared by the SP3 procedure.

Ultrasonicated 70PU/30PEMA IPN organoclay nanocomposites prepared by all synthesis procedures, SP series, show only an obvious PEMA transition with a less developed shoulder at the PU glass transition. See Figure 5.22. This implies that they

have to some extent of a phase separated morphology. These results confirm the findings of the TEM investigations.

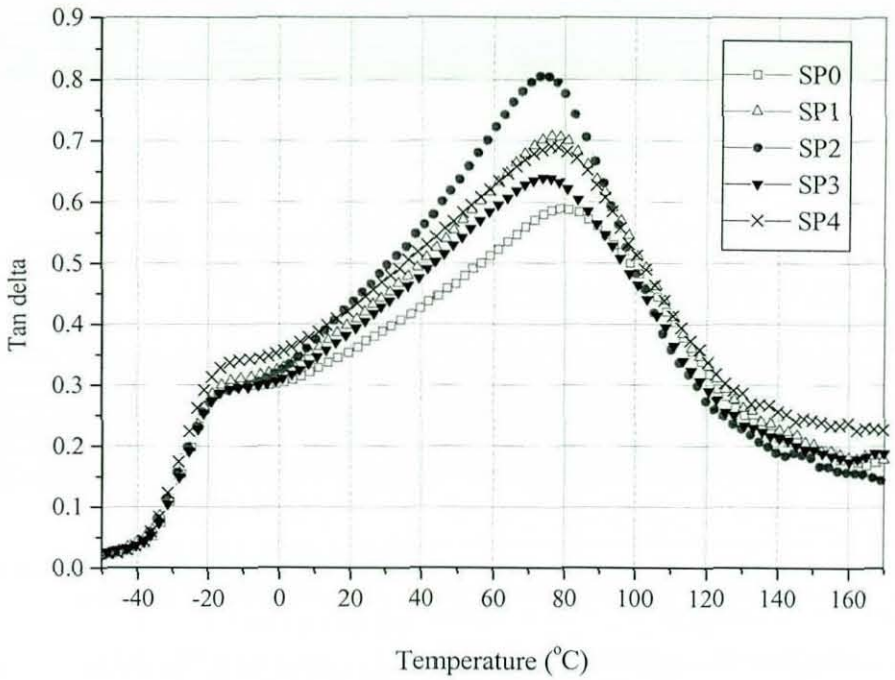


***Figure 5.22*** Loss factor versus temperature plots for the 70PU/30PEMA IPN organoclay nanocomposites from the various ultrasonic assisted synthesis procedures.

Correlation of damping mechanical properties of the 70PU/30PEMA IPN organoclay nanocomposites prepared by the various synthesis procedures with and without ultrasonication is given in Table 5.5. When the organoclay was mixed first with PPG1025 in SP0, a PU transition occurs at -14°C with a tan delta max value of 0.30, whereas a strong PEMA transition is observed at 80°C with a tan delta max value of 0.59. Ultrasonication causes the PEMA transition to shift from a value of 75°C to 80°C, but the tan delta max value decreases from 0.64 to 0.59, as compared to those of P0. This might probably be caused by the ultrasonic waves breaking some big clay agglomerates into smaller agglomerates and permitting a higher number of PEMA segments to adsorb onto the silicate surface. Thus, the PEMA network was less mobility (higher Tg and lower tan delta max).

***Table 5.5*** Dynamic mechanical properties of the 70PU/30PEMA IPN organoclay nanocomposites prepared by various synthesis procedures with and without the ultrasonication.

| Synthesis procedure | Tg at tan δ max (°C) | | | | Tan δ max value at Tg | | | |
|---|---|---|---|---|---|---|---|---|
| | PU | | PEMA | | PU | | PEMA | |
| | P | SP | P | SP | P | SP | P | SP |
| P0 | -14 | -14 | 75 | 80 | 0.31 | 0.30 | 0.64 | 0.59 |
| P1 | -15 | -15 | 75 | 77 | 0.27 | 0.30 | 0.70 | 0.71 |
| P2 | -16 | -16 | 71 | 74 | 0.30 | 0.28 | 0.74 | 0.80 |
| P3 | -14 | -14 | 79 | 75 | 0.32 | 0.29 | 0.57 | 0.64 |
| P4 | -15 | -13 | 77 | 77 | 0.33 | 0.33 | 0.68 | 0.69 |

In SP1, when the organoclay was mixed first with the mixture of PPG1025 and TMP, there was no significant change in either the glass transition or the tan delta max value at the PU Tg. Whereas, the PEMA Tg slightly decreased from 80°C to 77°C with an increase in tan delta max value from 0.59 to 0.70, as compared with those of SP0. This could be because both polyol and triol molecules could intercalate into the silicate galleries. So, a lesser amount of the PU constituents may interpenetrate with the PEMA network outside the silicate clay galleries. Consequently, the PEMA was predominant. Also, a slight reduction of the PEMA transition might probably be because a less crosslinked PEMA network is formed (lower Tg and higher tan delta max), owning to a lesser amount of reacted monomer/crosslinker to form the PEMA network. However, results for SP1 do not reveal any significant difference as compared to those of P1, except only a slight increase in both PU and PEMA tan delta max values

C20A organoclay was first mixed with the mixture of PPG1025, TMP and TMXDI in the ultrasonic-assisted synthesis procedure two, SP2. The PU transition showed no significant shift at -16°C. A reduction in glass transition from 80°C to 74°C, and a steep increase in tan delta max value at PEMA transition from 0.59 to 0.80 were observed, as compared to those of SP0. This IPN shows the greatest change in its morphology. Because TMXDI was incorporated with the organoclay in concurrence with the polyol

and triol, the PU segments can establish within the silicate galleries. Thus, a higher amount of the PU segments is constrained between the silicate layers. Consequently, the PEMA segments were less restricted when they interpenetrated with the reduced amount of PU networks outside the layered silicate. This might be a reason why the tan delta max value was increased at the PEMA transition, making the predominant network. Besides, the first formed PU network and higher fraction area of silicate particles could hinder the PEMA forming. Consequently, a PEMA network of lower crosslink density could be formed, exhibiting a lower glass transition and higher tan delta max. However, SP2 shows an increase in PEMA transition from a value of 71°C to a value of 74°C with higher tan delta max value from 0.74 to 0.80, while, the tan delta max at PU transition shows no significant changes, as compared to P2. Under the present reaction conditions, the PU reaction proceeded faster than the PEMA formation. Thus, the PEMA network might was trapped by the first formed PU network which was spread in an increasing number of areas in the matrix, as the silicate layers were under the ultrasonication. Consequently, an increasing number of interface interactions of the PEMA network, which was surrounded by the PU network and near the spread silicate layers, with the phases were possible. These could be some explanations for the significant increase in the glass transition at the PEMA transition.

In the ultrasonic-assisted synthesis procedure three, SP3, the organoclay was first added into a mixture of a monomer, EMA, and a crosslinker, TEGDM. As seen in Figure 5.22, the PEMA glass transition decreases from 80°C to 75°C with an increase in tan delta height from a value of 0.59 to a value of 0.64, as compared to those of SP0. On the other hand, it shows no significant changes at the PU transition. The PU shoulder has a tan delta max value of 0.29 at -14°C. This might prove that the PU component could intercalate into the silicate layers faster than the PEMA component. A decrease in the PEMA transition and an increase in tan delta max could result from a reduction in the degree crosslinking because of intercalated and non-reacted monomer/crosslinker, yielding more a flexible molecular network. However, the PEMA transition slightly decreased from 79°C to 75°C with an increase in tan delta max value from a value of 0.57 to a value of 0.64, as compared to those of P3. Whilst, the PU tan delta max slightly decreased from a value of 0.32 to a value of 0.29 with same PU transition at -14°C. Because of a better dispersion of smaller aggregates, there

is a greater extent of the intercalated and non-reacted monomer/crosslinker, consequently, a looser PEMA network could be formed.

All the chemicals were mixed first with the organoclay, except the PU catalyst, SnOct, and the initiator, AIBN, of the PEMA component in SP4. A PU transition still shows at the same position (-13°C) and a slight increase in tan delta max value from a value of 0.30 to a value of 0.33, as compared with those of SP0. Whilst, the PEMA transition shows a slight decrease from 80°C to 77°C with a significant increase in the tan delta max value from a value of 0.59 to a value of 0.69. These results can support an explanation that the PU component can intercalate into the layered silicates faster than the PEMA component. Therefore, the PU component might interpenetrate to a lesser extent with the PEMA component outside the silicate layers. Therefore, the PEMA network should be the predominant phase. Again, it is believed that a more flexible PEMA molecular structure, showing a lower Tg and a higher tan delta max, is formed because of intercalated and non-reacted monomer/crosslinker being constrained in the clay galleries. However, the PU and PEMA transitions show no changes as compared with the results of P4. Therefore, ultrasonication shows insignificant effects on synthesis procedure four.

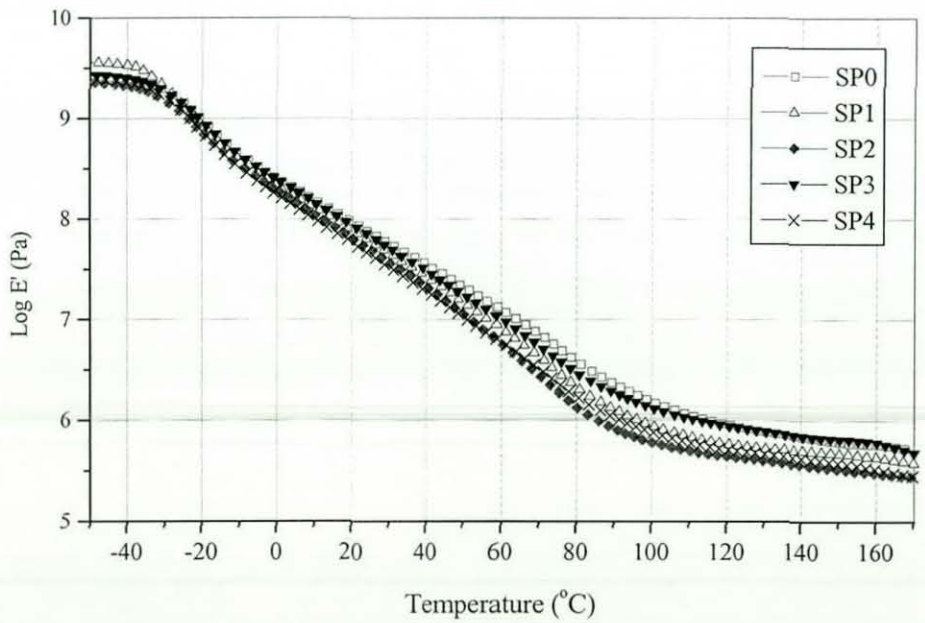


***Figure 5.23*** Storage modulus versus temperature plots for the 70PU/30PEMA IPN organoclay nanocomposites from the various ultrasonic assisted synthesis procedures.

Figure 5.23 shows the storage moduli for various ultrasonic assisted synthesis procedures. Again, they show a two-step drop through the measured temperature range, indicating some extent of phase separation. The storage moduli around the glassy state do not exhibit much different, while at temperatures beyond room temperature up to the rubbery plateau the storage moduli reveal significant changes, as the synthesis procedure varied. A similar comparative pattern as compared to those of unaided ultrasonicated samples, is found.

The storage modulus of SP2, reveals the lowest value. The ultrasonic-assisted original synthesis procedure, SP0, shows the highest value. These results correspond to the tan delta profiles in Figure 5.22. As can be seen in Figure 5.22, the SP2 seems likely to exhibit the highest extend of phase discontinuity, while the SP0 shows the largest extent of component mixing. Therefore, SP2 should has the lowest modulus value, which is the same as that found in P2, indicating that the ultrasonication did not help to change the modulus of the IPN prepared by this synthesis route. Besides, the other three specimens, SP1, SP2 and SP3, show lower modulus values than that SP0.

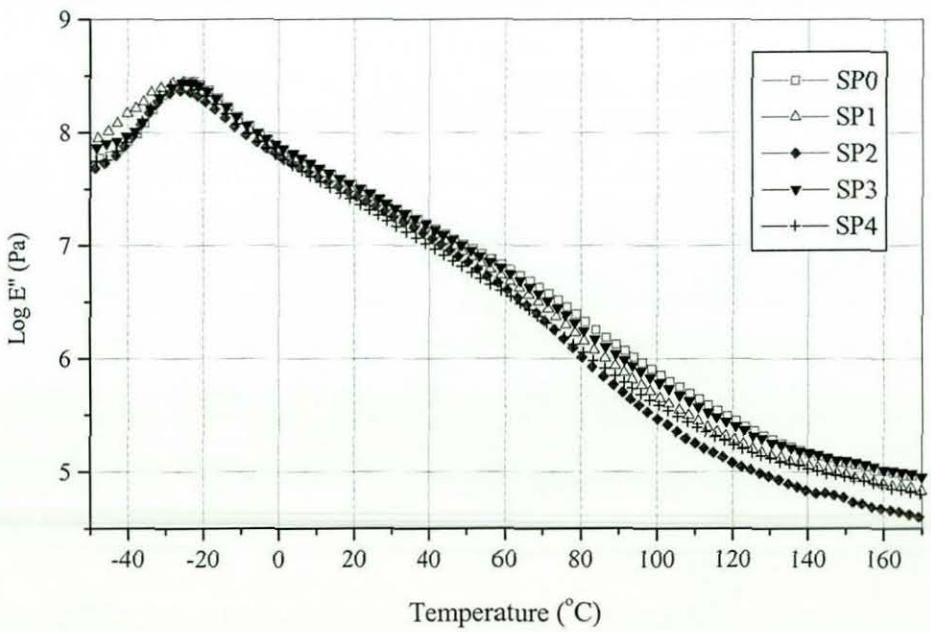


***Figure 5.24*** Loss modulus versus temperature plots for the 70PU/30PEMA IPN organoclay nanocomposites from the various ultrasonic assisted synthesis procedures.

The loss moduli for various ultrasonic-assisted synthesis procedures are shown in Figure 5.24. Again, they show some extent of phase separation. The loss moduli around the glassy state and also at the PU transition show no any differences, while at temperature above room temperature up to the rubbery plateau, the loss moduli reveal significant changes, as the synthesis procedure varied. These results show the same trend as found in the storage modulus. The lowest loss modulus was found for SP2. An alternative order between SP0 and SP3 profiles was also observed in a comparative of the loss modulus profile results between aided and unaided ultrasonication, as do in the storage modulus. Nevertheless, only a very small difference between those two profiles was noticed.

### 5.2.4 Modulated-temperature differential scanning calorimetry.

The 70PU/30PEMA IPN organoclay nanocomposites prepared via the various synthesis procedures aided by ultrasonication were also characterised by M-TDSC. The effects of variation of synthesis procedure on the glass transition temperatures are shown in Figure 5.25 and Table 5.6.

***Table 5.6*** M-TDSC data for the 70PU/30PEMA IPN organoclay nanocomposites from the various ultrasonication synthesis procedures.

| Synthesis procedure | Tg, °C | dCp/dT value, $J/g^{-1}°C^{-2}$ |
|---|---|---|
| | PU | PU |
| SP0 | -38 | 0.018 |
| SP1 | -39 | 0.019 |
| SP2 | -41 | 0.018 |
| SP3 | -37 | 0.016 |
| SP4 | -39 | 0.018 |

As can be seen from Figure 5.25, the M-TDSC curves in the form of the differential of heat capacity versus temperature plots for all specimens show a prominent dCp/dT peak with a very broad dCp/dT shoulder for the PU and PEMA-rich phase transitions, respectively, indicating microphase separation in these systems. However, there exists some degree of molecular mixing as indicated by the dCp/dT signal which has a

similar, non-zero, height continuously spanning the studied temperature range. Because of the very broad shoulder, it is very hard to assign the Tg of the PEMA-rich phase. Therefore, only the PU-rich phase transitions and their differential heat capacity values are summerised in Table 5.6.

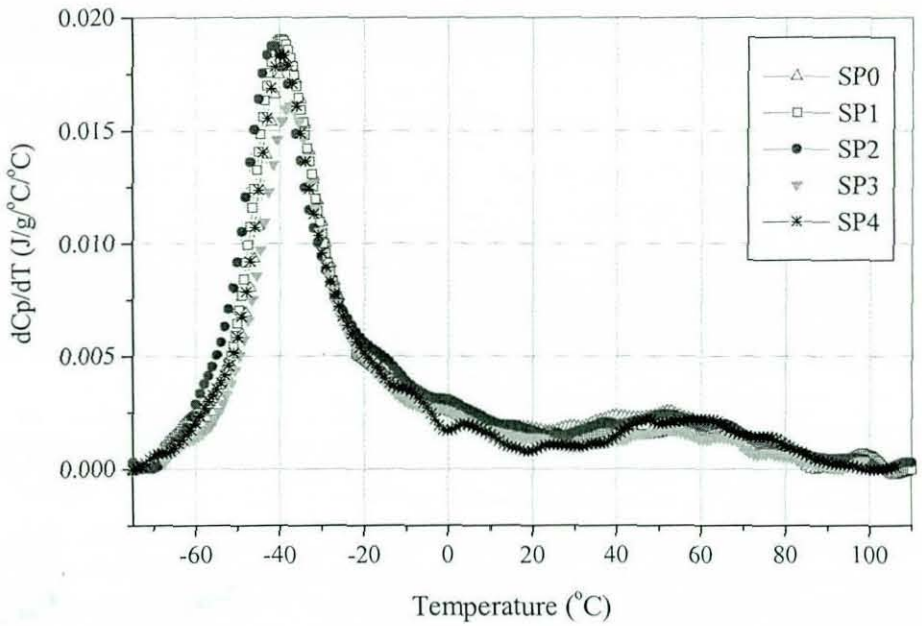


***Figure 5.25*** Differential heat capacity versus temperature plots showing the effect of the ultrasonic assisted synthesis procedures on the 70PU/30PEMA IPN organoclay nanocomposites.

As the synthesis procedure was changed, a slight shift of the PU-rich phase transition towards lower temperature, from -38°C, observed for SP0, to -41°C, obtained for SP2. The other IPNs show no significant changes in the PU transition in the temperature range measured in this study, as summerised in Table 5.6. The lowest of the PU-rich phase transitions might probably be caused by a lower extent of crosslinking in the PU network. As the PU constituents, except catalyst, SnOct, were intercalated first into the silicate layers, consequently, some parts were confined between the silicate galleries. Therefore, an incomplete PU network might be formed, showing a drop in the PU Tg. However, the differential heat capacity at the PU-rich phase shows no significant changes by changing the synthesis procedure. This conclusion was the same as for the specimens which were not sonicated.

### 5.2.5 Tensile behaviour.

The mechanical properties of 70PU/30PEMA IPN organoclay nanocomposites with variations in the ultrasonic assisted synthesis procedure were determined by tensile testing. The tensile strength, extension at break and the modulus of elasticity for each ultrasonic-assisted synthesis procedure are portrayed in Figure 5.26 and their data are summarised in Table 5.7. The tensile properties of the 70PU/30PEMA IPN organoclay nanocomposites prepared by the various synthesis procedures without ultrasonication are also shown in Table 5.7.

***Table 5.7*** Measured values of tensile strength, extension at break, and modulus of elasticity for the PU/PEMA organoclay nanocomposites with variation of the synthesis procedure with and without ultrasonication.

| Synthesis procedure | Tensile strength (MPa) | | Extension at break (%) | | Modulus of elasticity (MPa) | |
|---|---|---|---|---|---|---|
| | P | SP | P | SP | P | SP |
| 0 | 4.37 ±0.45 | 6.64 ± 0.41 | 506 ± 61 | 571 ± 27 | 18.9 ± 1.3 | 22.4 ± 1.8 |
| 1 | 2.84 ± 0.11 | 3.10 ± 0.18 | 392 ± 24 | 370 ± 27 | 17.9 ± 0.9 | 21.9 ± 1.7 |
| 2 | 1.96 ± 0.28 | 0.92 ± 0.07 | 381 ± 48 | 295 ± 15 | 15.5 ± 1.2 | 16.8 ± 1.4 |
| 3 | 5.28 ± 0.31 | 4.97 ± 0.37 | 516 ± 27 | 457 ± 40 | 18.4 ± 2.9 | 23.5 ± 0.7 |
| 4 | 2.76 ± 0.21 | 1.84 ± 0.17 | 471 ± 42 | 469 ± 11 | 10.6 ± 2.1 | 14.2 ± 0.9 |

In the ultrasonic-assisted original synthesis procedure, SP0, where the organoclay was first mixed with PPG1025, the tensile strength and extension at break show the highest values of 6.64 MPa and 571%, respectively. While the modulus of elasticity shows a fairly high value of 22.4 MPa. With respect to the P0 results, as shown in Table 5.7, the tensile strength is increased by 52%, the elongation at break and the storage modulus is moderately increased by 13% and 18%, respectively. These may be attributed to the influence of ultrasonication.

A severe decrease in the tensile strength and the elongation at break are illustrated in Figure 5.26, while the modulus of elasticity marginally decreases, as a mixture of PPG1025 and TMP was first mixed with the organoclay in the ultrasonic assisted

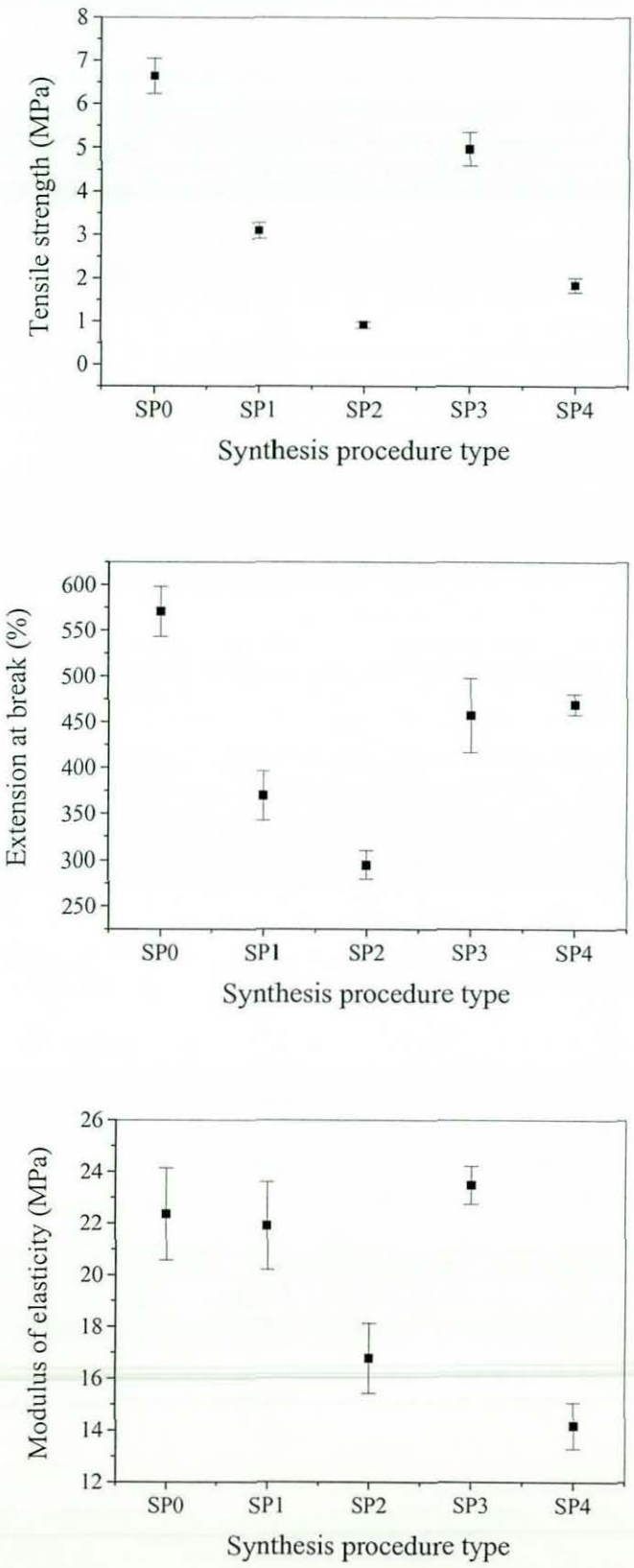


***Figure 5.26*** Tensile properties of the 70PU/30PEMA (5 wt% C20A) IPN organoclay nanocomposites as a function of ultrasonic assisted synthesis procedure.

synthesis procedure SP1. The tensile strength decreases by half from 6.64 to 3.10. The elongation at break decreased considerably from 571% to 370%. Roughly, the same value of 22 MPa was found for the modulus of elasticity, as compared to those of SP0. These might possibly be due to lower crosslink of PU hard segment as the crosslinker TMP was constrained between the silicate layers. Another reason may be caused a reduction in the degree of hydrogen bonding between the hard segments. However, the tensile strength and the modulus of elasticity significantly increase, whilst the elongation at break decreases, as compared to those of P1. The high frequency of the ultrasonic wave might break silicate agglomerates into silicate tactoids and individual silicate layers, consequently, the higher interface interaction between the nanoclay tactoids and the polymer matrix might be occured. Thus, the ultrasonication of premixed nanoclay/polymer considerably improved the mechanical properties.

In SP2, where all the PU constituents were mixed first with the organoclay, except SnOct, again the tensile strength and elongation at break revealed the lowest values of 0.92 MPa and 295 %, respectively. Besides, the modulus of elasticity also shows a low value of 16.78 MPa. Because of the TMXDI was incorporated with polyol and triol in the silicate galleries, it is possibly that the PU network, the soft and hard segments could establish within the silicate galleries during premixing with the organoclay, even though they might not be completely formed. Thus, a higher amount of the PU segment was constrained between the silicate layers. So, a looser network might be formed. Consequently, a reduction in the interfacial bonding between the PU and PEMA phases might be occurred. These could be some explanations for the severe reduction in the mechanical properties. However, as compared to the results of P2, a significant decreased tensile strength from 1.96 MPa to 0.92 MPa, and the elongation at break from 381% to 295%, and slightly increased modulus of elasticity from 8.55 MPa to 8.65 MPa, was as observed for P2 and SP2, respectively. These indicate less interfacial interaction because a greater extent of the PU segments was constrained between the silicate galleries, which were disaggregated to some extent by the ultrasonication during the premixing of organoclay and polymer.

Ultrasonication in SP3 showed a slight increase in the modulus of elasticity, while the tensile strength and the elongation at break revealed a significant decrease, as

compared to the SP0. This indicates that the silicate layers are not interacted to a great extent with the PEMA component, as the organoclay was first mixed with the EMA monomer and the crosslinker TEGDM, prior to combine with the PU component. TEM micrographs confirmed that the silicate layers were not intercalated to a great extent by the EMA monomer and the crosslinker. The PEMA domains seem to be more obviously continuous with sharp phase boundaries. This is possibly a reason for these findings. However, the modulus of elasticity for SP3 increases from a value of 18.35 MPa to 23.48 MPa, compared to that of P3. The tensile strength and the extension at break decrease from 5.28 MPa and 516% to 4.97 MPa and 457%, respectively. Again, a possible reason is that the PEMA tend to be in interconnected domains in the PU matrix with an inhomogeneous dispersion of the silicate tactoids, as seen in the TEM micrographs. Therefore, the PEMA should affect to some extent the whole mechanical properties of the IPN.

Compared to the SP0, a large decrease in the tensile strength and the storage modulus of elasticity were found in SP4, while a slight decrease in the elongation at break was also found. They were 1.84 MPa, 14.18 MPa and 469%, corresponding to the tensile strength, the modulus of elasticity and the extension at break, respectively. As stated before, because all constituents of both networks were first mixed with the organoclay, except SnOct and AIBN, a looser PU and PEMA networks might be formed. Consequently, the reduced extent of interpenetration of those two networks and interface interaction between the phases could exist. Therefore, the mechanical properties of this IPN decreased. However, incorporating ultrasonication tends to decrease the tensile strength and the elongation at break, but marginally increase the modulus of elasticity.

### 5.2.6 Hardness measurements.

Hardness Shore A measurements were conducted on all the ultrasonication assisted synthesis procedure specimens. An average value of Shore A hardness of the 70PU/30PEMA IPN organoclay nanocomposites versus synthesis procedure type is illustrated in Figure 5.27

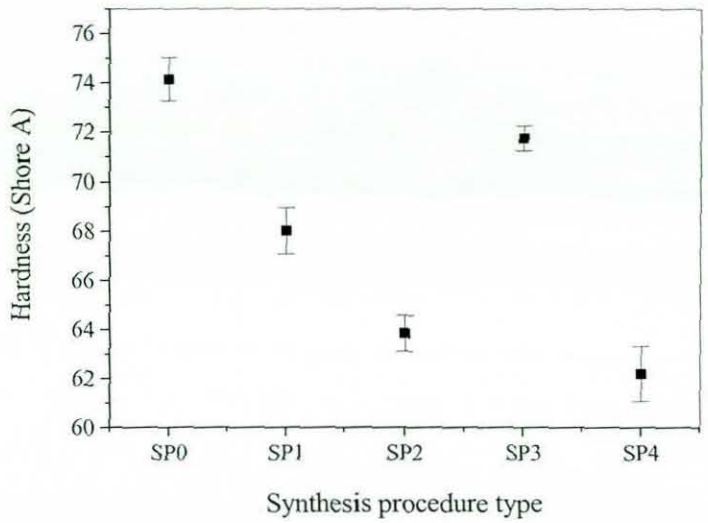


***Figure 5.27*** Shore A hardness values of the 70PU/30PEMA (5 wt% C20A) IPN organoclay nanocomposites as a function of ultrasonic assisted synthesis procedure.

Not surprisingly, the hardness profile shows the similar trend as the modulus of elasticity, shown in Figure 5.26, because the hardness of a material is strongly dependent upon its modulus of elasticity[154]. The Shore A hardness values are 74, 68, 64, 72, 62, for the SP0, SP1, SP2, SP3 and SP4, respectively. The lowest value is found for SP4, where all constituents were first mixed with the organoclay, except for the catalyst, SnOct, and an initiator, AIBN. The reaction of the diisocyanate and hydroxyl groups led to form the PU network. In general, the first formed network usually represents the continuous phase and plays an important role in IPN properties[2]. Moreover, an incomplete PU network might be formed because some of the PU constituents were confined in the silicate galleries. The silicate layers might restrict the hydrogen bonding between the hard segments. Therefore, this IPN shows the lowest hardness value. Besides, for the SP2, it also reveals a low Shore A hardness value. Again, this can be explained by the same reason as offered before for the SP4. However, when these values were compared with those of unaided ultrasonication specimens, which exhibited Shore A hardness values of 69, 68, 63, 70 and 64, as shown in Figure 5.14, for the P0, P1, P2, P3 and P4, respectively, they show a slight increase after ultrasonication, except for the SP4 and P4, but they are all within the experiment error range.

# CHAPTER 6

# OTHER NANOCLAYS

# CHAPTER 6
# OTHER NANOCLAYS

Clay nanocomposites can produce dramatic improvements in a variety of properties, especially in exfoliated nanocomposites compared with those of the neat resin and conventional composite materials. Thus, it is important to understand the factors which affect delamination of the clay. These factors include[14] the cation exchange capacity of the clay, the polarity of the polymer medium and the chemical nature of the modifier, e.g. onium ions. By modifying the surface polarity of the hydrophilic clay, onium ions allow thermodynamically favourable penetration of polymer precursors into the silicate interlayer regions. The ability of the onium ion to assist in the delamination of the clay galleries depends on its chemical nature such as its polarity[223,224].

The correct selection of modified clay is crucial to ensure effective penetration of the polymer, or its precursor, into the interlayer spacings of the silicate clay, resulting in the desired exfoliated or intercalated polymer-clay nanocomposites. Usuki et al.[225] studied polypropylene (PP) nanocomposites. They used a maleic anhydride grafted PP as a compatibiliser. They believed that the driving force for intercalation originated from the maleic anhydride group and the oxygen groups of the silicate through hydrogen bonding. In case of poly(ε-caprolactone) (PCL) layered silicate nanocomposites[226], partially delaminated/partially intercalated structures were formed in the presence of montmorillonite modified by alkylammonium cations bearing two hydroxyl groups. The grafting of the PCL chains by the hydroxyl groups attached to the alkylammonium cations were an explanation of the full delamination. Tien and Wei[196] synthesised polyurethane/ montmorillonite (PU/MMT) nanocomposites. They employed tris(hydroxylmethyl) aminomethane (THAM) in order to induce efficient exfoliation and dispersion of MMT layers in the PU matrix. The hydroxyl groups of THAM reacted with the isocyanate groups of the PU prepolymer, creating an exfoliated structure.

Therefore, in this chapter other types of the organoclay were investigated in order to find a more suitable organoclay type, which improves the dynamic damping and the

mechanical properties of the PU/PEMA IPN organoclay nanocomposites. There were four sections in this chapter. The first section is focused on the influence of C15A organoclay on the IPN properties. The effect of the C30A organoclay and Na clay on the IPN morphology and properties were examined in the second and the third sections. The last section reports a comparison of those clay/organoclay types with C20A organoclay.

### 6.1 C15A organoclay.

Cloisite 15A, C15A, is a natural montmorillonite modified with a quaternary ammonium salt, dimethyl dihydrogenated tallow quaternary ammonium chloride, as used for C20A. Its modifier concentration, 125 milliequivalents/100g clay, is higher than that of C20A, 95 milliequivalents/100g clay. It is a white powder with a specific gravity of 1.66 g/cm$^3$ and it also is used as an additive for plastics to improve various physical properties[169].

In this study, C15A at 0%, 1%, 3%, 5% and 7% by weight of PU were introduced into the 70PU/30PEMA IPN system by using an in-situ polymerisation method, in which C15A organoclay was first homogeneously mixed with PPG1025 at room temperature for 30 minutes by using a Silverson L2R mixing apparatus, as in the original synthesis procedure (Chapter 3). The PU network was based on TMXDI, PPG1025, TMP and SnOct, with PPG1025:TMP ratio of 3:1 and SnOct 1.2% by weight of PU, whereas the PEMA network had TEGDM 5 mol% of PEMA and was initiated by AIBN at 1 mol% of PEMA. The simultaneous IPN technique was used to combine intimately the crosslinked elastomeric PU with a high glass transition plastic, PEMA. The effects of the C15A organoclay on the IPN properties, glass transition temperature, damping and mechanical properties were analysed by several techniques discussed earlier. The results of these investigations are outlined as follows.

#### 6.1.1 Wide angle X-ray diffraction.

The x-ray diffraction patterns of the 70PU/30PEMA IPN organoclay nanocomposites at loadings of 0, 1 and 7 wt% of C15A are shown in Figures 6.1 and 6.2.

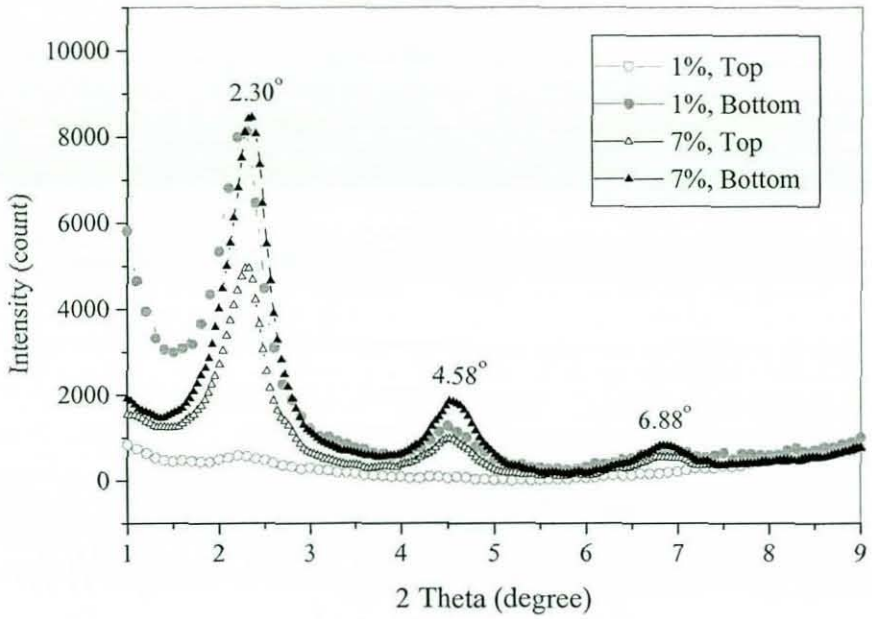


***Figure 6.1*** WAXD patterns for top and bottom sides of C15A organoclay-filled 70PU/30PEMA IPNs containing 1 and 7 wt% of C15A.

As can be seen in Figure 6.1, the WAXD data collected from both sides of cast samples show differences of intensity for the top and the bottom sides. Higher clay content exhibits a lower intensity difference. This indicates that the C15A organoclay did not homogeneously disperse in the polymer matrix. Moreover, the silicate particles tend to settle to the bottom side of the sheets during polymerisation process. Increasing the overall viscosity of the mixture, with increased organoclay loading, restricts the settlement of the clay particles during polymerisation. Consequently, the intensity difference between the top and the bottom is reduced. In the further comparative studies, only the diffraction patterns from the bottom side of those samples will be used.

The WAXD patterns for C15A organoclay, the 70PU/30PEMA IPNs, and the C15A organoclay-filled 70PU/30PEMA IPNs at 1 and 7 wt% of clay are shown in Figure 6.2. Only one diffraction peak is noticed in the C15A organoclay at 2.73°, corresponding to a $d_{001}$ of 3.24 nm, while, as expected, no diffraction peak is present in the unfilled 70PU/30PEMA IPNs. After in-situ intercalative polymerisation, three diffraction peaks are revealed. The first diffraction peaks have shifted towards lower angles of 2.29° and

2.35°, for 1% and 7% clay loading, respectively, which correspond to interlayer spacings of 3.86 and 3.76 nm. These results indicate that the polyether polyol molecules are intercalated in between the silicate layers to some extent at both the clay contents.

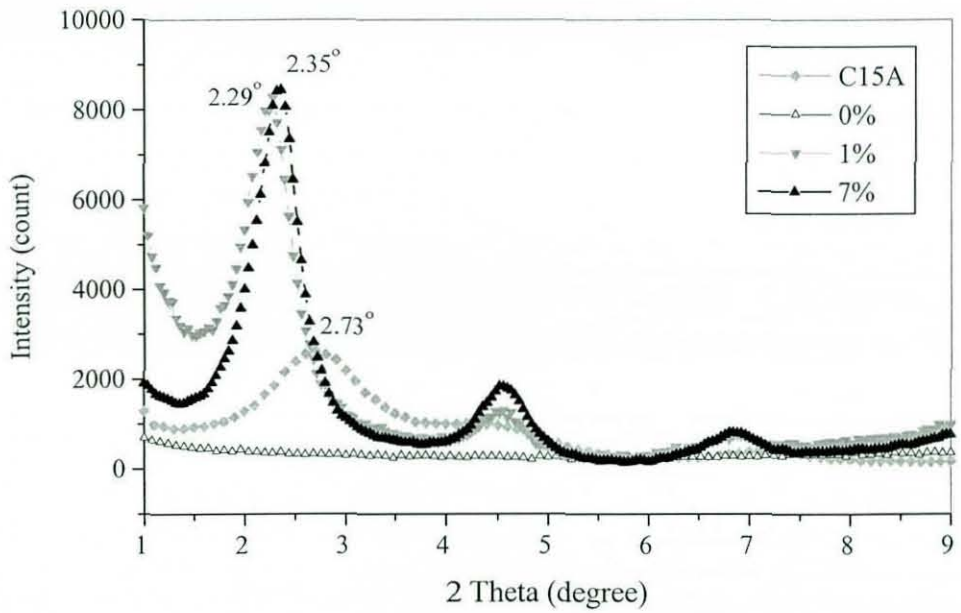


***Figure 6.2*** WAXD patterns for the C15A organoclay, the 70PU/30PEMA IPN, and the C15A-filled 70PU/30PEMA IPNs containing 1 and 7 wt% C15A.

### 6.1.2 Transmission electron microscopy.

WAXD is a useful screening technique for determining the type of nanocomposite prepared, but the results provided by WAXD can not be used alone to describe the exact nature of these nanocomposites. WAXD only gives the distance between clay layers, thus, revealing the relationship of the clay layers to themselves, not of the clay particles to the polymer. WAXD does not reveal how well dispersed the clay is throughout the polymer, nor does it define the degree of intercalation or exfoliation. TEM analysis can provide further information. Low magnification TEM will exhibit how well dispersed the clay is throughout the polymer matrix, and it can also show the degree of intercalation and/or exfoliation which has occurred.

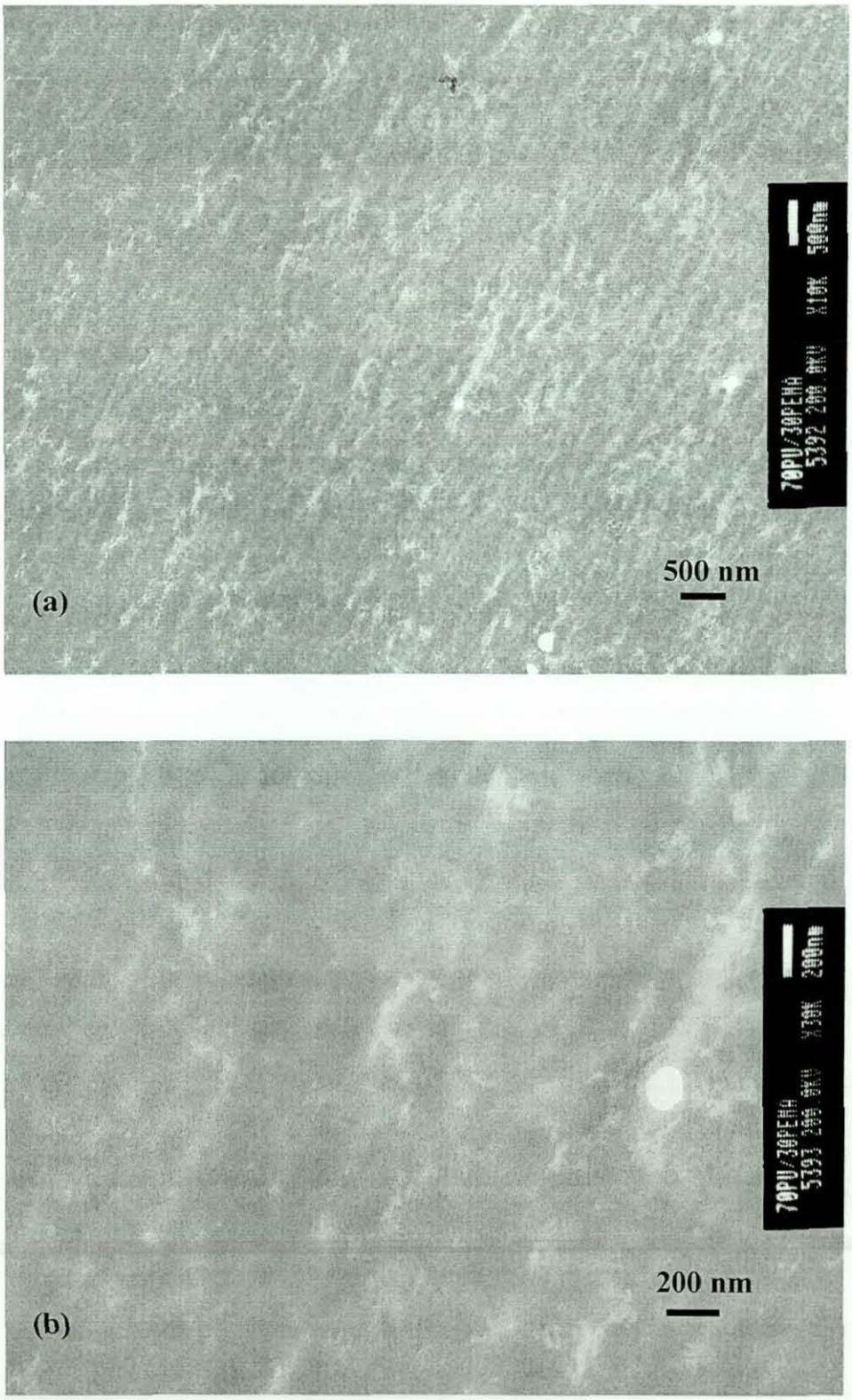


***Figure 6.3*** TEM micrographs for the unfilled 70PU/30PEMA IPN. (a) At 10k magnification. (b) At 30k magnification.

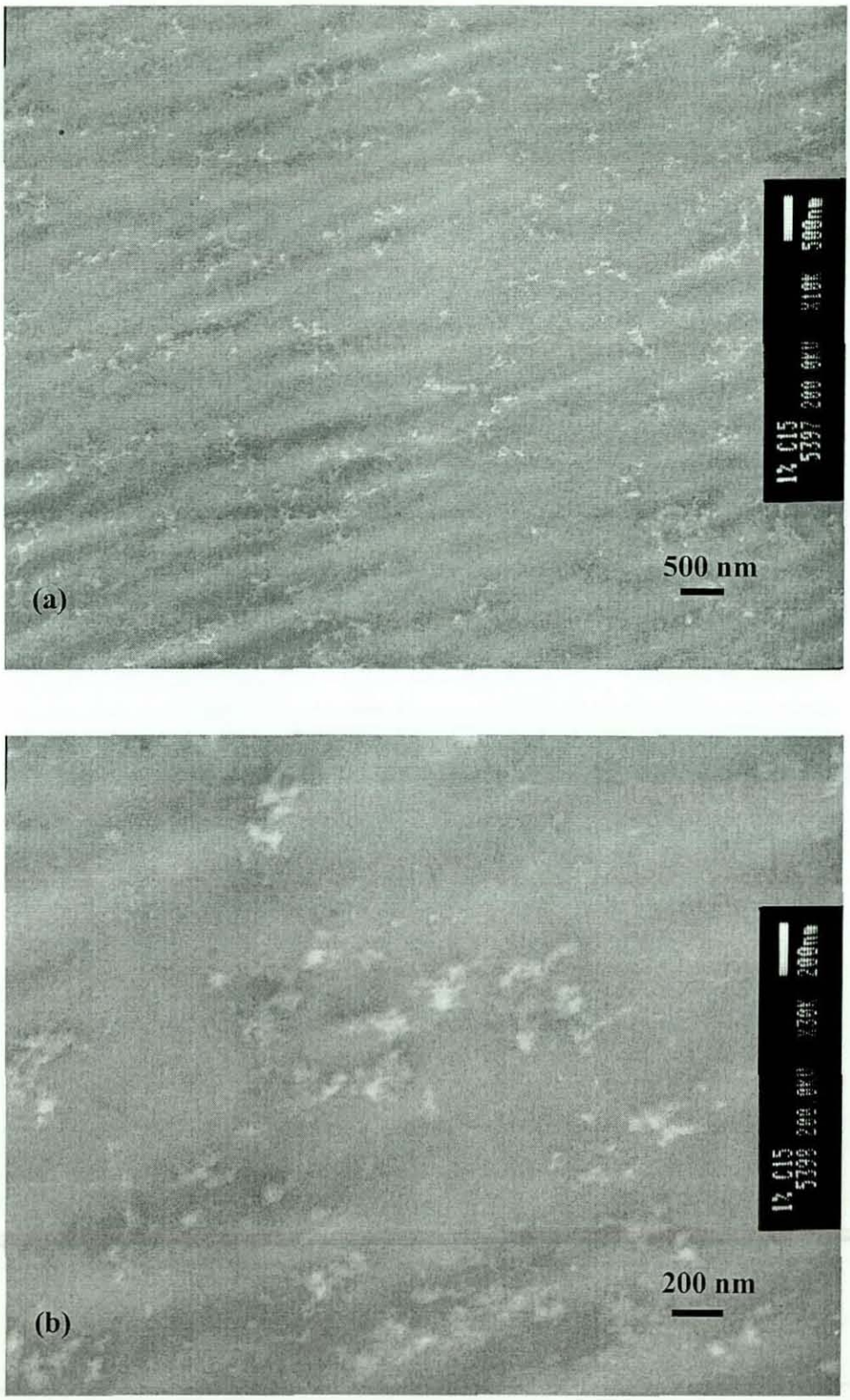


***Figure 6.4*** TEM micrographs for the 70PU/30PEMA (1 wt% C15A organoclay) IPN nanocomposites. (a) At 10k magnification. (b) At 30k magnification.

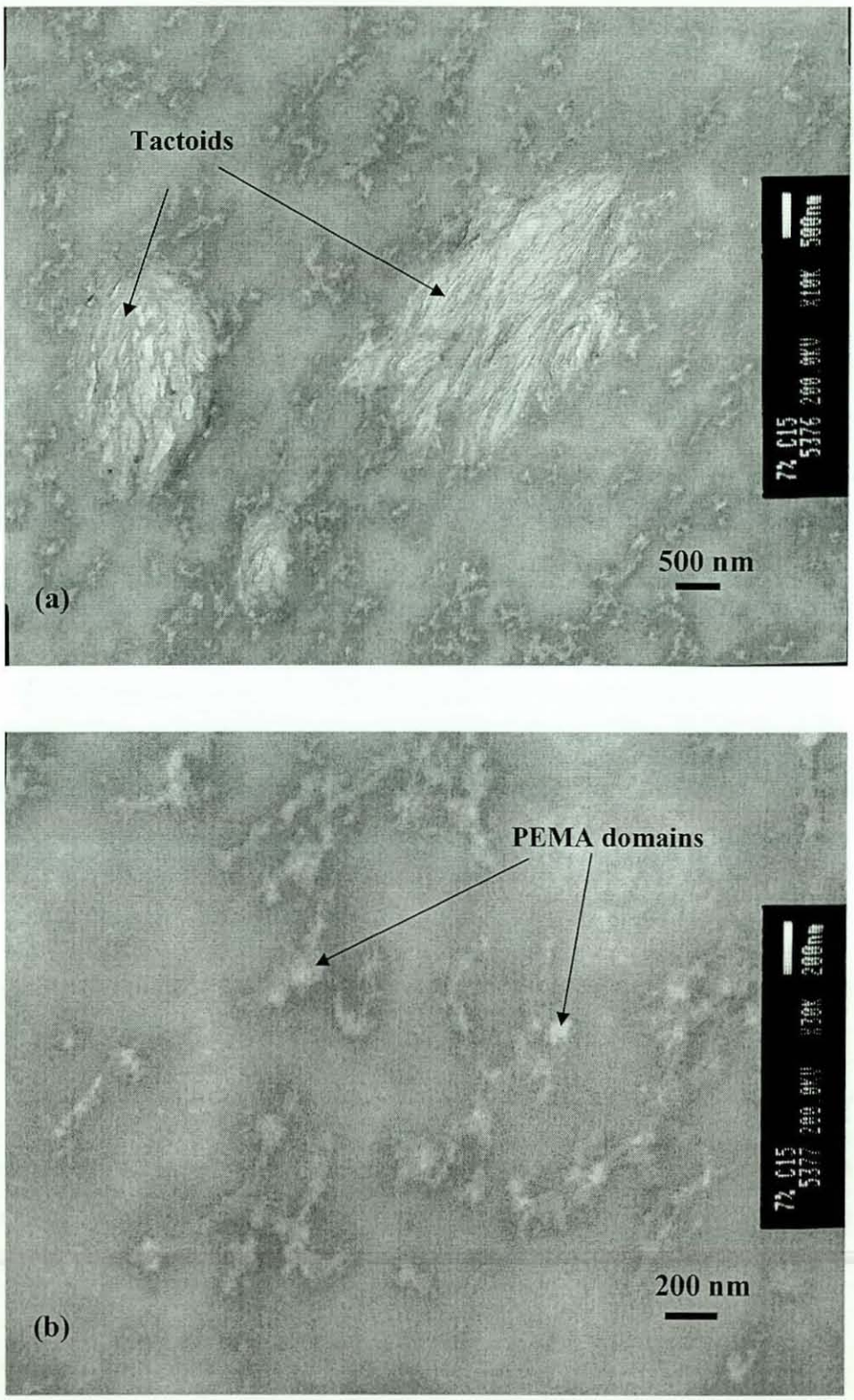


***Figure 6.5*** TEM micrographs for the 70PU/30PEMA (7 wt% C15A organoclay) IPN nanocomposites. (a) At 10k magnification. (b) At 30k magnification.

The TEM micrographs showing the morphology of the 70PU/30PEMA IPN and the 70PU/30PEMA IPN organoclay nanocomposites are given in Figures 6.3 to 6.5. Because of higher electron density than the surrounding polymer matrix, the organoclay particles appear as dark particles in the TEM images. As can be seen from the 70PU/30PEMA IPN organoclay nanocomposites compared with the 70PU/30PEMA IPN, Figures 6.3 to 6.5, again, the large and unevenly dispersed organoclay platelets are aggregated in the polymer matrix at low magnification, indicating poor dispersion of these clay particles. The size of these tactoids was in the order of 0.5-3 μm, as seen in Figure 6.5 (a). Unfortunately, exfoliation is not observed. Incorporation of C15A organoclay causes a significant change in the observed microstructure of the matrix. The light, interconnected PEMA domains become bigger, more obvious and more interconnected with increasing organoclay content. At 7 wt% C15A, a cellular structure can be observed more clearly. However, a lot of different shades of grey in the PU matrix can be seen, showing some extent of molecular mixing between the two components. Besides, darker matrix areas are more frequently observed around the PEMA domains and appear to be to some extent interconnected. Therefore, the morphology of these organoclay nanocomposites reveals some phase separation.

### 6.1.3 Dynamic mechanical thermal analysis.

DMTA was used to complement these morphology studies. The dynamic mechanical properties of the 70PU/30PEMA IPN organoclay nanocomposites with various C15A clay contents are plotted as a function of temperature in Figures 6.6 to 6.9. Peak positions and tan delta max values of their PU and PEMA components and peak widths at tan $\delta \geq 0.3$ are summerised in Table 6.1.

As seen in Figure 6.6, the DMTA plot for the unfilled 70PU/30PEMA IPN shows a semi-miscible system, where two shoulders corresponding to PU and PEMA-rich phases appear at 1°C and 90°C, respectively. Incorporating C15A organoclay causes the PU transition to decrease to lower temperatures with a lower tan delta max value for all the studied range. At 7 wt% C15A, the PU transition decreased from 1°C (tan δ max 0.50) obtained for the unfilled organoclay to -16°C (tan δ max 0.29). On the other hand, the PEMA transition exhibits a decrease in the glass transition with an increase

of the tan delta max value with increasing C15A organoclay content. The PEMA transition is at 90°C (tan δ max 0.49) for no C15A organoclay situation. Adding C15A clay, the PEMA transition continuously decreases to 71°C (tan δ max 0.79), shown by the sample of 7 wt% C15A organoclay. Besides, the peak width of tan $\delta \geq 0.3$ decreases at the higher C15A contents, as seen in the Table 6.1, indicating a lesser extent of matrix mixing with increasing the organoclay content.

***Table 6.1*** Dynamic mechanical properties of the 70PU/30PEMA IPN organoclay nanocomposites with various C15A contents.

| C 15A (% wt) | Tg at tan δ max. (°C) | | Tan δ max value at Tg | | Peak width tan $\delta \geq 0.3$ (°C) |
|---|---|---|---|---|---|
| | PU | PEMA | PU | PEMA | |
| unfilled | 1 | 90 | 0.50 | 0.49 | - |
| 1% | -11 | 81 | 0.38 | 0.54 | - |
| 3% | -11 | 79 | 0.36 | 0.60 | -21 ↔ 138 (159) |
| 5% | -15 | 77 | 0.32 | 0.72 | -19 ↔ 127 (146) |
| 7% | -16 | 71 | 0.29 | 0.79 | -8 ↔ 119 (127) |

The lower glass transition values and tan delta max at the PU transition might be because of an incomplete PU network formation. It was reported that the polyol and isocyanate could intercalate the clay galleries. Consequently, it is more likely that during the PU network polymerisation there was an imbalance in the hydroxyl : isocyanate ratio, resulting in a poor polymer network. This would explain the reduction in glass transition and tan delta max as fewer polyol molecules are involved. The PEMA constituents could also intercalate into the clay galleries. This may result in a poor network because of intercalated and non-reacted monomer/crosslinker, yielding a more flexible network. Consequently, it reveals a lower Tg and higher tan delta max at the PEMA transition. However, the influence of the C15A organoclay on the tan delta profiles of the 70PU/30PEMA IPNs shows the same aspect as found for the C20A organoclay (see section 4.1.3).

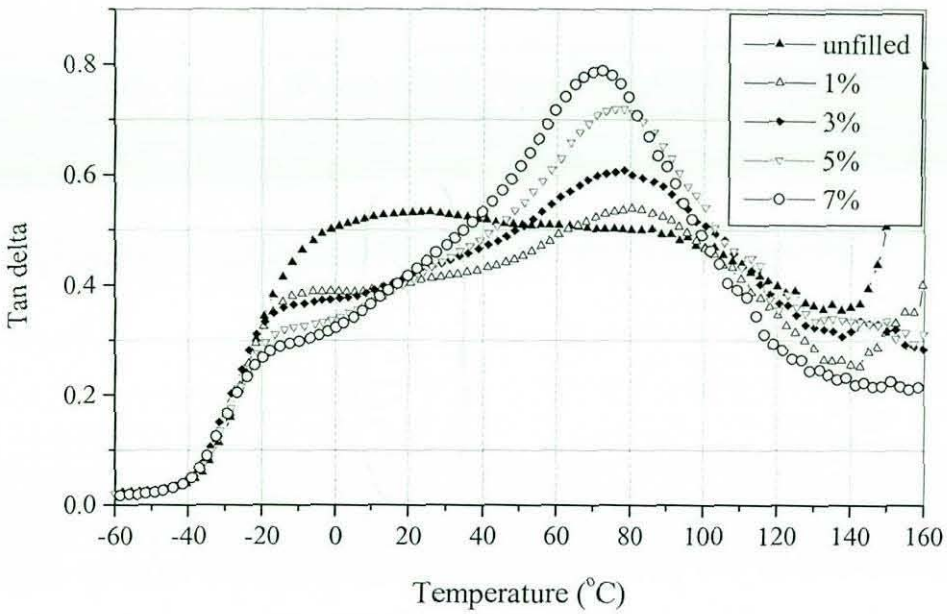


***Figure 6.6*** Loss factor versus temperature plots for the 70PU/30PEMA IPN organoclay nanocomposites: 0, 1, 3, 5 and 7 wt% C15A.

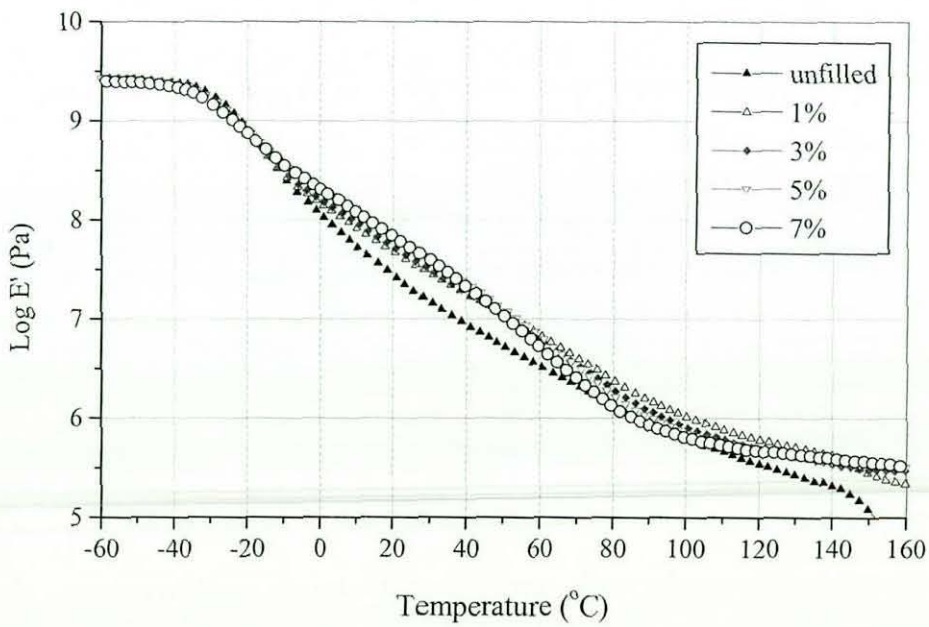


***Figure 6.7*** Storage modulus versus temperature plots for the 70PU/30PEMA IPN organoclay nanocomposites: 0, 1, 3, 5 and 7 wt% C15A.

Figure 6.7 shows the storage modulus of IPN organoclay nanocomposites as a function of temperature. Again, there is no sign of gross phase separation, which could be observed by sharp drops at the Tgs of both homopolymers. Instead, they show a broad transition interval with slight changes in slope around the homopolymer Tgs, especially the IPN with 7 wt% C15A.

In the glassy state, the incorporation of the organoclay does not have a significant influence on the storage modulus. The storage moduli above room temperature for the filled IPNs are higher than that of the unfilled system between their Tgs, as seen in Figure 6.7. Two changes of slope in each storage modulus-temperature plot are observed in regard to the location of PU and PEMA-rich phase transition temperatures. Thus, over the temperature range studied, the storage modulus can be divided into two regions at the mid point of their Tgs, which is at 50°C. In the first region, the storage moduli slightly increase as the C15A content is increased. On the contrary, the storage moduli slightly decrease with increasing amount of organoclay in the second region. For easier consideration, the storage modulus of the IPNs as a function of the C15A organoclay content at 20°C and 80°C, the mid points of the temperature range of each region, are provided in Figure 6.8.

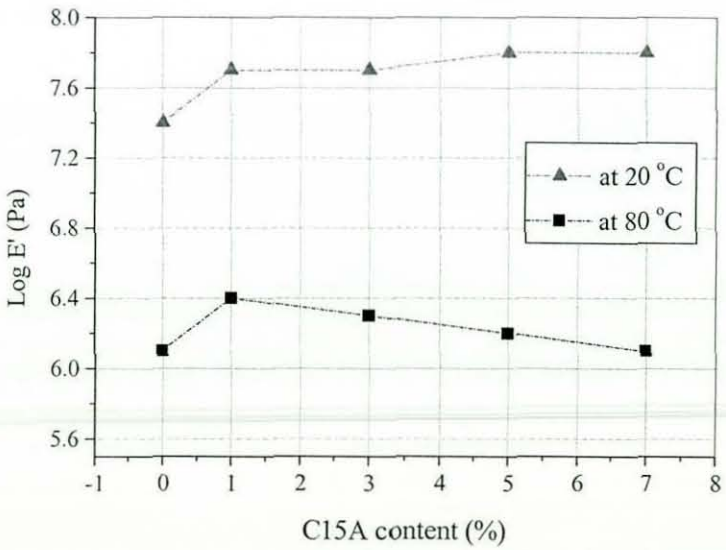


***Figure 6.8*** Storage modulus versus temperature plots at 20°C and 80°C for the 70PU/30PEMA IPN organoclay nanocomposites: 0, 1, 3, 5 and 7 wt% C15A.

The increase in the storage modulus with increasing C15A content in the first region could be due to the normal characteristics of conventional filled polymer system[180]. In the higher temperature region, the gradual decrease in the storage modulus might be explained in terms of the degree of crosslinking. Lower glass transitions for both networks were found from the tan delta profiles as clay increased. This implies that a lower degree of crosslinking of the PU and PEMA networks occurs. Consequently, the gradual decrease in the storage modulus in the second region might be explained.

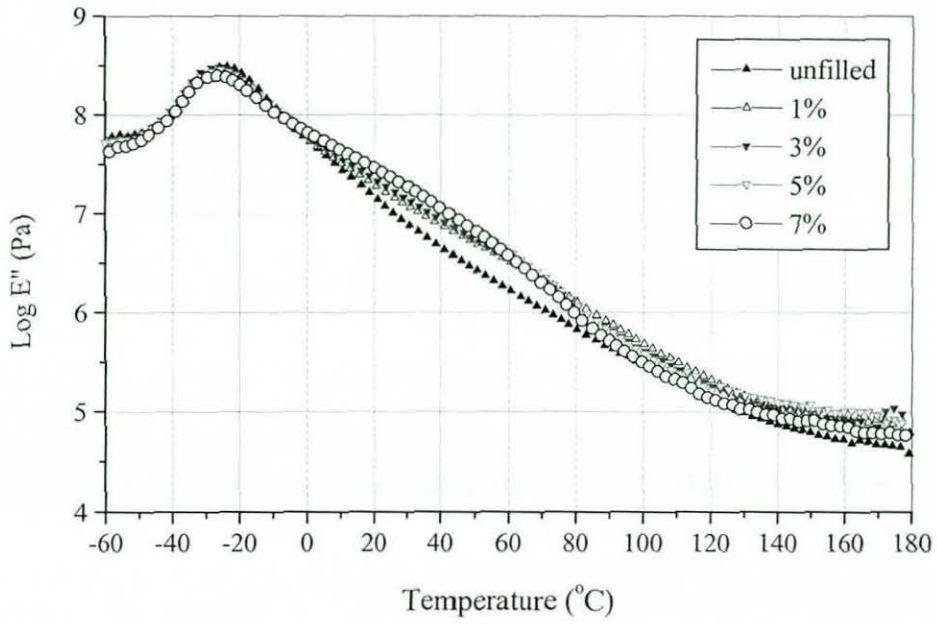


***Figure 6.9*** Loss modulus versus temperature plots for the 70PU/30PEMA IPN organoclay nanocomposites: 0, 1, 3, 5 and 7 wt% C15A.

A similar trend was observed for the loss modulus as shown in Figure 6.9. The unfilled organoclay IPN shows a gradual decrease in loss modulus over the temperature range, indicating a high extent of component mixing and interface content. Incorporation of C15A organoclay caused no sign of gross phase separation. All the filled IPNs showed two changes of slope around the PU and PEMA transitions in each loss modulus-temperature plot. Adding more the organoclay, the changes are more obvious, as seen for the 7 wt% C15A. Again, no significant changes in the loss modulus are found at the glassy stage, but there are increases in the inter-transition range and decreases around the PEMA transition and beyond the rubbery stage, as found in the storage modulus profiles. However, the loss modulus of the filled organoclay IPNs seems to be

increased at the rubbery stage as compared to that at the glassy stage, due to the stiffness of the silicate particles.

### 6.1.4 Modulated-temperature differential scanning calorimetry.

The effect of C15A organoclay content on the miscibility of the 70PU/30PEMA IPNs was studied by M-TDSC and reported in Figure 6.10 and the Tg data for each composite are given in Table 6.2.

***Table 6.2*** M-TDSC data for the 70PU/30PEMA IPN organoclay nanocomposites with varying C15A clay contents.

| C15A (%wt) | Tg, °C | | dCp/dT value, $J/g^{-1}{}^{o}C^{-2}$ | |
|---|---|---|---|---|
| | PU | PEMA | PU | PEMA |
| unfilled | -37 | 62 | 0.018 | 0.001 |
| 1% | -37 | 55 | 0.017 | 0.002 |
| 5% | -40 | 55 | 0.016 | 0.002 |
| 7% | -40 | 55 | 0.014 | 0.002 |

M-TDSC curves for the unfilled 70PU/30PEMA IPN exhibits a sharp peak at the PU transition and a very broad shoulder over the PEMA transition, indicating some extent of phase separation. Nevertheless, it also shows multi-phase morphology, owing to the spanning of transition spectra with almost the same height over wide temperature ranges between the transitions of the homopolymers. This implies that there no gross phase separation took place. The presence of C15A organoclay results in similar spectra where a sharp peak appears at the PU transition, but the broad shoulder at the PEMA transition is more obviously noticed over the entire clay content range. This indicates more extent of phase separation with incorporating of the C15A organoclay. It also can be seen that the Tg value of the PU network in the IPNs slightly decreases from -37°C, observed for unfilled IPN, to -40°C, revealed for 7 wt% C15A. After normalising for the clay loading, again, the dCp/dT value at the PU transition gradually decreases with increasing C15A loading, as was found earlier in the C20A-filled IPNs. At 1 wt% C15A, the PEMA exhibits a lower glass transition temperature from 62°C, observed for unfilled IPN, to 55 °C with an increase in the differential heat

capacity value from 0.001 to 0.002 $Jg^{-1}{}^{o}C^{-2}$, respectively. On adding more organoclay, the PEMA transition temperature and the dCp/dT values present no further changes.

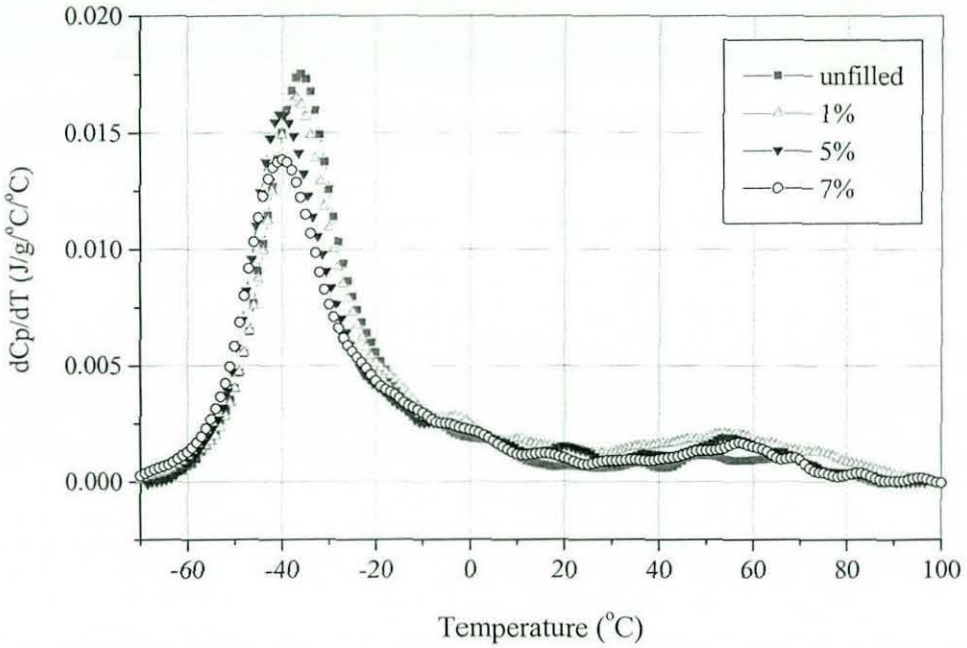


***Figure 6.10*** Differential heat capacity versus temperature plots showing the effect of C15A organoclay content on the 70PU/30PEMA IPN organoclay nanocomposites.

The reduction in the PU Tg might be because of an incomplete network formation, since the polyol and isocyanate can intercalate the clay galleries. Consequently, a more flexible network rather than a complete network may be formed, yielding a lower Tg. Besides, the segments that were constrained between the layered silicates are not involved in the glass transition. Therefore, the dCp/dT values decreased as the C15A content increased. In the case of the PEMA network, the dCp/dT values was approximately the same as the C15A content increased, while the PEMA Tg decreased by 7° C. The reduction in Tg could be because of some monomer and crosslinker were trapped within the silicate galleries. Consequently, a looser network could be formed, yielding a drop in the PEMA Tg.

### 6.1.5 Tensile behaviour and hardness measurements.

The mechanical properties of the IPN organoclay nanocomposites were also investigated by tensile testing and Shore A hardness measurements. The results of

tensile testing are listed in Table 6.3. Figure 6.11 illustrates the tensile properties: modulus of elasticity, tensile strength and elongation at break versus the C15A organoclay content, while the hardness profile is shown in Figure 6.12.

***Table 6.3*** Measured values of tensile strength, extension at break and modulus of elasticity for the IPN organoclay (C15A) nanocomposites.

| Clay content (wt%) | Tensile strength (MPa) | Extension at break (%) | Modulus of elasticity (MPa) |
|---|---|---|---|
| unfilled | 4.58 ± 0.24 | 736 ± 37 | 4.52 ± 0.72 |
| 1% | 5.68 ± 0.48 | 663 ± 25 | 9.05 ± 1.09 |
| 3% | 3.78 ± 0.39 | 610 ± 20 | 8.22 ± 0.22 |
| 5% | 2.62 ± 0.25 | 504 ± 42 | 10.23 ± 0.37 |
| 7% | 1.31 ± 0.67 | 329 ± 42 | 10.97 ± 0.50 |

A typical behaviour of a filled polymer[154,227] is observed in Figure 6.11. An increase in the modulus of elasticity is combined with a decrease in the extension and the tensile strength at break. The modulus of elasticity gradually increases from 4.52 MPa for the unfilled IPN to 10.97 MPa for the IPN with 7 wt% C15A. On the other hand, the extension at break decreases considerably from 736% for the unfilled IPN to 329%, for the 7 wt% clay loading. For the tensile strength, at 1 wt% clay content, the tensile strength at break is slightly higher than that of the unfilled IPN. Adding more clay results in a gradual decrease of the tensile strength from a value of 5.68 MPa, revealed for 1 wt% C15A, to 1.31 MPa when the organoclay was 7 wt%. The reduction of the tensile strength and the percentage extension to failure might be attributable to the restriction of intercalated segments to stretch between the silicate galleries and possible also the reduction of the interfacial bonding between the polymer matrix and the organoclay particles. Incorporation of silicate particles usually increases stiffness comparative to an unfilled sample[228].

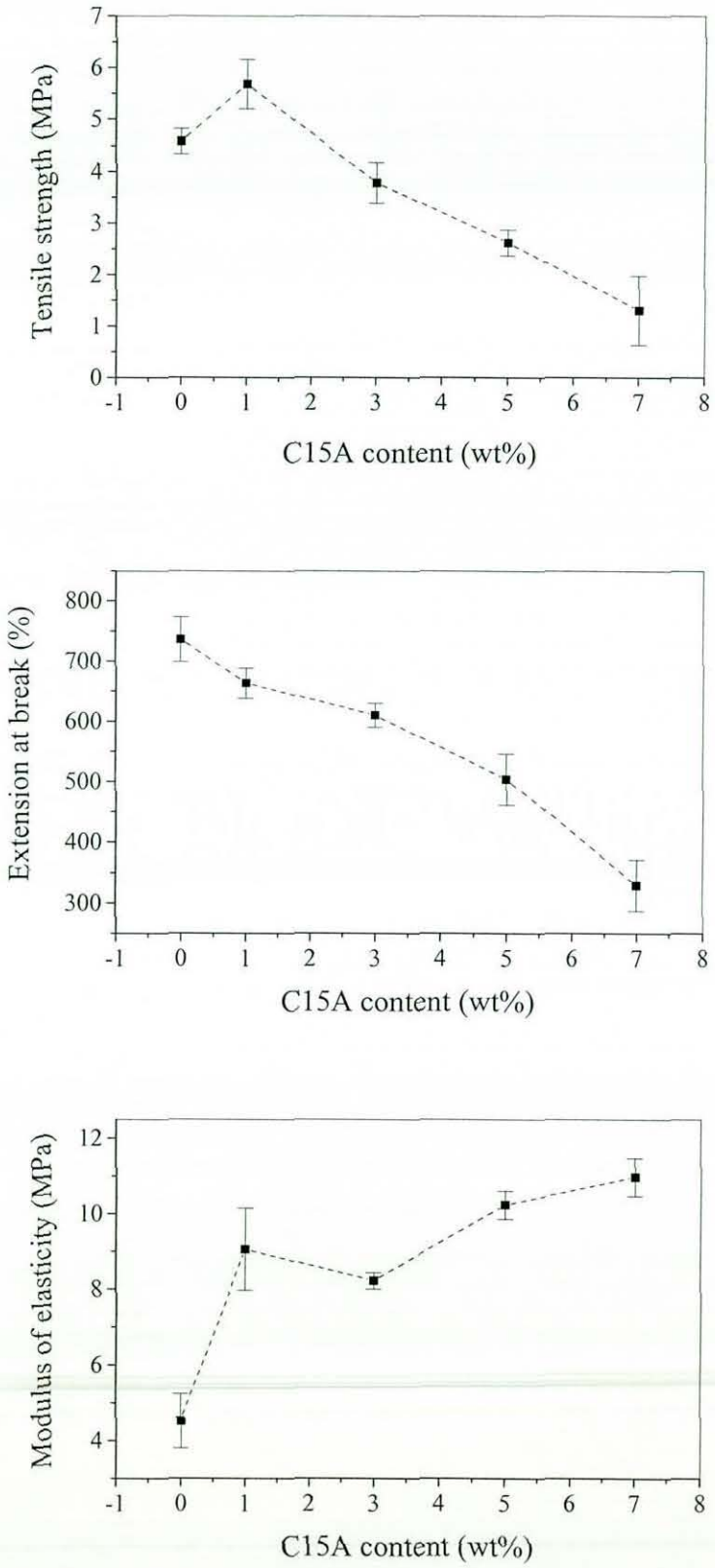


***Figure 6.11*** Tensile properties of the IPN organoclay nanocomposites as a function of C15A clay loading.

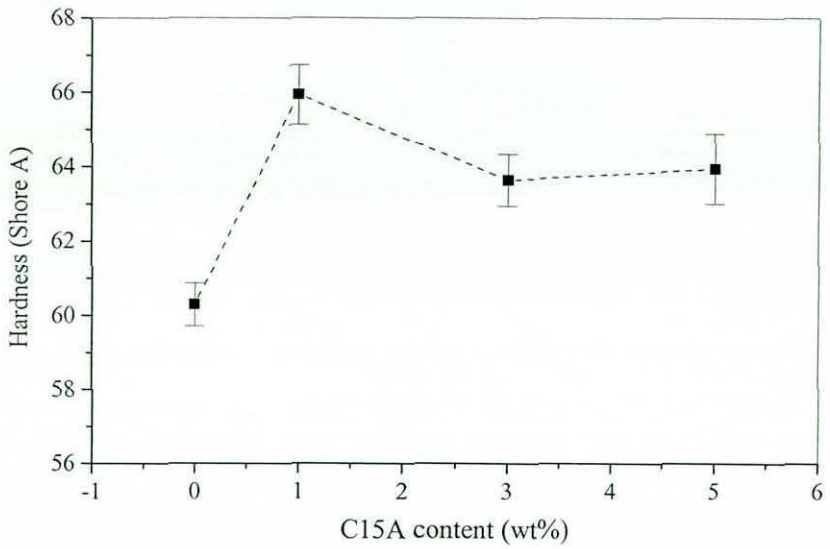


***Figure 6.12*** Shore A hardness values of the IPN organoclay nanocomposites as a function of C15A clay loading.

Shore A hardness profile of these IPN organoclay nanocomposites shows the same trend as found in the modulus of elasticity. With an addition in the C15A organoclay content, the hardness of the 70PU/30PEMA IPN shows a significant increase from Shore A 60, observed for the unfilled IPN, to Shore A 64 at 5 wt% clay content, indicating that the IPN nanocomposites are stiffer than the unfilled IPN. This is due to a hydrodynamic effect[228].

**6.2 C30B organoclay.**

Cloisite 30B, C30B, is a natural montmorillonite modified with a quaternary ammonium salt, methyl tallow bis(2-hydroxy ethyl) quaternary ammonium chloride. See its chemical structure in Figure 3.1. Its modifier concentration is 90 milliequivalents/100g clay. It is a white powder with a high specific gravity of 1.98 $g/cm^3$ and is also used as an additive for plastics to improve various physical properties[169].

In this study, C30B at 0%, 1% and 5% by weight of PU were introduced into the 70PU/30PEMA IPN system by using an in-situ polymerisation method, in which C30B organoclay was first homogeneously mixed with PPG1025 at room temperature for 30

minutes with a Silverson L2R mixer, as in the original synthesis procedure (Chapter 3). The PU network was based on TMXDI, PPG1025, TMP and SnOct, with PPG1025:TMP ratio of 3:1 and SnOct 1.2% by weight of PU, whereas the PEMA network was prepared containing TEGDM 5 mol% of PEMA and was initiated by AIBN at 1 mol% of PEMA. The simultaneous IPN technique was used to combine intimately the crosslinked elastomeric PU with a high glass transition plastic PEMA. Finally, according to the settlement of organoclay during polymerisation found in the previous chapter, the filled steel mould was turned over every 30 minutes in the first four hours. Subsequently, it was turned every one hour for another 3 hours to diminish extent of the clay settlement during the curing process. The effects of the C30B organoclay on the IPN properties, glass transition temperature, damping and mechanical properties were analysed and the results of these investigations are shown below.

### 6.2.1 Wide angle X-ray diffraction.

The resulting WAXD patterns for C30B organoclay, 70PU/30PEMA IPNs, and C30B organoclay-filled 70PU/30PEMA IPNs with 1 and 5 wt% C30B are shown in Figure 6.13. No diffraction peak is present in the 70PU/30PEMA IPNs, because it is an amorphous composite. Only one prominent diffraction peak is observed for the C30B organoclay at 4.79°, corresponding to the first diffraction of an interlayer spacing of 1.84 nm. After the in-situ intercalative polymerisation, the diffraction peak was still located at the original position, 4.79°. The crystalline structure of the C30B organoclay has not changed. This indicates that both PU and PEMA constituents did not intercalate the silicate nanolayers. Moreover, they still exhibit some settlement of the C30B organoclay. However, it is clear that the variation of amount of C30B has no effect on the interlayer spacing of the C30B clay galleries. It is believed that driving force for intercalation originated from the hydroxyl groups attached on the silicate surface and the hydroxyl groups on polyol and/or isocyanate groups through hydrogen bonding. Since the modifier of C30B clay has two hydroxyl groups, which could form H-bonding with the hydroxyl groups on the silicate platelets, there is less chance for the polyol / isocyanate molecules to diffuse into the silicate galleries. Therefore, these materials might exhibit the properties of traditional filled polymer composites instead of those of nanocomposites.

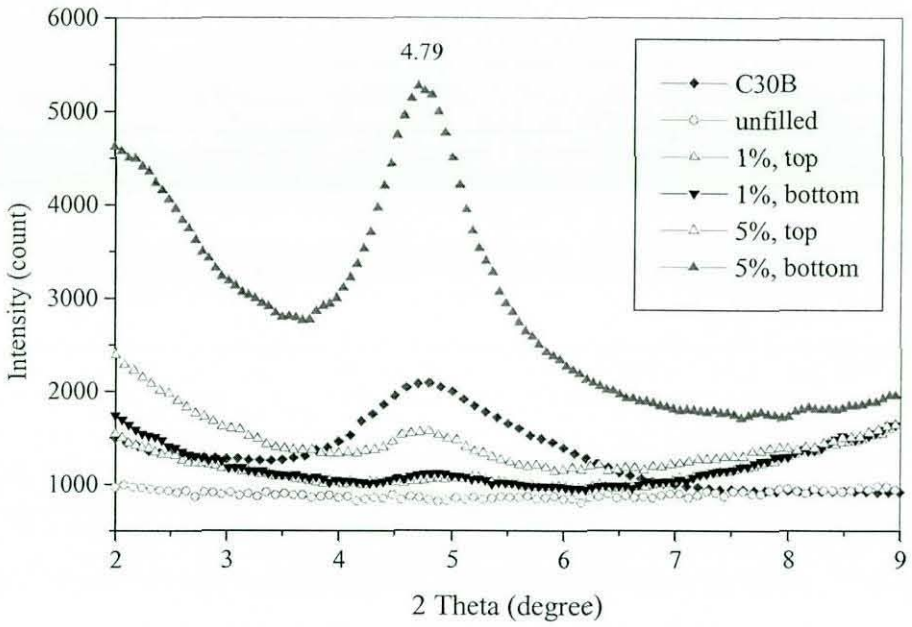


***Figure 6.13*** WAXD patterns for C30B organoclay, the 70PU/30PEMA IPN and the C30B-filled 70PU/30PEMA IPNs containing 1 and 5 wt% C30B.

### 6.2.2 Transmission electron microscopy.

The TEM micrographs showing the morphology of the 70PU/30PEMA IPN with C30B organoclay composites are given in Figures 6.14 to 6.15.

Incorporation of C30B organoclay gives a marginal change in the observed microstructure. The light, interconnected PEMA domains spreading through the PU matrix seem to be bigger and more interconnected as the organoclay content increased. A high extent of different shades of grey in the PU matrix can be seen. Besides, the darker matrix is more frequently observed around the PEMA domains and appeared to be to some extent interconnected, showing some degree of molecular mixing between the two components.

### 6.2.3 Dynamic mechanical thermal analysis.

The dynamic mechanical properties of the C30B organoclay-filled 70PU/30PEMA IPN composites are plotted as a function of temperature in Figures 6.16 to 6.18. Peak positions and values in tan delta max of their PU and PEMA homopolymers and peak widths at tan $\delta \geq 0.3$ are summerised in Table 6.4.

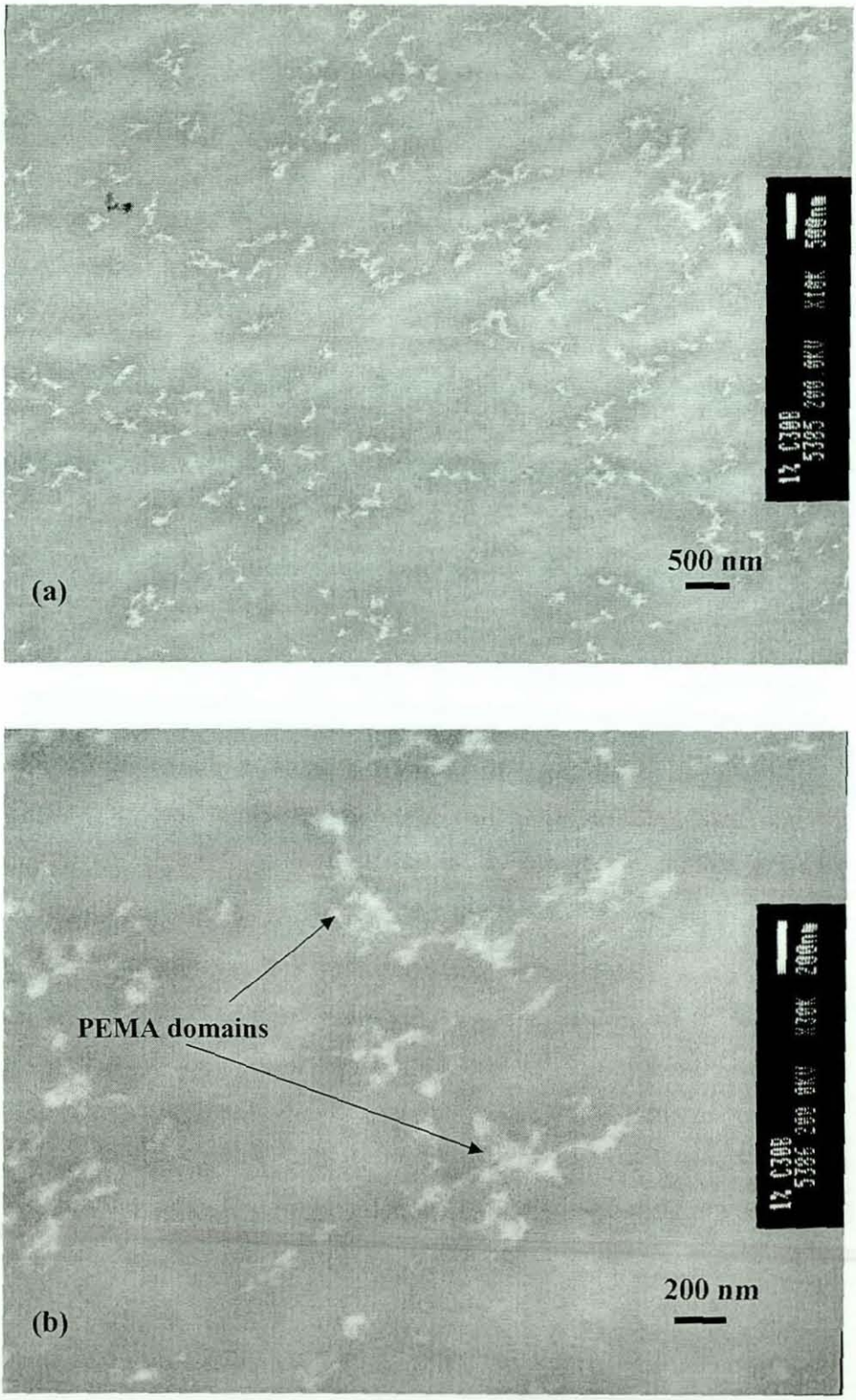


***Figure 6.14*** TEM micrographs for the 70PU/30PEMA (1 wt% C30B organoclay) IPN composites. (a) At 10k magnification. (b) At 30k magnification.

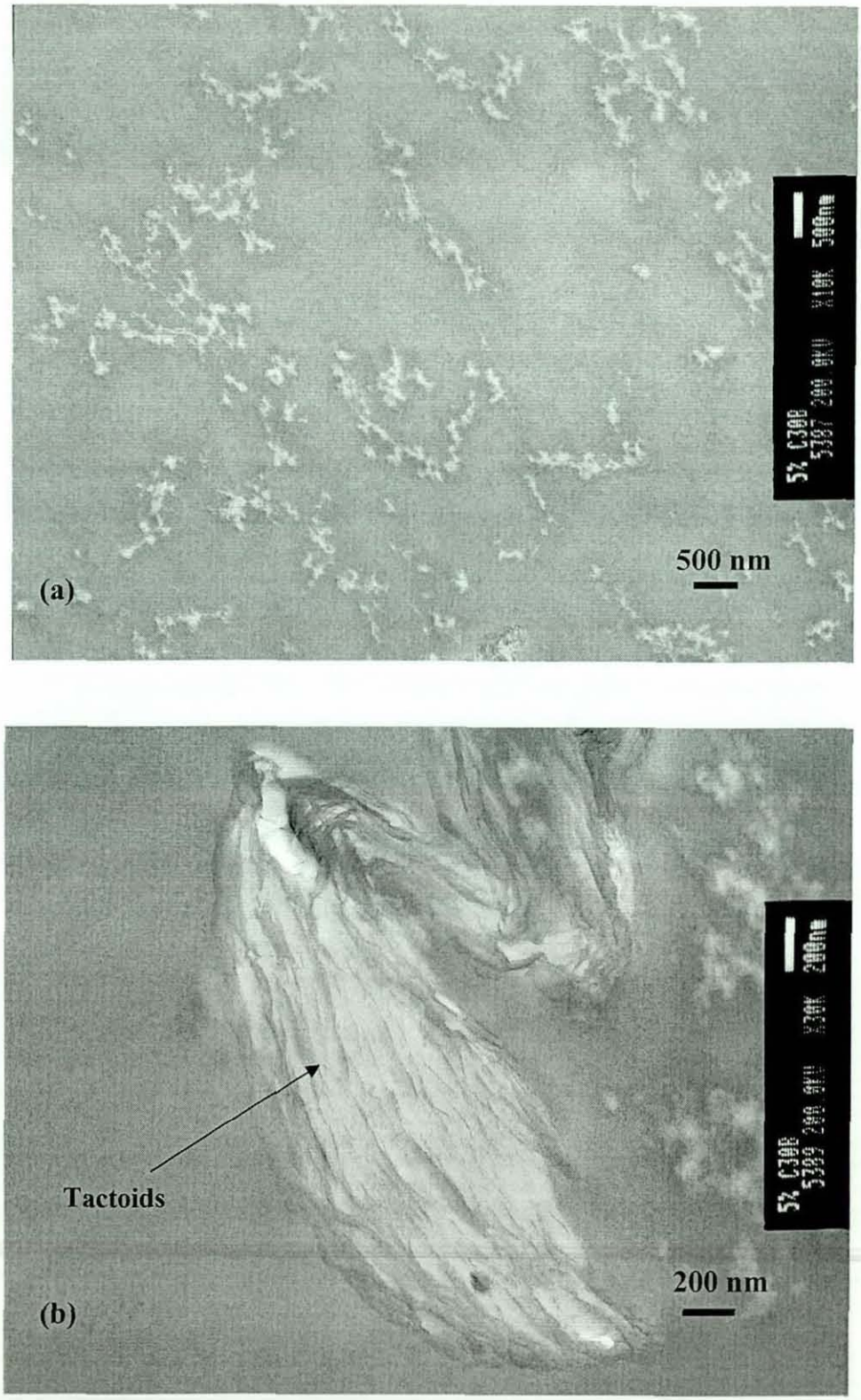


***Figure 6.15*** TEM micrographs for the 70PU/30PEMA (5 wt% C30B organoclay) IPN composites. (a) At 10k magnification. (b) At 30k magnification.

***Table 6.4*** Dynamic mechanical properties of organoclay filled 70PU/30PEMA IPN composites with various C30B contents.

| C 30B ( % wt) | Tg at tan δ max. (°C) | | Tan δ max value at Tg | | Peak width tan δ ≥ 0.3 (°C) |
|---|---|---|---|---|---|
| | PU | PEMA | PU | PEMA | |
| unfilled | 1 | 90 | 0.50 | 0.49 | - |
| 1% | -11 | 79 | 0.36 | 0.60 | -21 ↔ 138 (159) |
| 5% | -15 | 77 | 0.32 | 0.72 | -19 ↔ 127 (146) |

Over the studied temperature range of -60°C to 160°C, the DMTA plots of the PU/PEMA IPNs show that the two polymers are a semi-miscible, where two shoulders corresponding to PU and PEMA-rich phases appeared at 1°C and 90°C, respectively, with a broad and almost rectangular tan delta profile, indicating a high damping temperature range. On adding C30B organoclay, the glass transition of both networks shift to lower temperatures. Moreover, the PU does not exhibit a maximum value in tan δ profile, despite being the major component. The higher value is shown at the PEMA transition for each clay loading.

The PEMA transition occurs at 90°C (tan δ max 0.49) in the absence of C30B organoclay. Incorporation of 1% C30B shifted the transition to 79°C (tan δ max 0.60). Further increase in C30B content to 5 wt% brings the transition down to 77°C (tan δ max 0.72). There is also a slight downward shift of the PU transition over the range of filled IPN composites, with also a reduction of the tan delta max value at PU Tg. The PU transition decreases from 1°C (tan δ max 0.50) observed for the unfilled IPN to -15°C (tan δ max 0.32) shown by the sample of 5 wt% C30B content. Moreover, the peak width at tan δ ≥ 0.3, tends to be narrower as the C30B organoclay content increases. These results may arise because some chain segments might have been adsorbed on the surface of organoclay particles, owning to the high aspect ratio of the silicate platelets. Subsequently, the IPNs of lower crosslink density could be formed in the presence of the C30B organoclay, showing lower glass transitions for both polymer networks.

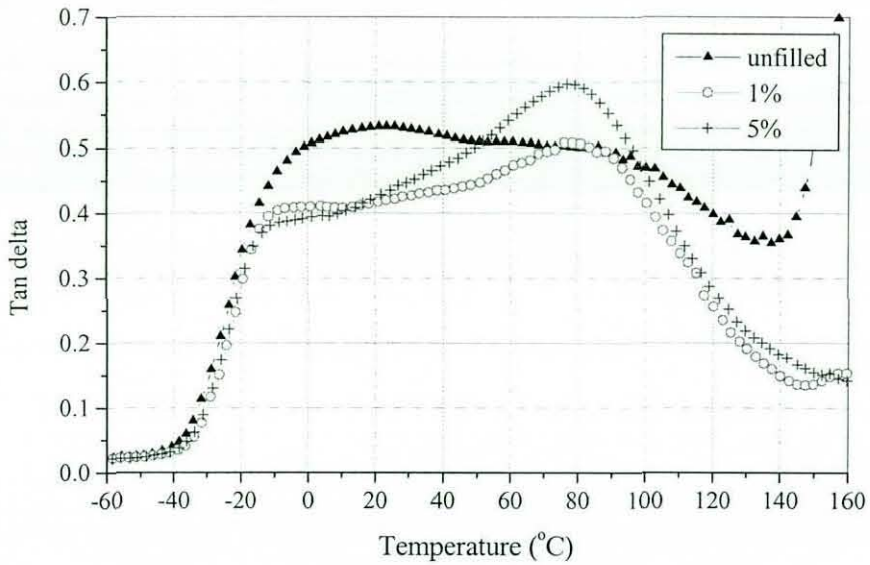


***Figure 6.16*** Loss factor versus temperature plots for the 70PU/30PEMA IPN organoclay composites: 0, 1 and 5 wt% C30B.

Figure 6.17 shows the storage modulus of the IPNs with added C30B organoclay as a function of temperature. There is no sign of gross phase separation. No significant change in slope was observed. Incorporation of the C30B organoclay results in an increase in storage modulus around room temperature up until the rubbery stage. This behaviour can be explained by the typical filled system.

A similar trend is observed for the loss modulus as shown in Figure 6.18. The unfilled organoclay IPN shows a gradual decrease in loss modulus over the temperature range, indicating a high extent of component mixing and interface content. Incorporation of C30B organoclay causes no sign of gross phase separation. Again, no significant changes in the loss modulus were found at the glassy stage, but there are increased around the room temperature and beyond, as found in the storage modulus profiles. However, the loss modulus of the filled organoclay IPNs is increased in the rubbery region as compared to that at the glassy state, this being due to the relative stiffness of the silicate particles.

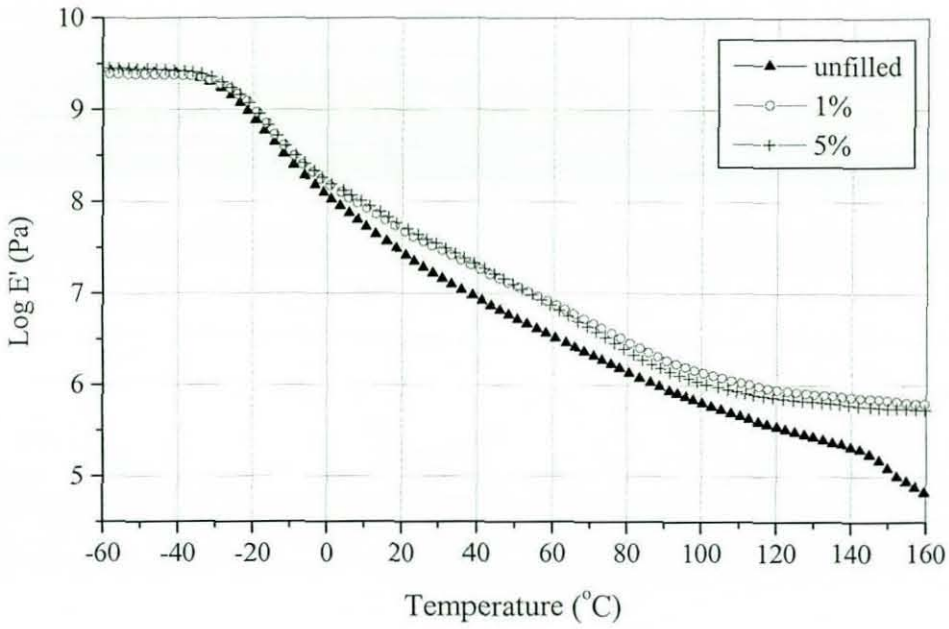


***Figure 6.17*** Storage modulus versus temperature plots for the 70PU/30PEMA IPN organoclay composites: 0, 1 and 5 wt% C30B.

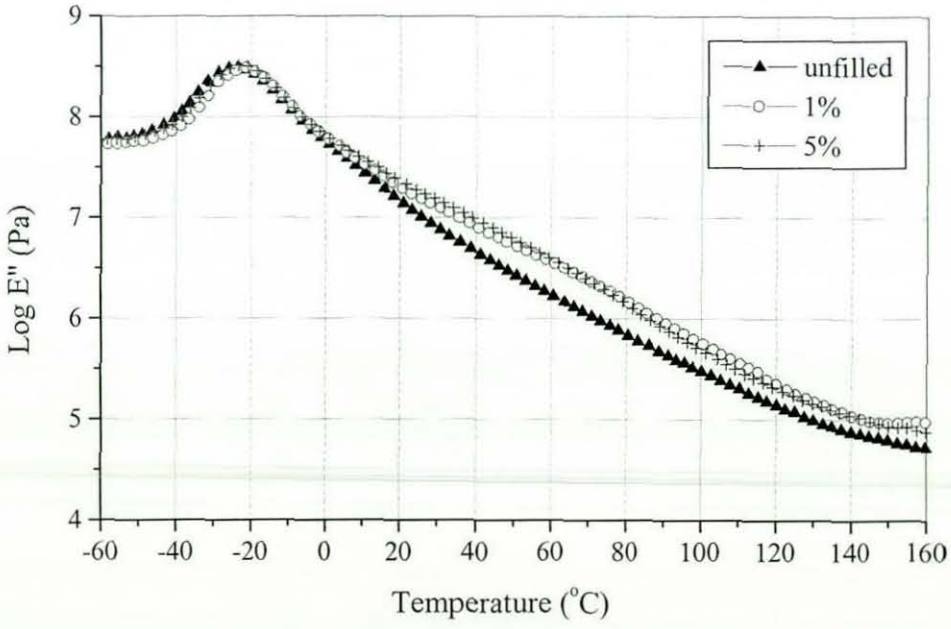


***Figure 6.18*** Loss modulus versus temperature plots for the 70PU/30PEMA IPN organoclay composites: 0, 1 and 5 wt% C30B.

### 6.2.4 Modulated-temperature differential scanning calorimetry.

The effect of C30B organoclay content on the glass transition temperatures and the miscibility of the 70PU/30PEMA IPNs were measured by M-TDSC and are presented in Figure 6.19.

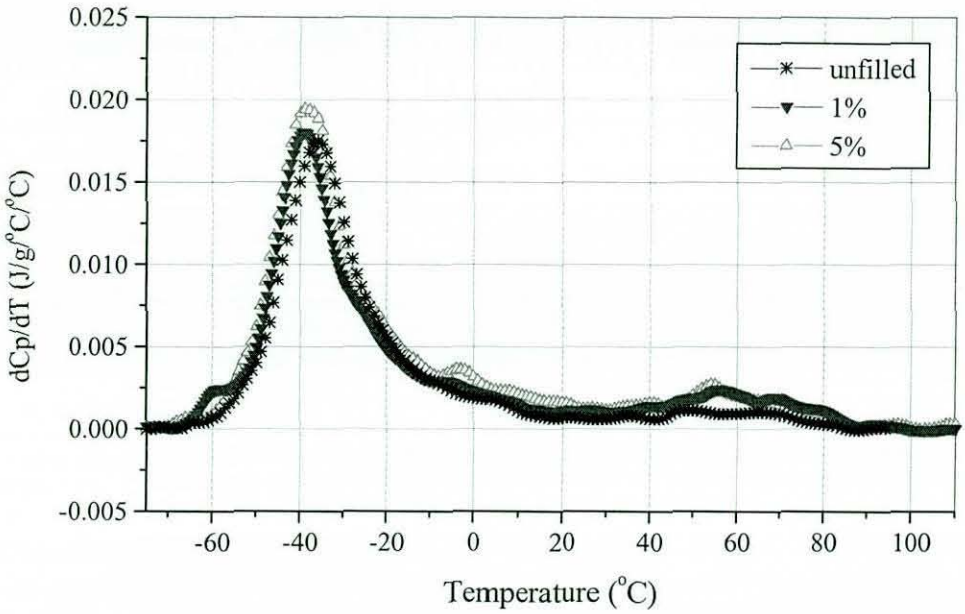


***Figure 6.19*** Differential heat capacity versus temperature plots showing the effect of C30B organoclay on the 70PU/30PEMA IPN organoclay composites.

M-TDSC curves for the C30B organoclay filled 70PU/30PEMA IPNs exhibit similar thermograms to the unfilled IPN, showing a sharp peak at the PU transition and a very broad shoulder at the PEMA transition. Moreover, it also shows some degree of multi-phase morphology, due to the retention of high value of the differential heat capacity over wide temperature range. Gross phase separation can not be seen. Increasing the organoclay content, the PU Tg shows no significant change as does the differential heat capacity value. This might be due to the fact that no segments are entrapped between the silicate layers. Therefore, as expected, peak heights, dCp/dT values, at the PU transition are approximately same. The slight, possibly within experimental error, changes are consistent with a looser PU networks. For the PEMA transition, no significant changes are observed.

### 6.2.5 Tensile behaviour and hardness measurements.

The mechanical properties of the IPN organoclay composites were also investigated by tensile testing and Shore A hardness measurements. The results of tensile testing and hardness measurements are shown in Figures 6.20 and 6.21, respectively. Table 6.5 shows the tensile results.

***Table 6.5*** Values of tensile strength, extension at break and modulus of elasticity for the IPN organoclay nanocomposites.

| Clay content (wt%) | Tensile strength (MPa) | Extension at break (%) | Modulus of elasticity (MPa) |
|---|---|---|---|
| unfilled | 4.58 ± 0.24 | 736 ± 37 | 4.52 ± 0.72 |
| 1% | 4.56 ± 0.34 | 642 ± 35 | 7.66 ± 0.81 |
| 5% | 2.80 ± 0.08 | 531 ± 33 | 8.01 ± 0.75 |

The tensile strength and the elongation at break gradually decrease with increasing organoclay content. At 5 wt% C30B, approximately a 40% decrease in stress at break and around 30% reduction of elongation at break are noticed. On the other hand, the modulus of elasticity and the Shore A hardness values show some increase. The modulus of elasticity exhibits around 70% increment for the 1 wt% filled IPN, and 80% for the 5 wt% filled IPN, as compared with unfilled IPN. The Shore A hardness usually relates to the modulus of elasticity. Varying the organoclay content in the IPN system results in changes of the Shore A values from 60, observed for unfilled IPN, to 62, obtained for 5 wt% filled IPN. Since the polymer did not intercalate, this system behaves like a conventional polymer composite[180,184].

## 6.3 Na clay.

Cloisite Na, Na clay, is a natural montmorillonite. No organic modifier is included in this clay. It is a white powder with a specific gravity of 2.86 g/cm$^3$. It is used as a filler for plastics to improve various physical properties[169].

In this study, Na clay at 0%, 1% and 5% by weight of PU were introduced into the 70PU/30PEMA IPN system by using an in-situ polymerisation method, in which the

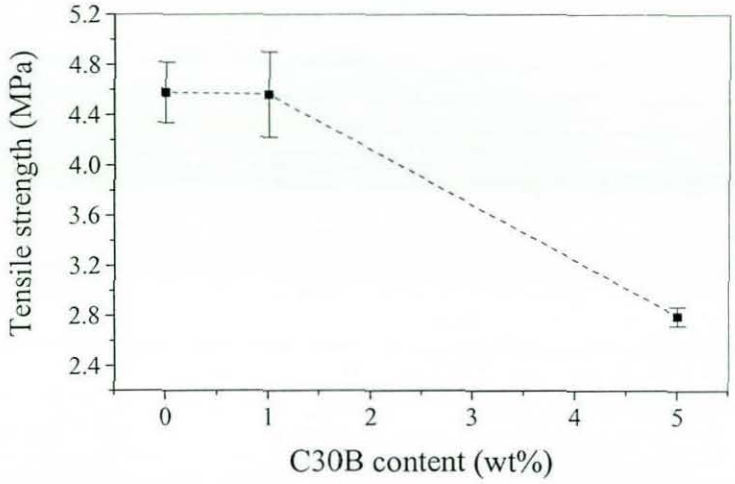


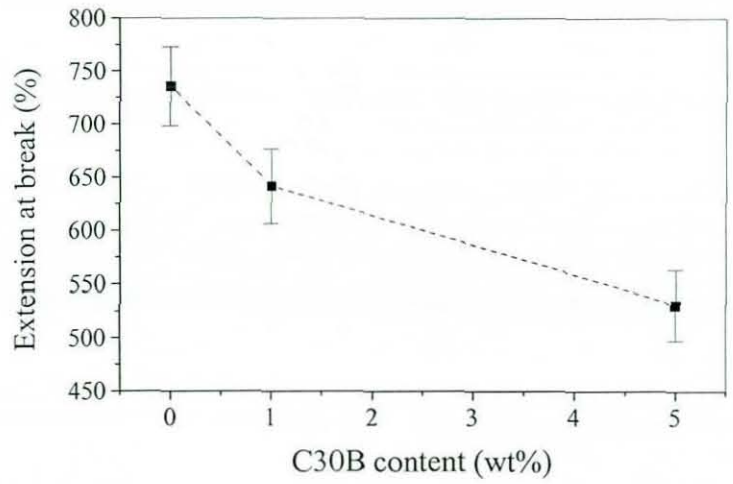


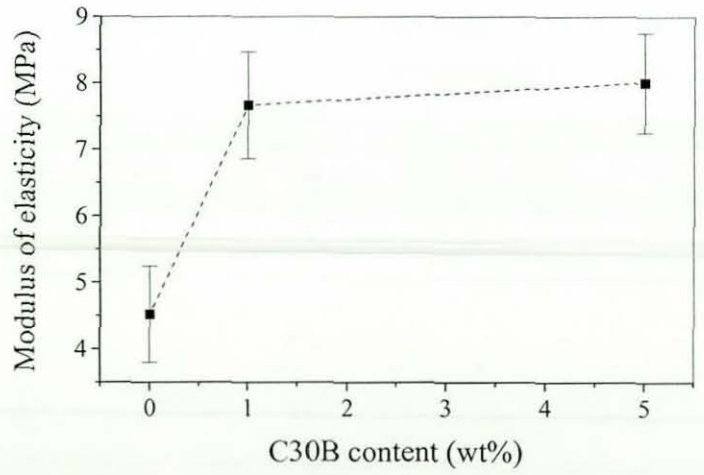


***Figure 6.20*** Tensile properties of the IPN organoclay nanocomposites as a function of C30B clay loading.

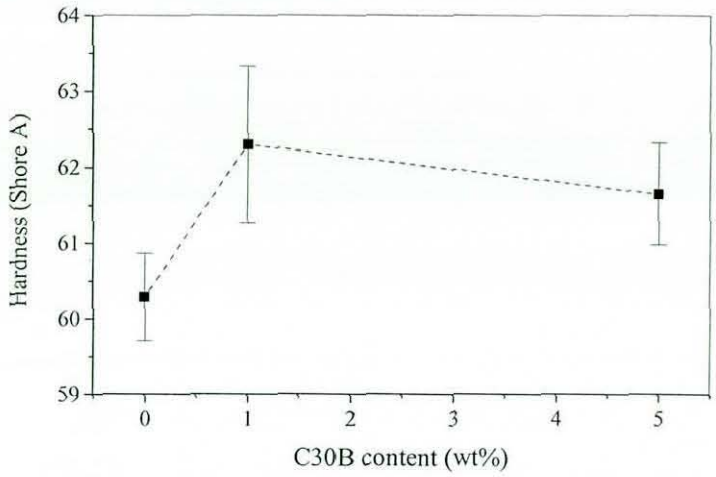


***Figure 6.21*** Shore A hardness values of the IPN organoclay composites as a function of C30B clay loading.

Na clay was first homogeneously mixed with PPG1025 at room temperature for 30 minutes using a Silverson L2R mixer, as in the original synthesis procedure (Chapter 3). The PU network was based on TMXDI, PPG1025, TMP and SnOct, with PPG1025:TMP ratio of 3:1 and SnOct 1.2% by weight of PU, whereas the PEMA network was prepared with TEGDM 5 mol% of PEMA and was initiated by AIBN at 1 mol% of PEMA. The simultaneous IPN technique was used to combine intimately the crosslinked elastomeric PU with the high glass transition plastic, PEMA. Finally, because of the settlement of organoclay during polymerisation reported in a previous chapter, the filled steel mould was turned every 30 minutes in the first four hours, and, subsequently, it was turned over every one hour for another 3 hours to diminish the extent of the clay settlement during curing process. The effects of the Na clay on the IPN properties, glass transition temperature, damping and mechanical properties were analysed by several techniques. The results of these investigations are shown below.

### 6.3.1 Wide angle X-ray diffraction.

The resulting WAXD patterns for Na clay, 70PU/30PEMA IPNs, and Na clay-filled 70PU/30PEMA IPNs with 1 and 5 wt% Na clay are shown in Figure 6.22. No diffraction peak is present for the 70PU/30PEMA IPNs because it is an amorphous composite. One prominent diffraction peak was observed for the Na clay at 7.94° corresponding to an interlayer spacing of 1.11 nm.

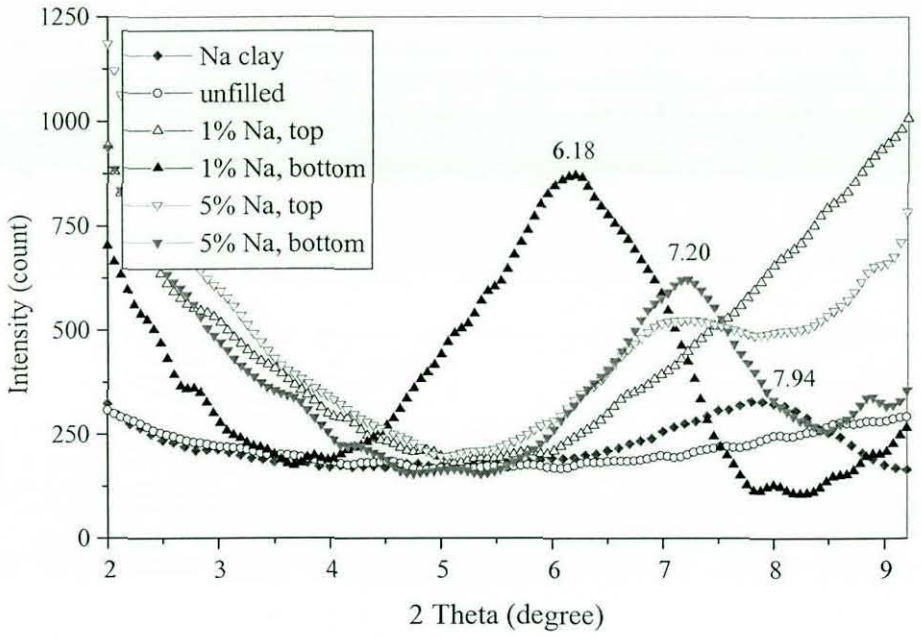


***Figure 6.22*** WAXD patterns for Na clay, the 70PU/30PEMA IPN and the Na clay-filled 70PU/30PEMA IPNs containing 1 and 5 wt% Na clay for both top and bottom sides.

After in-situ intercalative polymerisation with 70PU/30PEMA, the diffraction peak is shifted towards a lower angle value of 6.18° and 7.20°, for the 1% and 5% clay loadings, respectively. These correspond to interlayer spacings of 1.43 and 1.23 nm. These results indicate that the polyether polyol molecules are intercalated to some degree in the silicate layers at both the clay contents. Besides, they still exhibit some settlement of the Na clay as compared between the top and the bottom sides of a sample sheet. At higher clay contents, lesser differences of diffraction intensity were obtained. A dramatic difference occurs at 1 % clay content.

### 6.3.2 Transmission electron microscopy.

The TEM micrographs showing the morphology of the 70PU/30PEMA IPN with Na clay nanocomposites are given in Figures 6.23 and 6.24. Incorporation of Na clay gives a marginal change in the microstructure. The light, interconnected PEMA domains spreading through the PU matrix seem to be bigger and more interconnected, as the clay content increases. Moreover, there are some small, light PEMA domains dispersed uniformly in the continuous PU matrix, as seen in Figure 6.24 (b). A range

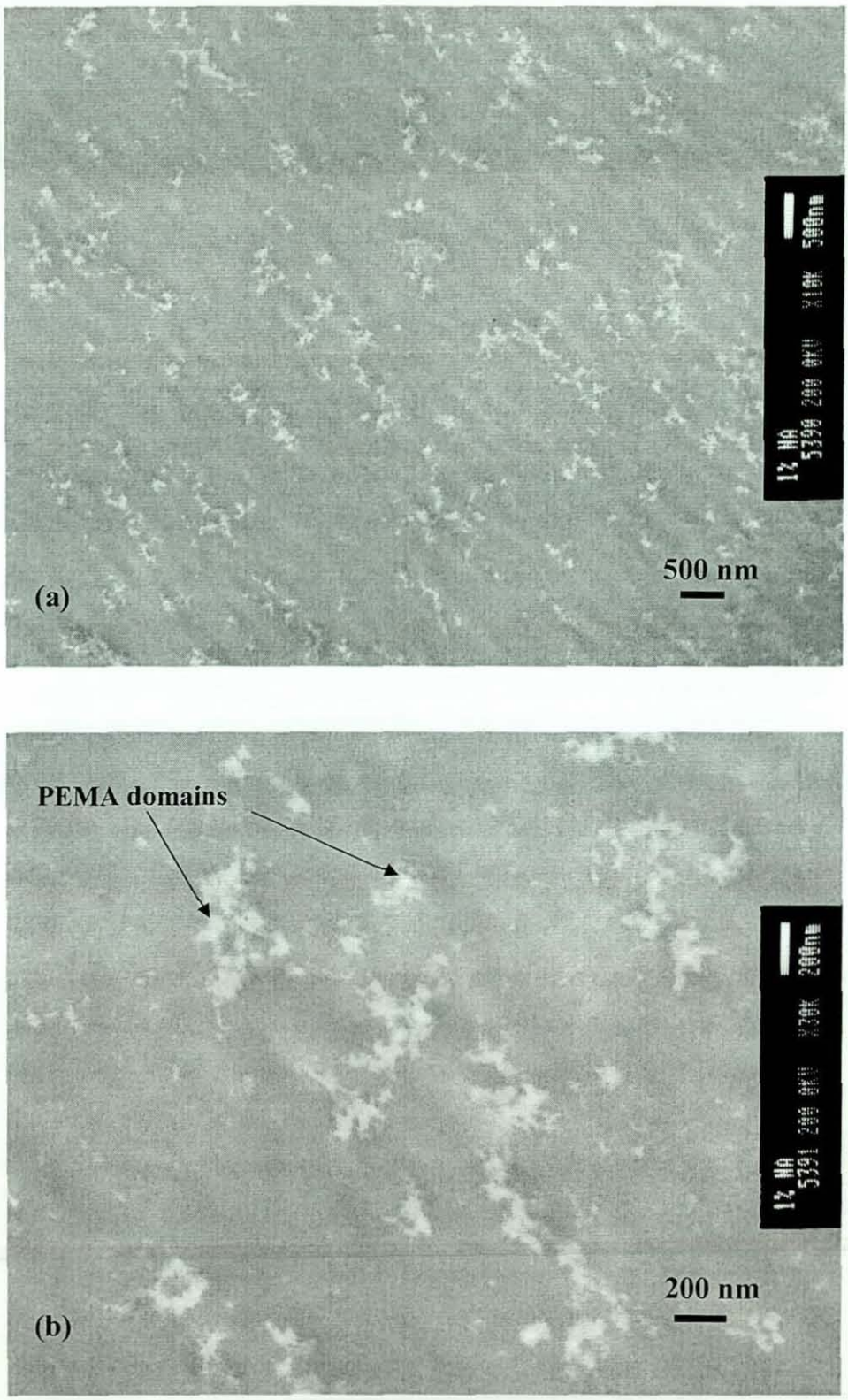


***Figure 6.23*** TEM micrographs for the 70PU/30PEMA (1 wt% Na clay) IPN nanocomposites. (a) At 10k magnification. (b) At 30k magnification.

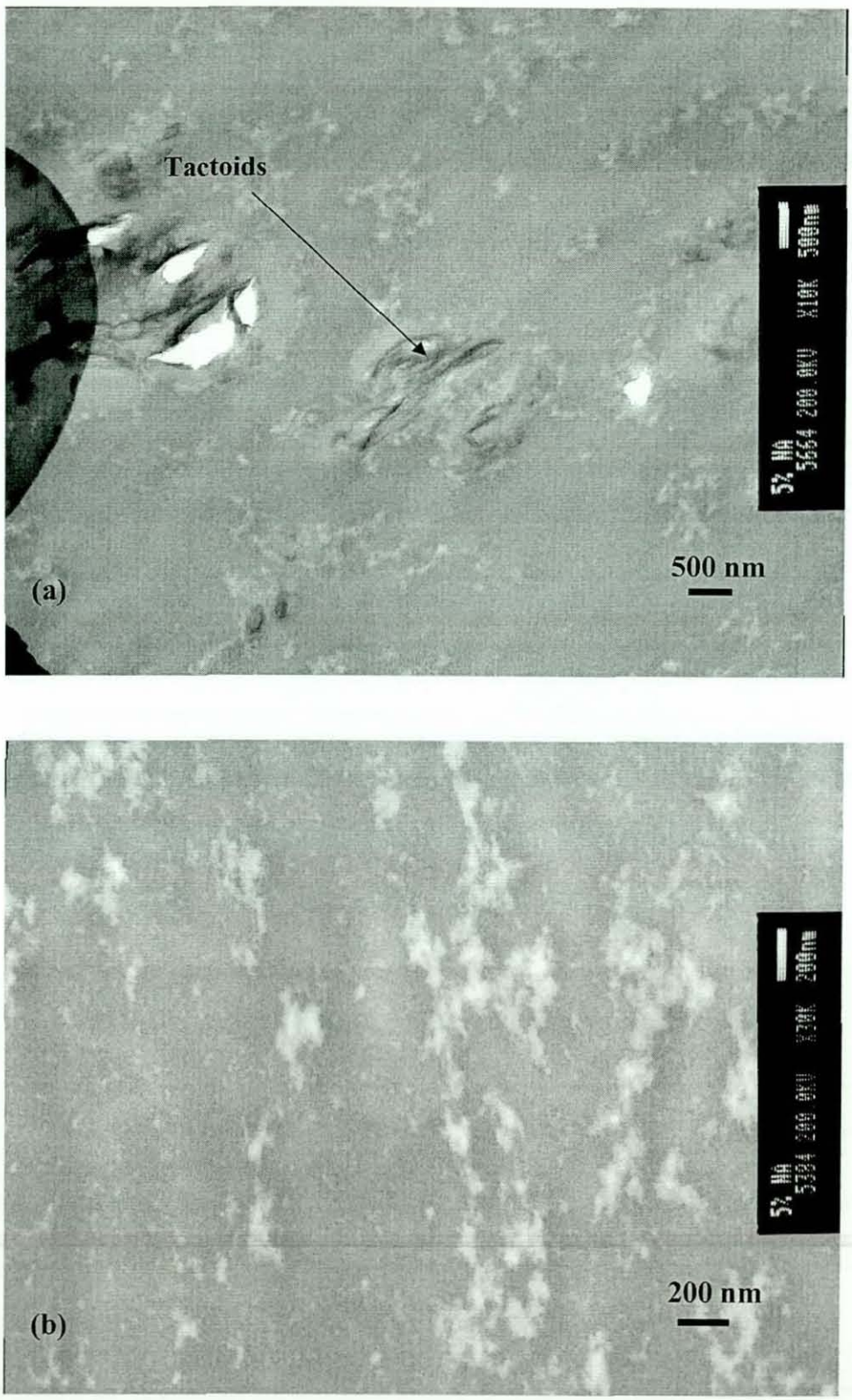


***Figure 6.24*** TEM micrographs for the 70PU/30PEMA (5 wt% Na clay) IPN nanocomposites. (a) At 10k magnification. (b) At 30k magnification.

of different shades of grey in the PU matrix can be seen. Also, the darker matrix areas are more frequently observed around the PEMA domains, indicating some degree of molecular mixing between the two components. Therefore, the morphology of these nanocomposites reveals some significant degree of component mixing.

### 6.3.3 Dynamic mechanical thermal analysis.

The dynamic mechanical properties of the Na clay-filled 70PU/30PEMA IPN composites at various Na clay contents are plotted as a function of temperature in Figures 6.25 to 6.27. Peak positions and values in tan delta max values of their PU and PEMA components and the peak widths at tan $\delta \geq 0.3$ are summerised in Table 6.6.

***Table 6.6*** Dynamic mechanical properties of filled 70PU/30PEMA IPN composites with various Na clay contents.

| Na clay ( % wt) | Tg at tan δ max. (°C) | | Tan δ max value at Tg | | Peak width tan $\delta \geq 0.3$ (°C) |
|---|---|---|---|---|---|
| | PU | PEMA | PU | PEMA | |
| unfilled | 1 | 90 | 0.50 | 0.49 | - |
| 1% | 0 | 84 | 0.46 | 0.44 | -15 ↔ 114 (129) |
| 5% | -2 | 81 | 0.46 | 0.47 | -18 ↔ 112 (130) |

In the temperature range from -60°C to 160°C, the DMTA plots of the PU/PEMA IPNs show that the two polymers form a semi-miscible system, where two shoulders corresponding to PU and PEMA-rich phases appear at 1°C and 90°C, respectively. Broad and almost rectangular tan delta profiles indicate a high damping temperature range. Adding Na clay, the glass transitions of both networks shift towards to lower temperatures with a slight decrease in tan delta max values for both networks. Both filled IPNs still show the broad tan delta profiles. Therefore, it is fairly difficult to verify accurate the individual glass transition temperatures of the homopolymer networks. They still reveal a high damping characteristic, showing a broad loss factor, tan $\delta \geq 0.3$, spanning a temperature range of 130°C, but the tan delta max values are a little lower when the Na clay is incorporated.

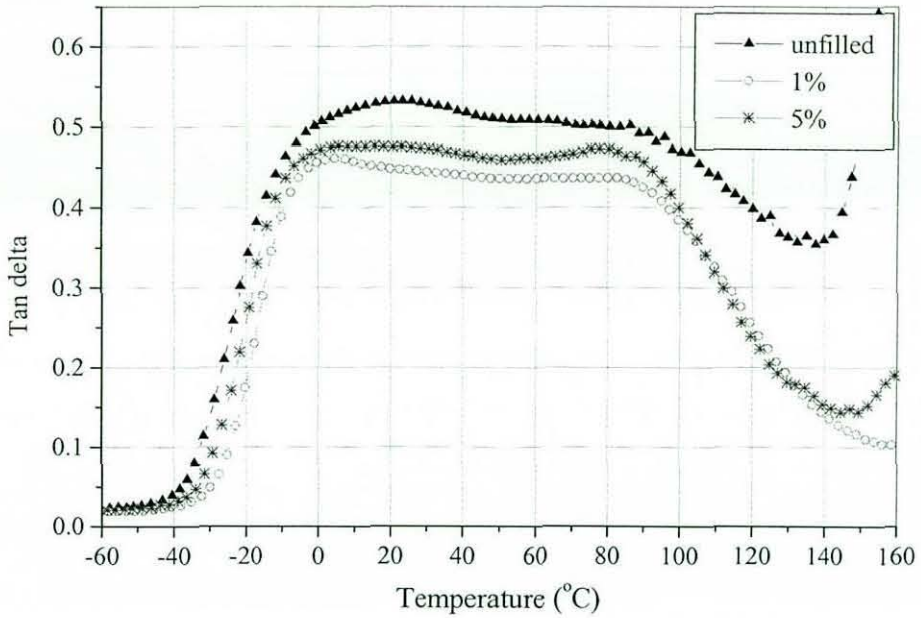


***Figure 6.25*** Loss factor versus temperature plots for the 70PU/30PEMA IPN organoclay nanocomposites: 0, 1 and 5 wt% Na clay.

The storage moduli of the IPNs with added Na clay as a function of temperature are shown in Figure 6.27. They show gradual and continuous shape changes. This indicates extensive mixing between the polymer components. Incorporation of the Na clay results in an increase in storage modulus around room temperature and above. This behaviour is typical of a conventionally filled system[180,184].

A similar trend was observed for the loss modulus as shown in Figure 6.27. All IPNs show a gradual decrease in loss modulus over the temperature range studied, indicating a high extent of component mixing and a high interface content. Incorporation of Na clay shows a slight increase of the PU network Tg. This may arose from restricted PU segments. The loss modulus values are also increased around room temperature and above. However, the loss modulus of the filled IPNs seems to be increased in the rubbery state as compared to that at the glassy state, due to the stiffness of the silicate platelets and the internal friction between the silicate platelets and the polymer matrix.

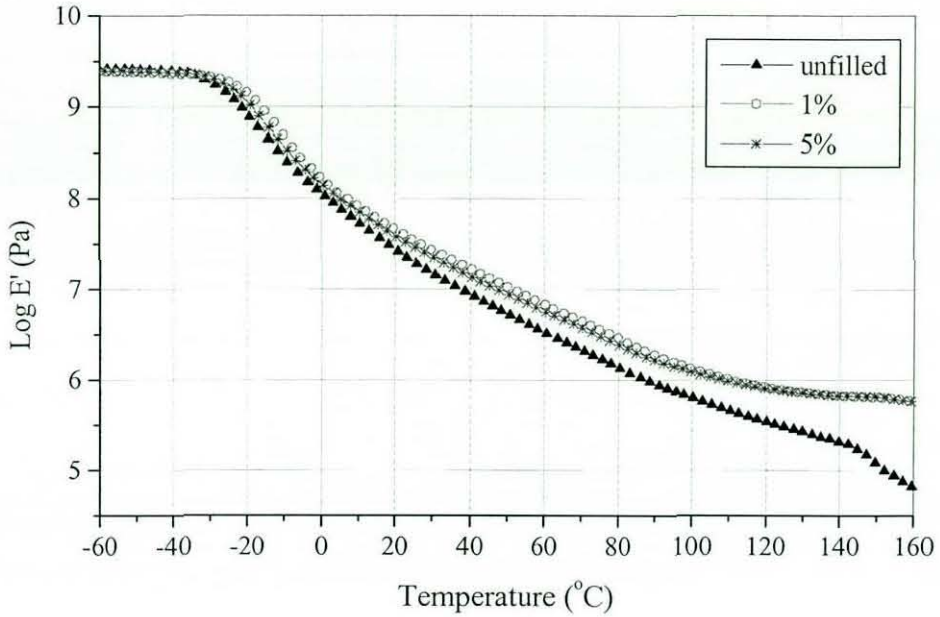


***Figure 6.26*** Storage modulus versus temperature plots for the 70PU/30PEMA IPN nanocomposites: 0, 1 and 5 wt% Na clay.

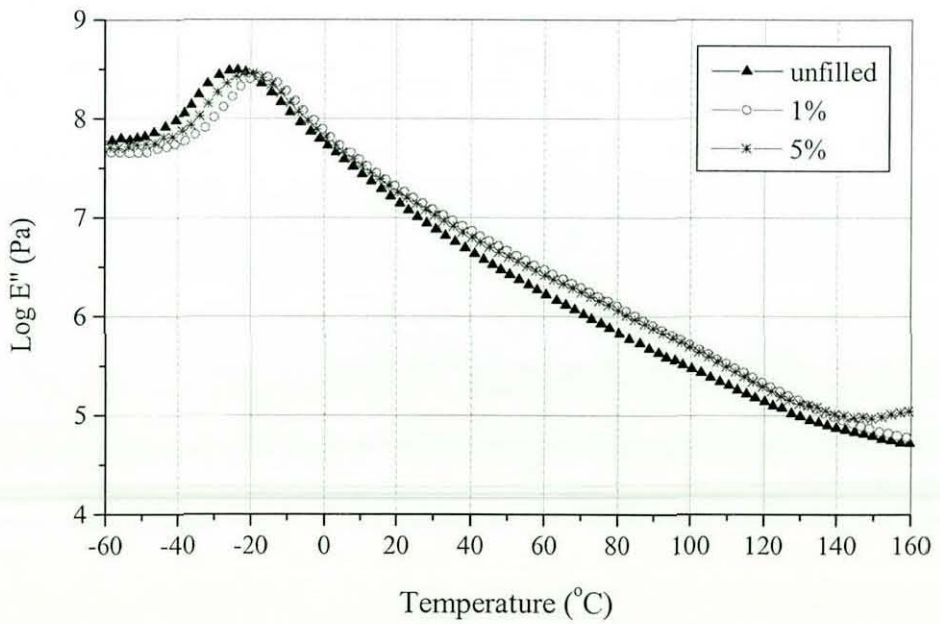


***Figure 6.27*** Loss modulus versus temperature plots for the 70PU/30PEMA IPN nanocomposites: 0, 1 and 5 wt% Na clay.

### 6.3.4 Modulated-temperature differential scanning calorimetry.

The effect of Na clay content on the glass transition temperatures and the miscibility of the 70PU/30PEMA IPNs measured by M-TDSC are presented in Figure 6.28.

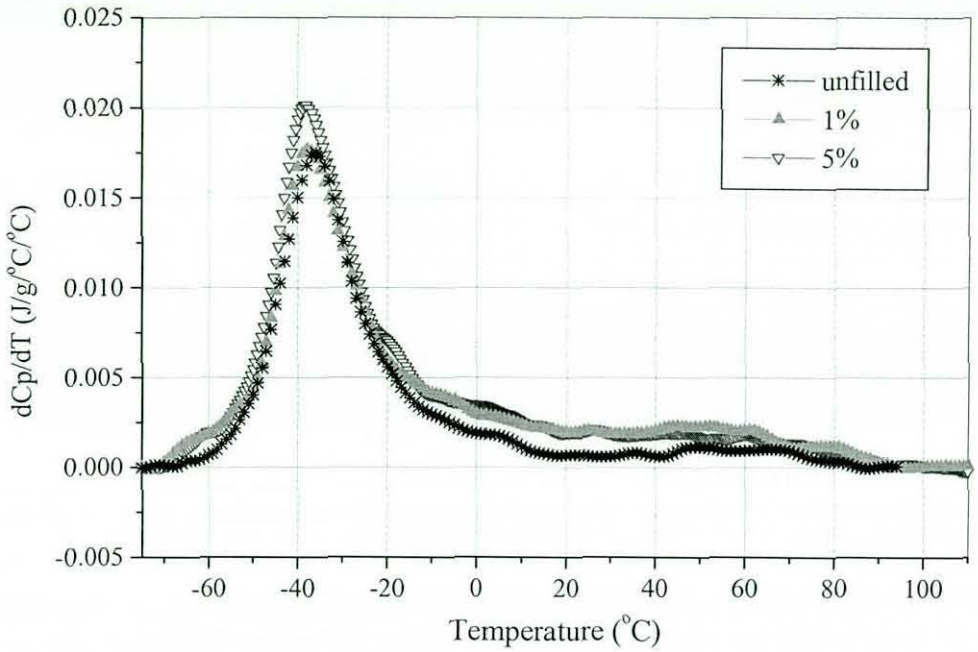


***Figure 6.28*** Differential heat capacity versus temperature plots showing the effect of Na clay content on the 70PU/30PEMA IPN nanocomposites.

M-TDSC curves for the Na clay filled 70PU/30PEMA IPNs exhibit the similar traces to that found for the unfilled IPN, showing a sharp PU transition and a very broad shoulder over the PEMA transition region. Moreover, it also shows some multi-phase morphology, due to the spanning of high value of the differential heat capacity over a wide temperature range. Gross phase separation is not indicated. Increasing the clay content, the PU Tg shows no significant change, while the differential heat capacity values at the PU transition slightly change. The slight, possibly within experiment error, changes are consistent with a looser PU network. However, for PEMA transition shows no significant change.

### 6.3.5 Tensile behaviour.

Mechanical properties of the IPN nanocomposites were investigated by tensile testing. Figure 6.29 shows the tensile strength, elongation at break and the modulus of elasticity versus Na clay content. Their tensile property results are shown in Table 6.7.

***Table 6.7*** Values of tensile strength, extension at break and modulus of elasticity for the IPN nanocomposites.

| Clay content (wt%) | Tensile strength (MPa) | Extension at break (%) | Modulus of elasticity (MPa) |
|---|---|---|---|
| unfilled | 4.58 ± 0.24 | 736 ± 37 | 4.52 ± 0.72 |
| 1% | 4.68 ± 0.36 | 637 ± 18 | 4.58 ± 0.40 |
| 5% | 4.45 ± 0.32 | 607 ± 22 | 5.80 ± 0.59 |

The tensile properties for unfilled and filled IPN samples are shown in Figure 6.29. Incorporation of Na clay tends to reduce elongation at break, but increases the modulus of elasticity. No significant change is observed for the tensile strength. The stress and elongation at break of the unfilled IPN are 4.58 MPa and 736%, and the modulus of elasticity is 4.52 MPa. The values of stress and elongation at break decrease slightly to 4.45 MPa and 607% for the 5 wt% Na clay-filled IPN, whereas a value of 5.80 MPa is detected for the modulus of elasticity.

## 6.4 Comparison of the various clay types.

Comparisons of the DMTA and tensile testing results are examined in this section. The correct selection of the clay type should show optimum values in the dynamic mechanical and physical properties, especially damping behaviour.

### 6.4.1 Dynamic mechanical thermal analysis.

The DMTA results for the 70PU/30PEMA composites with 1 wt% of clay are shown in Figures 6.30 to 6.32, corresponding to loss factor and the storage and loss moduli profiles, respectively, whilst those of the 5 wt% filled IPNs are illustrated in Figures 6.33 to 6.35.

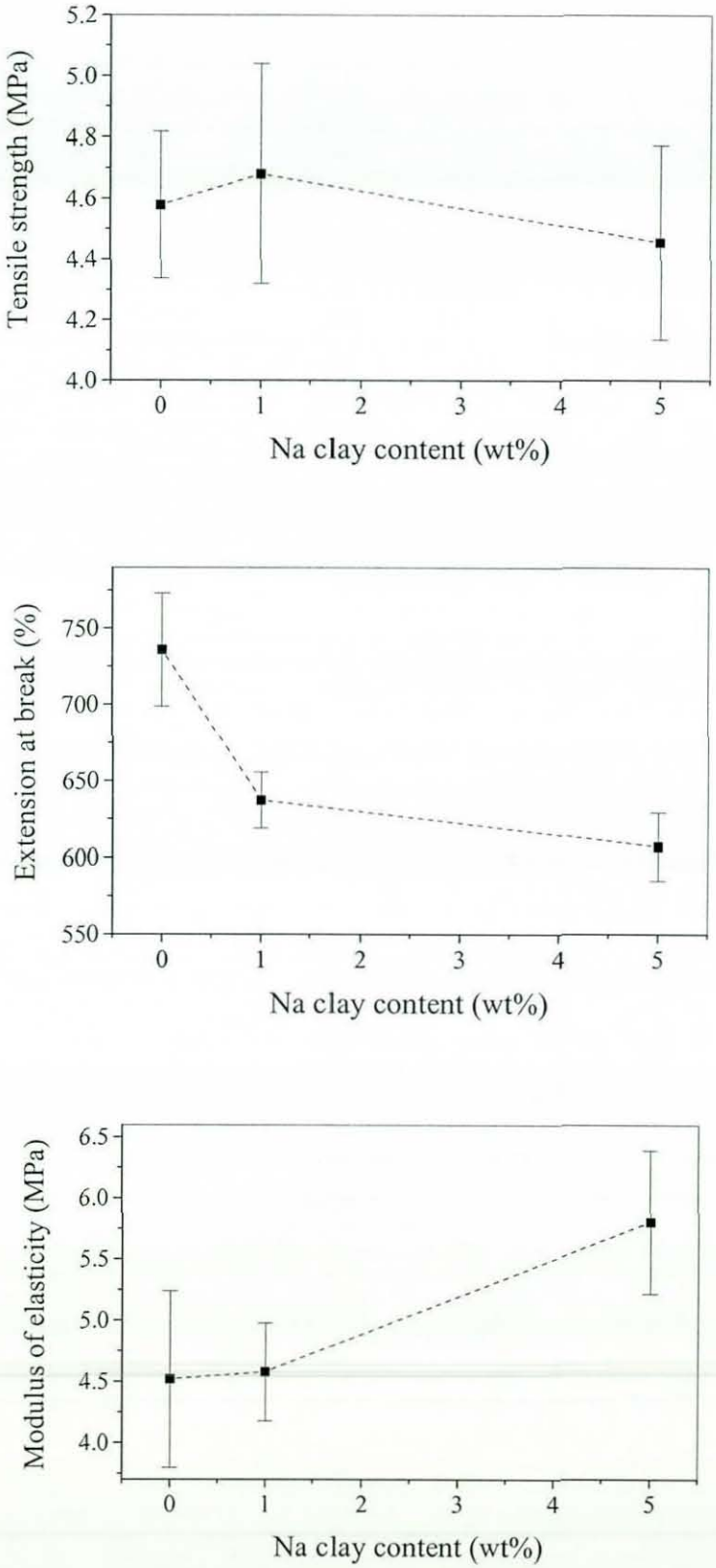


***Figure 6.29*** Tensile properties of the IPN nanocomposites as a function of Na clay loading.

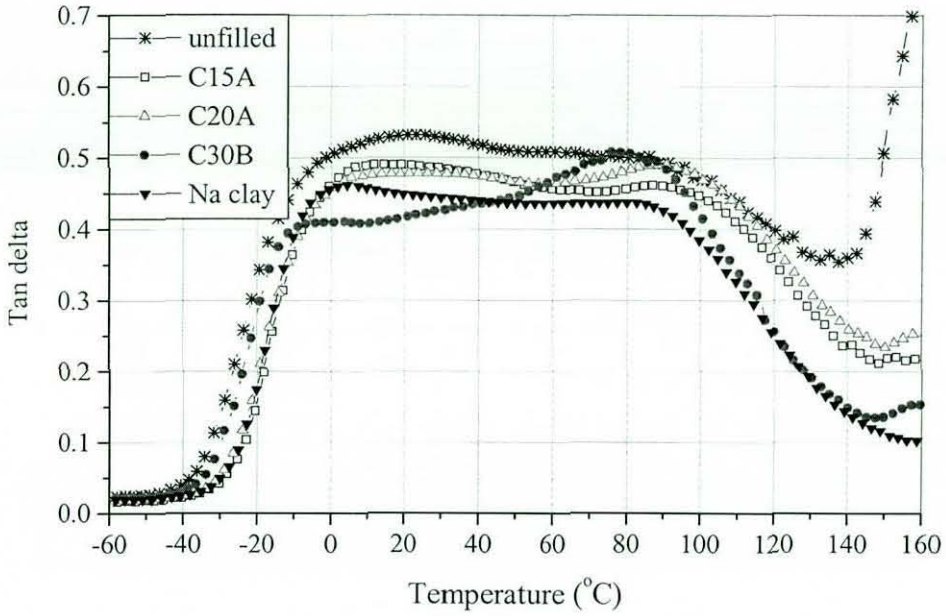


***Figure 6.30*** Loss factor versus temperature plots for the 70PU/30PEMA IPN composites at 1 wt% loading.

1 wt% C15A and C20A show similar loss factor profiles, as seen in Figure 6.30. They show broad and rectangular tan delta profiles. Their loss factor values are slightly reduced compared to the unfilled IPN. The 1 wt% C15A- and C20A-filled IPN nanocomposites still exhibit high damping characteristics, with tan $\delta$ of $\geq 0.3$ spanning a temperature range of 130°C. Na clay-filled IPN nanocomposite exhibits high damping characteristics also, even though it shows a significant decrease in loss factor values. Thus, these three filled IPN nanocomposites reveal micro-heterogeneity with some extent of molecular mixing, showing the broadened glass transitions. For C30B organoclay, the filled IPN composite shows a significant change in loss factor profile. The loss factor value at PU transition decreases, while that at PEMA transition increases, indicating that some more phase separation takes place. This might be attributed to the incompatibility of the C30B organoclay and polyether polyols etc., since the latter could not intercalate the silicate layers.

The corresponding storage and loss moduli data, seen in Figures 6.31 and 6.32, indicate that no gross phase takes place for any of the IPN composites. All the filled IPNs exhibit a gradually change the storage and loss moduli over the measured

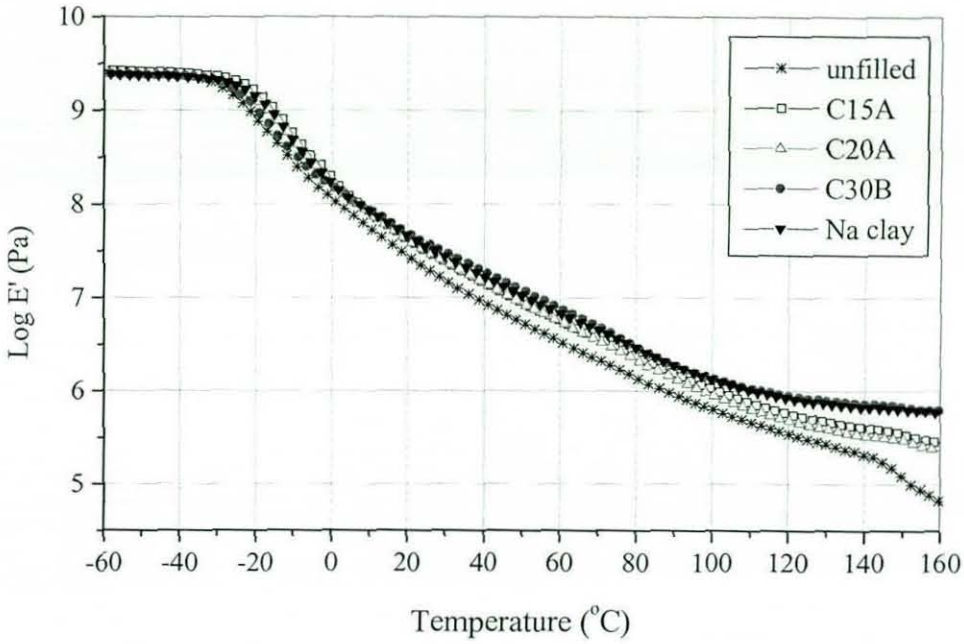


***Figure 6.31*** Storage modulus versus temperature plots for the 70PU/30PEMA IPN composites at 1 wt% loading.

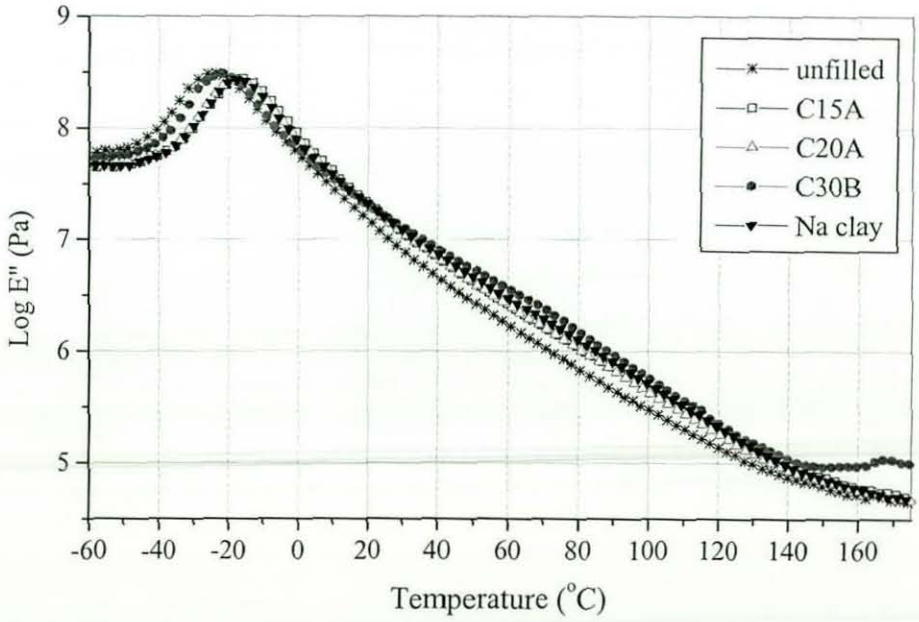


***Figure 6.32*** Loss modulus versus temperature plots for the 70PU/30PEMA IPN composites at 1 wt% loading.

temperature range, except the C30B-filled IPN. A slight change in slope at the homopolymer Tgs for the C30B-filled IPN can be seen in the loss modulus profile. Moreover, the PU Tg is shifted towards higher temperature by around 5°C, as compared to that of the unfilled IPN, after C15A, C20A or Na clay were added, but no obvious change was found for the C30B-filled IPN. The possible reason is some PU segments are restricted in the galleries of the C15A, C20A and Na clays. However, the filled IPN composites reveal higher storage and loss modulus than those of the unfilled IPN.

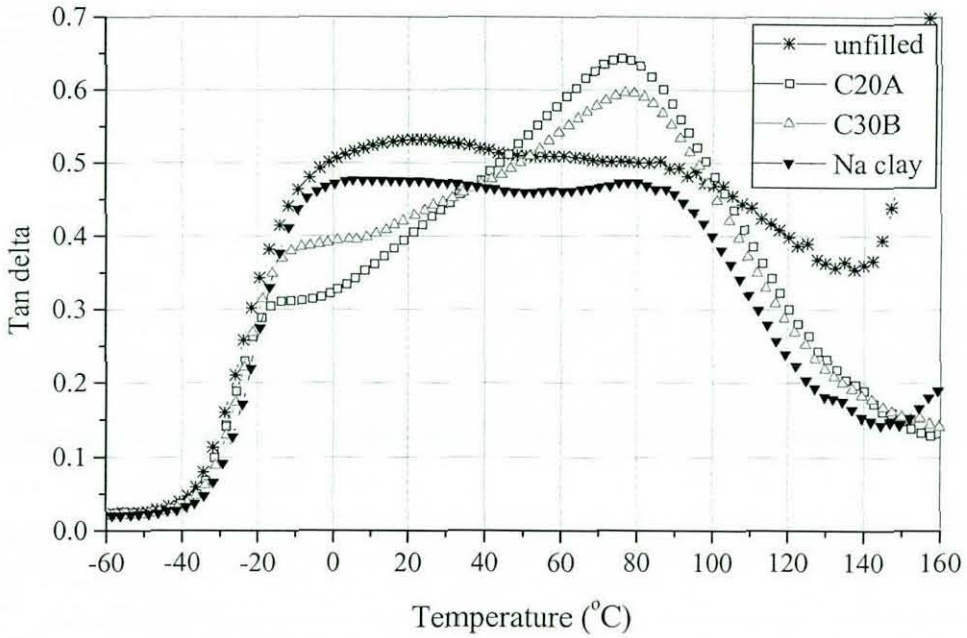


***Figure 6.33*** Loss factor versus temperature plots for the 70PU/30PEMA IPN composites at 5 wt% loading.

At 5 wt% nanoclay content, the C20A- and C30B-filled IPNs show a PU transition and a strong PEMA transition, as seen in Figure 6.33. These results tend to reveal some extent of phase separation for higher contents of nanoclay, as compared to those with 1 wt% filled IPNs. While, 5 wt% Na clay-filled IPN, the loss factor profile remains showing a broadening and a rectangular in shape over a studied temperature range, indicating high extent of molecular mixing in this IPN composite. The reason for these findings was not clear. More detailed research was needed.

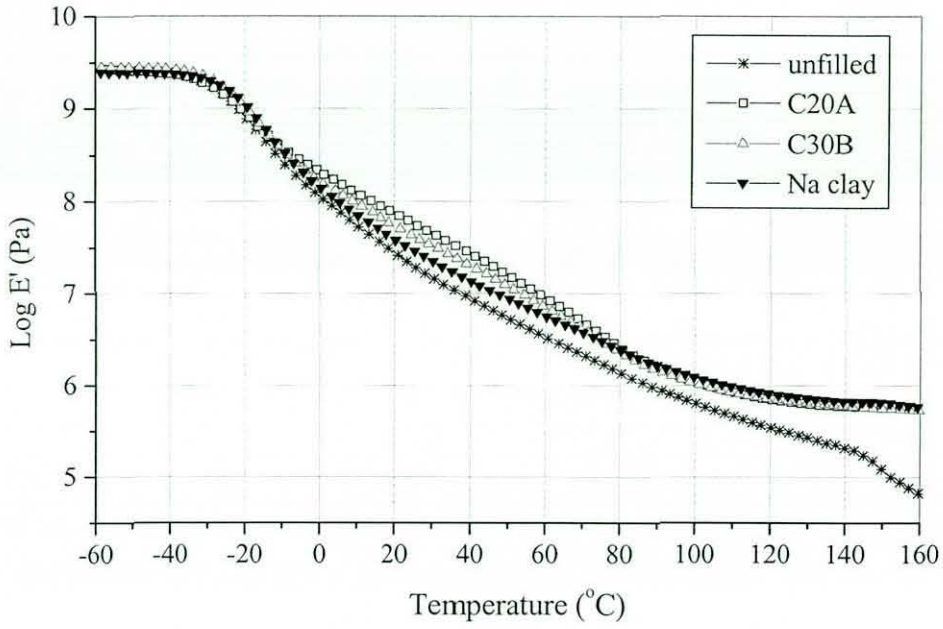


***Figure 6.34*** Storage modulus versus temperature plots for the 70PU/30PEMA IPN composites at 5 wt% loading.

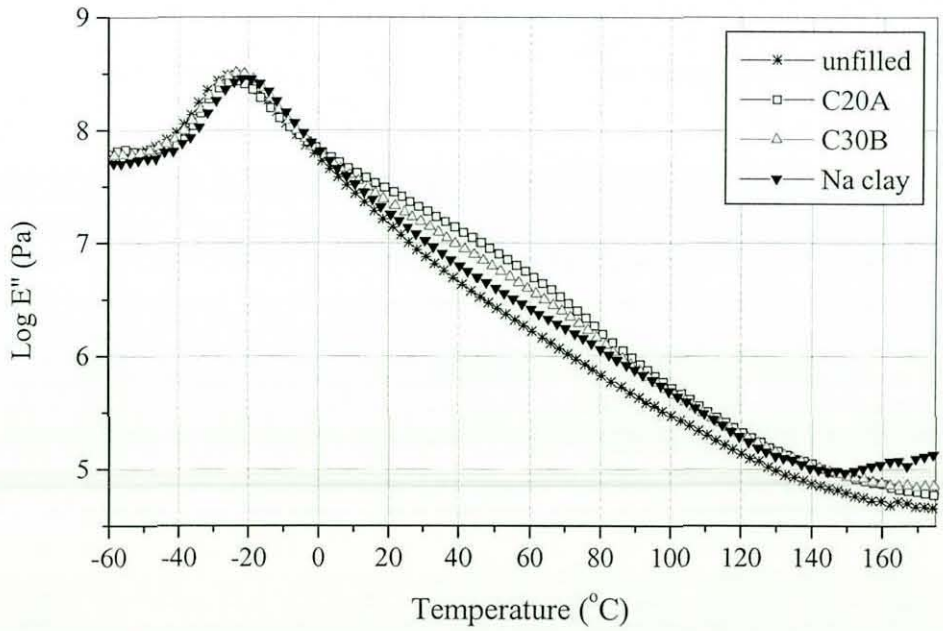


***Figure 6.35*** Loss modulus versus temperature plots for the 70PU/30PEMA IPN composites at 5 wt% loading.

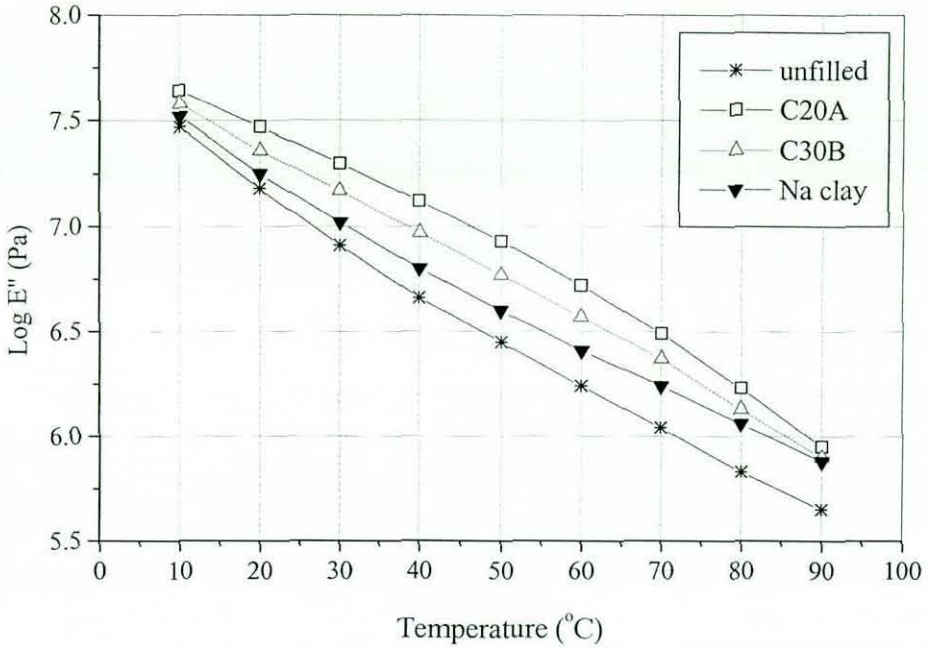


***Figure 6.36*** Loss modulus for the 70PU/30PEMA IPN composites with 5 wt% loading at various temperatures.

C20A- and C30B-filled IPNs show a two-step change for both storage and loss modulus profiles at the Tgs of their homopolymers, as seen in Figures 6.34 and 6.35. A gradual change in slope of storage and loss moduli is found for the Na clay-filled IPN. In the glassy state, both moduli do not show any significant changes, but they reveal a significant increase above the PU transition and continuously increase until the rubbery state for all filled IPNs.

The C20A-filled IPN shows the highest loss modulus value at each observed temperature, as seen in Figure 6.36. This could be because some chain segments intercalated, yielding a higher extent of physical interaction between the nanoclay and the polymer. Another reason could be internal friction between the silicate platelets themselves. The C30B-filled IPN also shows a high loss modulus value, even though C30B was not intercalated in this IPN. This could be because of a strong internal friction between polymer matrix and silicate particles and between the silicate particles themselves. The Na clay-filled IPN shows the lowest loss modulus value amongst the filled-IPN composites.

### 6.4.2 Tensile behaviour.

Tensile behaviour of the filled IPNs with the different types of nanoclay is shown in Figures 6.37 to 6.39.

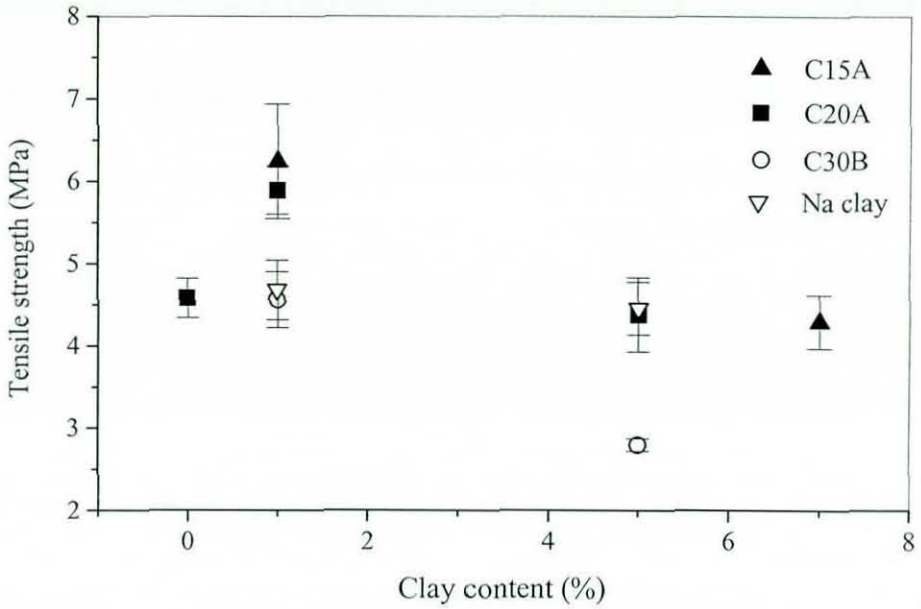


***Figure 6.37*** Tensile strength of the 70PU/30PEMA IPN composites as a function of clay loading.

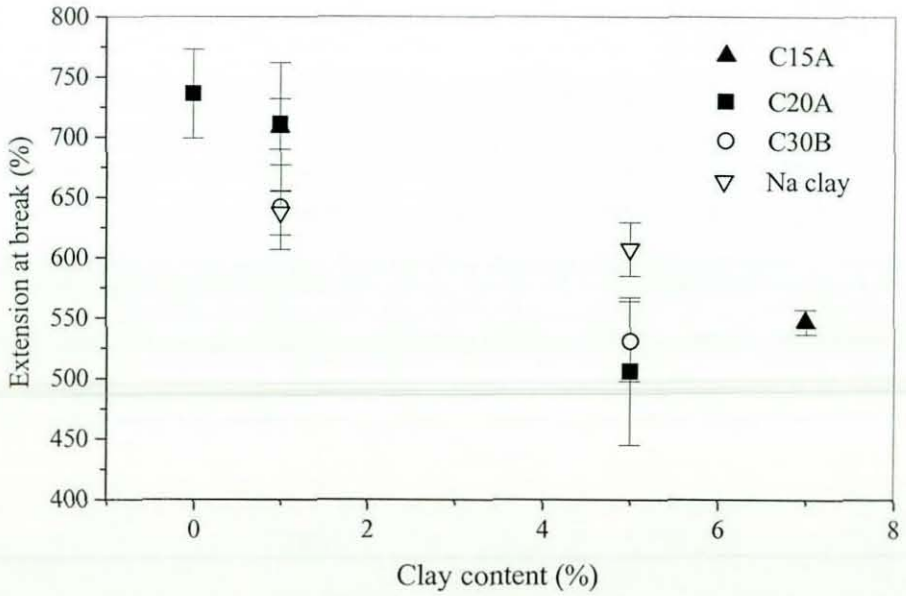


***Figure 6.38*** Elongation at break of the 70PU/30PEMA IPN composites as a function of clay loading.

Tensile strength at 1 wt% clay content increases around 33 % for C15A- and C20A-filled IPNs, as seen in Figure 6.37, but no significant change for the C30B- and Na clay-filled IPNs was observed. The high tensile strength for C15A- and C20A-filled IPN could be attributed to a high extent of interaction between the intercalated polymer segments and the silicate platelets. Because of no modifier, the Na clay-filled IPNs might have a weak interphase interaction. Consequently, it exhibits an insignificant change in the tensile strength. For the C30B-filled IPN, no intercalation took place, and, therefore, it shows no significant change. Further addition of clay results in a decrease in the tensile strength for all the filled IPNs. This could be because the clays tend to aggregate when they were incorporated at higher contents. Such big aggregates may act as defects and/or stress concentrators.

Figure 6.38 shows a reduction in elongation at break for all the filled IPNs. Further addition of clay leads to a gradual further decrease in the elongation at break. Again, this is due to defects and/or stress concentrators tending to form at higher clay contents. Consequently, a reduction in the elongation at break could happen. However, there is no obvious difference when compares amongst all nanoclay types.

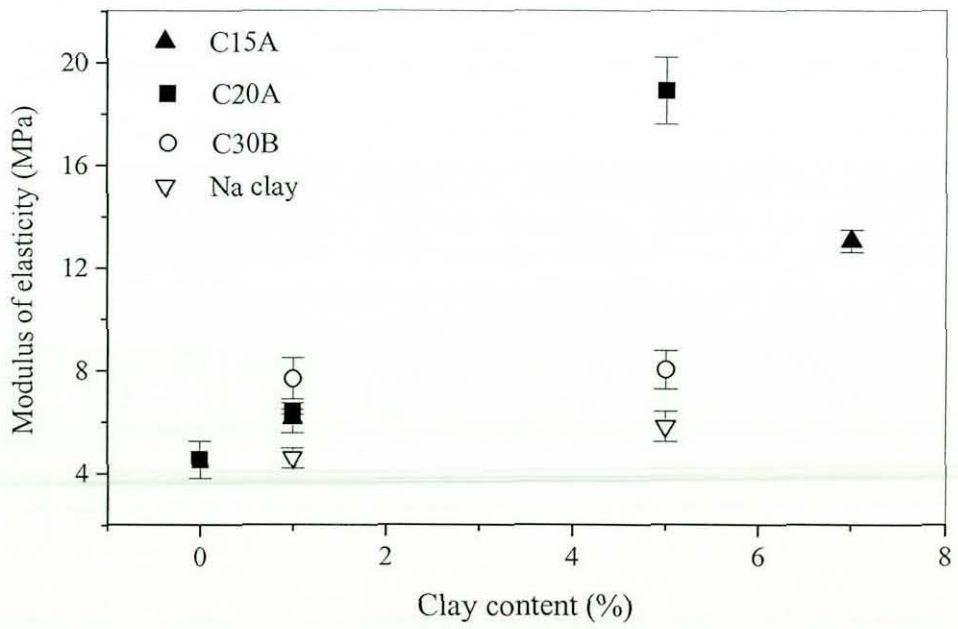


***Figure 6.39*** Modulus of elasticity of the 70PU/30PEMA IPN composites as a function of clay loading.

The increase in modulus of elasticity as clay content increased for all the filled-IPNs, see Figure 6.39, can be attributed to the difference in modulus between the polymer matrix and the clay. Incorporation of silicate clay usually increases stiffness comparative to the unfilled sample[118]. At 5% clay content, C20A-filled IPN reveals much higher modulus of elasticity than those of the C30B- and the Na clay-filled samples. This could come from the stronger interaction between the intercalated polymer segments and the silicate platelets.

# CHAPTER 7

# CONCLUSIONS AND FUTURE WORK

# CHAPTER 7

# CONCLUSIONS AND FUTURE WORK

## 7.1 Conclusions.

### 7.1.1 Selection of suitable formulations and conditions.

IPN morphology and mechanical properties, especially the damping behaviour, were investigated for 70PU/30PEMA IPN filled with organoclay particles. Formulations and conditions used to alter the IPN properties were the variation of organoclay content, IPN composition ratio, organoclay mixing time and PU catalyst content.

70PU/30PEMA IPNs filled with C20A, a modified clay in which the modifier is dimethyl dihydrogenated tallow quanternary ammonium, were systhesised by the in-situ polymerisation method via the original systhesis procedure with polyether polyol. The effects of the C20A organoclay content were observed in a range of 0 to 15% by weight of PU. X-ray diffraction results indicated that the interlayer distance increased almost the same amount from 2.29 nm, observed for C20A organoclay, to 3.92 nm, observed for IPN nanocomposites, for all cases. That meant the intercalation of polymer chains occurred. The diffusion ability of polymer chains into clay galleries was not controlled by the clay loading. Corresponding results revealed by TEM micrographs confirmed that the 70PU/30PEMA IPN nanocomposites had developed partial intercalation. Addition of C20A clay brought the IPN Tgs to lower temperatures. Besides, tan δ height at the PU Tg was decreased, while the PEMA Tg was increased with the C20A content. Higher clay contents tended to reveal high extents of phase separation. Introducing the C20A organoclay resulted in a stiffening effect and increased the modulus of elasticity and hardness of the IPNs, but decreased the tensile strength and elongation at break.

WAXD and TEM results for the C20A-filled PEMA showed the same results as found for the C20A-filled PU, where only partial intercalation could be achieved. The intercalated layer spacings were 3.92 nm and 3.81 nm for filled PU and filled PEMA, respectively. This meant that both PU and PEMA constituents could intercalate into the clay galleries. Increasing the clay content, showed no significant change of the PU Tg, while the PEMA Tg increased. Also, tan δ max values decreased at the glass

transitions for both PU and PEMA. Filled PU showed a reduction in storage modulus and modulus of elasticity with increasing organoclay content. On the other hand, filled PEMA revealed an increase in storage and loss modulus. These differences may be attributed to the number of crosslinking sites formed, strengthening the interaction between the organoclay and PEMA, which might not have occurred with PU.

A better approach was needed to enhance the dynamic and mechanical properties of the IPN system. Composition ratio was one of the crucial factors used to search for an optimised formulation. DMTA results showed that at the 70PU/30PEMA IPN composition exhibited the highest value of component mixing, as seen from a broad tan δ peak and gradual almost linear decreases in storage and loss moduli over the studied temperature ranges, as compared to those of the 50PU/50PEMA and 80PU/20PEMA IPN with 5 wt% C20A. As the PU content in the IPNs was increased, the tensile strength at break, the modulus of elasticity and hardness tended to reduce, but there was an increase in the elongation at break.

Variation of mixing time for dispersing the nanoclay into the polymer matrix showed a slight increase in phase separation with increased mixing time, which was exhibited by the DMTA results and also confirmed by M-TDSC thermograms. The tensile properties and Shore A hardness of the IPN nanocomposites revealed a slight improvement with increasing the mixing time. The values went through a maximum at 9 hour mixing time. Further increase in the mixing time led to a deterioration of the properties.

The PU catalyst content showed a slight change in component mixing of IPN. Increasing the catalyst content, the tan δ profile showed more extent of mixing, giving lower tan delta max values and lower glass transition of the PEMA component. These might be because of a higher degree of restriction of PEMA segmental mobility and incomplete network formation of the PEMA. The elongation at break marginally increased with catalyst content, but a large increase was found for the tensile strength and modulus of elasticity. The tensile properties showed optimum values at 1.6 wt% SnOct.

### 7.1.2 Optimisation of synthesis procedures.

**Variation of synthesis procedure.**

Variation of synthesis procedure by changing clay dispersion and the IPN component preparation steps were investigated. Details of these procedures and their flow diagrams are shown in chapter 3.

For all synthesis routes, X-ray diffraction results indicated that the interlayer distance increased by almost the same amount from 2.29 nm, observed for the C20A organoclay, to 3.84 nm, obtained for the IPN composites. This meant that the synthesis procedures did not affect the intercalation of the polymer molecules. Even though intercalation occurred in all IPN composites, regardless of the synthesis procedure, they were not pure nanocomposites.

TEM micrographs showed some large clay aggregates. Unfilled IPNs revealed a fine morphology with light, interconnected domains of PEMA in the dark, dominant PU matrix. Besides, the TEM micrographs also revealed a high extent of interphase as seen by the different shades of grey dispersed in the PU matrix. Incorporation of the C20A organoclay, by various synthesis procedures, exhibited no gross phase separation. The light, interconnected PEMA domains for all synthesis routes, became bigger and more distinct, indicating some extent of phase separation. Synthesis procedures one, two and four showed cellular structures, implying a higher extent of phase separation as compared to those of the original and synthesis procedure three.

Corresponding data for the extent of phase separation of the IPNs, prepared by the various synthesis routes, were confirmed by tan delta profiles. Those of the original synthesis procedure and synthesis procedure three revealed a lesser extent of phase separation. Consequently, they exhibited a higher storage and loss moduli compared to those of synthesis procedures one, two and four. Synthesis procedure three, which revealed the least extent of phase separation, showed the highest values of the tensile properties and of hardness.

**Use of ultrasonication.**

Ultrasonication was used for 1 hour after finishing the clay mixing step in all the synthesis procedures. The influence of various ultrasonic-assisted synthesis procedures on the intercalation showed that nothing changed. X-ray diffraction patterns revealed a similar interlayer distance to the unaided ultrasonication procedures. This indicated that the ultrasonic waves were unable to promote intercalation of polymer segments into the silicate clay galleries and improve the dispersion ability of the organoclay in this IPN system.

TEM micrographs revealed some large aggregates, which meant that these were not pure intercalated IPN composites. The aided synthesis procedures SP0, SP1 and SP4 morphologies revealed a cellular structure with an incorporation of light PEMA domains in the cellular matrix. There were very fine domains for SP0, but they became bigger for SP1. The biggest cellular domains were found for SP4. However, the different shades of grey areas at the phase boundaries revealed some extent of phase mixing.

The tan delta profiles showed that the ultrasonication aided original synthesis and synthesis procedure three exhibited a higher extent of mixing compared to those of SP1, SP2 and SP4. The storage and loss moduli of the SP0 and SP3 revealed higher values as compared to those of the SP1, SP2 and SP4. The same trends were also observed for the tensile strength and the elongation at break, the modulus of elasticity and the hardness.

### 7.1.3 Influence of other nanoclays.

**C15A organoclay.**

With incorporation of C15A organoclay in the IPN matrix, X-ray results showed an increase of the interlayer spacing from 3.24 nm, observed for C15A organoclay, to around 3.80 nm, observed for IPN nanocomposites. This meant that the intercalation of polymer chains occurred. However, the clay loading was not a factor that controlled the diffusion of polymer chains into clay galleries.

TEM micrographs revealed that the light, interconnected PEMA domains became bigger, more obvious and more interconnected with increasing organoclay content. However, a large range of different shades of grey dispersed in the PU matrix could be seen, indicating some extent of molecular mixing between the two polymer components.

DMTA results confirmed the TEM micrographs. Increasing the C15A content tended to exhibit a higher extent of phase separation. Tan delta profiles showed a less dominant PU transition and a higher and more distinctive peak at the PEMA transition. The storage and loss moduli exhibit two-step broad profiles with increasing clay loading. They also revealed some degree of phase separation. Incorporation the C15A organoclay decreased the tensile strength and elongation at break, but increased in the modulus of elasticity and hardness of the IPNs.

**C30B organoclay.**

C30B acted as a common filler in the IPN systems. X-ray diffraction results showed no change in the interlayer spacing, indicating that the polyol and polymer molecules were unable to intercalate into the clay galleries. TEM micrographs revealed that the light, interconnected PEMA domains became bigger, and more interconnected with increasing the C30B content. This showed some extent of phase separation. Tan delta profiles tended to show a high degree of phase separation with increasing clay content. However, adding the organoclay exhibited an increase in the modulus of elasticity and hardness value, whilst it decreased the strength and the elongation at break.

**Na clay.**

Intercalation of the polymer segments into the Na clay was revealed by the X-ray diffraction. The interlayer distance increased from 1.11 nm, obtained from the pure Na clay, to 1.43 and 1.23 nm at 1 and 5 wt% clay contents, respectively.

The light, interconnected PEMA domains were slightly bigger, and more interconnected, as the Na clay content increased. Besides, there were some small, light PEMA domains dispersed uniformly in the continuous PU matrix. Thus, the

morphology of these nanocomposites revealed some degree of component mixing. This was also supported by the DMTA results.

Tan delta-temperature traces revealed a very broad and nearly rectangular profile spanning the studied temperature range for the Na clay-filled IPN. The storage and loss moduli showed a gradual decrease with increasing the clay loading. Increasing the Na clay content caused the modulus of elasticity to increase, whilst the elongation at break decreased.

**Comparison of the clay types.**

At 1 wt% clay loading, the C15A-, C20A- and Na clay-filled 70PU/30PEMA IPNs exhibited high damping characteristics. They showed a broad loss factor, tan $\delta \geq 0.3$, spanning a temperature range of 130°C, implying micro-heterogeneity with some extent of molecular mixing. However, Na clay-filled IPNs showed a slightly lower loss factor value, as compared to those of the C15A- and C20A-filled IPNs. The C30B-filled IPN tended to exhibit some phase separation as shown by a decrease in the tan $\delta$ max value at the PU Tg and an increase in tan $\delta$ max value at the PEMA Tg.

At 5 wt% clay content, the C20A- and C30B-filled IPNs showed high extents of phase separation, revealing a PU transition shoulder with a strong PEMA transition. This was attributed to a restricted mobility of segmental chains in both polymer networks. The loss and storage moduli also showed a two-step change at homopolymer Tgs. Na clay-filled IPN still revealed a broad loss factor profile spanning the measured temperature range, but exhibited a slightly lower value as compared to that of unfilled IPN.

Tensile behaviour of filled IPNs with various types of nanoclay showed that filled IPNs revealed some improvement in tensile strength at break and modulus of elasticity with a decrease in the elongation at break. The C15A- and C20A-filled IPNs with 1 wt% clay loading showed the optimum tensile strength, which was around 33% of that for the unfilled IPN. Modulus of elasticity, for all clay types, gradually increased with increasing clay content. The C15A- and C20A-filled IPNs showed much improvement, more than two times, at 5 wt% clay loading, when they were compared to that of the pure IPN. Less pronounced improvements were shown by the C30B- and Na clay-

filled IPNs. The reduction in the elongation at break gradually decreased as the nanoclay content increased for all filled IPNs, especially at the higher clay content.

## 7.2 Recommendations for future work.

Only partially intercalated IPN nanocomposites have been obtained and characterised in this study. Thus, the hoped for great improvement in dynamic and mechanical properties has not yet been achieved. To achieve the full intercalation/exfoliation with high damping characteristic, the following investigation should be attempted.

1. An attempt should be make to study the effect of temperature and the combination of the temperature with other important factors such as mixing order and mixing time.

2. Other types of organoclay such as C10A, C25A and C93A, should be examined. For C10A, C25A and C93A, their modifiers are more hydrophilic than those of C15A and C20A.

3. Synthesis of new organically-modified clay might be another way to achieve full exfoliation/intercalation for this IPN system. The ability of the onium ion to assist in intercalation/delamination of the clay depends on its chemical nature.

4. Work should be conducted on other techniques to study damping characteristics and to measure the damping ability of these materials. One of the interesting ways is sound absorption measurements and also the use of these modified materials in extensional and constrained layer damping systems under controlled conditions, such as at various temperatures and frequencies.

# REFERENCES

## REFERENCES


1) L.H.Sperling, "Interpenetrating Polymer Networks and Related Materials", Plenum Press, New York (1981).
2) L.H.Sperling, in "Interpenetrating Polymer Networks", Eds., D. Klempner, L.H. Sperling and L.A. Utracki, Advances in Chemistry Series 239, American Chemical Society, Washington DC (1994).
3) X. Yu, G. Gao, J. Wang, F. Li and X. Tang, *Polym. Int.,* **48**, 805 (1999).
4) R. Hu, V.L. Dimonie, M.S. El-Aasser, R.A. Pearson, A. Hiltner, S.G. Mylonaki and L.H. Sperling, *J. Polym. Sci. B: Polym. Phys.*, **35**, 1501 (1997).
5) Y.C. Chern, S.M. Tseng and K.H. Hsieh, *J. Appl. Polym. Sci.*, **74**, 335 (1999).
6) K.R. Kim, J.H. An, K.W. Cho and C.E. Park, *J. Appl. Polym. Sci.*, **47**, 305 (1993).
7) W. Peng and S.J. Li, *J. Appl. Polym. Sci.*, **58**, 967 (1995).
8) M. Patri, A. Samui and P.C. Deb, *J. Appl. Polym. Sci.*, **48,** 1709 (1993).
9) C.J. Tung and T.C. Hsu, *J. Appl. Polym. Sci.*, **46**, 1759 (1992).
10) J.J. Fay, C.J. Murphy, D.A. Thomas and L.H. Sperling, *Polym. Eng. Sci.*, **31**, 1731 (1991).
11) Q. Chen, H. Ge, D. Chen, M. He and X. Yu, *J. Appl. Polym. Sci.*, **54**, 1191 (1994).
12) D.J. Hourston and F.U. Schafer, *J. Appl. Polym. Sci.*, **62**, 2025 (1996).
13) M.Xu, W.J. MacKnight, C.H.Y. Chen and E.L. Thomas, *Polymer*, **28**, 2183 (1987).
14) M. Alexandre and P. Dubois, *Mater. Sci. Eng.*, **28**, 1 (2000).
15) E.P. Giannelis, *Adv. Mater.*, **8**, 29 (1996).
16) P.C. Le Baron, Z. Wang and T.J. Pinnavaia, *Appl. Clay Sci.*, **15**, 11 (1999).
17) R.A. Vaia, H. Ishii and E.P.Giannelis, *Chem. Mater.*, **5**, 1694 (1993).
18) D.C. Lee and L.W. Jang, *J. Appl. Polym. Sci.*, **61**, 117 (1996).
19) Y. Kojima, A. Usaki, M. Kawasumi, A. Okada, T. Kurauchi and O. Kamigaito, *J. Polym. Sci. Part A: Polym. Chem.*, **31**, 1755 (1993).
20) T. Lan and T.J. Pinnavaia, *Chem. Mater.*, **6**, 2216 (1994).
21) T. Lan, P.D. Kaviratna and T.J. Pinnavaia, *Chem. Mater.*, **7**, 2144 (1995).
22) C. Zilg, R. Mulhaupt and J. Finter, *Macromol. Chem. Phys.*, **200**, 661 (1999).
23) L.M. Liu, Z.N. Qi and X.G. Zhu, *J. Appl. Polym. Sci.*, **71**, 1133 (1999).

24) A. Blumstein, *J. Polym. Sci.*, **A3**, 2665 (1965).

25) S.D. Burnside and E.P. Giannelis, *Chem. Mater.*, **7**, 1597 (1995).

26) S.J. Wang, C.F. Long, X.Y. Wang, Q. Li and Z.N. Qi, *J. Appl. Polym. Sci.*, **69**, 1557 (1998).

27) J.W. Gilman, T. Kashiwagi, S. Lomakin, E.P. Giannelis, E. Manias, J.D. Lichtenhan and P. Jones, "Proceedings of the 6th European Meeting on Fire Retardancy of Polymeric Materials (FRPM 97), University of Lille, France, 24-26 September (1997).

28) J.W. Gilman, T. Kashiwagi, J.E.T. Brown and S. Lomakin, *SAMPE J.*, **43**, 1053 (1998).

29) K. Yano, A. Usaki and A. Okada, *J. Polym. Sci. A: Polym. Chem.*, **35**, 2289 (1997).

30) T. Lan, P.D. Kaviratna and T.J. Pinnavaia, *Chem. Mater.*, **6**, 573 (1994).

31) P.B. Messersmith and E.P. Giannelis, *J. Polym. Sci. A: Polym. Chem.*, **33**, 1047 (1995).

32) H.G. Jean, H.T. Jung, S.W. Lee and S.D. Hudson, *Polym. Bull.*, **41**, 107 (1998).

33) B. Lepoittevin, M. Devalckenaere, N. Pantoustier, M. Alexandre, D. Kubies, C. Calberg, R.J. Jerome and P. Dubois, *Polymer*, **43**, 4017 (2002).

34) J.H. Park and S.C. Jana, *Macromolecules*, **36**, 2758 (2003).

35) K.C. Frisch, D. Klempner and S. Migdal, *J. Polym. Sci. A: Polym. Chem.*, **12**, 885 (1974).

36) L.H. Sperling, *Polym. Eng. Sci.*, **25**, 517 (1985).

37) K.C. Frisch and D.Klempner, *Polym. Sci. Technol.*, **11**, 203 (1980).

38) M. Akay and S.N. Rollins, *Polymer*, **34**, 1865 (1993).

39) M. Akay, S.N. Rollins and E. Riordan, *Polymer*, **29**, 37 (1988).

40) D. Klempner, L. Berkowski, K.C. Frisch and K.H. Hsieh, *Rubber World*, **6**, 16 (1985).

41) Z. Wirpsza, "Polyurethanes: Chemistry, Technology and Applications", Ellis Horwood, London (1993).

42) F.W. Billmeyer, "Textbook of Polymer Science", Third edition, John Wiley & Sons, New York (1984).

43) T. Pabunruang, "Damping Characteristics of Unfilled and Filled-Polyurethane/Poly(ethyl methacrylate) Simultaneous Interpenetrating Polymer Networks", Ph.D thesis, Loughborough University (2000).

44) F.U. Schafer, "Polyurethane-Based Simultaneous IPNs", Ph.D thesis, Loughborough University (1996).

45) J.G. Ryu, S.W. Park, H. Kim and J.W. Lee, *Mater. Sci. Eng.*, **C24**, 285 (2004).

46) M. Okamoto, S.Morita, H. Taguchi, Y.H. Kim, T. Kotaka and H. Tateyama, *Polymer*, **41**, 3887 (2000).

47) B. Finnigan, D. Martin, P. Halley, R. Truss and K. Campbell, *Polymer*, **45**, 2249 (2004).

48) http://www.pslc.ws/macrog/mpm/ipn/example.htm on 07 September 2005.

49) F.D. Roemer and L.H. Tateosian, European Patent 0,014,515 (1984).

50) D.J. Hourston and J.J. Romaine, *J. Appl. Polym. Sci.*, **39**, 1587 (1990).

51) D.J. Hourston, R. Satgurunathan and H. Varma, *J. Appl. Polym. Sci.*, **34**, 901 (1987).

52) http://www.silon.com/silon-ipn.htm on 07 September 2005.

53) K.E. Mueller and S.J. Heiber, *J. Appl. Polym. Sci.*, **27**, 4043 (1982).

54) C.F. Mason, Europe Patent 390307 A2 (1990).

55) S. Suzuki, M. Sakah and A. Shiba, *J. Biomed. Mater. Res.*, **24**, 1091 (1990).

56) M.K. Lindeman and K. Deacon, U.S. Patent 4,686,260 (1987).

57) M.K. Lindeman and K. Deacon, U.S. Patent 4,683,165 (1987).

58) R.H. Pater, *Polym. Eng. Sci.*, **31**, 20, 28 (1991).

59) O. Olabisi and L.M. Robeson, "Polymer-Polymer Miscibility", Acedemic Press, New York (1979).

60) L.A. Utracki, "Polymer Alloys and Blends", Hanser Publishers, Munich (1990).

61) D.S. Kaplan, *J. Appl. Polym. Sci.*, **20**, 2615 (1976).

62) W.Y. Chiang and D.M. Chang, *Eur. Polym. J.*, **13**, No.8, 709 (1995).

63) M. Kamal and A.K. Srivastava, *Reactive & Functional Polymers*, **49**, 55 (2001).

64) S.S. Hon and P.L. Kuo, *Polymer*, **42**, 9505 (2001).

65) D.J. Hourston, M. Song, F.U. Schafer, H.M. Pollock and A. Hammiche, *Themochimica Acta*, **324**, 109 (1998).

66) M. Song, D.J. Hourston and F.U. Schafer, *Polymer*, **40**, 5773 (1999).

67) M. Song, D.J. Hourston, F.U. Schafer, H.M. Pollock and A. Hammiche, *Themochimica Acta*, **315**, 25 (1998).

68) V.D. Athawale and S.S. Raut, *Euro. Polym. J.*, **38**, 2033 (2002).

69) T.T. Alekseeva, Y.S. Lipatov, N.V. Babkina, S.I. Grishchuk and N.V. Yarovaya, *Polymer*, **46**, 419 (2005).

70) J.M. Widmaier, A. Nilly, J.M. Chenal and A. Mathis, *Polymer*, **46**, 3318 (2005).

71) http://saule.u-strasbg.fr/~anglais/equipe2/widmaierfcadre3.html on 07 September 2005.

72) L.H. Sperling, in "Comprehensive Polymer Science", Eds., G. Allen and J.C. Bevington, Vol. 6, Pergamon Press, New York (1989).

73) A.A. Donatelli, L.H. Sperling and D.A. Thomas, *J. Appl. Polym. Sci.*, **21**, 1189 (1977).

74) D.J. Hourston and J.A. McCluskey, *J. Appl. Polym. Sci.*, **31**, 645 (1986).

75) D.J. Hourston and Y. Zia, *J. Appl. Polym. Sci.*, **28**, 3849 (1983).

76) D.J. Hourston and J.A. McCluskey, *J. Appl. Polym. Sci.*, **30**, 2157 (1985).

77) M.I. Felisberti and R. Stadler, *Macromolecules*, **22**, 4128 (1989).

78) B.J. Bauer and R.M. Briber, *Macromolecules*, **22**, 940 (1989).

79) B.J. Bauer and R.M. Briber, *Macromolecules*, **24**, 1899 (1991).

80) V. Huelck, D.A. Thomas and L.H. Sperling, *Macromolecules*, **5**, 340 (1972).

81) A.A. Donatelli, L.H. Sperling and D.A. Thomas, *Macromolecules*, **9**, 671 (1976).

82) R.B. Fox, J.L. Bittner, J.A. Hinkley and W. Carter, *Polym. Eng. Sci.*, **25**, 157 (1985).

83) D.J. Hourston and M.G. Huson, *J. Appl. Polym. Sci.*, **45**, 1753 (1992).

84) S.C. Kim, D. Klempner, K.C. Frisch, W. Radigan and H.L. Frisch, *Macromolecules*, **9**, 263 (1976).

85) S.C. Kim, D. Klempner, K.C. Frisch, W. Radigan and H.L. Frisch, *Macromolecules*, **10**, 1187 (1977).

86) S.C. Kim, D. Klempner, K.C. Frisch, H.L. Frisch and H. Ghiradella, *Polym, Eng. Sci.*, **15**, 339 (1975).

87) D.R. Paul and S. Newman, "Polymer Blends", Vol.2, Academic Press, New York (1981).

88) J.R. Millar, *J. Chem. Soc.*, **263**, 1311 (1960).

89) D. Klempner, H.L. Frisch and K.C. Frisch, *J. Polym. Sci. A2*, **8**, 921 (1970).

90) K. Shibayama and Y. Suzuki, *Kobunshi Kagaku*, **23**, 24 (1966).

91) D. Klempner, K.C. Frisch and H.L. Frisch, *J. Elast. Plastics*, **3**, 2 (1971).

92) D. Klempner, H.L. Frisch, T.K. Kwei and M. Matsui, *Polym. Eng. Sci.*, **10**, 327 (1970).

93) H.C. Van de Hulst, "Light Scattering by Small Particles", Wiley, New York (1973).

94) R.G. Bauer, R.M. Pierson, W.C. Mast, N.C. Bletso and L. Shepherd, *Adv. Chem. Ser.*, **99**, 237 (1971).

95) R.G. Bauer and M.S. Guillod, *Adv. Chem. Ser.*, **142**, 231 (1975).

96) D.R. Pual and J. Altamirano, *Adv. Chem. Ser.*, **142**, 371 (1975).

97) J.D. Lipko, H.F. George, D.A. Thomas and S.C. Hargest, *J. Appl. Polym. Sci.*, **23**, 2739 (1979).

98) K.C. Frisch, D. Klempner, H.L. Frisch and H. Ghiradella, in "Recent Advances in Polymer Blends, Grafts and Blocks", Ed., L.H. Sperling, Plenum, New York (1974).

99) R.L. Imken, D. Paul and J.W. Barlow, *Polym. Eng. Sci.*, **16**, 593 (1976).

100) J.A. Manson and L.H. Sperling, "Polymer Blends and Composites", Plenum Press, New York (1976).

101) A.J. Curtins, M.J. Covitch, D.J. Thomas and L.H. Sperling, *Polym. Eng. Sci.*, **12**, 101 (1972).

102) L.H. Sperling, "Introduction to Physical Polymer Science", Second edition, John Wiley & Sons, New York (1992).

103) C.E. Carraher, Jr., "Polymer Chemistry: An Introduction", Marcel Dekker Inc., New York (1996).

104) J.D. Ferry, "Viscoelastic Properties of Polymers", John Wiley & Sons Inc., New York (1980).

105) N.G. McCrum, "Principles of Polymer Engineering", Second edition, Oxford University Press Inc., New York (1997).

106) S.R. Sandler, W. Karo, J. Bonesteel and E.M. Pearce, "Polymer Synthesis and Characterization: A Laboratory Manual", Academic Press, London (1998).

107) G.W. Ehrenstein, "Polymeric Materials: Structure-Properties-Applications", Hanser Gardner Publications Inc., Cincinnati (2001).

108) E.E. Unger, in "Noise and Vibration Control", Ed., L.L. Beranek, McGraw Hill, New York (1979).

109) M.C. Chang, D.A. Thomas and L.H. Sperling, *J. Polym. Sci. Part B: Polym. Phy.*, **26**, 1627 (1988).

110) J.N. Forster and L.H. Sperling, *J. Appl. Polym. Sci.*, **33**, 2637 (1987).

111) D.J. Hourston and J.A. McCluskey, *Polymer*, **20**, 1573 (1979).

112) M. Akay and S.N. Rollins, *Polymer*, **34**, 967 (1993).

113) D. Sophiea, D. Klempner, V. Sendijarevic, B. Suthar and K.C. Frisch, in "Interpenetrating Polymer Networks", Eds., D. Klempner, L.H. Sperling, and L.A. Utracki, Advance in Chemistry Series 239, American Chemical Society, Washington DC (1994).

114) L.H. Sperling, "Polymeric Multicomponent Materials: An Introduction", John Wiley & Sons, New York (1997).

115) B.K.G. Theng, "The Chemistry of Clay-Organic Reactions", Wiley, New York (1974).

116) M. Ogawa and K. Kuroda, *Bull. Chem. Soc. Jpn.*, **70**, 2593 (1997).

117) A. Okada, M. Kawasumi, A. Usaki, Y. Kojima, T. Kurauchi and O. Kamigaito, *Mater. Res. Soc. Proc.*, **171**, 45 (1990).

118) T.J. Pinnavaia and G.W. Beall, "Polymer-Clay Nanocomposites", John Wiley & Sons, New York (2000).

119) E.P. Giannelis, R. Krishnamoorti and E. Manias, *Adv. Polym. Sci.*, **118**, 108 (1999).

120) G. Lagaly, *Solid State Ionics*, **22**, 43 (1986).

121) R.A. Vaia, R.K. Teukolsky and E.P. Giannelis, *Chem. Mater.*, **6**, 1017 (1994).

122) C. Oriakhi, *Chem. Br.*, **34**, 59 (1998).

123) X. Kornmann, "Synthesis and Characterisation of Thermoset-Layered Silicate Nanocomposites", Ph.D. thesis, Lulea University of Technology (2001).

124) P.B. Messersmith and E.P. Giannelis, *Chem. Mater.*, **6**, 1719 (1994).

125) B.K.G. Theng, "Formation and Properties of Clay-Polymer Complexes, Elsevier, Amsterdam (1979).

126) N. Hasegawa, M. Kawasumi, M. Kato, A. Usaki and A. Okada, *J. Appl. Polym. Sci.*, **67**, 87 (1998).

127) M.W. Noh and D.J. Lee, *Polym. Bull.*, **42**, 619 (1999).

128) Y. Kojima, A. Usaki, M. Kawasumi, A. Okada, Y. Fukushima, T. Karauchi and O. Kamigaito, *J. Mater. Res.*, **6**, 1185 (1993).

129) Z. Wang and T.J. Pinnavaia, *Chem. Mater.*, **10**, 1820 (1998).

130) Z. Wang and T.J. Pinnavaia, *Chem. Mater.*, **10**, 3769 (1998).

131) M. Laus, O. Francesangeli and F. Sandrolini, *J. Mater. Res.*, **12**, 3134 (1997).

132) K. Yano, A. Usaki and A. Okada, *J. Polym. Sci. A: Polym. Chem.*, **35**, 2289 (1997).

133) A. Okada and A. Usuki, *Mater. Sci. Eng.*, **C3**, 109 (1995).

134) D.C. Lee and L.W. Jang, *J. Appl. Polym. Sci.*, **68**, 1997 (1998).

135) H.L. Tyan, Y.C. Liu and K.H. Wei, *Polymer*, **40**, 4877 (1999).

136) J.W. Gilman, *Appl. Clay Sci.*, **15**, 31 (1999).

137) F. Dietsche and R. Mulhaupt, *Polym. Bull.*, **43**, 395 (1999).

138) G.W. Beall, "Annual Technical Conference-Society of Plastics Engineers", 57$^{th}$, Vol. 3, 3979 (1999).

139) C. Hepburn, "Polyurethane Elastomers", Second edition, Elsevier Applied Science, London (1992).

140) W.F. Gum, W. Riese and H. Ulrich, Eds., "Reaction Polymers", Hanser Publishers, Munich (1992).

141) J.H. Saunders and K.C. Frisch, "Polyurethane Chemistry and Technology", Part I, Interscience Publishers, New York (1962).

142) G. Oertel, "Polyurethane Handbook", Second edition, Carl Hanser Verlag, Munich (1994).

143) G. Odian, "Principles of Polymerization", Third edition, Wiley-Interscience, New York (1991).

144) K. Uhlig, "Discovering Polyurethanes", Hanser Publishers, Munich (1999).

145) J. Bhattachryya, "Handbook of Polymer Science and Technology", Vol.2, Marcel Dekker, New York (1989).

146) F. Rodriguez, "Principles of Polymer Systems", Fourth edition, Taylor & Francis, London (1996).

147) A. Ravve, "Principles of Polymer Chemistry", Second edition, Kluwer Academic/Plenum Publishers, New York (2000).

148) S. Inoue, Chapter 5 in "Structure and Mechanism in Vinyl Polymerisation", Eds., T. Tsuruta and K.F.O. Driscoll, Dekker, New York (1969).

149) J.M.G. Cowie, "Polymers: Chemistry & Physics of Modern Materials", Second edition, Stanley Thornes Publishers Ltd, Cheltenham (1991).

150) R.W. Richards, "Scattering Methods in Polymer Science", Ellis Horwood Limited, New York (1995).

151) L.E. Alexander, "X-ray Diffraction Methods in Polymer Science", John Wiley & Sons, New York (1969).

152) D. Campbell, "Polymer Characterization: Physical Techniques", Second edition, Eds., R.A. Pethrick and J.R. White, Stanley Thornes (Publishers) Ltd, Cheltenham (2000).

153) J.F. Rabek, "Experimental Methods in Polymer Chemistry: Physical Principles and Applications", John Wiley & Sons, Chichester (1980).

154) L.E. Nielson, "Mechanical Properties of Polymers and Composites", Vol.1 & 2, Dekker, New York (1974).

155) DMTA Mk II User Manual, Rheometric Scientific (1995).

156) U.W. Gedde, "Polymer Physics", Chapman & Hall, London (1995).

157) D.J. Hourston, M. Song, A. Hammiche, H.M. Pollock and M. Reading, *Polymer*, **38**, 1 (1997).

158) S.L. Simon, *Thermochimica Acta*, **374**, 55 (2001).

159) M. Reading, *Trends Polym. Sci. 1*, **8**, 248 (1993).

160) A. Riga and R. Collins, "Encyclopedia of Analytical Chemistry": Differential Scanning Calorimetry and Differential Thermal Analysis, Ed., R.A. Mayers, John Wiley & Sons, New York (1995).

161) M. Song, H.M. Pollock, A. Hammiche, D.J. Hourston and M. Reading, *Polymer*, **38**, 503 (1995).

162) M. Song, A. Hammiche, H.M. Pollock, D.J. Hourston and M. Reading, *Polymer*, **36**, 3313 (1995).

163) TA Instruments Operator's Manual, New Castle (1997).

164) B.J. Hunt and M.I. James, "Polymer Characterisation", Blackle Academic & Professional. Glasgow (1993).

165) A.Y. Malkin, A.A. Askadsky, V.V. Kovriga and A.E. Chalykh, "Experimental Methods of Polymer Physics", Prentice-Hall Inc., New Jersey (1983).

166) P.I. Donnelly, "Mechanical Properties of Polymers", Wiley-Interscience, New York (1971).

167) D.W. Clegg and A.A. Collyer, "The Structure and Properties of Polymeric Materials", The Bourne Press, Bournemouth (1993).

168) H. Gletter, *Adv. Matter.*, **4**, 474 (1992).

169) http://www.nanoclay.com on 07 September 2005.

170) H. Djomo, A. Morin, M. Damyanidu and G. Meyer, *Polymer*, **24**, 65 (1983).

171) J. Brandrup and E.H. Immergut, "Polymer Handbook", Wiley-Interscience, Third edition, New York (1984).

172) P.C. LeBaron and T.J. Pommavaia, *Chem. Mater.*, **13**, 3760 (2001).

173) C.I.L. Park, W.W. Choi, M.H.O. Kim and O.O.K. Park, *J. Polym. Sci. B: Polym. Phys.*, **42**, 1685 (2004).

174) D.S. Lee and S.C. Kim, *Macromolecules*, **17**, 268 (1984).

175) E. Cassidy, H. Xiao, K.C. Frisch and H. Frisch, *J. Polym. Sci., Polym. Chem. Edn.*, **22**, 1839 (1984).

176) L. Sperling, D. Taylor, M. Kirkpatrick and H. George, *J. Appl. Polym. Sci.*, **14**, 73 (1970).

177) S. Kim, D. Klempner, K.C. Frisch and H. Frisch, *Macromolecules*, **9**, 258 (1976).

178) Y.S. Lipatov, T.T. Alekseeva, V.F. Rosovitsky and N.V. Babkina, *Polym. Int.*, **37**, 97 (1995).

179) Y. Li, R. Liu, J. Wang and X. Tang, *Progress in Organic Coatings*, **21**, 101 (1992).

180) G. Wypych, "Fillers", Chem Tec Publishing, Ontario (1993).

181) H. Lu and S. Nutt, *Macromolecules*, **36**, 4010 (2003).

182) K.J. Yao, M. Song, D.J. Hourston and D.Z. Luo, *Polymer*, **43**, 1017 (2002).

183) M.Y. Gelfer, H.H. Song, L. Liu, B.S. Hsiao, B. Chu, M. Rafailovich, M. Si and V. Zaitsev, *J. Appl. Polym. Sci. Part B: Polym. Phys.*, **42**, 44 (2002).

184) H.S. Katz and J.V. Milewski, "Handbook of Fillers for Plastics", Van Nostrand Reinhold Company, New York (1987).

185) T.J. Siddaramaiah, *Eur. Polym. J.*, **39**, 569 (2003).

186) J.J. Luo and I.M. Daniel, *Compos. Sci. Technol.*, **63**, 1607 (2000).

187) Y.T. Vu, J.E. Mark, L.H. Pham and M. Engelhardt, *J. Appl. Polym. Sci.*, **82**, 1392 (2001).

188) Y.Q. Zhang, L.H. Lee, H.J. Jang and C.W. Nah, *Compos. Part B: Eng.*, **35**, 133 (2004).

189) M. Tortora, G. Gorrasi, V. Vittoria, G. Galli, S. Ritrovati and E. Chiellini, *Polymer*, **43**, 6147 (2002).

190) N. Sheng, M.C. Boyce, D.M. Parks, G.C. Rutledge, J.I. Abes and R.E. Cohen, *Polymer*, **45**, 487 (2004).

191) S. Kloe, A. Bhattacharya, D.K. Tripathy and K. Bhowmick, *J. Appl. Polym. Sci.*, **48**, 529 (1993).

192) A.R. Payne and J.R. Scott, "Engineering Design with Rubber", Interscience Publishers, New York (1960).

193) Z.S. Petrovic and J. Ferguson, *Prog. Polym. Sci.*, **16**, 695 (1991).

194) Y.I. Tien and K.H. Wei, *J. Appl. Polym. Sci.*, **86**, 1741 (2002).

195) Y.I. Tien and K.H. Wei, *Polymer*, **42**, 3213 (2001).

196) Y.I. Tien and K.H. Wei, *Macromolecules*, **34**, 9045 (2001).

197) M. Song, D.J. Hourston, H.M. Pollock, F.U. Schafer and A. Hammiche, *Thermochim Acta*, **304/305**, 335 (1997).

198) S.Y. Moon, J.K. Kim, C. Nah and Y.S. Lee, *Eur. Polym. J.*, **40**, 1615 (2004).

199) J.A. Miller, S.B. Lin, K.K.S. Hwang. K.S. Wu, P.E. Gibson and S.L. Cooper, *Macromolecules*, **18**, 32 (1985).

200) W. Zhang, X. Shen, Y. Li and Y. Fang, *Radiation Physics and Chemistry*, **67**, 651 (2003).

201) A. Tabtiang, S. Lumlong and R.A. Venables, *Euro. Polym. J.*, **36**, 2599 (2000).

202) T. Xie, G. Yang, X. Fang and Y. Ou, *J. Appl. Polym. Sci.*, **89**, 2256 (2003).

203) V. Mishra, F.D. Prez and L.H. Sperling, *Polym. Mater. Sci. Eng.*, **72**, 124 (1995).

204) M.T. Tabka, J.M. Widmaier and G.C. Meyer, *Plastics Rubber Comp. Process. Appl.*, **16**, 11 (1991).

205) J. Jordan, K.I. Jacob, R. Tannenbaum, M.A. Sharaf and I. Jasiuk, *Mater. Sci. Eng. A.*, **393**, 1 (2005).

206) M.Z. Rong, M.Q. Zhang, Y.X. Zheng, H.M. Zeng, R. Walter and K. Friedrich, *Polymer*, **42**, 167 (2001).

207) K.C. Frisch, in "Polyurethane Technology", ed. P.E. Bruins, Interscience Publishers, New York (1969).

208) P. Tan, in "Interpenetrating Polymer Networks", Eds., D. Klempner, L.H. Sperling, and L.A. Utracki, Advance in Chemistry Series 239, American Chemical Society, Washington DC (1994).

209) J.W. Gilman, T. Kashiwagi, M. Nyden, J.E.T. Brown, C.L. Jackson, S.Lomakin, E.P. Giannelis and E. Manias, "Chemistry and Technology of Polymer Additives", The Royal Society of Chemistry, Cambridge (1999).

210) A.B. Morgan, J.W. Gilman, M.R. Nyden and C.L. Jackson, "National Institute of Standard & Technology Internal Report (NISTIR) 6465", Feb 2000.

211) K. Gonsalves and X. Chen, in "Materials Research Soc. Symposium Procedding", Materials Research Society : Warrendale, PA (1996).

212) H. Ishida, S. Campbell and J. Blackwell, *Chem. Mater.*, **12**, 1260 (2000).

213) X.Y. Huang and W.J. Brittain, *Macromolecules*, **34**, 3255 (2001).

214) J. Massan and T.J. Pinnavaia, *Mater. Res. Soc. Symp. Proc.*, **520**, 223 (1998).

215) E.P. Giannelis, R. Krishnamoorti and E. Manias, *Adv. Polym. Sci.*, **138**, 107 (1999).

216) R.A. Vaia, G. Price, P.N. Ruth, H.T. Nguyen and J. Lichtenhan, *Appl. Clay. Sci.*, **15**, 67 (1999).

217) M. Biswas and S.S. Ray, *Adv. Polym. Sci.*, **155**, 167 (2001).

218) A.B. Morgan and J.W. Gilman, *J. Appl. Polym. Sci.*, **87**, 1329 (2003).

219) S.S. Ray and M. Okamoto, *Prog. Polym. Sci.*, **28**, 1539 (2003).

220) J.G. Doh and L. Cho, *Polym. Bull.*, **41**, 511 (1998).

221) H. Kim and J.W. Lee, *Polymer*, **43**, 2585 (2002).

222) B. Chen, J.R.G. Evans and S. Holding, *J. Appl. Polym. Sci.*, **94**, 548 (2004).

223) http://www.azon.com/details.asp?ArticleID=936 on 06 November 2005.

224) A. Pattanayak and S.C. Jana, *Polymer*, **46**, 3394 (2005).

225) M. Kawasumi, N. Hasegawa, M. Kato, A. Usuki and A. Okada, *Macromolecules*, **30**, 6333 (1997).

226) B. Lepoittevin, N. Pantoustier, M. Devalckenaere, M. Alexandre, C. Calberg, R. Jerome, C. Henrist, A. Rulmont and P. Dubois, *Polymer*, **44**, 2033 (2003).

227) A.W. Birley, B. Haworth and J. Batchelor, "Physics of Plastics", Hanser Publishers, Munich (1991).

228) W.C. Wake, "Fillers for Plastics", Plastics Institute, London (1971).